# *Biodynamics of lens sterols and their role in membrane homeostasis*

ALEXIA ANNE-MAJ KALLIGERAKI

# BIODYNAMICS OF LENS STEROLS AND THEIR ROLE IN MEMBRANE HOMEOSTASIS

A thesis submitted for the degree of Doctor of Philosophy

**Alexia A. Kalligeraki**



**DURHAM UNIVERSITY**
**Department of Biosciences**
**Hatfield College**
**31/10/2020**

Biodynamics of lens sterols and their role in lens membrane homeostasis

Alexia A. Kalligeraki

**Abstract**

Lifelong lens transparency is reliant on the physiological interactions between the lens proteome and the lens lipidome. The age-related collapse of α-crystallin chaperone activity, the increase of high molecular weight protein aggregates, and the progressive stiffening of lens fibre cell membranes due to cholesterol enrichment all contribute to the terminal manifestation of lens ageing which is cataract. The use of oxysterols as a pharmacotherapeutic agent for cataract has been proposed, though there is limited understanding behind the mechanisms underpinning the interactions of supplemental sterols with endogenous lens lipids and proteins. We have analysed the gross phenotypic effect of inhibition of cholesterol synthesis in the developing zebrafish and analysed the absorption and retention of deuterated sterols by the larval lens in the context of human syndromes presenting with congenital and juvenile cataract. The inhibition of cholesterol synthesis reduces the optomotor response in developing zebrafish by negatively affecting the visual acuity of the larvae, while changes in the lens epithelium affect the aspect ratio of the tissue. Lanosterol or cholesterol supplementation do not immediately rescue the physical phenotypes of synthesis inhibited zebrafish, but both sterols are absorbed, transported, and retained in the lens. *In vitro* analysis of the protein-lipid interactions of lens lysates revealed an α-crystallin dependent, temporal solubilisation of proteins including the cytoskeletal proteins vimentin and BFSP1, and the transmembrane water channel protein AQP0. This effect was not preserved in material derived from cataractous lenses and was inhibited using cysteine protease inhibitors E-64 and leupeptin. Finally, the supplementation of exogenous α-crystallin restored the temporal solubility of E-64-treated lens proteins and this effect was accelerated via the sensitisation of α-crystallin with oxysterols. These findings highlight the need for a better understanding of the pharmacokinetics of oxysterols in relation to their fate in the lens and support the concept of targeting the chaperone activity of α-crystallin as an intervention against the progression of cataract.

# Table of Contents

List of tables ..... 8

List of Figures ..... 8

List of abbreviations ..... 12

Declaration and Statement of Copyright ..... 22

Acknowledgements ..... 23

1 Chapter 1: Introduction ..... 24

1.1 The physiology of the lens ..... 24

1.1.1 Lens structure and development ..... 25

1.1.2 Lens ageing and cataract ..... 28

1.1.3 Lens fibre cell membranes ..... 30

1.1.4 Age-related changes in the lens proteome ..... 38

1.1.5 Lipidome- proteome dynamics ..... 40

1.2 Cholesterol metabolic disorders and congenital cataract ..... 42

1.2.1 Congenital cataract in systemic disorders ..... 42

1.3 The lipidome and proteome of age-related cataract ..... 43

1.3.1 Lens membrane lipids in cataract ..... 44

1.3.2 Lens proteins and cataract ..... 44

1.3.3 A role for α-crystallin in the prevention and treatment of cataract ..... 46

1.4 Hypothesis: Connecting α-crystallin to cholesterol ..... 46

2 Chapter 2: Aims and Objectives ..... 48

2.1 Aim 1: Characterise the effect of impaired cholesterol synthesis on the developing zebrafish ..... 48

2.2 Aim 2: Investigate the efficacy of sterol supplements as rescue treatments in cholesterol synthesis-impaired zebrafish ..... 48

2.3 Aim 3: Investigate the absorption, trafficking, and metabolism of supplemented sterols in the developing zebrafish ..... 48

2.4 Aim 4: Identify relationships between lipid classes and proteins in lens lysates and lens membranes ..... 49

2.5 Aim 5. Examine the effect of exogenous sterols on the distribution of major lens proteins ..... 49

2.6 Aim 6: Analyse the influence of lanosterol and cholesterol on the aggregation of lens membranes ..... 49

3 Chapter 3: Materials and Methods ..... 50

3.1 Isolation of integral membrane proteins from bovine lenses ..... 50

3.1.1 Bovine lens isolation and dissection ..... 50

3.1.2 Isolation of high protein content lens membranes ..... 50

3.1.3 Isolation of integral membrane proteins ..... 50
3.2 Protein solubility assays ..... 51
3.2.1 High protein content lens membranes ..... 51
3.2.2 Low protein content lens membranes ..... 52
3.3 Growth of zebrafish larvae ..... 52
3.3.1 Growth of zebrafish embryos to 5 days post fertilisation ..... 52
3.3.2 Euthanasia of zebrafish larvae ..... 52
3.4 Pharmacological treatment of zebrafish larvae ..... 53
3.4.1 LXR agonist treatment ..... 53
3.4.2 Cholesterol inhibitor treatment ..... 53
3.4.3 Sterol supplementation ..... 53
3.4.4 Deuterium-tagged sterol supplementation ..... 53
3.4.5 Fluorescent cholesterol tracking ..... 54
3.5 Analysis of lipid content ..... 54
3.5.1 Isolation of lipids from zebrafish larvae ..... 54
3.5.2 Isolation of lipids from bovine lens membranes ..... 54
3.5.3 Liquid chromatography – mass spectrometry ..... 55
3.6 Preparation of protein samples for polyacrylamide gel electrophoresis (PAGE) ..... 55
3.6.1 Sample preparation for sodium dodecyl sulphate (SDS)-PAGE ..... 55
3.6.2 Sample preparation for clear native (CN)-PAGE ..... 55
3.7 Protein quantification assays ..... 55
3.7.1 SDS-PAGE and CN-PAGE ..... 55
3.7.2 Western blot ..... 56
3.8 Data capture of zebrafish physical and behavioural phenotypes ..... 57
3.8.1 Behavioural phenotype capture ..... 57
3.8.2 Physical phenotype capture ..... 57
3.9 Statistical analyses ..... 57
3.9.1 Kaplan-Meier survival curves ..... 57
3.9.2 Behavioural phenotype analysis ..... 58
3.9.3 Physical phenotype analysis ..... 58
3.9.4 LCMS analysis ..... 58
3.9.5 Protein quantification assays ..... 58
3.10 List of reagents ..... 58
3.10.1 Zebrafish procedures ..... 58

4 Chapter 4: Alterations of cholesterol metabolism produce behavioural and physical phenotypes in zebrafish larvae ..... 64
4.1 Lipid metabolism in the zebrafish ..... 64
4.1.1 The cholesterol synthesis pathway ..... 64
4.1.2 Cholesterol metabolism ..... 65
4.1.3 Sterol metabolism in the developing zebrafish ..... 66
4.2 Experimental design and objectives ..... 67
4.3 Pharmacological inhibition of cholesterol synthesis produces physical and behavioural phenotypes in viable zebrafish larvae ..... 68
4.3.1 LXR agonists and cholesterol synthesis inhibitors have varied effects and lethal concentrations ..... 68
4.3.2 Partial inhibition of cholesterol synthesis reduces zebrafish independent motion and optomotor responses ..... 69
4.3.3 Pharmacological alteration of cholesterol synthesis in zebrafish larvae results in increased lethality at 5 days post fertilisation ..... 72
4.3.4 Pharmacological inhibitors of cholesterol synthesis reduce larval body size and yolk size 76
4.3.5 Some pharmacological cholesterol synthesis inhibitors reduce eye size in zebrafish larvae, but do not alter eye aspect ratio ..... 80
4.4 Sterol supplementation has a variable effect on phenotype recovery of cholesterol synthesis-inhibited zebrafish larvae ..... 83
4.4.1 Lanosterol and cholesterol supplementation of inhibitor-treated zebrafish is viable in both a concentration-dependent and a treatment-dependent manner ..... 84
4.4.2 Lanosterol supplementation successfully rescues yolk size, but not body and eye size in RO48-8071 treated zebrafish ..... 87
4.4.3 Cholesterol supplementation rescues body and yolk size and increases eye size in AY994 treated zebrafish ..... 90
4.5 The inhibition cholesterol synthesis impacts lens shape in zebrafish larvae ..... 92
4.5.1 The inhibition of LSS alters larval lens aspect ratio but does not cause microphakia ..... 92
4.5.2 The inhibition of cholesterol synthesis results in decreased LEC height ..... 94
4.6 Tracking of sterols in zebrafish larvae ..... 95
4.6.1 Pharmacological synthesis inhibitors reduce total cholesterol levels in treated zebrafish and lead to the accumulation of upstream metabolites ..... 95
4.6.2 Lanosterol and cholesterol supplementation partially recover total cholesterol levels in whole bodies and lenses ..... 99
4.6.3 Fluorophore-conjugated cholesterol does not penetrate the lens ..... 100
4.6.4 Supplemented sterols are retained and metabolised in zebrafish larvae ..... 103
4.7 General summary ..... 106

5 Chapter 5: The effect of cholesterol and lanosterol supplementation on lens fibre cell proteins and lipids....108
5.1 Protein-lipid relationships in lens membranes....108
5.2 Bovine lens membrane proteins have distinct sedimentation profiles....109
5.2.1 Transmembrane bovine lens proteins sediment in cholesterol-rich fractions .111
5.2.2 Cytoskeletal filaments have variable sedimentation profiles in bovine lens membranes....114
5.2.3 αB crystallin is present in all fractions, while γC-crystallin is enriched in nucleus-derived membranes....117
....118
5.3 High-protein content membranes contain a variably soluble protein fraction....119
5.3.1 Aquaporin 0 is present in soluble and insoluble membrane fractions, in contrast with insoluble connexin 50....122
5.3.2 The filaments vimentin and BFSP1 are found in insoluble and soluble lens fractions 124
5.3.3 αB-crystallin is enriched in soluble membrane fractions in a temporal, sterol supplementation-independent manner....127
5.4 Co-incubation with lanosterol or cholesterol does not alter the solubility of endogenous cholesterol in bovine lens membranes....129
5.5 Co-incubation with lanosterol or cholesterol does not alter the solubility of endogenous lanosterol in bovine lens membranes....131
5.6 General summary....133
6 Chapter 6: The sedimentation of lens proteins is influenced by α-crystallin....135
6.1 The solubility status of α-crystallin....135
6.1.1 Age-dependent changes in α-crystallin of mammalian lenses....135
6.1.2 The aggregation of α-crystallin in cataract....135
6.2 The solubility of high protein content membranes fractions can be altered....136
6.2.1 High protein content membranes from cataractous lenses do not contain a temporally soluble fraction....136
6.2.2 The release of soluble material from high protein content lens membranes is time and temperature dependent....137
6.2.3 Cysteine and serine protease inhibitors prevent the release of soluble protein from high content membranes....139
6.2.4 The cysteine protease inhibitor E-64 prevents the release of soluble material more efficiently than the serine/cysteine/threonine protease inhibitor leupeptin....141
6.3 The co-incubation of lens fibre cell membranes with whole α-crystallin fractions has variable results....144
6.3.1 The solubility of α-crystallin is fraction and concentration-dependent when co-incubated with integral protein lens membranes....144

6.3.2 The solubility of α-crystallin is fraction and concentration-dependent when co-incubated with high protein content lens membranes treated with cysteine/serine/threonine protease inhibitors ..... 148

6.4 The sensitisation of α-crystallin fractions with sterols influence the interactions with high protein content lens membranes ..... 155

6.4.1 Cholesterol sensitisation increases the efficacy of native soluble α-crystallin in aiding the solubilisation of high protein content membranes ..... 155

6.4.2 25-hydroxycholesterol sensitisation increases the amount of total soluble protein but does not restore the temporal solubilisation seen in control membrane samples 157

6.4.3 Lanosterol sensitisation increases the amount of total soluble protein and partially restores the temporal solubilisation in E-64-incubated membranes ..... 159

6.5 General summary ..... 162

7 Chapter 7: Discussion and general findings ..... 163

7.1 The effect of cholesterol metabolism alteration in the developing zebrafish ..... 163

7.1.1 The partial inhibition of cholesterol synthesis decreases larval independent movement and affects the optomotor response ..... 163

7.1.2 The pharmacological inhibition of cholesterol synthesis proportionately reduces larval size but accelerates yolk consumption ..... 164

7.1.3 The pharmacological inhibition of cholesterol synthesis has a limited impact on the gross morphology of zebrafish eyes ..... 165

7.1.4 Lanosterol supplementation rescues the synthesis inhibition-associated reduction in yolk size, but cholesterol supplementation is lethal for all inhibitors apart from AY9944 ..... 165

7.1.5 The inhibition of cholesterol synthesis has a limited effect on lens development and structure ..... 167

7.1.6 The pharmacological inhibition of cholesterol synthesis reduces total cholesterol in zebrafish and results in the accumulation of relevant upstream metabolites ..... 168

7.1.7 Lanosterol and cholesterol supplementation recover total cholesterol levels in synthesis-inhibited larvae ..... 169

7.1.8 The incorporation of supplemental lanosterol and cholesterol in the developing zebrafish is variable and subject to downstream metabolism ..... 169

7.1.9 General conclusion and future work ..... 170

7.2 The sedimentation of lens material is dependent on the protein and lipid content of lens fractions ..... 172

7.2.1 The protein content of isolated lens membranes influences its sedimentation pattern 172

7.2.2 Lens proteins are associated with distinct lipid fractions ..... 173

7.2.3 A cortex-enriched specific lens protein fraction transiently sediments and is partially influenced by lanosterol or cholesterol co-incubation ..... 174

7.2.4 Lanosterol or cholesterol supplementation do not alter the sedimentation profile of endogenous lens sterols ..... 175

7.3 The solubility of α-crystallin influences the sedimentation of lens material ..... 176

7.3.1 The temporal release of a soluble protein fraction from high protein content lens membranes is temperature-dependent, and is absent in cataractous lenses ..... 176

7.3.2 The temporal release of a soluble protein fraction for high protein content lens membranes can be inhibited via the use of protease inhibitors ..... 177

7.3.3 Lenticular α-crystallin solutions have a variable effect on the sedimentation of integral membrane protein membrane samples ..... 179

7.3.4 Lenticular α-crystallin solutions influence the sedimentation of high protein content membranes treated with protease inhibitors and partially restore the temporal release of material from leupeptin and E-64-treated high protein content membranes. 180

7.3.5 Sterol and oxysterol sensitisation of α-crystallin solutions has a variable effect on the sedimentation profile of high protein content membranes treated with leupeptin and E-64 181

7.3.6 General conclusions and future work ..... 182

8 Chapter 8: Conclusion ..... 184

References ..... 187

Appendix 1: The synthesis of cholesterol ..... 214

# List of tables

Table 3.1. Buffers and reagents used in zebrafish larvae growth, maintenance, and euthanasia. ..... 58
Table 3.2. Buffers used in fractionation of high protein content and low protein content integral lens membranes ..... 59
Table 3.3. Reagents used in SDS-PAGE and CN-PAGE ..... 59
Table 3.4. Reagents used in semi-dry Western blot transfer and membrane visualisation ..... 60
Table 3.5. Primary and secondary antibodies used in western blot ..... 61
Table 3.6. Pharmacological inhibitors used in zebrafish cholesterol metabolism studies, lipids and lipid standards used in mass spectrometry and zebrafish metabolism studies, chemicals used in protein solubility studies ..... 62
Table 4.1. Summary of cholesterol synthesis inhibitors and their effects.. ..... 69

# List of Figures

Figure 1.1 The structure of the lens.. ..... 24
Figure 1.2. The FGF gradient maintains the cell cycle profile of LECs.. ..... 28
Figure 1.3 The crystallin composition of the lens. ..... 33
Figure 1.4. The major structural lens proteins, their distribution in the lens and core functions ..... 37
Figure 1.5. Cataractogenic load is a multifactorial path to the development of cataract ..... 47
Figure 4.1.The major steps in the cholesterol synthesis pathway ..... 64
Figure 4.2. Independent motion was measured in treated wildtype zebrafish larvae ..... 70
Figure 4.3.Zebrafish larvae were exposed to three different stimuli to assess their startle response ..... 71
Figure 4.4. LXR agonists were tested against three concentration to assess toxicity. ..... 73
Figure 4.5. Pharmacological cholesterol synthesis inhibitors were tested against increasing concentrations to assess toxicity. ..... 75
Figure 4.6. Zebrafish treated at 24 hours post fertilisation. ..... 77
Figure 4.7. Zebrafish treated at 24 hours post fertilisation. ..... 78
Figure 4.8. Treated zebrafish yolk sac size was expressed as a percentage of body size. ..... 79
Figure 4.9. Zebrafish treated at 24 hours post fertilisation ..... 80
Figure 4.10. Zebrafish treated at 24 hours ..... 82
Figure 4.11. Treated zebrafish eye size was expressed as a percentage of body size to account for relative changes. ..... 83
Figure 4.12. The sterol lipids lanosterol and cholesterol were tested against increasing concentrations to assess toxicity. ..... 84
Figure 4.13. Survival rates of cholesterol inhibitor-treated zebrafish which were supplemented with 20µM lanosterol or cholesterol.. ..... 86
Figure 4.14. Lanosterol supplementation successfully restores yolk size to control levels.. ..... 88
Figure 4.15. Lanosterol supplementation rescues proportionate yolk size and has no effect on relative eye size in zebrafish larvae.. ..... 89
Figure 4.16. Cholesterol supplementation at 48 hpf rescued body and yolk size in AY9944 treated zebrafish and increases eye size. ..... 91
Figure 4.17. Relative eye size is increased in AY9944-treated zebrafish supplemented with cholesterol ..... 92

Figure 4.18. Inhibition of LSS alters zebrafish lens aspect ratio. .....93
Figure 4.19. The inhibition of cholesterol synthesis decreases zebrafish LEC height.. .....94
Figure 4.20. Inhibition of cholesterol synthesis with all tested reagents reduces the total cholesterol in zebrafish larvae. .....96
Figure 4.21. Total cholesterol reduction following inhibitor treatment is apparent in whole body and lens tissue samples, while oxidosqualene accumulates in bodies and lenses of RO48-8071-treated zebrafish.....97
Figure 4.22. 7-dehycrocholesterol accumulates in bodies and lenses of AY9944-treated zebrafish, while U-18666A treatment leads to the accumulation of desmosterol in bodies but not lenses.....99
Figure 4.23. Lanosterol and cholesterol supplementation at 48 hpf partially restore total cholesterol levels in bodies and lenses of inhibitor-treated zebrafish. .....100
Figure 4.24. TopFluor Bodipy cholesterol 488 penetrates the yolk and sclera of developing zebrafish.....101
Figure 4.25. TopFluor Bodipy cholesterol 488 penetrates the yolk and sclera of developing zebrafish.....102
Figure 4.26. TopFluor Bodipy cholesterol is detected at 20 hpf in the yolk of larvae supplemented at 6 hpf but is absent at 30 hpf.. .....103
Figure 4.27. D6 cholesterol incorporation was detected in the lens at 20 hpf following d6 cholesterol supplementation, while d6 lanosterol was detected in the yolk at 20 hpf following d6 lanosterol supplementation in zebrafish larvae. .....104
Figure 4.28. Increased d6 cholesterol incorporation was detected in lenses of d6 cholesterol supplemented zebrafish at 30 hpf, while increased d6 lanosterol was detected in both lenses and yolk of d6 lanosterol supplemented larvae. .....105
Figure 4.29.D3 27-hydroxycholesterol was detected as the major metabolite in yolks from d6 cholesterol and d6 lanosterol supplemented zebrafish.. .....106
Figure 5.1. . Protein profile of bovine lens cortex membranes prior to and following fractionation in an 8M urea buffer.....109
Figure 5.2. Protein profile of bovine lens nucleus membranes prior to and following fractionation in an 8M urea buffer.....110
Figure 5.3. Sequential centrifugation of high protein content bovine lens membranes yields different sedimentation profiles for cortex-derived and nucleus-derived protein. .....110
Figure 5.4. The enrichment of cholesterol in pelletable cortex and nucleus membranes is substantially increased as compared to the enrichment of phosphatidylcholine. .....112
Figure 5.5. The major membrane-associated proteins AQP0, CAV-1, and CX50 are enriched in insoluble cortical lens membranes.....113
Figure 5.6. The cytoskeleton proteins vimentin and actin were detected in cortical lens membranes. .....115
Figure 5.7. The beaded filament proteins BFSP1 and BFSP2 show different sedimentation profiles for their distinct isoforms in cortical and nuclear lens membranes. .....116
Figure 5.8. Low molecular weight αB-crystallin is enriched ubiquitously in cortex and nucleus-derived lens membranes, while γC-crystallin is enriched in nucleus fractions. .....118
Figure 5.9. High protein content lens membrane fractions release soluble protein material in a temporal manner. .....120

Figure 5.10. High protein content lens membrane fractions release soluble protein material in a temporal manner following co-incubation with 10 µM lanosterol at 37$^{O}$C in light-safe conditions..... 121
Figure 5.11. High protein content lens membrane fractions release soluble protein material in a temporal manner following co-incubation with 10 µM cholesterol at 37$^{O}$C in light-safe conditions..... 122
Figure 5.12. The time-dependent solubilisation of high molecular weight AQP0 is inhibited by lanosterol co-incubation in lens cortex membranes. ..... 123
Figure 5.13. Neither lanosterol nor cholesterol co-incubation influence the sedimentation of Cx50 in lens cortex membranes. ..... 124
Figure 5.14. Vimentin is subject to a time-dependent, increasing solubilisation in cortex-derived lens membranes. ..... 125
Figure 5.15. Lanosterol co-incubation suppresses the solubilisation of the ~50 kDa minor band, while neither lanosterol nor cholesterol co-incubation have any effect on the major 60 kDa band.. ..... 126
Figure 5.16. BFSP1 is subject to a time-dependent, increasing solubilisation in cortex-derived lens membranes.. ..... 127
Figure 5.17. The time-dependent solubilisation of αB-crystallin in cortex-derived lens membranes. ..... 128
Figure 5.18. Co-incubation of cortex lens membranes with 10 µM lanosterol or 10 µM cholesterol has no effect on the time-dependent solubilisation of αB-crystallin. ..... 129
Figure 5.19. The co-incubation of high-protein content lens membranes with lanosterol or cholesterol has no effect on the endogenous total cholesterol content of insoluble and soluble membrane fractions. ..... 130
Figure 5.20. Deuterated cholesterol was detected in all cortex and nucleus-derived insoluble fractions co-incubated with d6 cholesterol. ..... 131
Figure 5.21. No significant fluctuation in endogenous lanosterol levels was recorded for cortex and nucleus membranes co-incubated with cholesterol or lanosterol.. ..... 132
Figure 5.22. Deuterated lanosterol was not detected in any soluble membrane fraction. ..... 133
Figure 6.1. High protein content membranes from lenses with nuclear cataract do not show the time-dependent release of soluble material seen in age-matched clear lenses. ..... 137
Figure 6.2. The temporal release of soluble material in cortical and nuclear membrane samples is temperature dependent. ..... 138
Figure 6.3. The incubation of high protein content membranes in a commercial serine/cysteine protease inhibitor complex greatly reduces the amount of temporally soluble protein in cortex and nucleus-derived membranes. ..... 140
Figure 6.4. Iodoacetamide reduces the total amount of temporally soluble protein in nuclear membranes, but not in cortical membranes. ..... 141
Figure 6.5. E-64 inhibits the temporal release of soluble protein from cortical high protein content membranes more efficiently than leupeptin. ..... 142
Figure 6.6. Leupeptin and E-64 successfully reduce the amount of temporally soluble protein released from nuclear high protein content membranes isolated from clear lenses. ..... 143
Figure 6.7. Native soluble α-crystallin, but not commercial α-crystallin results in a modest release of soluble protein for integral protein membranes. ..... 145
Figure 6.8. Native soluble α-crystallin, but not commercial α-crystallin results in an increased release of soluble protein for integral protein membranes. ..... 146

Figure 6.9. Native soluble α-crystallin produces an initial inversion of the insoluble to soluble protein ratio of integral membrane proteins but is followed by a temporal increase in insoluble material. ..... 147
Figure 6.10. All α-crystallin fractions produce a static release of a soluble protein fraction from integral protein lens membranes at 120 $\mu gmL^{-1}$.. ..... 148
Figure 6.11. Commercial a-crystallin at 15 $\mu gmL^{-1}$ has no effect on the solubility of high protein content membranes treated with an inhibitor protease complex. ..... 149
Figure 6.12. Commercial a-crystallin at 30 $\mu gmL^{-1}$ has no effect on the solubility of high protein content membranes treated with an inhibitor protease complex. ..... 150
Figure 6.13. Commercial a-crystallin at 60 $\mu gmL^{-1}$ showed a transition of all protein to the insoluble fraction, except for a minimal amount of transiently soluble protein at 24 hours. ..151
Figure 6.14. All α-crystallin samples produce a relatively static amount of soluble protein, with an excess of insoluble protein at all tested timepoints. ..... 152
Figure 6.15. Commercial and SEC-isolated α-crystallin partially restore the temporal solubilisation seen in high protein content membranes extracted from clear lenses. ..... 153
Figure 6.16. All α-crystallin fractions partially restore the temporal increase in released soluble material in membranes pre-treated with E-64 ..... 154
Figure 6.17. Sensitisation of α-crystallin with cholesterol increases the concentration of soluble protein in cortical high protein content membranes incubated with a commercial protease inhibitor complex. ..... 156
Figure 6.18. Sensitisation of α-crystallin with cholesterol increases the concentration of soluble protein in cortical high protein content membranes incubated with the cysteine peptidase inhibitor E-64. ..... 157
Figure 6.19. Sensitisation of α-crystallin with 25-hydroxycholesterol increases the concentration of soluble protein in cortical high protein content membranes incubated with a commercial protease inhibitor complex. ..... 158
Figure 6.20. Sensitisation of α-crystallin with 25-hydroxycholesterol increases the concentration of soluble protein in cortical high protein content membranes incubated with the cysteine peptidase inhibitor E-64. ..... 159
Figure 6.21. Sensitisation of α-crystallin with lanosterol increases the concentration of soluble protein in cortical high protein content membranes incubated with a commercial protease inhibitor complex.. ..... 160
Figure 6.22. Sensitisation of α-crystallin with lanosterol increases the concentration of soluble protein in cortical high protein content membranes incubated with the cysteine peptidase inhibitor E-64. ..... 161
Figure 8.1. The recovery of α-crystallin chaperone function is essential in the reversal of lens lysate sedimentation…… 185

# List of abbreviations

25-OHC 25-hydroxycholesterol

27-OHC 27-hydroxycholesterol

ACAT2 Acetyl-CoA acetyltransferase

ANOVA Analysis of variance

AQP0 Aquaporin 0

AQP1 Aquaporin 1

AQP5 Aquaporin 5

ARNC Age-related nuclear cataract

ATP Adenosine triphosphate

BFSP1 Beaded filament protein 1

BFSP2 Beaded filament protein 2

BMP Bone morphogenic protein

CAV-1 Caveolin-1

CDCA chenodeoxycholic acid

CLSM Confocal Scanning Laser Microscopy

CN-PAGE Clear native polyacrylamide gel electrophoresis

CoA Coenzyme A

CTX Cerebrotendinous Xanthomatosis

Cx43 Connexin 43

Cx46 Connexin 46

Cx50 Connexin 50

CYP27A1 Cytochrome p27a1

DCM Dichloromethane

DHCR24 24-dehydrocholesterol reductase

DHCR7 7-dehydrocholesterol reductase

di$H_2O$ Deionised water

DMSO Dimethyl sulfoxide

DNase IIβ Deoxyribonuclease II-beta

DPF Days post fertilisation

DRM Detergent-resistant membranes

DSM Detergent-soluble membranes

ER Endoplasmic reticulum

EtOH Ethanol

FA Formic acid

FDFT Farnesyl diphosphate farnesyltransferase 1

FDPS Farnesyl diphosphate synthase

FGF Fibroblast growth factor

FPP Farnesyl pyrophosphate

GPP Geranyl pyrophosphate

HH Hedgehog

HMG-CoA 3-hydroxy-3-methylglutaryl-conezyme A

HMGS1 HMG-CoA synthase 1

HPF Hours post fertilisation

HRP Horse radish peroxidase

HSD Honestly significant difference

HSPB4 Heat shock protein 4

HSPB5 Heat shock protein 5

IC Inner cortex

IDA Iminodiacetic acid

IN Inner nucleus

IPP Isopentenyl pyrophosphate

LCMS Liquid Chromatography Mass Spectrometry

LEC Lens Epithelial Cell

LFC Lens Fibre Cell

LSS Lanosterol synthase

LXR Liver X receptor

MeOH Methanol

MVD Diphosphomevalonate decarboxylase

MVK Mevalonate kinase

OC Outer cortex

OFZ Organelle-free zone

ON Outer nucleus

PBS Phosphate buffered saline

PKC Protein Kinase C

PMVK Phosphomevalonate kinase

PSC Posterior subcapsular cataract

RCF Relative centrifugal force

RPM rotations per minute

SAB Sequestered actin bundle

SDS Sodium dodecyl sulphate

SDS-PAGE Sodium dodecyl sulphate polyacrylamide gel electrophoresis

SEC Size exclusion chromatography

SHH Sonic Hedgehog

sHSP Small heat shock protein

SLOS Smith-Lemli-Opitz Syndrome

SQLE Squalene epoxidase

SREBP Sterol regulatory element binding protein

TBS Tris buffer saline

TBST Tris buffered saline Tween

TDCA tauroursodeoxycholic acid

UDCA ursodeoxycholic acid

# Declaration and Statement of Copyright

The content of this thesis has been composed by Alexia A. Kalligeraki for the degree of Doctor of Philosophy at Durham University, and has not been submitted in whole or in part for any other qualification. Except where stated otherwise by reference or acknowledgement, the work presented has been conducted in its entirety by the author.

All previously published work has been appended.

# Acknowledgements

This thesis is a syncytium of the care and affection of all the people who brought me here.

For Mum and Dad, who have always let me do what I want.

For Granny Jean, who has always been a role model and an unwavering source of support.

For Ben, who listens but most importantly tells me I am wrong when others refuse to.

For Miguel, who taught me all the practical lab skills I know and who lost too much time listening to me in the lab.

For Alice, whose infectious optimism kept Miguel sane.

For Ian, whose patience and support are the only reason Chapter 4 exists. He is and will be sorely missed.

For all the RAQ lab members and PhD researchers in ACaS, who have made this experience a constant celebration.

For all the friends and collaborators I've had the opportunity to meet through the project, whose love for the work constantly sustains my enthusiasm.

And finally, but most importantly, for Roy, whose refusal to walk the trodden path has taught me more about the scientific endeavour than anyone else.

# 1 Chapter 1: Introduction

## 1.1 The physiology of the lens

The lens is an avascular, non-innervated tissue which lies in the anterior portion of the eye; its function is to refract light onto the retina in conjunction with the cornea. To accurately perform its refractive role, lifelong lens transparency and an appropriate gradient refractive index is required to be maintained in the face of age-related deleterious insults. The lens achieves this by a combination of a unique lipidome and proteome which develop and support the structure-function of the tissue.

The lens is comprised of an encapsulated population of two cell types: lens epithelial cells (LECs) form a cuboidal monolayer covering the anterior portion of the tissue, while the bulk is formed by organelle-free lens fibre cells (LFCs) as seen in figure 1.1. Mammalian LECs are organised into three distinct groups: the central zone consists of quiescent cells in the anterior region of the lens. The germinative zone consists of a high density, near-equatorial region of cells where proliferation takes place. Finally, cells from the germinative zone align to form the meridional rows which house the precursors of all fibre cells. Epithelial cells from the meridional rows undergo an elongation and organelle-shedding process during the differentiation into mature LFCs (1).

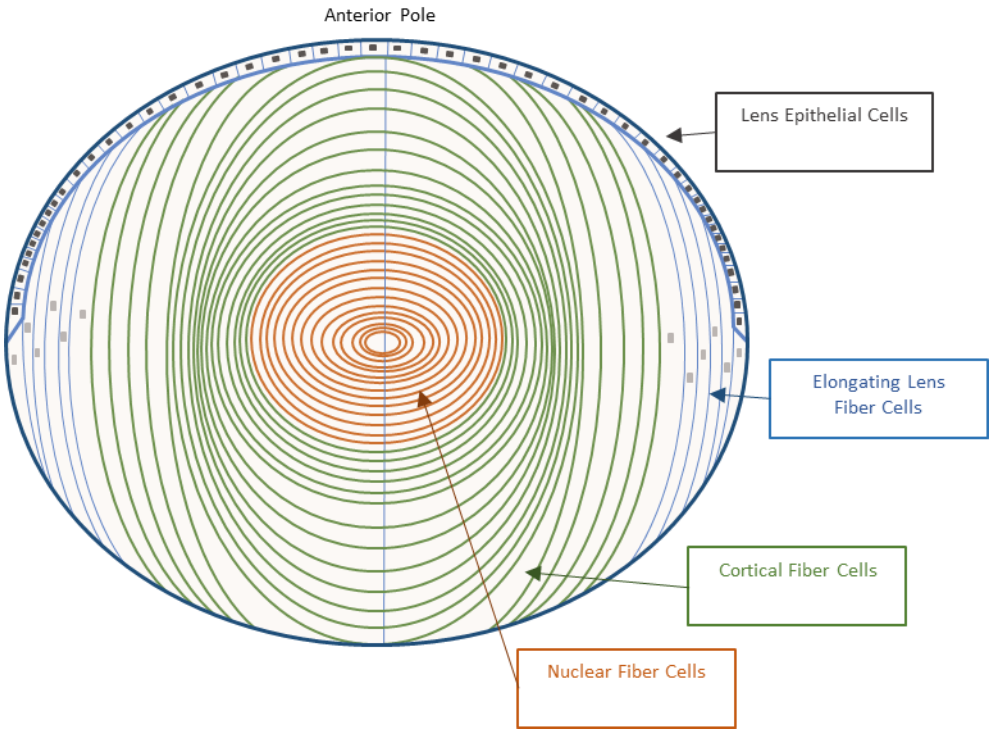


Figure 1.1 The structure of the lens. A cuboidal epithelial monolayer covers the anterior portion of the tissue, with a dense proliferative zone located around the equator. Differentiating lens

fibre cells elongate and migrate towards the interior of the lens, where LFC maturation occurs. Adapted with permission from Kalligeraki et al, 2020 (2).

### 1.1.1 Lens structure and development

#### *1.1.1.1 Embryonic lens development*

Lens morphogenesis is initiated through the formation of the lens placodes on the head surface ectoderm and is followed by an invagination of these cells to produce the presumptive lens vesicle. From this, cells in the anterior portion of the lens vesicle give rise to the lens epithelium, while cells in the posterior undergo an elongation and differentiation event to form the primary lens fibre cells. The proliferation and differentiation of LECs at the equator goes on to generate secondary fibre cells, which surround the embryonic lens nucleus and add to the continual growth of the lens throughout life.

From a developmental perspective, the formation of the presumptive lens placode is *Pax6/Six-3/Sox-2* induction-dependent (3,4) in conjunction with the inhibition of *Wnt* signalling in the presumptive lens ectoderm, endogenous and exogenous fibroblast growth factor (FGF) and bone morphogenic protein (BMP) signalling (5) both from the presumptive lens and its surrounding tissues, and retinoic acid (RA) signalling from the retina (6). Increased cell proliferation and crowding in the les placode forces placode invagination in conjunction with the transient formation of basal filopodia, a collection of F-actin rich cell protrusions in the lens pit that regulate pit curvature by adhering to the basal lamina of the retinal neuroepithelium (7). A gradient of growth factors, including FGF and BMP secreted from the surrounding tissues, regulate the polarity of the developing lens, and maintain it throughout life. Cells in the anterior portion of the lens vesicle adopt an epithelial phenotype, with FGF promoting cell proliferation and BMP promoting cell cycle exit in an-FGF dependent manner (8). Cell in the posterior portion of the lens vesicle undergo primary differentiation and adopt a fibre cell phenotype, which is characterised by an accumulation of crystallin proteins (9), migration and elongation concurrent to cytoskeletal remodelling, and the loss of intracellular organelles (10).

#### *1.1.1.2 Lens growth*

In contrast with the eye as a whole which follows a determinate growth model, reaching maturity and its terminal size at the end of the second decade of life in humans, the lens has been shown to grow continually throughout life (11). Two phases of growth have been identified in vertebrate lenses, monophasic growth where the lens grows at an increased rapid rate during embryonic development and drastically slows down postnatally, and biphasic growth which is characterised by an initial asymptotic growth during embryogenesis and the first postnatal years of life and is followed by a near-linear increase in size thereafter (12–14). The human lens is one of the few lenses which follow a biphasic growth pattern, while most

animal lenses including mouse, rat, and zebrafish are monophasic. Embryonic lenses are largely spherical and fibre cell deposition contributes to uniform growth in mature spherical lenses such as those seen in zebrafish. Transitions from spherical to ellipsoidal shapes which coincide with the establishment of emmetropia have been observed in mammals such as the mouse (2), with the human lens showing a radical development of an ellipsoidal shape due to an increase in equatorial diameter during early childhood(15), which impact the compaction of nuclear fibre cells (15). In adulthood, the equatorial diameter and the sagittal diameter increase linearly at similar rates preserving a relatively stable aspect ratio (14).

LECs are a group of polarised cells with the apical membranes in contact with LFCs and the basolateral membranes in contact with the aqueous humour in the anterior chamber of the eye, and contain bona fide adult progenitor cells which express the pluripotency factor Sox2 (16). These progenitors are the reservoir for all LFCs by ensuring the maintenance of the lens epithelium following the proliferation of LECs and differentiation of prospective LFCs. Whether these progenitors are true adult stem cells remains a matter of debate, as evidence has shown they are exhibit multiple established characteristics of stem cells such as thymidine label retention (17), express stem cell associated markers (16), and express telomerase reverse transcriptase activity (18). Simultaneously, cultured human lens cells lack an extensive proliferative capacity *in vitro* (19) and have no discernible stem cell niche (11), both characteristics associated with pluripotent stem cell populations.

Disruption of the lens epithelium has a direct impact on the deposition of LFCs and thus the structure-function of the tissue (20–22). The formation of cataract due to the loss of organisation and cell programming has been studied with particular interest in the development of post-surgical posterior subcapsular cataract (PSC) (23), but the retention of long-term damage in LECs which then successfully undergo differentiation and how these contribute to the instability of fibre cell organisation is still a topic to be explored.

Secondary LFC differentiation is driven by the same FGF/BMP/Wnt pathway utilised in embryogenesis, with FGF2 concentrations of 3 $ngmL^{-1}$ and 40 $ngmL^{-1}$ respectively being capable of inducing cell migration and differentiation in cultured primary LECs (22). The differentiation of cells has been shown to be BMP-dependent (8) as seen in figure 1.2, with the Notch-mediated suppression of BMP signalling leading to the loss of fibre cell-specific protein expression (24) suggesting that Notch signalling could define the border between the germinative zone and the meridional rows by preventing early withdrawal from the cell cycle (25). The expression of crystallin proteins in LFCs is spatiotemporally regulated in the lens (26), and their accumulation leads to the development of the gradient refractive index (9). Cortical

LFCs undergo a dramatic elongation which is mediated by the remodelling of the actin cytoskeleton and the spectrin membrane cytoskeleton (27,28), while formation of the lens-specific beaded filament network of BFSP1 and BFSP2 follows (29). The basal and apical tips of elongating LFCs form sutures at the posterior and anterior pole, with cells adopting a hexagonal cross-section profile, a continuation of cell organisation in the meridional rows, with two broad faces and four narrow faces which facilitate increasingly tight packing and the minimising of extracellular space. As fibre cells progress through their differentiation, interlocking protrusions emerge which connect neighbouring fibres into radial columns in a ball-and-socket fashion (9). The development and maintenance of lens transparency requires the removal of all light-scattering bodies within fibre cells, with LFCs which have successfully shed their organelles forming the organelle-free zone (OFZ) across the optical axis (30). Initiation of mitochondrial degradation in differentiating LFCs precedes denucleation (31), while autophagolysosomes have been detected in developing chick fibres and adult human lens fibres containing multilamellar membranes and mitochondrial fragments, implicating autophagy and mitophagy as essential processes in organelle degradation (32). The major class of cysteine proteases implicated in organelle breakdown has been shown to be calpains, with calpain-cleaved spectrin being detected in LFCs directly adjacent to the OFZ (33). This finding, in combination with the relatively sharp border of the OFZ, suggest that organelle degradation is a highly coordinated rapid process. Denucleation in differentiating fibre cells has been proven particularly challenging to study as it is a rapid process, though reports have indicated that chromatic condensation follows the remodelling and breakdown of the nuclear envelope, with deoxyribonuclease II-beta (DNase IIβ) being responsible for the final degradation of genetic material (34–36). The loss of nuclei and mitochondria in the OFZ result in the absence of protein synthesis and the exclusive reliance on glycolysis for all energy needs.

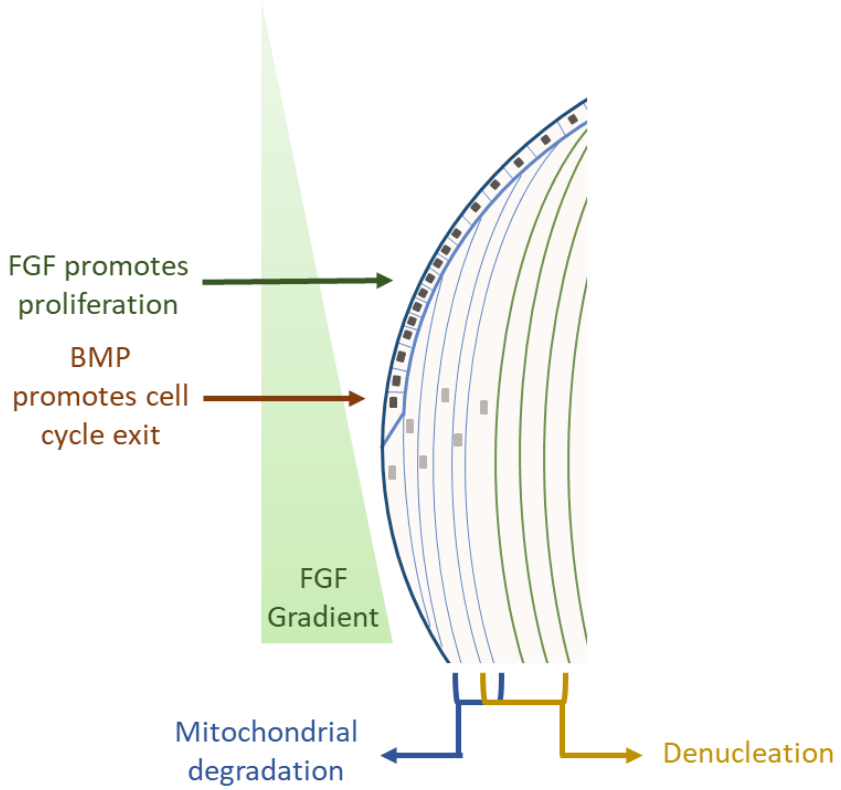


Figure 1.2. The FGF gradient maintains the cell cycle profile of LECs. An increasing concentration of FGF promotes cell proliferation, while the synergistic effect of BMP promotes cell cycle exit and the initiation of LFC differentiation. Mitochondrial degradation and denucleation occur prior to the remodelling zone in the lens cortex, after which organelle-free LFCs complete their maturation process.

The lifelong retention of macromolecules in the differentiating LFCs creates and environment where cells are susceptible to the accumulation of deleterious, light scattering aggregates consisting of damaged proteins and lipids. The high concentration of crystallins, often exceeding 450 $mgmL^{-1}$ (9) in the lens core, accounts for this problem via the chaperone action of α-crystallin (37). Further, this high protein concentration ensures that α-, β- and γ-crystallins repel each other in solution and form short-range, liquid like order without periodicity (38–40) which contributes to the gradient refractive index of the lens. In addition, the enrichment of nuclear fibre cell membranes in cholesterol and sphingomyelins at the expense of phospholipids alters the refractive index of plasma membranes to be closer to the cytoplasmic index, reducing light scatter and increasing transparency (21,41–43).

### 1.1.2 Lens ageing and cataract

The continued growth of the lens in conjunction with the incredibly limited turnover of macromolecules in mature LFCs (44–47) creates a system where the age-related accumulation of damage is inevitable. The hypothesis that ocular lenses can tolerate a certain amount of

age-related damage prior to the formation of cataract is termed cataractogenic load, and has been discussed extensively by Uwineza et al (48) in the context of radiation-induced damage.

The natural ageing process of the lens involves changes to the lipidome and the proteome of cells which increase the rigidity of the tissue, the distribution of proteins between the water soluble and water insoluble fractions, the enrichment of material in the lens nucleus, and the decreased diffusion of antioxidants such as glutathione.

The lens epithelium is subject to the standard ageing processes seen in other nucleated, metabolically active cells including an accumulation of DNA damage (13), a reduction in the expression of DNA repair genes (49,50), and telomere shortening (51,52). These are coupled with changes in the gross morphology and cell distribution of the epithelium, where an age-related decay in LEC density is seen in the central zone in addition to increased disorganisation of the meridional rows (53). As new fibre cells are continuously added throughout the lifespan of the organism, it is possible to appreciate the impact of aged LECs on the physiological LFCs differentiation process.

The constant deposition of new LFCs, in combination with the retention of all fibre cells and their compaction in the nucleus (9,11,54) produces an environment where damaged cells are most likely retained (55,56). LFCs regulate the ageing process via the reduction of oxidative stress as a damage prevention measure, and by the chaperone function of α-crystallin as a damage control measure. Fibre cells boast a selection of antioxidant enzymes including glutathione, catalase, superoxide dismutase, and peroxiredoxins. The major antioxidant in the lens is the glutathione redox cycle, where reduced glutathione is synthesised in the epithelium and the cortical fibre cells and diffuses through the nucleus via gap junctions. With age, an impermeable glutathione barrier develops and glutathione diffusion halts after the fourth decade of life in humans (57) leaving the nuclear core of the lens susceptible to oxidative damage.

Cataract is a disease where a progressive opacification of the lens leads to decreased visual acuity and eventual blindness. Age-related, congenital, and injury related cataracts (58–60) have all been documented as multifactorial processes with a vibrant selection of phenotypes including differences in the location and colour of related opacities (61–64).

Congenital cataracts have an average incidence rate of 72 in 100,000 births, with a higher prevalence in regions with an increased risk of environmental damage and disease during gestation (65). Though the majority of congenital cataracts are spontaneous, inherited forms account for between 8% and 25% of cases (66,67) and are mostly well characterised either as

part of systemic disorders or as Mendelian traits. Further discussion on congenital cataracts can be found in section 1.2.

Age-related cataracts can be summarised as the collective output of genetic predisposition, environmental insults, and dietary intake in the broader context of lifestyle (68–70). Cumulative macromolecule damage in lens proteins and lens lipids as a function of ageing results in increased lens permeability and susceptibility to oxidative damage, which in turn accelerates the damage inflicted on aged peptides. Further discussion on the lipidome and proteome of cataract, and the mechanisms underpinning the development of light-scattering aggregates, can be found in section 1.3.

### 1.1.3 Lens fibre cell membranes

The fundamental roles of LFC membranes can be summarised in three points: to match the refractive index of the cytoplasm and decrease light scatter, to house essential proteins which facilitate the circulation of molecules including antioxidants and ions, and to provide a barrier in order to maintain the hypoxic environment (71) which protects lens macromolecules from oxidative stress throughout the lifespan of the organism. These are achieved by the content of the bilayer, which favours lipids durable to withstand the maximum lifespan of an organism without being subjected to excessive oxidative damage.

#### *1.1.3.1 The lipidome of LFCs confers lifelong stability*

LFC membranes from adult human lenses are highly ordered and rich in saturated phospholipids. The cholesterol content of fibre cell membranes is one of the highest in the body at a ratio of 8:1 compared to phospholipid in its core (72,73), with cholesterol rafts and cholesterol crystalline domains being prevalent throughout (73,74). In addition to the highly saturated lipid content, most LFC membrane lipids are associated with proteins (75,76) further limiting their lateral mobility.

The phospholipid content of LFCs has been shown to be species-specific and directly related to the maximum lifespan of the organism (77). LFC membranes of vertebrates with relatively low lifespans such as rodents contain a higher proportion of unsaturated glycerolipids, including phosphatidylcholine and phosphatidylserine, while membranes of mammals with longer lifespans such as domestic cattle contain higher proportion of saturated sphingolipids. Interestingly, mammals with similar maximum lifespans have been shown to have increased levels of sphingolipids in LFCs membranes if they are endemic to harsh environmental conditions, with camels and polar bears having almost double the sphingolipid content as compared to lifespan-matched vertebrates (77).

The most abundant phospholipid in the human lens is dihydrosphingomyelin, which is also prevalent in other primate lenses at considerable amounts. The relative ratio of sphingomyelins to glycerolipids increases with age and in cataract, with the relative amount of sphingolipid rising from approximately 35% at birth to over 60% of phospholipid content by the eight decade of life, and the relative amount of phosphatidylcholine reducing from 5% to less than 2% in the same timeframe (21,73,78,79). This ratio is further skewed in cataractous lenses in favour of sphingolipids, with the complete loss phosphatidylcholine and dramatic depletion of other glycerolipids due to selective oxidation being contrasted against an enrichment of sphingomyelin in excess of 80% of the total phospholipid content of the lens (21,76,80,81).

The age-related loss of glycerolipids in combination with the increase in sphingolipids and cholesterol enrichment seen in human lenses (21,42) results in the progressive loss of accommodation due to increases stiffness of the lens. These membrane events, in conjunction with the transition of α-crystallin to a majority membrane bound protein by the fifth decade of life manifest as the first universal consequence of lens ageing which is known as presbyopia (82–84). The onset of presbyopia has been considered a major point of intervention in the delay of age-related cataract, due to the shared baseline phenotypes between the two conditions (82,85,86).

#### *1.1.3.2 Major lens proteins*

The proteome of LFCs is essential in conferring lifelong transparency and stability, in addition to developing and supporting the gradient refractive index of the lens which is required for its function (86,87). Multiple studies have characterised the LFC membrane proteome in model organisms including mouse (88), cow (89), and zebrafish (90) in addition to human lenses (91,92).

The most abundant cytoplasmic proteins in LFCs are the crystallins as seen in figure 1.3, which account for up to 90% of the dry weight of the tissue and include α-crystallin, β- and γ-crystallin in mammalian and fish lenses. The conservation of crystallin proteins varies among species, with vertebrates employing a mix of α-, β-, γ-, and δ- crystallins to achieve lens function while non-chordate lenses rely on a radically different protein composition (93). This finding points towards the hypothesis that crystallins have been recruited for a lens-specific role from an ancestral pool of proteins which is further supported by phylogenetic data which show that the βγ domain, a four Greek-key containing domain which is essential in conferring protein stability in β- and γ-crystallins, is encountered in hundreds of proteins with diverse functions from different taxonomic groups (93–96).

Lens α-crystallin refers to a polydisperse mix of αA- and αB-crystallin homo and heterooligomers of varying molecular weights (97–99). The origin of αA-crystallin has been suggested to be a lens-specific ancestral duplication of the αB-crystallin gene CRYAB, since both proteins show a relatively high sequence homology of 57% (100) and the common tissue expression of αB-crystallin is ubiquitous unlike αA-crystallin which is only expressed at low levels outside the lens (101–106). Lenticular α-crystallin functions as a chaperone protein, with both αA- and αB-crystallin also exhibiting chaperone functions in their own right (37,107) and being known as heat shock protein 4 (HSPB4) and heat shock protein 5 (HSPB5) in the mammalian small heat shock protein (sHSP) family (108). The chaperone function of α-crystallin in the lens results in the binding and stabilising of denatured and misfolded proteins such as other crystallins (109,110). This finding is further supported by the age-related increase in high molecular weight α-crystallin aggregates (82,111), which form due to the minimal protein turnover in the lens and the lifelong retention of damaged macromolecules.

Although no clear biological activity has been identified for β- and γ-crystallins in the lens, the current understanding of their role is limited to their contribution to the development of the refractive gradient index (85,86) and the prevention of extensive protein crystallisation and phase separation one would expect at the high concentrations native to LFCs (9,41,112). The abundance of γ- crystallins has been shown to influence the stiffness of lenses, with hard non-accommodating lenses of fish containing a broad range of γM-crystallins (90,95,112). Both β- and γ-crystallins are differentially expressed in mammalian development, with γ-crystallins being prevalent in the embryonic lens nucleus while β-crystallins are found in the cortex and the increasingly in the nucleus (111,113,114).

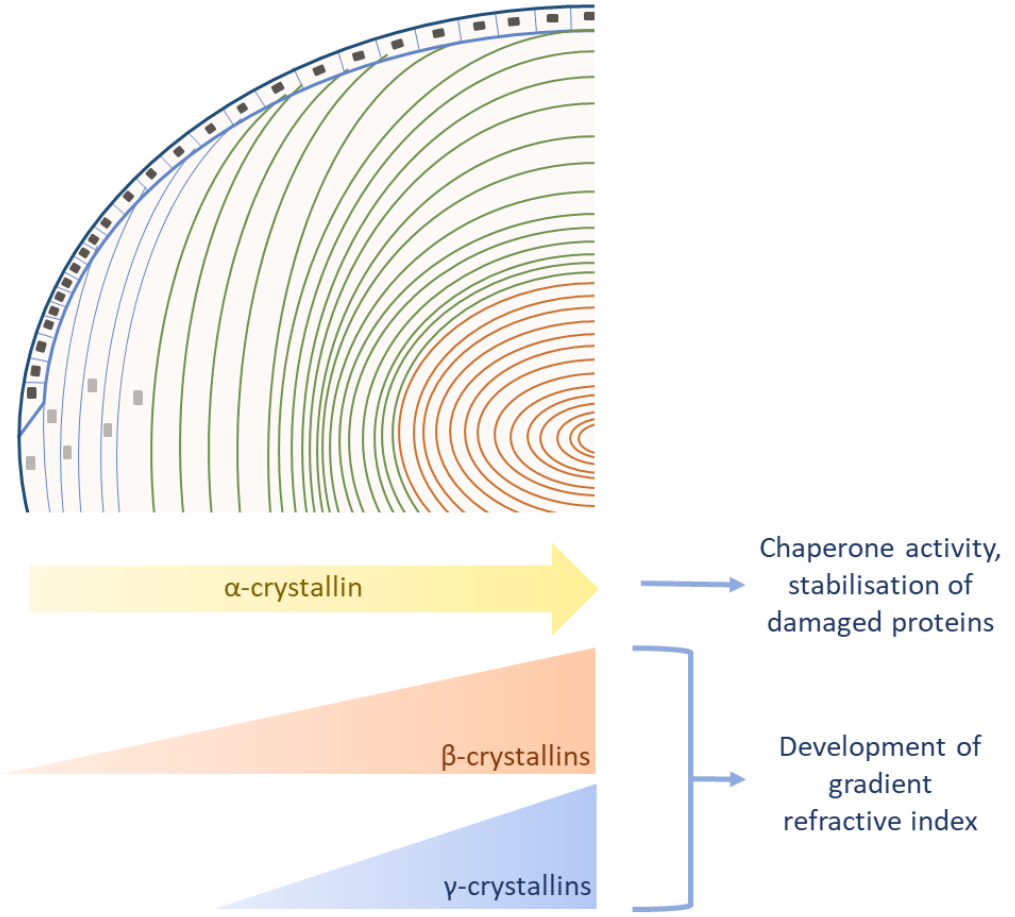


Figure 1.3 The crystallin composition of the lens. A high concentration of α-crystallin acts as a molecular crowder and prevents unwanted protein-protein interactions while also acting as a chaperone protein to prevent the aggregation of damaged macromolecules. Lens β- and γ-crystallins support the development of the gradient refractive index of the lens.

The shape change of differentiating LFCs is supported by cytoskeletal proteins including actin (28), vimentin (91,115,116), and the lens-specific beaded filament proteins BFSP1 and BFSP2 (117–119). Filament assemblies of vimentin and BSFP1/BFSP2 have been identified in the lens (118,120), while evidence suggest a preferential co-assembly with α-crystallin is also present (121,122). Some mutations in the human genes and the equivalent mouse *bfsp1* and *bfsp2* knockouts present with progressive, pre-senile cataract while others lead to altered optical properties of affected lenses (123–127). In a physiological context, a switch from membrane-associated vimentin to beaded filaments has been documented as a major component of fibre cell maturation in the 20-40μm remodelling zone (128) of the lens cortex (91), indicating distinct roles for each filament family in the process of cell differentiation. LFC interdigitations including ball and socket interdigitations have been shown to develop in the remodelling zone (128) while the knockout of *bfsp1* and *bfsp2* has been shown to result in the loss of LFC organisation after this boundary, further supporting the role of beaded filaments in the

physiological maturation of LFCs and the maintenance of membrane stability in nuclear fibres. Interestingly, vimentin filaments have been shown to compensate for the loss of Bfsp2 by associating with the reduced levels of Bfsp1 (123,124). The proteolytic post translational modification of BFSP1 has been shown to produce distinct fragments, with the N-terminal region co-assembling with BFSP2 to form the lens beaded filaments while the C-terminal region localises to the plasma membrane (129,130). C-terminal BFSP1 has been shown to alter the calcium-dependent regulation of AQP0 water permeability (131), while the C-terminal region of AQP0 has also been shown to interact with BFSP1 and BFSP2 (132).

While beaded filaments are integral to the mechanical support of LFCs (29,116,133) and microtubules are involved in fibre elongation (86,134,135), the actin cytoskeleton is involved in the organisation of fibre cell packing and mechanical stiffness of the lens (133,136,137). In the lens epithelium, actin stress fibres and lamellipodia in the basal face aid the adherence of LECs to the lens capsule via focal adhesions and integrin receptors (138,139) and are thought to maintain the quiescent state of central zone cells, while actin stress fibres, polygonal F-actin arrays and sequestered actin bundles (SABs) on the apical face of LECs maintain the cuboidal shape of the cells via contact with LFCs (139–141). The restructuring of basal F-actin in LECs is associated with the migration of cells through the meridional rows (28), with the differentiation of LFCs accompanying an increase in polymerised F-actin at the expense of globular G-actin (142). Basal F-actin bundles, via the action of integrin α5 and fibronectin 1, facilitate the migration of LFCs along the posterior lens capsule (138,143,144). The actin network in cortical fibre cells, in conjunction with the beaded intermediate filaments formed by BFSP1 and BFSP2, have been shown to modulate lens mechanical stiffness via association with the plasma membrane (91,133,137) in addition to facilitating the formation of gap junction plaques (145). In mature LFCs, F-actin and tropomodulin survive proteolytic degradation and remain associated with the cell membrane highlighting a lasting role for the actin cytoskeleton in the maintenance of fibre cell stability (28,136).

Organelle degradation and the subsequent loss of proteostatic machinery in mature LFCs creates the need for a stable circulation system by which ions and macromolecules can be transferred between nuclear and cortical fibres. Two major protein classes, aquaporins and connexins, form water channels and gap junctions in lens fibres and contribute to the adhesion of cells, the circulation of nutrients, and the accommodation function of softer lenses as seen in figure 1.4. The mode of lens circulation in the absence of blood flow has been a controversial subject (146,147), though evidence suggests a unique microcirculation system is generated by the flux of $Na^+$ from the extracellular space at the anterior and posterior poles which flows to the core of the lens and diffuses to the equatorial surface via gap junction

channels (148–151). The flow of water through gap junction channels generates a hydrostatic pressure gradient of 335 mmHg in the lens centre to 0 mmHg in the peripheral cortex, which is preserved across species (150,152) and is essential to maintaining an appropriate ratio of water to protein in different lens compartments for the development and maintenance of the gradient refractive index (153).

The main lens aquaporin is AQP0, while AQP1 and AQP5 are also expressed in LECs and LFCs (154,155). The developing embryonic lens is supported by the hyaloid vascular system (156) and as such has no need for an organ-specific circulation system; AQP0 acts as a structural protein during development, before undergoing a C-terminal truncation in the nucleus while AQP5 transitions from a cytoplasmic to a transmembrane protein at the same time (154,157). AQP1 is a constitutively open water channel protein (155,158) expressed in the lens epithelium, whose deletion has been shown to decrease lens water permeability in mice while upregulated levels have been detected in human cataractous lenses (159,160). AQP5 is expressed as a cytoplasmic protein in LECs and differentiating fibres in the cortex of adult lenses, though levels are significantly lower than AQP0 throughout the tissue (88,92,154,155).

AQP0 is the most abundant membrane protein the lens, accounting for approximately 30% of the total membrane proteome (88,89,92). Though classified as a water channel protein, AQP0 also mediates cell to cell adhesion in LFCs; this has been demonstrated in the zebrafish were Aqp0a and Aqp0b are the products of a genomic duplication event with Aqp0a functioning as a water channel and suture-stabilising protein (161) while Aqp0b appears to have an adhesion role but no channel permeability (162,163). Both isoforms have been shown to be essential to lens clarity, as deletion of either one produces cataracts (162). An additional role for AQP0 in regulating the structure of LFCs has been proposed as a result of its C-terminal interaction with the beaded intermediate filaments BFSP1 and BFSP2 (132,164), further supporting the hypothesis that membrane organisation in fibre cells is an essential component of the mechanical structure of the lens. Though both AQP0 and AQP5 are co-expressed in mature LFC membranes only AQP0 appears to affect the structural properties of lenses (165), implicating the protein in the development of presbyopia and cataract. The permeability of the tetrameric AQP0 channels has been shown to be regulated in a $Ca^{2+}$ dependent manner with calmodulin interaction sites at the C-terminal domain and the arginine-rich intracellular loop (166–168), with calmodulin binding inducing the closing of extracellular and intracellular gates in model membranes (169). The phosphorylation of AQP0 at the C-terminal domain, which decreases with age in the inner cortex, effectively disrupts calmodulin binding and increases the permeability of the water channel (170,171). These factors have been suggested to contribute to the diffusion barrier which forms at the inner cortex in aged lenses (148,172), though no

direct evidence has been produced in support of this hypothesis. Further regulation of AQP0 water permeability has been shown to occur due to the surrounding lipid environment of the membrane, with membrane trafficking being dependent on the lipidation profile of the protein. N-terminal and C-terminal fatty acid modifications have been reported in AQP0 from bovine and human lenses which correlate with the acyl composition of neighbouring phosphoethanolamines (173,174), with lipidated AQP0 detected in detergent resistant lipid raft domains while non-lipidated AQP0 has been detected in detergent soluble lipid raft domains (89,174). Age-related post translational modifications in the C-terminus of AQP0 have been predicted to affect both the water permeability of the channel and the structural integrity of the surrounding membranes due to the calmodulin and beaded filament interaction sites reported in the region (132,164,165,168,171), though further work is required to establish the connections between these events and the onset of presbyopia and cataract.

The lack of organelles in the lens nucleus creates an environment where nutrients, ions, and macromolecules need to freely flow through cells to satisfy the energy needs of the oldest LFCs. As such, LFCs are connected through a network of gap junctions formed by the connexins Cx43, Cx46, and Cx50. Connexin proteins oligomerise to form connexons, which are hexameric homotypic and heterotypic hemichannels, and are embedded in the plasma membrane before making contact with connexons from adjacent cells and completing the cell to cell channel (175). Finally, membrane domains rich in intercellular connexon channels are called gap junctions.

Lens connexins are spatiotemporally expressed, with Cx50 being ubiquitously and highly expressed in LECs and LFCs (176–178) in addition to being essential for normal tissue growth (179), while Cx46 expression is upregulated in the fibre cell cortex (145,180) and Cx43 is exclusively expressed in LECs at low levels (181). This distribution of connexins is conserved across mammals, mirroring the identity of the lens circulation system in all organisms in which it has been studied to date (150,152) and highlighting the significance of gap junctions in the preservation of lens physiology. Gap junctions have been found to form between adjacent LECs, adjacent LFCs, and between LECs and LFCs at different ratios depending on the polar angle of the epithelial region. Less than 10% of LECs in the anterior polar region form gap junctions with underlying fibre cells, while these connections drastically increase at the equatorial zone as inferred from dye tracking and coupling conductance studies (9,182). Similarly, the coupling conductance of LFCs ranges from its minimum at the poles through to its maximum at the equator demonstrating the enrichment of gap junctions at the equatorial region which contributes to the lens circulation (147,183). Though Cx50 and Cx46 staining is mostly uniform across the lens cortex (178), the gating of gap junctions appears to be

regulated similarly to the promotion of LFC differentiation with the combination of FGF/BMP upregulation inducing an increase in coupling conductance (8,24,184,185). In contrast, the coupling conductance of mature LFCs is relatively uniform across the entire length of the cells with C-terminally cleaved Cx50 channels constitutively gated open (186), supporting the syncytium nature of the lens nucleus.

While Cx46 and Cx50 copolymerise to form heteromeric connexons, with the selective knockout of Cx46 effectively eliminating the nuclear uptake of reduced glutathione in aged murine lenses (187) while Cx50 knockout and Cx50/AQP0 double knockout lenses showed a significant loss of LFC architecture resulting in microphthalmia, microphakia, extensive cataracts and a loss of lens elasticity (188,189).

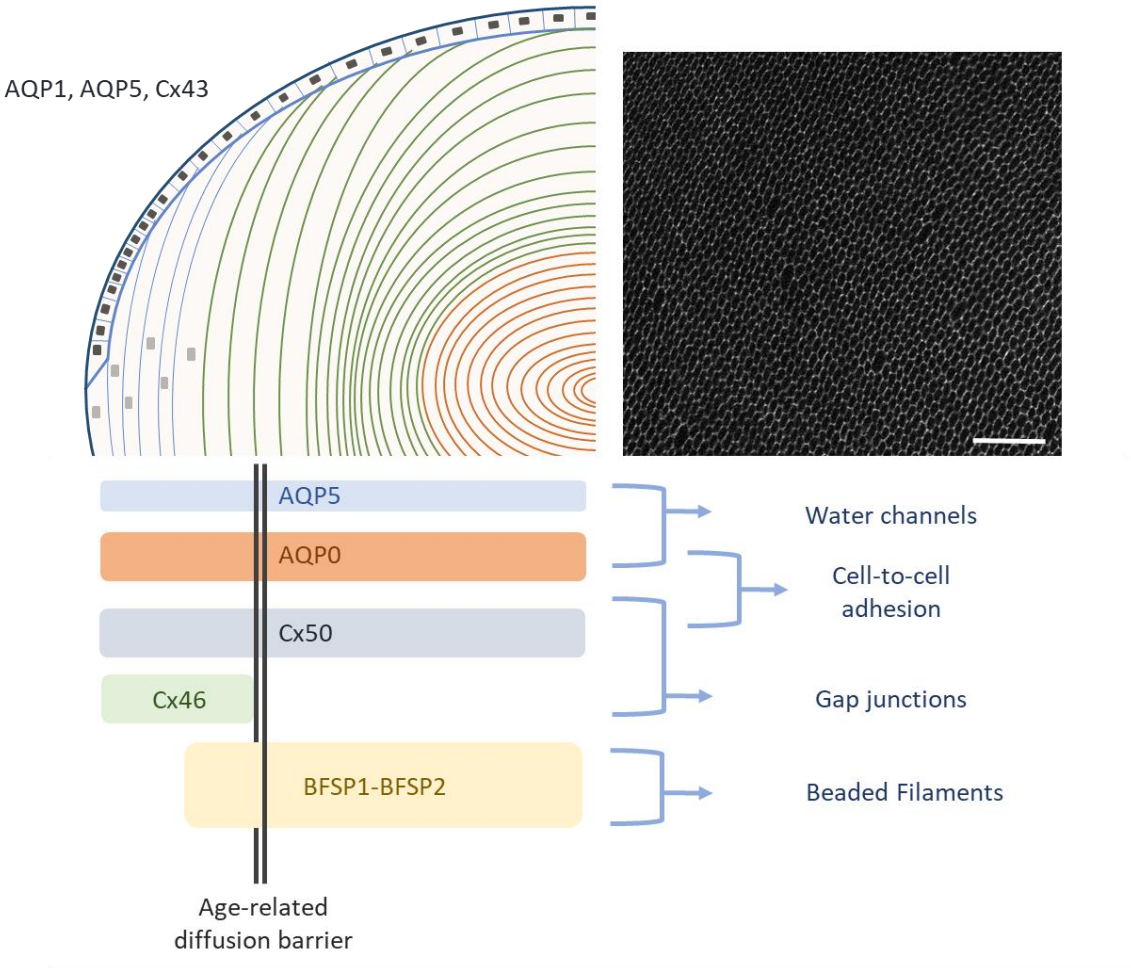


Figure 1.4. The major structural lens proteins, their distribution in the lens and core functions. A cross-section of LFCs reveals tightly-packed, hexagonal arrays of cells in a bovine lens immunolabelled against AQP0 (scale bar length = 80 µm). This unique cellular structure is directly supported by the lens fibre cell proteome through the synergistic actions of aquaporin water channels, cell-to-cell adhesion proteins, and gap junction proteins at the membranes, while beaded filament proteins support this structural network.

### 1.1.4 Age-related changes in the lens proteome

The lifelong retention of macromolecules, in addition to the extensive interactions between proteins in the lens, create an environment where age-related modifications are abundant and mostly accessible for examination.

The major source of age-related alterations in the lens are post-translational modifications, with effects impacting a range of lens characteristics from the ultrastructure of membranes and cellular architecture to the circulation of ions and the propagation of oxidative damage.

One of the most significant ageing events in the lens is the loss of all soluble α-crystallin by the fifth decade of life in humans (190–193) due to the increased binding of denatured proteins as part of its chaperone function (107,191), contributing to the hypothesis that the optimal amount of lenticular α-crystallin has been established as a consequence of reproductive pressure. The increased amount of high molecular weight protein aggregates in the lens nucleus, along with the increased binding of α-crystallin to LFC membranes (191,194,195) and the depletion of chaperone-functional protein (196) all contribute to increased lens stiffness in the form of presbyopia in addition to the age-depended accumulation of damaged macromolecules.

The post-translational modification of α-crystallin has been associated with ageing and cataractogenesis, with extensive deamidation and racemisation found in aged clear lenses (97,197,198). A direct structure-function relationship has been demonstrated for the deamidation of Asn123 in αA- and Asn146 in αB-crystallin (198,199) with both significantly reducing the chaperone function of α-crystallin. High molecular weight aggregates from aged lenses have been found to contain a multitude of truncated peptides including crystallins (200,201) both as a result of autolytic degradation and proteolytic cleavage (10,33,202,203), with C-terminal non-enzymatic truncation of α-crystallins being the most abundant and influencing the multimerization of the protein with a distinct reduction in chaperone capacity (199,201,204,205). Phosphorylation of α-crystallin is thought to be an irreversible process which increases with age and has been demonstrated to coincide with the transition of protein to the water insoluble fraction (97,206,207).

The major deleterious effect which contributes to cataractogenesis is thought to be the cross-linking of α-crystallin, which arises from the oxidation of thiols. Disulfide linked cysteines are not abundant in clear aged lenses while cataractous lenses show extensive cross linking of proteins including crystallins (205,208–210), highlighting the significance of irreversible oxidative damage as a cataractogenic agent (211).

Age-related changes in the membrane proteome of the lens have been suggested to contribute to the increase in oxidative agents early in life, mostly through the depletion of antioxidants in the lens nucleus as a result of the diffusion barrier which develops early in the 4$^{th}$ decade of life in humans (57). A progressive loss of connexin proteins Cx46 and Cx50 has been observed in mice and is accompanied by a dramatic reduction in nuclear coupling conductance (212), which in combination with the increasing hydrostatic pressure in the lens nucleus indicate an age-related decrease in open gap junctions and a decrease in the rate of water circulation (150,212).

AQP0 is extensively post-translationally modified in its C-terminus in an age-dependent manner, possibly to regulate its dual function as a water channel and cell to cell adhesion protein. Human AQP0 is C-terminally truncated in early adolescence, with up to 50% being truncated by 24 years of cellular age (213). The precise role of this increasing truncation in the lens nucleus is not entirely understood mostly due to conflicting structural and functional data on the water permeability of the cleaved protein (214–216), and the implications of losing the protein region responsible for interacting with the cytoskeleton (132) are yet to be elucidated. Covalent cross linking of AQP0 has been observed in an age-dependent manner and is enriched in cataractous lenses (217).

A modest increase in the oxidation of intermediate filament proteins has been shown for clear aged lenses, with moderate Cys167 disulfide formation found in BFSP1 and Cys236 in BFSP2. The oxidation profile of these residues, in addition to Cys65 in BFSP2, has also been shown to drastically increase in aged-matched cataractous human lenses, further highlighting the involvement of extensive oxidation of macromolecules in the formation of lens opacities (211,218).

Despite the extensive post translational modifications and the significant loss of chaperone activity in human lenses at the fifth decade of life, the onset of cataract is often delayed by a further couple of decades (219,220) which illustrates the concept that the lens is characterised by a damage tolerance threshold. This limit has been called the “cataractogenic load” and has been reviewed recently by Uwineza et al., (48) and is summarised in figure 1.5.

The structure-function relationship of the lens proteome is further substantiated in the ageing process of these macromolecules, as lifelong protein degradation in the lens still aims to support the integral functions of the organ: transparency, and appropriate refractive power. Though ageing effects including presbyopia become apparent by the middle of the average human lifespan, life-altering deleterious conditions such as cataract do not begin to occur until much later when a substantial fraction of the lens proteome is irreversibly damaged. The

theory of cataractogenic load has been proposed to extend a step further, where the accumulation of specific aged proteins aids the extended transparency of the lens. This is further supported by the conserved nature of pre-cataract protein modifications, while mature cataracts contain highly heterogeneous protein fragments.

### 1.1.5 Lipidome- proteome dynamics

The structural importance of LFC membranes in maintaining the hypoxic lens core and allowing the regulated circulation of ions and small molecules becomes apparent when considering the unique lipid and protein composition of these bilayers and how these vary spatially and temporally.

The close structure-function relationship of the lens lipidome and the lens proteome is best illustrated by lipid raft domains, which form as a consequence of the cholesterol enrichment of fibre cell membranes (72) and house important structural proteins such as AQP0 (72,89,221). The marked increase in cholesterol content coupled with the loss of DRM rafts in cataractous lenses (72) further emphasises the conclusion that membrane content alone is not enough to maintain lens physiology, but instead the organisation of membrane domains is essential.

#### *1.1.5.1 The proteome of lens lipid rafts*

Lipid rafts are cholesterol and sphingolipid-enriched membrane domains that range from 10-200nm and are involved in processes such as cell to cell adhesion, signal transduction, and cytoskeletal protein recruiting (222,223). Lens lipid rafts have been shown to contain raft marker proteins such as caveolin-1 and flotillins 1 and 2, in addition to the transmembrane proteins AQP0, AQP5, Cx46, and Cx50 (89,224,225). Cholesterol depletion of detergent resistant rafts has revealed possible interactions between lens lipid rafts and soluble proteins including αB-crystallin, though whether these interactions are due to protein-protein or protein-lipid binding remains to be examined.

Previous studies have shown that Cx43 and Cx46 co-localise with caveolin-1, in contrast with Cx50 which preferentially associated with detergent soluble membrane fractions (226). In the lens, AQP0 localises to the lateral faces of LFCs and Cx46/Cx50 to the apical ends, while Cx46 and Cx50 are sorted to different raft domains in cultured kidney cells. Considering that Cx46 and Cx50 have been shown to form heteromeric connexons in fibre cells (183), these differences in membrane localisation further complicate our understanding of raft assembly and function. Model proteoliposome preparations have evidenced a sorting of Cx50 into detergent soluble membranes, while AQP0 domain sorting was dependent on the molar ratio of protein to lipid. At a low ratio of 1:1200 AQP0/lipid, AQP0 was found almost exclusively in detergent soluble membranes while an enriched preparation of 1:100 shifted approximately

50% of the protein to the detergent resistant membrane fraction (221). Further proteoliposome studies of AQP0 found a lipid bilayer-dependent regulation of the water permeability of the protein unit, with increasing cholesterol and sphingomyelin content resulting in reduced channel permeability (227). The cholesterol/sphingomyelin enriched liposomes in combination with the AQP0 1:100 proteoliposome closely mimic the bilayer environment in the lens nucleus and thus shed light on the potential characteristics of raft targeted AQP0.

Beyond their role as membrane protein housing domains, cholesterol lipid rafts in LFCs have been proposed to act as a buffering agent which maintain the physical properties of the lipid bilayer- namely the order, fluidity, oxygen diffusion, and hydrophobicity- consistent during the lifelong depletion of glycerolipids such as phosphatidylcholine (84,228,229). Subsequently, the loss of lipid rafts in cataract (72) but not in age-matched clear donor lenses has widespread consequences for the preservation of LFC architecture, the continuing lens circulation, and the maintenance of the hypoxic nuclear core through the loss of essential membrane proteins regulating these processes; the exact nature of these interactions remains to be fully characterised.

#### *1.1.5.2 Membrane interactions of α-crystallin*

Apart from its role as a protein chaperone, lens α-crystallin has been shown to non-covalently bind native and synthetic lipid bilayers (191,194,195,230–233). The observation that high molecular weight α-crystallin aggregates are increasingly membrane bound in ageing and in cataract (191) in combination with the reduced chaperone activity of these aggregates have been proposed as an essential cataractogenic event which is complete by the onset of presbyopia (23,82,193).

*In vitro* preparations have demonstrated the ability of α-crystallin to stabilise denaturing membrane proteins such as AQP0 (234), while a competitive interaction between the two proteins has also been seen in transfected HeLa cells (235).

As the most abundant lens protein, any interaction between α-crystallin and the lens lipidome or the lens proteome will have a direct impact on the maintenance of tissue clarity and structure. Therefore, it is unsurprising that α-crystallin has been considered as a therapeutic target in the treatment of cataract both in the context of a protein aggregation disease and of a loss of membrane integrity.

## 1.2 Cholesterol metabolic disorders and congenital cataract

Congenital cataract can occur as an isolated phenotype or as part of systemic disorders, as recently reviewed by Shiels and Hejtmancik (59). Nonsyndromic congenital or early onset cataracts have been associated with mutations in genes encoding structural lens proteins such as *GJA8*, *GJA3*, *MIP*, *BFSP1*, *BFSP2*, and *VIM* which produce the proteins Cx50, Cx46, AQP0, BFSP1, BFSP2, and vimentin; the γ-crystallins *CRYGB*, *CRYGC*, and *CRYGD*; the β-crystallins *CRYBA4*, *CRYBA2*, *CRYBA1*, *CRYBB3*, *CRYBB2*, *CRYBB1*; and both α-crystallins *CRYAA* and *CRYAB* (64,125,243–248,127,236–242).

Systemic disorders of lipid metabolism have also been associated with the sporadic incidence of congenital or juvenile cataract, with the cholesterol synthesis gene lanosterol synthase *LSS* (249,250) gaining prominence due to the reported efficacy of lanosterol in dissolving lens opacities and crystallin aggregates (249,251); the lipid transporter ATP-binding cassette A3 *ABCA3* has also been involved in congenital cataract as part of a respiratory syndrome (252). Alterations in the synthesis of cholesterol via the use of statins is currently a controversial subject, as epidemiological and *in vitro* data suggest prolonged statin use reduce *de novo* cholesterol synthesis in the lens and increase the risk of cataractogenesis (253–256) though no alternative medication currently offers a more favourable risk-reward odds in relation to the atheroprotective effects of statins (257,258).

Despite the significance of elevated cholesterol in the maintenance of lens health (259), few cholesterol synthesis, transport, and metabolism gene mutants have been involved in cataractogenesis in humans (260), implying a complex mechanism of control underpins the regulation of intralenticular cholesterol levels and organisation.

### 1.2.1 Congenital cataract in systemic disorders

Two rare systemic disorders of cholesterol metabolism consistently present with congenital or juvenile cataract, namely cerebrotendinus xanthomatosis (CTX) and Smith-Lemli-Opitz syndrome (SLOS).

CTX is an autosomal recessive disorder which arises from mutations in the cytochrome P450 *CYP27A1*, an enzyme responsible for one of the first steps in the breakdown of cholesterol to the bile acid 27-hydroxycholesterol (261,262). The main pathology associated with CTX is an accumulation of cholesterol and cholestanol in the brain and other cholesterol rich tissues, resulting in bilateral juvenile cataracts (263), tendon xanthomas, and neurologic dysfunction such as ataxia (264,265). Due to the variety of mutations associated with the disorder, penetrance is also variable and affects the age of onset and severity of the major symptoms. Standard treatment for CTX involves the oral administration of the oxysterol chenodeoxycholic

acid (CDCA), which has been shown to improve the biochemical profile of patients and certain neurological aspects of the disorder (264,266), while cholic acid has also been recommended as a potential pharmaceutical treatment (267). Interestingly, CDCA treatment does not improve or resolve cataracts in CTX patients (262,266,268), raising questions about the bioavailability of orally administered oxysterols in the lens (269).

SLOS is an autosomal recessive disorder which arises from a cholesterol deficiency due to reduced 7-dehydrocholesterol reductase activity as encoded by the *DHCR7* gene. The biochemical characteristics of the disorder involve the accumulation of 7-dehydrocholesterol and reduction of cholesterol levels in all tissues, while symptom severity is variable but includes growth retardation, congenital or juvenile cataracts, neurological dysfunction such as intellectual dysfunction and microcephaly (270–272). As with CTX, cholesterol supplementation has been shown to improve the majority of physical and neurological phenotypes, but no improvement of developed cataracts has been reported to date (273).

Cataracts have been produced *ex vivo* and *in vivo* in model systems to mimic rare, sporadic cholesterol metabolism disorders such as mevalonic aciduria (260), desmosterolosis (274), and SLOS (275). However, translation to the equivalent human disorders is lacking both due to the complexity of cholesterol metabolism and its downstream signalling targets, but also due to our limited understanding of the mechanistic and structural impact of cholesterol-related dysfunction in the lens.

## 1.3 The lipidome and proteome of age-related cataract

Age-related cataract is broadly classified into nuclear, cortical, or posterior subcapsular depending on the location of light scattering aggregates in the lens. Nuclear cataract is by far the most prevalent subtype accounting for up to 50% of cases, followed by PSC and cortical opacities (62,219,220,276). When controlled for age, cortical cataract is more prevalent in people <50 years of age (219), implicating the lens cortex in an increased susceptibility to acute damage as opposed to the age-related cataractogenic load which is associated with nuclear cataract.

Cataractogenic events include direct macromolecule damage of lens lipids and proteins, genetic damage, and mutations. Association studies have highlighted several polymorphisms which may contribute to increased risk of age-related cataract, including *ATM, GJA3, BMP4, CYP46A1, TP53, APOE,* and *ERCC2* (248), all of which are involved in diverse cellular roles such as DNA damage, cell adhesion, and lipid metabolism and transport. Epidemiological studies have suggested genetic factors contributing to cataract incidence could account for up to 35-48% of the risk in nuclear and up to 75% for the risk of cortical cataract (68,69,220,276), while

environmental factors such as cigarette smoking and obesity (277,278) and elevated blood glucose levels in combination with statin use (253,279) have been proposed as risk factors for nuclear and cortical cataract respectively.

### 1.3.1 Lens membrane lipids in cataract

The unique lipidome of LFC membranes favours an age-related enrichment of cholesterol at the expense of glycerolipids (21), creating a bilayer environment that initially aids in the shielding of the hypoxic lens core but provides a platform for the propagation of oxidative damage as the cataractogenic load increases. Increased levels of autooxidised cholesterol have been detected in lenses with age-related cataract (21,280) including 7β-hydroxycholesterol, 7-ketocholesterol, 5α6α-epoxycholestanol, and 25-hydroxycholesterol, which affect the order of membrane lipids and influencing the fluidity of the lipid bilayer (280). The depletion of glycerolipids in human lenses >40 years of age (80) in combination with the enrichment of saturated, oxidation-resistant phospholipids such as dihydrosphingomyelin, favours the autoxidation of cholesterol which disrupts the function of proteins housed in cholesterol-rich domains (75). Apart from their structural disruption of lipid membranes and propagation of oxidative damage to surrounding macromolecules, oxysterols act as signalling molecules; 7-ketocholesterol has been shown to modify Na/K ATPase activity (281), which is instrumental in regulating lens ion transport (147,282). Lipids isolated from cataractous lenses have been shown to be devoid of raft domains (72), further implicating the role of lipid-protein interactions in the maintenance of lifelong lens health. The oxidation of lipids in the lens has commonly been hailed as the initiating cataractogenic event (52,211,283–285) due to the structural barrier membranes create to maintain the hypoxic environment in the nucleus.

Beyond the systemic damage created by cholesterol oxides, the ordering of lipids in LFC membranes has been shown to increase with age and with the development of cataract (76,79,280) which in turn has been associated with a 20% increase in membrane light scattering (286). As mentioned previously, the matching of the refractive index of the cytoplasm and the lipid bilayer is an essential component of lens clarity (21,41–43) and any deviation in nuclear LFCs from the ratios seen in clear lenses will lead to increased light scatter (9).

### 1.3.2 Lens proteins and cataract

In a proteomic context, cataract can be summarised as an irreversible aggregation of proteins which form light scattering adducts and permanently alter lens transparency. Aggregates in age-related nuclear cataract (ARNC) mostly consist of insoluble high molecular weight α-

crystallin bound to denatured proteins including other crystallins (191,207,287,288) and are increasingly membrane associated as the severity of the cataract progresses (191).

The early loss of soluble α-crystallin by the fourth decade of life (190,193,289) and subsequent development of presbyopia have recently been reconsidered as the defining moment in cataractogenesis due to the continuous decline of α-crystallin chaperone activity. This depletion of soluble α-crystallin with age is a testament to its appropriate function as a chaperone protein, but lenses of long-lived organisms do not contain enough chaperone to stabilise other damaged macromolecules indefinitely. Regardless, denatured α-crystallin remains relatively stable until the critical threshold of cataractogenic load has been crossed (48). Membrane-bound high molecular weight aggregates continue to increase in protein content in the ageing lens, with approximately 60% of the total LFC protein content associated with these aggregates after the seventh decade of life in humans during which ARNC prevalence increases rapidly (289,290).

The formation of the lens barrier between the lens cortex and the lens nucleus results in the depletion of reduced glutathione in mature LFCs, effectively eliminating the major oxygen scavenger in the organelle-free lens core and leaving α-crystallin as the final frontier against protein denaturation. Though the exact mechanism underpinning the barrier development has not been elucidated, evidence suggests a loss of open gap junctions at the border of the cortex remodelling zone could be responsible (91,128). As the selective knockout of Cx46 in mice mimics the barrier seen in human lenses and drastically decreases the amount of reduced glutathione in the lens nucleus (187) and Cx46 has been detected in detergent resistant lipid rafts which are lost in cataractous lenses, it is possible to suggest a changing role for Cx46 containing gap junctions in the ageing lens which is influenced by the surrounding lipid environment. Similarly, the membrane partitioning of Cx50 and AQP0 into detergent soluble and detergent insoluble domains (89,189,221,227) likely impacts the cell to cell adhesion properties of the proteins in cataractous lenses where cholesterol-rich membrane rafts are lost.

Lenses presenting with ARNC can be distinguished from clear aged-matched lenses by the increased amount of insoluble total protein. The proteome of advanced ARNC contains the highest amount of oxidised amino acids with approximately 90% of cysteines cross linked by disulfides and 40-50% of methionines converted to methionine sulfoxides (218,291–296).

### 1.3.3 A role for α-crystallin in the prevention and treatment of cataract

The introduction of a non-surgical intervention as a prophylactic or therapeutic approach to cataract has long been an alluring prospect, with a range of pharmacological and dietary methods examined to varying results.

Studies utilising a preventative approach have mostly sought to expand the timeframe of soluble and chaperone active α-crystallin, though epidemiological data have often yielded mixed results (297). Oral supplementation of tocopherol and glutathione, the two main lens antioxidants, had no effect on the incidence of cataract in a clinical setting (298), while long-term dietary intake of vitamin A, riboflavin, niacin, and thiamin were associated with decreased incidence of nuclear cataract (62) though no molecular mechanism has been proposed or identified.

The stabilisation of aggregated α-crystallin using pharmacological agents after the development of cataract has also been examined. The topical application of oxysterols including lanosterol were shown to reverse lens opacities both *in vivo* and *in vitro* (249,299), though the replication of this effect in human lenses has failed (300). The *in vitro* application of the oxysterols ursodeoxycholic acid (UDCA) and tauroursodeoxycholic acid (TDCA) enhance the chaperone activity of α-crystallin and suppress the thermal aggregation of αA-, αB-crystallin, and insulin (269), while topical UDCA was found to suppress selenite-induced cataract in rats by up to 80% (301).

Numerous plant-derived antioxidants have been proposed as potential pharmacological interventions, as reviewed by Heruye et al., with varying efficacy observed *in vitro* and *ex vivo*. Most successful *in vivo* pharmacological interventions have been reported against induced cataract, and as such very little convincing data is available in favour of the reversal of ARNC through topical means (302).

## 1.4 Hypothesis: Connecting α-crystallin to cholesterol

A pharmacological treatment option for ARNC would significantly improve the quality of life for almost 10 million people globally every year, who would otherwise be blinded due to the lack of access to affordable surgical interventions. The administration of antioxidants is a promising avenue for the delaying of the onset of cataract, but the impenetrability of the lens nucleus to reduced glutathione from 30 years of age limits the bioavailability of therapeutic molecules in the region where denatured protein aggregates are found. As such, oxysterols and oxysterol derivatives are currently the most attractive option for ARNC treatment due to their demonstrated ability to improve the chaperone activity of α-crystallin and to dissolve crystallin aggregates *in vitro* (251,269,301). Despite this, the topical application of oxysterols to the lens

has the potential to significantly disrupt lens architecture either through off-target interactions with cholesterol rich membrane domains (72,89,303,304) or through the induction of pro-oxidative cascades which are not currently understood (281,305,306).

At its core, our hypothesis proposes that sterols including cholesterol, lanosterol, and 25-hydroxycholesterol interact with and influence the function of α-crystallin while also being bioavailable throughout the lens following topical application.

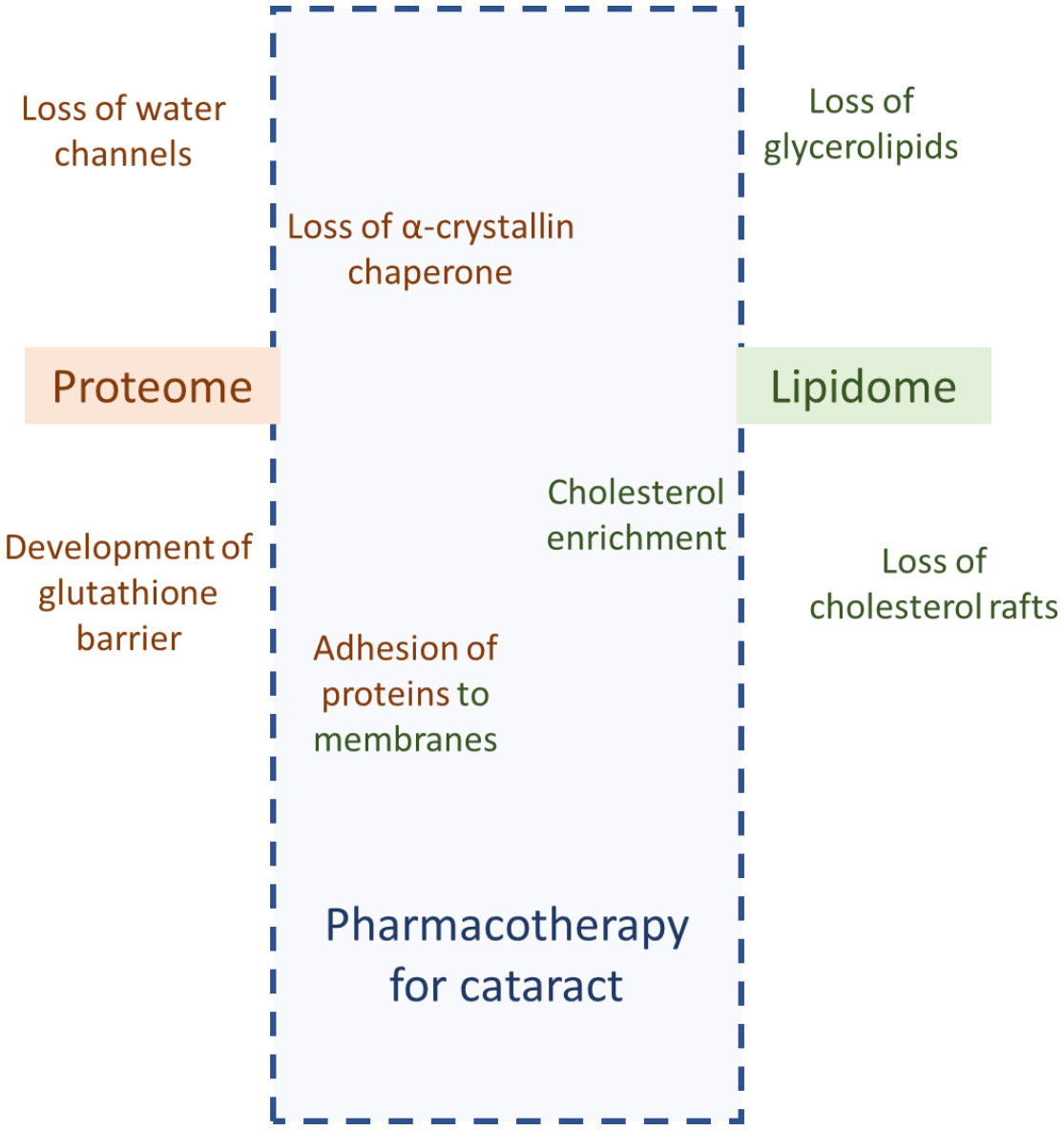


Figure 1.5. Cataractogenic load is a multifactorial path to the development of cataract, with no one event exclusively influencing the onset of ARNC. However, a successful pharmacotherapy for cataract will have to address the interface between the major proteomic and major lipidomic events that contribute to cataractogenesis, namely the loss of chaperone activity for α-crystallin, the adhesion of high molecular weight aggregates to LFC lipid membranes, and the increased rigidity of membranes due to cholesterol enrichment which are hallmarks of cataract and presbyopia.

# 2 Chapter 2: Aims and Objectives

The use of oxysterols as a prophylactic or a non-surgical treatment for cataract could have an enormous global impact by introducing an affordable and accessible method of restoring vision to patients who would otherwise be condemned to lifelong blindness. As with all novel therapeutics, rigorous safety testing is imperative; often this does not translate to informed understanding of the underlying mechanisms at play but is limited to the binary question of whether the compound safely works. Furthermore, prolonged use of cholesterol-modifying drugs such as statins has been associated with increased incidence of cataract (253–255). In this project, we have addressed five major research questions to understand how sterols influence lens health through lipid-protein interactions both *in vivo* and *in vitro*.

## 2.1 Aim 1: Characterise the effect of impaired cholesterol synthesis on the developing zebrafish

Congenital cataracts resulting from impaired lipid synthesis have been identified and characterised in humans, as discussed in section 1.3 (249,271). We have used the developing zebrafish as a model to study the effect of reduced cholesterol synthesis on the lens and the broader physiology and behaviour of impaired larvae to identify distinct ocular phenotypes. We address this objective in chapter 4.

## 2.2 Aim 2: Investigate the efficacy of sterol supplements as rescue treatments in cholesterol synthesis-impaired zebrafish

Oxysterol application has previously been reported as a method to reverse lens opacities both *ex vivo* and *in vivo* (249,251,269,299), though data remain inconclusive and contradictory on the global suitability of these compounds in the treatment of cataract (300). We have examined the effect of sterol supplements on pharmacologically inhibited cholesterol synthesis zebrafish and have proposed disease-rescue pairs for different checkpoints in this metabolic pathway. We address this objective in chapter 4.

## 2.3 Aim 3: Investigate the absorption, trafficking, and metabolism of supplemented sterols in the developing zebrafish

The mechanism by which exogenously introduced sterols are utilised by the lens have not previously been described for the zebrafish. In chapter 4, we have investigated the absorption of the supplement sterols lanosterol and cholesterol by the developing zebrafish larvae and have examined their distribution in lipid rich tissues such as the yolk sac and lens. Further, we have analysed the initial steps of downstream metabolism of supplement sterols and their retention in the lens.

## 2.4 Aim 4: Identify relationships between lipid classes and proteins in lens lysates and lens membranes

The high cholesterol content in lens fibre cell membranes results in the formation of pure cholesterol bilayers (228,259,307), which are essential in the organisation of gap junction and cell adhesion proteins. The preferential association of proteins with different lipid classes has been previously characterised in the lens (72,89,104,221,226); we have explored the dynamics of these relationships under different environmental conditions and whether altering the protein content of lysates affects the distribution of lens lipids. This objective is addressed in chapter 5.

## 2.5 Aim 5. Examine the effect of exogenous sterols on the distribution of major lens proteins

The lipid content of lens membranes is both species-specific and lifespan dependent (77,308), serving as a critical component in maintaining functional lens clarity. Critical thresholds in cholesterol content have been identified and associated with physiological ageing and the development of cataract (72–74,83,305,308), suggesting any disruption to this balance via the application of exogenous sterols may compromise the redox equilibrium of the organ. We have examined the influence of exogenous sterols on the stability of lens membrane fractions and the distribution of major lens protein classes, as reported in chapter 5.

## 2.6 Aim 6: Analyse the influence of lanosterol and cholesterol on the aggregation of lens membranes

Lanosterol and lanosterol-related sterols have been proposed as therapeutics for the reversing of cataract in animal models via their effect on stabilising aggregated α-crystallin and restoring its soluble form (249,251,269). We have analysed the effect of lanosterol, cholesterol, and 25-hydroxycholesterol on insoluble lens membrane fractions to assess their interactions with native lens proteins and lipids, with the results presented in chapter 6.

# 3 Chapter 3: Materials and Methods

## 3.1 Isolation of integral membrane proteins from bovine lenses

### 3.1.1 Bovine lens isolation and dissection

Bovine eyes were acquired from Linden Burradon Food Supply (Food Standards Agency SRM Dispatch approval number 2056) within two hours of culling. All animals were between 12 and 36 months old from UK farms and were sacrificed for human consumption. Twenty-four lenses were manually dissected out of the capsule and submerged in 120mL buffer 1. Four lens fractions were serially hydrodissected to produce outer cortical, inner cortical, outer nuclear, and inner nuclear material of equal volumes. Fraction sizes were determined as four concentric shells of equal radius. All buffer recipes can be found in Table 3.1.

### 3.1.2 Isolation of high protein content lens membranes

Total lens fractions were homogenised in 120 mL of buffer 1, followed by a 15-minute centrifugation at 15000 rpm ($RCF_{AV}$ 17640 x g) in a JA-20 rotor (Beckman Coulter) using an Avanti J20 centrifuge (Beckman Coulter) chilled to $4^{O}C$. The supernatant was discarded, and pellets were serially resuspended and centrifuged in 120 mL buffers 1, and 2. Homogenised protein in buffer 2 was stored on an agitator at $4^{O}C$ overnight. Following further centrifugation, pellets were resuspended and centrifuged in 120 mL buffers 1, and 3. Pellets recovered from the centrifugation of buffer 3 were resuspended in buffer 1 at a concentration of 400 $mgmL^{-1}$ for short-term storage at $4^{O}C$.

### 3.1.3 Isolation of integral membrane proteins

For the isolation of integral membrane protein fractions, pellets recovered from the centrifugation of buffer 3 were resuspended in 80 mL buffer 4 and agitated at room temperature for 20 minutes before being centrifuged for 45 minutes at 25000 rpm ($RCF_{AV}$ 51275 x g) in a JA-25.50 rotor (Beckman Coulter) using an Avanti JA-20XP ultracentrifuge (Beckman Coulter) chilled to $4^{O}C$. Pellets were resuspended in 60 mL buffer 1, and centrifuged at 15000 rpm ($RCF_{AV}$ 17640 x g) in a JA-20 rotor (Beckman Coulter) using a Avanti J20 centrifuge (Beckman Coulter) chilled to $4^{O}C$. Pellets were further resuspended in 60 mL buffer 5 and centrifuged, and the final protein pellets were homogenised in buffer 1 to a concentration of 100 $mgml^{-1}$ for short-term storage at $4^{O}C$.

## 3.2 Protein solubility assays

### 3.2.1 High protein content lens membranes

#### *3.2.1.1 Native solubility assay*

Cortical and nuclear high protein content bovine lens membranes were pooled to 10 $mgmL^{-1}$ and serially centrifuged to determine their solubility status. Material was serially centrifuged at $RCF_{AV}$ 14000 x g (3800 rpm) in a tabletop VWR Micro Star 17R centrifuge (VWR), and supernatants were collected. Pellets were resuspended in equivalent volume buffer 1 and centrifuged further. Supernatants and pellets were assessed via SDS-PAGE for their protein content.

High protein content bovine lenses were serially centrifuged four times at $RCF_{AV}$ 14000 x g for pre-clearance, with each supernatant discarded and the remaining pellet resuspended in equivalent volume buffer 1.

Pre-cleared bovine lens membranes were pooled to 10 $mgmL^{-1}$ and incubated in light safe conditions at $4^{O}C$, $25^{O}C$, $37^{O}C$, and $42^{O}C$ to assess their solubility status. Samples were collected after 30 minutes, 2 hours, 12 hours, 24 hours, and 72 hours and centrifuged at $RCF_{AV}$ 14000 x g in a tabletop VWR Micro Star 17R centrifuge (VWR) at $4^{O}C$. Supernatants were collected, and the remaining pellets were resuspended in equivalent volume buffer 1. Samples were stored at $-20^{O}C$ prior to analysis.

#### *3.2.1.2 Chemical-mediated solubility assays*

Pre-cleared bovine lens membranes were pooled at 10 $mgmL^{-1}$ and co-incubated with varying concentrations of Roche cOmplete Mini Protease inhibitor cocktail (Sigma-Aldrich), or iodoacetamide (Sigma-Aldrich, 144-48-9), or E-64 (Sigma-Aldrich, 66701-25-5), or leupeptin (Sigma-Aldrich, 103476-89-7) as shown in table 3.6. Samples were incubated at $37^{O}C$ in light safe conditions and collected after 30 minutes, 2 hours, 12 hours, 24 hours, and 72 hours. All samples were centrifuged at $RCF_{AV}$ 14000 x g, supernatants were collected, and pellets were resuspended in equivalent volume buffer 1.

#### *3.2.1.3 α-crystallin mediated solubility assays*

Pre-cleared bovine lens membranes and pellets from section 3.2.1.1. were co-incubated with varying concentrations of commercial α-crystallin (Sigma-Aldrich, 11046-99-4), size-exclusion chromatography (SEC) isolated bovine α-crystallin, and native soluble α-crystallin from the first supernatant in section 3.2.1.2. Samples were incubated at $37^{O}C$ in light safe conditions and collected after 30 minutes, 2 hours, 12 hours, 24 hours, and 72 hours. All samples were

centrifuged at $RCF_{AV}$ 14000 x g, supernatants were collected, and pellets were resuspended in equivalent volume buffer 1.

#### *3.2.1.4 Lipid-mediated solubility assays*

Pre-cleared bovine lens membranes and pellets from section 3.2.1.2. and 3.2.1.3. were co-incubated with 1 µM, 10 µM, or 100 µM lanosterol d6 (Avanti Polar Lipids, 28290-39-3), cholesterol d6 (Avanti Polar Lipids, 60816-17-3), or 25-hydroxycholesterol d6 (Avanti Polar Lipids, 64907-22-8) in light safe conditions at $37^{O}C$. Samples were collected at 30 minutes, 2 hours, 12 hours, 24 hours, and 72 hours and centrifuged at $RCF_{AV}$ 14000 x g in a tabletop VWR Micro Star 17R centrifuge (VWR) at $4^{O}C$. Supernatants were collected and pellets were resuspended in equivalent volume of buffer 1.

### 3.2.2 Low protein content lens membranes

#### *3.2.2.1 Lipid-mediated solubility assays*

Cortical and nuclear low protein content bovine lens membrane fractions were co-incubated at 10 $mgmL^{-1}$ with 10 µM or 20 µM lanosterol (Sigma-Aldrich, 79-63-0) or cholesterol (Avanti Polar Lipids, 60816-17-3) at $37^{O}C$ in light safe conditions. Samples were retrieved at 2, 10, and 24 hours and centrifuged at $RCF_{AV}$ 14000 x g in a tabletop VWR Micro Star 17R centrifuge (VWR). The supernatant was collected, and the remaining pellet was resuspended in equivalent volume buffer 1.

## 3.3 Growth of zebrafish larvae

### 3.3.1 Growth of zebrafish embryos to 5 days post fertilisation

Wildtype (Wik) zebrafish were kept in the Durham zebrafish facility on a 14-h light/10-h dark cycle at 28.5°C. All the experiments were carried out in accordance with the animal ethics guidelines of the UK Animals Act 1986 and Amendment Regulations 2012 and had ethical approval from Durham University. Groups of 4 zebrafish were gender-segregated overnight in mating tanks using transparent partitions. Fertilised eggs were recovered in the morning at t=0 hours post fertilisation and adults were returned to their housing tanks. Recovered eggs were transferred to 16mm CytoOne petri dishes (StarLab) and divided into groups of 50. Eggs were then stored in the dark at $28^{O}C$ in E3 zebrafish growth medium and monitored once every twenty-four hours. At 24 hours post fertilisation, non-fertilised eggs were removed from the dishes and discarded according to protocol.

### 3.3.2 Euthanasia of zebrafish larvae

Zebrafish larvae were stunned on ice and euthanised using 1X MS-222 (Sigma-Aldrich, 886-86-2) in E3 growth medium at room temperature. All larvae were decapitated prior to the

collection of tissue for analysis. Lenses and yolks were manually dissected from embryos and stored in phosphate buffered saline (PBS) 1X at -20$^{O}$C.

## 3.4 Pharmacological treatment of zebrafish larvae

### 3.4.1 LXR agonist treatment

LXR agonists T0901317 (Sigma-Aldrich, 293754-55-9) and GW3965 (Sigma-Aldrich, 405911-17-3) were diluted in 100% DMSO (Sigma-Aldrich, 67-68-5) to 10 mM and stored at -20$^{O}$C. Zebrafish were pooled in groups of 10 and manually dechorionated at 24 hours post fertilisation and treated with 1 µM, 2 µM, or 5 µM of either compound in E3 growth medium with a maximum concentration of 0.1% (v/v) DMSO. Larvae were then returned to the incubator and kept in solution until 5 days post fertilisation.

### 3.4.2 Cholesterol inhibitor treatment

Cholesterol synthesis inhibitors RO48-8071 (Enzo Life Sciences, 89197-69-1), U-18666A (Enzo Life Sciences, 3039-71-2), and AY9944 (Calbiochem, 366-93-8) were diluted in 100% DMSO to 10mM and stored at 4$^{O}$C. Zebrafish were pooled in groups of 10 and manually dechorionated at 24 hours post fertilisation and treated with 1 µM, 2 µM, or 5 µM RO48-8071; 5 µM, 10 µM, or 20 µM U-18666A; 5 µM, 10 µM, or 20 µM AY9944 in E3 growth medium. A staggered combination treatment of AY9944 and U-18666A was applied at either 10 µM or 20 µM of both compounds, with AY9944 treatment preceding U-18666A treatment by one hour. The total concentration of DMSO did not exceed 0.1% (v/v) in any treatment group. Larvae were returned to the incubator and kept in solution until 5 days post fertilisation.

### 3.4.3 Sterol supplementation

Lanosterol (Sigma-Aldrich, 79-63-0) was dissolved in ethanol (Sigma-Aldrich, 64-17-5) at 10 mM. Inhibitor-treated zebrafish were supplemented with 20 µM or 40 µM lanosterol in E3 growth medium at 30 or 48 hours post fertilisation. Ethanol concentration did not exceed 0.1% (v/v) in any treatment group. Supplemented zebrafish were kept in E3 growth medium until euthanasia at 5 days post fertilisation.

### 3.4.4 Deuterium-tagged sterol supplementation

Deuterated lanosterol d6 (Avanti Polar Lipids, 28290-39-3), and deuterated cholesterol d6 (Avanti Polar Lipids, 60816-17-3) were dissolved in dichloromethane (Sigma-Aldrich, 64-17-5) at 10 mM. Inhibitor-treated zebrafish were supplemented with 20 µM or 40 µM deuterated sterol in E3 growth medium at 30 or 48 hours post fertilisation. Dichloromethane concentration did not exceed 0.1% (v/v) in any treatment group. Supplemented zebrafish were kept in E3 growth medium until euthanasia at 5 days post fertilisation.

### 3.4.5 Fluorescent cholesterol tracking

Zebrafish were incubated with 100 µM TopFluor Bodipy cholesterol (Avanti Polar Lipids, 878557-19-8) at 2 days post fertilisation for 5, 6, 18 and 24 hours. Larvae were washed in E3 growth medium and then stunned on ice and anaesthetised with 1X MS-222 in fresh E3 growth medium prior to being imaged with a Leica SP5 II (Leica) laser scanning confocal microscope equipped with an argon 488 laser. Images were captured using a Leica HCX PL APO lambda blue 10X 1.52 OIL UV and a Leica HCX PL APO lambda blue 40X 1.52 OIL UV objective and processed using Fiji (309).

Fertilised zebrafish eggs were manually dechorionated at 6 hours post fertilisation (approximately 70% epiboly) and incubated with 100 µM TopFluor Bodipy cholesterol until the 25-somite developmental stage at 30 hours post fertilisation. Larvae were anaesthetised and imaged as mentioned previously.

## 3.5 Analysis of lipid content

### 3.5.1 Isolation of lipids from zebrafish larvae

Lipids were isolated using a modified Bligh-Dyer method (310). Tissue from euthanised zebrafish was pooled to 10 $mgmL^{-1}$ wet weight per sample and kept on ice in PBS 1X. All glassware was serially rinsed with methanol and hexane. Each tissue sample was added to a clean glass culture tube (Pyrex) and suspended in 2 mL dichloromethane : methanol (1:2). Tubes were vortexed for 30 seconds and incubated for 30 minutes at room temperature. Following incubation, 0.67 mL dichloromethane was added, and tubes were vortexed. A further 1.2 mL of 0.9% (w/v) KCl was added, and tubes were vortexed for 30 seconds and centrifuged for 5 minutes at $RCF_{AV}$ 1000 x g (2250 rpm) at room temperature in a GS6r centrifuge (Beckman Coulter). The organic phase was collected via aspiration and dried in a glass culture tube under a nitrogen gas stream using a sample evaporator (VLM Labtec). Desiccated lipids were resuspended in 0.2 mL iminodiacetic acid (Sigma-Aldrich, 142-73-4) : dichloromethane (Sigma-Aldrich, 75-09-2) (1:1) and stored in glass autosampler tubes (Pyrex) at -20$^{O}$C.

### 3.5.2 Isolation of lipids from bovine lens membranes

Membrane fractions from bovine lenses were diluted to 10 $mgmL^{-1}$ wet weight per and kept on ice in PBS 1X. All glassware was serially rinsed with methanol and hexane. Each tissue sample was added to a clean glass culture tube (Pyrex) and suspended in 2mL dichloromethane : methanol (1:2). Tubes were vortexed for 30 seconds and incubated for 30 minutes at room temperature. Following incubation, 0.67 mL dichloromethane was added and tubes were vortexed. A further 1.2 mL of 0.9% (w/v) KCl was added, and tubes were vortexed for 30

seconds and centrifuged for 5 minutes at $RCF_{AV}$ 1000 x g (2250 rpm) at room temperature in a GS6r (Beckman Coulter) centrifuge. The organic phase was collected via aspiration and dried in a glass culture tube under a nitrogen gas stream using a sample evaporator (VLM Labtec). Desiccated lipids were resuspended in 0.2m L iminodiacetic acid : dichloromethane (1:1) and stored in glass autosampler tubes (Pyrex) at -20$^{O}$C.

### 3.5.3 Liquid chromatography – mass spectrometry

Spike-in deuterated control lipids were introduced to samples prior to loading. Lipid detection and quantification was performed using a Shimadzu UHPLC system linked to a triple-quadrupole mass spectrometer, with electrospray ionisation in positive mode (ESI+, QTRAP 6500, AB Sciex). Chromatographic separation was performed on a Cortecs UPLC column (100x2.1 mm, 1.6 µm pore, Waters) with mobile phases A and B. Mobile phase A consisted of acetonitrile (Sigma-Aldrich, 75-05-8) : $H_2O$ (Merck Millipore) (60:40), 10 mM $NH_4HCO_2$ (Sigma-Aldrich, 540-69-2), 0.1% (w/v) formic acid (Sigma-Aldrich, 64-18-6). Mobile phase B consisted of acetonitrile : isopropanol (Sigma-Aldrich, 67-63-0) (1:1), 10 mM $NH_4HCO_2$, 0.1% (w/v) formic acid. The column was programmed to a flow rate of 140 µL/minute at maintained at 60$^{O}$C. The analyte peak area of elution curves was calculated in the quantification mode of the Analyst 1.6.2 software package (Sciex).

## 3.6 Preparation of protein samples for polyacrylamide gel electrophoresis (PAGE)

### 3.6.1 Sample preparation for sodium dodecyl sulphate (SDS)-PAGE

Protein samples were diluted to the desired concentration in loading buffer (see recipe Table 3.3) and mixed with loading dye prior. Bovine lens membrane material was not boiled prior to use.

### 3.6.2 Sample preparation for clear native (CN)-PAGE

Protein samples were diluted to the desired concentration in SDS-free loading buffer (see recipe Table 3.3) and mixed with SDS-free loading dye. Samples were not boiled prior to use.

## 3.7 Protein quantification assays

### 3.7.1 SDS-PAGE and CN-PAGE

Sodium dodecyl sulphate polyacrylamide gels (SDS-PAG) were cast with acrylamide concentrations of 8%, 10%, 12%, or 15%. Polyacrylamide separating gels were topped with 5% polyacrylamide stacking gels. Gels for clear native polyacrylamide gel electrophoresis (PAGE) were cast in the absence of SDS. All gel recipes can be found in Table 3.3 in section 3.10.1.1.

Gels were run in a Bio-Rad Mini-PROTEAN Tetra vertical electrophoresis cell (Bio-Rad) at a constant voltage 150 V for 45 minutes in 1X running buffer. All gels were fixed in gel fixative solution and stained with 0.25% (w/v) Coomassie brilliant blue R-250 (Sigma-Aldrich, 6104-59-2) prior to imaging. Gels were visualised on a Fujifilm LAS-1000plus Luminescent Image Analyser and processed in Fiji (manufacturer).

### 3.7.2 Western blot

#### *3.7.2.1 Semi-dry transfer*

Whatman cellulose filter paper (Whatman) was cut to size to cover a Bio-Rad Mini-PROTEAN Tetra front glass plate. Six pieces of filter paper were submerged in transfer buffer A, three pieces in transfer buffer B, and nine pieces in transfer buffer C. Transfers were performed as described by Kyhse-Andersen (311).

Nitrocellulose membranes were then washed in di$H_2O$ and stained for 5 minutes at room temperature with 0.1% (w/v) Ponceau S (Sigma-Aldrich, 6226-79-5) in light safe conditions to confirm sufficient protein binding. Membranes were washed three times in di$H_2O$ and blocked with blocking buffer A or C for one hour at room temperature prior to antibody probing.

#### *3.7.2.2 Primary antibody probing*

Primary antibodies were titrated in appropriate blocking buffer and stored at -20$^{O}$C. Nitrocellulose membranes were probed with primary antibodies in sealed polyurethane bags for 16 hours at 4$^{O}$C on an agitating plate. Membranes were washed three times in TBST 1X, and the primary antibody solution was reserved and stored at 4$^{O}$C until further use. Primary antibody solutions were used a maximum of ten times or until binding quality was insufficient against control samples.

#### *3.7.2.3 Secondary antibody probing*

HRP-conjugated goat anti-mouse (manufacturer) and anti-rabbit (manufacturer) antibodies were diluted in blocking buffer B at 1:10000 (v/v) concentration as per manufacturer's protocol. Nitrocellulose membranes were probed in sealed polyurethane bags for 1 hour at room temperature on an agitating plate. Membranes were washed three times in TBST 1X prior to immediate visualisation.

#### *3.7.2.4 Visualisation*

Equal volumes of ECL1 and ECL2 solutions were mixed and immediately applied to probed nitrocellulose membranes. Membranes were incubated in the dark at room temperature prior to being imaged on a Fujifilm LAS-1000plus Luminescent Image Analyser. Membranes were washed with TBST 1X and stored in TBS 1X at 4$^{O}$C.

#### *3.7.2.5 BCA*

Protein stock concentrations were recorded using a Nanodrop 2000 (Thermo Fisher). Protein concentrations of samples were determined via the Pierce BCA (bicinchoninic acid) assay kit (Thermo Scientific) using a BioTek ELx800 spectrophotometer (BioTek Instruments) equipped with a 562 nm filter (BioTek Instruments).

## 3.8 Data capture of zebrafish physical and behavioural phenotypes

### 3.8.1 Behavioural phenotype capture

Zebrafish were removed from total dark conditions and equilibrated at ambient artificial light and room temperature for 5 minutes without agitation or further visual stimuli. Larvae were then exposed to diffuse light from and LED source on a Nikon SMZ1270i stereo microscope (Nikon) and were observed for five minutes. Slow scoots were manually recorded for the following five minutes to assess independent movement of zebrafish (312). Larvae were then allowed five minutes to equilibrate to ambient artificial lighting conditions without physical agitation.

Each group of zebrafish was then exposed to a different stimulus to assess the startle response (313). Groups were either exposed to a strong burst of light from the microscope LED source, to light agitation for 5 seconds, or to physical contact on the tail with a dissection needle. C-starts and burst swims were recorded manually for the following minute.

### 3.8.2 Physical phenotype capture

Zebrafish were stunned on ice and anaesthetised using 0.5X MS-222 (Sigma). Pooled zebrafish were imaged using a Nikon SMZ1270i stereo microscope (Nikon) equipped with an LED diascopic illumination stand at 5X optical zoom. Images were recorded using the accompanying Nikon software suite, and physical size data were obtained using Fiji (309).

## 3.9 Statistical analyses

### 3.9.1 Kaplan-Meier survival curves

Zebrafish larvae were pooled into groups of fifty per clutch and followed until 5 days post fertilisation to calculate the survival rate S=(t) of different experimental conditions. A Kaplan-Meier estimate (314) was used to analyse the direct effect of treatments and supplementations on zebrafish viability. Unfertilised eggs were excluded from the analysis. All data processing and statistical analysis was performed in Microsoft Excel (Microsoft).

### 3.9.2 Behavioural phenotype analysis

Baseline activity and startle response indicators were manually recorded and pooled per treatment group. Welch ANOVA was used to analyse the difference between groups in Prism 5.01 (GraphPad Software Inc.), with $\alpha=0.05$.

### 3.9.3 Physical phenotype analysis

Measurements from the physical phenotype analysis were pooled per treatment group. Barlett's test was used to establish homoscedasticity, and Welch's ANOVA with $\alpha=0.05$ was used to determine the effect of pharmacological treatment on body size, yolk size, eye size, and eye aspect ratio. Games-Howell was used for post-hoc analysis to identify significantly different means, with $\alpha=0.05$.

### 3.9.4 LCMS analysis

All LCMS lipidomic experiments were conducted in triplicate using pooled biological samples. Lipid peak analyte absolute areas were normalised against the peak area values of spiked-in lipid standards.

### 3.9.5 Protein quantification assays

Protein quantification assays were conducted in triplicate from pooled, age-matched biological samples. Barlett's test was used to establish homogeneity of variance, and one-way ANOVA with $\alpha=0.05$ was used to determine the effect chemical treatment on protein solubility. Tukey's HSD test was used for post-hoc analysis to identify statistical significance between group means, with $\alpha=0.05$.

## 3.10 List of reagents

### 3.10.1 Zebrafish procedures

Table 3.1. Buffers and reagents used in zebrafish larvae growth, maintenance, and euthanasia.

| REAGENT | COMPONENTS | AMOUNT | SPECIFICATIONS |
|---|---|---|---|
| E3 Zebrafish Growth Medium 60X | NaCl<br>KCl<br>$CaCl_2$ 2H2O<br>$MgCl_2$ $6H_2O$ | 34.8g<br>1.6g<br>5.8g<br>9.78g | Make up to 1L with deionised water ($diH_2O$)<br>Adjust to pH 7.2, Store at room temperature |
| MS-222 (Tricaine) 20X | MS-222<br>1M Tris pH 7<br>$diH_2O$ | 400mg<br>2.1mL<br>97.9mL | Adjust to pH 7, store at -20$^{O}$C |
| PBS 10X | NaCl<br>KCl<br>$Na_2HPO_4$<br>$KH_2PO_4$ | 80g<br>2g<br>14.4g<br>2.4g | Make up to 1L with $diH_2O$<br>Adjust to pH 7.4, Store at room temperature |

#### *3.10.1.1 Protein assays*

Table 3.2. Buffers used in fractionation of high protein content and low protein content integral lens membranes

| REAGENT | COMPONENTS | FINAL CONCENTRATION | SPECIFICATIONS |
|---|---|---|---|
| Buffer 1 | $NaPO_4$ pH 7.4<br>NaCl<br>EDTA | 10mM<br>100mM<br>5mM | Store at room temperature |
| Buffer 2 | $NaPO_4$ pH 7.4<br>KCl<br>EDTA | 10mM<br>1.5M<br>5mM | Store at room temperature |
| Buffer 3 | $(NH_4)HCO_3$<br>EDTA | 100mM<br>1mM | Store at room temperature |
| Buffer 4 | $NaPO_4$ pH 7.4<br>Urea<br>EDTA | 10mM<br>8M<br>5mM | Make fresh |
| Buffer 5 | NaOH | 100mM | Store at room temperature |

Table 3.3. Reagents used in SDS-PAGE and CN-PAGE

| REAGENT | COMPONENTS | AMOUNT or CONCENTRATION | SPECIFICATIONS |
|---|---|---|---|
| SDS-PAGE Running buffer 10X | Tris base<br>Glycine<br>SDS | 30.3g<br>144.4g<br>10g | Make up to 1L with $diH_2O$<br>Store at room temperature |
| Sample buffer 5X | bromophenol blue<br>DTT<br>Glycerol<br>SDS<br>Tris pH 8 | 0.25% (w/v)<br>0.5M<br>50% (w/v)<br>10% (w/v)<br>0.25M | Filter and store at -20$^{O}$C |
| Stacking polyacrylamide gel (5% v/v) 5mL | $diH_2O$<br>30% acrylamide : bis-acrylamide (37.5:1)<br>0.5M Tris pH 6.8<br>10% (w/v) SDS<br>10% (w/v) APS<br>TEMED | 3mL<br>0.67mL<br>1.25mL<br>50µL<br>75µL<br>5µL | Store hydrated at 4$^{O}$C |
| Separating polyacrylamide gel (10% v/v) 8mL | $diH_2O$<br>30% acrylamide : bis-acrylamide (37.5:1)<br>1.5M Tris pH 8.8<br>10% (w/v) SDS<br>10% (w/v) APS<br>TEMED | 3.2mL<br>2.67mL<br>2mL<br>80µL<br>80µL<br>8µL | Store hydrated at 4$^{O}$C |
| Separating polyacrylamide gel (12% v/v) 8mL | $diH_2O$<br>30% acrylamide : bis-acrylamide (37.5:1)<br>1.5M Tris pH 8.8<br>10% (w/v) SDS<br>10% (w/v) APS<br>TEMED | 3.4mL<br>2.4mL<br>2mL<br>80µL<br>80µL<br>8µL | Store hydrated at 4$^{O}$C |
| Separating polyacrylamide gel (15% v/v) 8mL | $diH_2O$<br>30% acrylamide : bis-acrylamide (37.5:1)<br>1.5M Tris pH 8.8<br>10% (w/v) SDS<br>10% (w/v) APS<br>TEMED | 2.8mL<br>3mL<br>2mL<br>80µL<br>80µL<br>8µL | Store hydrated at 4$^{O}$C |
| Gel fixative | Methanol<br>Acetic acid glacial<br>$diH_2O$ | 50% (v/v)<br>10% (v/v)<br>40% (v/v) | Store at room temperature |
| Gel destain | Methanol<br>Acetic acid glacial<br>$diH_2O$ | 50% (v/v)<br>10% (v/v)<br>40% (v/v) | Store at room temperature |
| Coomassie staining solution | Coomassie Brilliant Blue R-250<br>Methanol<br>Acetic acid glacial<br>$diH_2O$ | 0.25% (w/v)<br><br>20% (v/v)<br>10% (v/v) | Store at room temperature in light-safe conditions |
| PageRuler Plus prestained protein ladder 10kDa to 250kDa (Thermo Scientific) | | 2µL per well | Store at -20$^{O}$C |

Table 3.4. Reagents used in semi-dry Western blot transfer and membrane visualisation

| REAGENT | COMPONENTS | AMOUNT or CONCENTRATION | SPECIFICATIONS |
|---|---|---|---|
| TBS 10X | Tris base<br>NaCl | 24g<br>88g | Make up to 1L with $diH_2O$<br>pH to 7.6 and store at room temperature |
| TBST 1X | TBS 10X<br>Tween-20 | 10% (v/v)<br>0.1% (v/v) | Store at room temperature |
| Transfer buffer A | Tris base<br>Methanol | 0.3M<br>20% (v/v) | Store at room temperature |
| Transfer buffer B | Tris base<br>Methanol | 0.025M<br>20% (v/v) | Store at room temperature |
| Transfer buffer C | Tris<br>Glycine<br>Methanol | 0.025M<br>0.04% (w/v)<br>20% (v/v) | Store at room temperature |
| Blocking buffer A | skimmed milk powder<br>TBST 1X | 5% (w/v) | Store at -20$^{O}$C |
| Blocking buffer B | Bovine serum albumin<br>TBST 1X | 2% (w/v) | Store at -20$^{O}$C |
| Blocking buffer C | skimmed milk<br>Bovine serum albumin<br>TBST 1X | 5%(w/v)<br>2% (w/v) | Store at -20$^{O}$C |
| ECL 1 | luminol 250mM<br>coumaric acid 90mM<br>Tris 1M pH 8.5<br>$dH_2O$ | 1mL<br>0.44mL<br><br>10mL<br>Make up to 100mL | Store at -20$^{O}$C |
| ECL 2 | hydrogen peroxide 30% (v/v)<br>Tris 1M pH 8.5<br>$dH_2O$ | 64µL<br><br>10mL<br>Make up to 100mL | Store at -20$^{O}$C |
| Ponceau staining solution | Ponceau S<br>Acetic acid glacial<br>$diH_2O$ | 0.1% (w/v)<br>1% (v/v)<br>99% (v/v) | Store at room temperature in light safe conditions |
| Mild stripping buffer | Glycine<br>SDS<br>Tween-20 | 15g<br>1g<br>10mL | Adjust to pH 2.2, make up to 1L with $diH_2O$<br>Store at room temperature |

### *3.10.1.2 Primary and secondary antibodies*

Table 3.5. Primary and secondary antibodies used in western blot

| ANTIBODY | CODE AND MANUFACTURER | FINAL CONCENTRATION |
|---|---|---|
| Anti-mouse HRP conjugated | Sigma 12-349 | 0.1µgmL$^{-1}$ |
| Anti-rabbit HRP conjugated | Sigma 12-348 | 0.1µgmL$^{-1}$ |
| Anti-AQP0 (mouse) | Sigma-Aldrich B-11 | 1µgmL$^{-1}$ |
| Anti-connexin 50 | Abcam ab222885 | 1µgmL$^{-1}$ |
| Anti-actin AC 40 | Abcam11003 | 0.5µgmL$^{-1}$ |
| Anti-vimentin | In-house 3052 | 2µgmL$^{-1}$ |
| Anti-phosphovimentin (S38) | Abcam ab52942 | 1µgmL$^{-1}$ |
| Anti-caveolin 1 | Abcam ab2910 | 1µgmL$^{-1}$ |
| Anti-BFSP1 | In-house 3241 | 2µgmL$^{-1}$ |
| Anti-BFSP2 | In-house 2981 | 2µgmL$^{-1}$ |
| Anti-αA crystallin | In-house 3273 | 2µgmL$^{-1}$ |
| Anti-αB crystallin | In-house 3148 | 1µgmL$^{-1}$ |
| Anti-γC crystallin | In-house | 1µgmL$^{-1}$ |

#### *3.10.1.3 Pharmacological inhibitors, lipids, and chemicals*

Table 3.6. Pharmacological inhibitors used in zebrafish cholesterol metabolism studies, lipids and lipid standards used in mass spectrometry and zebrafish metabolism studies, chemicals used in protein solubility studies

| REAGENT | CODE AND MANUFACTURER | STOCK CONCENTRATION |
|---|---|---|
| T0901317 | Sigma-Aldrich 293754-55-9 | 10mM in DMSO |
| GW3965 | Sigma-Aldrich 405911-17-3 | 10mM in DMSO |
| RO48-8071 | Enzo Life Sciences 189197-69-1 | 10mM in DMSO |
| AY9944 | Calbiochem 366-93-8 | 10mM in DMSO |
| U-18666A | Enzo Life Sciences 3039-71-2 | 10mM in DMSO |
| Lanosterol | Sigma-Aldrich 79-63-0 | 500µM in ethanol |
| Lanosterol d6 | Avanti Polar Lipids 28290-39-3 | 500µM in dichloromethane |
| Cholesterol d6 | Avanti Polar Lipids 60816-17-3 | 10mM in dichloromethane |
| TopFluor Bodipy Cholesterol 488 | Avanti Polar Lipids 878557-19-8 | 10mM in DMSO |
| 25-hydroxycholesterol d6 | Avanti Polar Lipids 64907-22-8 | 10mM in dichloromethane |
| Roche cOmplete Mini | Sigma-Aldrich | As per manufacturer's instruction |
| Iodoacetamine | Sigma-Aldrich 144-48-9 | 1M in DMSO |
| E46 | Sigma-Aldrich 66701-25-5 | 1mM in DMSO |
| Leupeptin | Sigma-Aldrich 103476-89-7 | 1mM in DMSO |
| Bovine α-crystallin | Sigma-Aldrich 11046-99-4 | 3.3mgmL$^{-1}$ in 100mM NaCl 5mM EDTA |

# 4 Chapter 4: Alterations of cholesterol metabolism produce behavioural and physical phenotypes in zebrafish larvae

## 4.1 Lipid metabolism in the zebrafish

### 4.1.1 The cholesterol synthesis pathway

Cholesterol biosynthesis is a regulated process which is highly conserved across vertebrates. Due to near identity of the biosynthetic pathway across a wide range of animals, synthesis inhibitors including human cholestatic drugs are highly effective in the majority of model organisms including the zebrafish (315).

There are five major regulatory units in vertebrate cholesterol synthesis, starting from the conversion of acetyl-CoAs to 3-hydroxy-3-methylglutaryl-CoA (HMG-CoA), the conversion of HMG-CoA to mevalonate, mevalonate to isopentenyl pyrophosphate (IPP), IPP to squalene, and finally the conversion of squalene to cholesterol. A full flow diagram can be found in Appendix 1, while an abridged version can be seen below in figure 4.1.

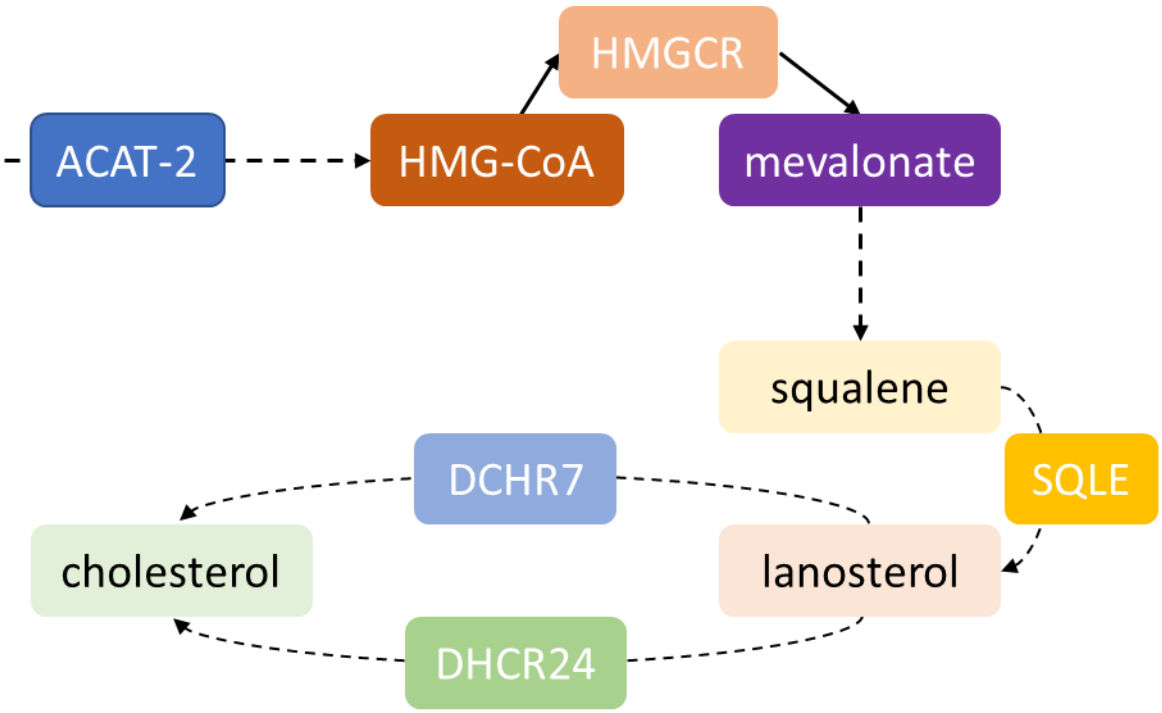


Figure 4.1.The major steps in the cholesterol synthesis pathway

Cytosolic synthesis of acetoacetyl-CoA from acetyl-CoA is initiated by the action of acetyl-CoA acetyltransferase 2 (ACAT2) and is followed by a further addition of acetyl-CoA by HGM-CoA synthase (HMGS1) to form HMG-CoA. The endoplasmic reticulum (ER) bound enzyme HMG-CoA reductase (HMGR) then mediates the conversion of HMG-CoA to mevalonate via the consumption of $NADPH^{+}$, which is the major rate limiting step in cholesterol biosynthesis (316).

Mevalonate is serially phosphorylated in an adenosine triphosphate (ATP) dependent manner by mevalonate kinase (MVK) to produce mevalonate 5-phosphate and then by phosphomevalonate kinase (PMVK) to produce mevalonate 5-diphosphate. Finally, an ATP dependent decarboxylation catalysed by diphosphomevalonate decarboxylase (MVD) converts mevalonate 5-diphosphate to isopentenyl pyrophosphate (IPP).

IPP is converted to squalene in three steps. The conversion of IPP to geranyl pyrophosphate (GPP) is followed by its further conversion to farnesyl pyrophosphate (FPP) via the action of farnesyl diphosphate synthase (FDPS). Two molecules of FPP are then used by farnesyl diphosphate farnesyltransferase 1 (FDFT1) to produce squalene.

Squalene undergoes two serial cyclizations, initially catalysed by squalene epoxidase (SQLE) to produce 2,3-oxidosqualene and followed by lanosterol synthase (LSS) to produce lanosterol.

Lanosterol is eventually converted to cholesterol via two distinct pathways which take place in the ER and peroxisomes. In the Bloch pathway (317), four reactions lead to the formation of zymosterol which is the first 27-carbon cholesterol precursor. In the Kandutsch-Russell pathway (317), zymostenol is the equivalent 27-carbon molecule. Zymosterol is converted to desmosterol in three steps in the Bloch pathway, which is then converted to cholesterol in a final step catalysed by dehydrocholesterol reductase 24 (DHCR24), whereas zymostenol is converted to lathosterol and then 7-dehydrocholesterol which is the major cholesterol precursor. Dehydrocholesterol reductase 7 (DHCR7) catalyses the conversion of 7-dehydrocholesterol to cholesterol, with vitamin D being a major alternative product of 7-dehydrocholesterol processing.

### 4.1.2 Cholesterol metabolism

Cholesterol undergoes further modifications either via oxidation in the liver to produce bile acids, or via conversion to steroid hormones in the adrenal glands and the gonads (318). In the context of bile acid synthesis, the two major enzymes cytochrome P7A1 (CYP7A1) and CYP27A1 catalyse hydroxylation of cholesterol on carbons 7 and 27 respectively. CYP7A1 is the rate limiting enzyme in the classic pathway of bile acid synthesis (317) and deficiencies in its function result in increased total cholesterol and relevant cardiovascular and neurological pathologies. CYP27A1 is a mitochondrial enzyme and acts with cofactor proteins ferrodoxin 1 and ferrodoxin reductase on several different sterols. Deficiencies in CYP27A1 have been associated with progressive neurological disorders and congenital bilateral cataracts, as discussed in section 1.3.

Oxysterols are bioactive molecules which influence cholesterol metabolism via their function on liver x receptors (LXR) and sterol regulatory element binding protein (SREBP) activation. Two LXR variants have been characterised in humans; LXRα is expressed in tissues involved in lipid metabolism such as liver, small intestine, and adipose while LXRβ is ubiquitously expressed (319). Major oxysterol regulators of LXR activity include 27-hydroxycholesterol (27-OHC), which has also been implicated in ocular health (264). Downstream targets of LXRs include metabolic rate-limiting enzymes such as CYP7A1, and in the liver LXR activation induces the expression of SREBP-1c (320). The cleavage and activation of SREBP-1c directly regulates the degradation of HMGR, which is the rate limiting enzyme in cholesterol biosynthesis, via the action insulin-induced proteins 1 and 2 (INSIG-1, -2). While LXRs are not known to be mechanistically linked with lens components such as crystallins, their major function as sterol metabolism regulators presents an interesting target both for local and systemic oxysterol homeostasis.

### 4.1.3 Sterol metabolism in the developing zebrafish

#### *4.1.3.1 Direct inhibition of cholesterol synthesis*

The zebrafish has gained increasing popularity as an *in vivo* model of lipid metabolism and associated pathologies due to its ease of use and its conserved similarities as compared to human lipid synthesis and trafficking (90,315,319). Zebrafish larvae form the major lipid metabolism organs including the liver, intestine, pancreas, and gallbladder early in development in addition to the cardiovascular system. Unlike rodents such as the mouse, zebrafish express the same transcription factors as humans in the regulation of sterol synthesis including SREBP (320) and have been shown to closely mimic human biological processes better than the mouse in drug trials (321,322).

Embryos rely on the yolk supply of maternal lipids for nutrient needs until 4 days post fertilisation (dpf) (315), which provides triacylglycerol (TAG), lipid-soluble vitamins and sterols. During this time, the yolk-syncytial layer (YSL) harbours the lipoproteins and enzymes required for lipid transport and processing in intestinal absorption of the adult zebrafish, further highlighting the early developmental function of these pathways. Larvae typically deplete their yolk supply by 5 to 6 dpf and rely on a lipid-rich diet throughout their remaining lifespan, with a minimum 10% (w/w) phospholipid and sterol content.

Pharmacological inhibition of cholesterol synthesis by statins has been shown to result in developmental arrest of larvae due to impaired primordial germ cell (PGC) migration which arises from deficiencies in the prenylation pathway (323). As such, it is evident that

manipulating cholesterol synthesis at a critical step such as HMGR has broad consequences on zebrafish development.

Inhibition of HMGR at the beginning of organogenesis has also been shown to result in impaired ciliogenesis and loss of ciliary function due to cholesterol depletion in zebrafish, an effect which can be rescued via concurrent cholesterol supplementation (316).

#### *4.1.3.2 The role of LXRs in zebrafish vision*

Previous reports have established that zebrafish express a single LXR form *lxr* which resembles human LXRα and has been detected both in metabolic tissues such as intestine and liver, but also in brain, neural retina, and the lens (319); this expression profile remains ubiquitous from development through to adulthood. The LXR agonists T0901317 and GW3965 (see appendix figure A1. 0-4) have shown to activate lxr *in vivo* from 4 dpf, which has downstream effects on genes involved in lipid metabolism and ocular health. In the lens, upregulation of the gamma crystallins *crygs2* and *crygs3* and downregulation of the zebrafish-specific crystallins *crygm2* and *crygm3* have been observed as a result of T0901317 and GW3965 treatment, in parallel to increased uptake of yolk lipids at 6 dpf (319). At the earlier developmental timepoint of 6 hours post fertilisation (hpf) these agonists have been shown to result in disorganised retinal and lens epithelia, though whether this is a consequence of lens- and retina-specific processes or a result of altered cholesterol metabolism remains to be established (319).

## 4.2 Experimental design and objectives

Aberrations in the cholesterol synthesis and metabolism pathways have been shown to implicate a broad variety of tissues, and as such it is important to take into consideration the overall viability of model organisms in the pursuit of either eye or lens specific phenotypes and potential cardiovascular or neurological adverse effects. In this study, targets were selected based on prior reports of human congenital cataracts being characteristic of metabolic pathologies: pharmacological agents were employed to examine the effects of reduced cholesterol synthesis due to LSS, DHCR7, DHCR24, and the combined DHCR7/DHCR24 inhibition. As previous reports have implicated LXR regulation in ocular development in zebrafish (319), pharmacological agonists were also utilised.

Zebrafish larvae were treated with the aim of observing the effect of reduced cholesterol synthesis on development and eye health. Further, sterol supplementation was explored as a method for phenotype rescue.

## 4.3 Pharmacological inhibition of cholesterol synthesis produces physical and behavioural phenotypes in viable zebrafish larvae

Zebrafish larvae were manually dechorionated at 24 hours post fertilisation (hpf) and separated into groups of 10 in separate culture dishes. Each dish group was treated with either an *LXR* agonist or a cholesterol synthesis inhibitor as described in Table 4.1.

### 4.3.1 LXR agonists and cholesterol synthesis inhibitors have varied effects and lethal concentrations

*LXR* agonists T0901317 and GW3965 were assessed for the production of any behavioural phenotype including altered independent motion and startle responses to light, agitation, or physical contact in order to determine whether dysfunction was purely optical or extended to a broader neurological effect. Concentrations tested were 1 µM, 2 µM, and 5 µM and zebrafish were followed to 5 days post fertilisation (dpf). Mortality measurements were recorded daily as shown in Figure 4.3. As neither GW3965 nor T0901317 produced a physical phenotype at tested maximum concentrations, the compounds were not used for further studies.

Similar to the above, cholesterol inhibitors RO48-8071, U-18666A, AY9944, and the staggered combination treatment AY9944/U-18666A were assessed for resulting behavioural and physical phenotypes, and lethality at 5 dpf following treatment of zebrafish at 24 hpf. Concentrations tested followed a geometric progression at 5 µM, 10 µM, and 20 µM for RO48-8071, U-18666A, and AY9944, whereas the AY9944/U-18666A treatment was limited to equal 10 µM or 20 µM doses, as seen in table 4.1. All treatment groups exhibited both behavioural and physical phenotypes, while all maximum concentrations tested resulted in >25% lethality at 5 dpf.

Table 4.1 Summary of cholesterol synthesis inhibitors and their effects. The *LXR* agonists T0901317 and GW3965 were used at concentrations of 1 µM, 2 µM, and 5 µM and produced behavioural phenotypes only while demonstrating lethality lower than 25% at the endpoint of 5 days post fertilisation. The LSS inhibitor RO48-8071 was used at identical concentrations and produced both behavioural and physical phenotypes while exhibiting significant lethality at the highest concentration of 5 µM. The DHCR24 and DHCR7 inhibitors U-18666A and AY9944 were used at concentrations of 5 µM, 10 µM, and 20 µM; both inhibitors produced behavioural and physical phenotypes and resulted in >25% lethality at the experimental endpoint. The staggered combination of AY9944/U-18666A inhibitors was used at paired concentrations of 10 µM and 20 µM, resulting in behavioural and physical phenotypes in the zebrafish larvae and significant lethality at 5 days post fertilisation at maximum concentration.

| COMPOUND | TARGET | CONCENTRATION | | | BEHAVIOURAL PHENOTYPE | | | PHYSICAL PHENOTYPE | | | >25% LETHALITY AT S(t) | | |
|---|---|---|---|---|---|---|---|---|---|---|---|---|---|
| T0901317 | LXR | 1 µM | 2 µM | 5 µM | YES | YES | YES | NO | NO | NO | NO | NO | NO |
| GW3965 | LXR | 1 µM | 2 µM | 5 µM | YES | YES | YES | NO | NO | NO | NO | NO | NO |
| RO48-8071 | LSS | 1 µM | 2 µM | 5 µM | YES | YES | YES | YES | YES | YES | NO | NO | YES |
| U-18666A | DHC24 | 5 µM | 10 µM | 20 µM | YES | YES | YES | YES | YES | YES | NO | NO | YES |
| AY9944 | DHCR7 | 5 µM | 10 µM | 20 µM | YES | YES | YES | YES | YES | YES | NO | NO | YES |
| AY9944 / U-18666A | DHCR7 / DHCR24 | 10 µM / 10 µM | 20 µM / 20 µM | N/A | YES | YES | N/A | YES | YES | N/A | NO | YES | N/A |

### 4.3.2 Partial inhibition of cholesterol synthesis reduces zebrafish independent motion and optomotor responses

All *LXR* concentrations produced behavioural phenotypes which included a dampened optokinetic response. At medium concentration of 2 µM, both T0901317 and GW3965 produced a complete loss of independent slow scoots at ambient light conditions following a 5-minute light equilibration period, as seen in Figure 4.2. A minimal slow scoot incidence of 1 was recorded at four minutes post equilibration in T0901317 zebrafish.

Similarly, at minimum concentration of 5 µM all cholesterol synthesis inhibitors reduced the total number of independent slow scoots, which are a form of undulatory locomotion (312,324,325). RO48-8071 treated zebrafish exhibited a complete loss of independent motion at all timepoints apart from two minutes post-equilibration, where one scoot was recorded in a group of 10 larvae. Zebrafish treated with U-1866A showed a similar movement pattern to the 0.1% (v/v) DMSO control group with a limited 2 scoots at one-minute post-equilibration as

opposed to 6 motions recorded in the control group. The combination treatment of AY9944/U-18666A resulted in a complete loss of all independent motion at 5 dpf, as shown in Figure 4.2.

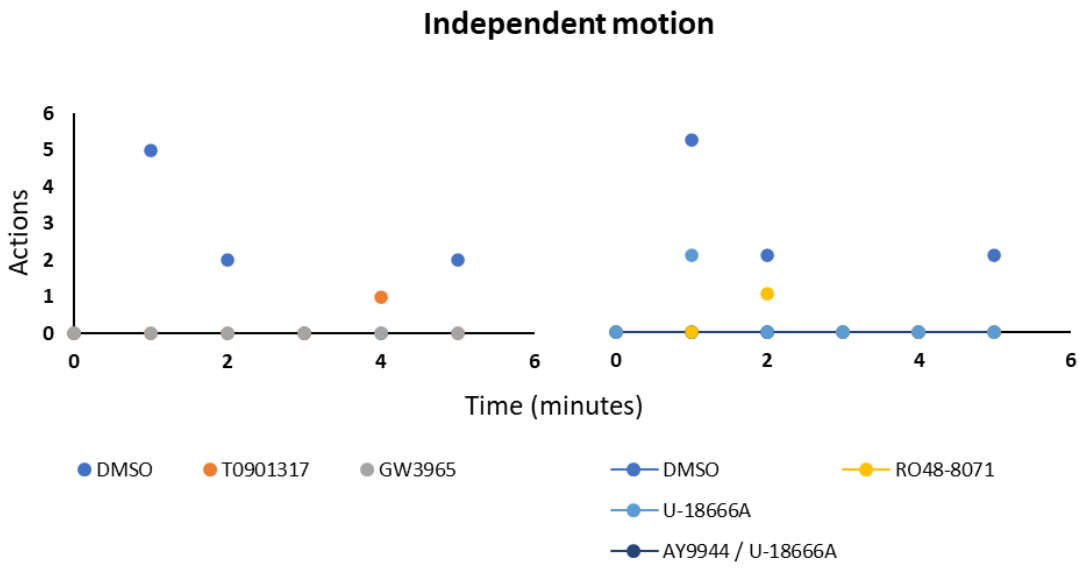


Figure 4.2. Independent motion was measured in treated wildtype zebrafish larvae at 5 days post fertilisation to assess the optokinetic response. Zebrafish were kept in total darkness from fertilisation to 5 days post fertilisation. Following a 5-minute equilibration at ambient artificial lighting conditions, the larvae were placed under a Nikon SMZ1270i dissection microscope and exposed to diffuse illumination and followed for a further five minutes. Slow scoots were recorded to quantify baseline movement at minute increments. Control zebrafish activity was concentrated to the first three minutes of increased light exposure, peaking at the first minute. Zebrafish exposed to *LXR* agonists had diminished baseline movement, with only one scoot recorded for the T0901317 group during the observation time. Similarly, cholesterol synthesis inhibitors reduced independent movement in larvae, with U-18666A and RO48-8071 treated fish showing 2 and 1 scoot within the first two minutes of observation. N=10 per treatment group pooled from separate clutches.

Following the equilibration and independent motion observation periods, zebrafish were exposed to one of three distinct stimuli to assess the effect of different treatments on the optokinetic and touch responses.

*LXR* treated groups showed a significantly reduced response to a sudden increase in illumination, as seen in Figure 4.3. Larvae treated with 2 µM GW3965 showed no response to a light pulse, whereas T0901317 treated zebrafish showed a significantly reduced number of movements with one burst swim recorded within one minute of stimulus exposure (p=0.048). The agitation response of T0901317 treated fish was not significantly reduced, whereas

GW3965 treatment resulted in a total of 3 burst swims over the first minute post-stimulus (p=0.0012). Neither T0901317 nor GW3965 treatment eliminated the touch-mediated startle response, as seen in Figure 4.4.

As with GW3965, all cholesterol synthesis inhibitor treatments resulted in the complete loss of the light-mediated startle response at the minimum tested concentrations (see table 4.1). Inhibitors RO48-8071 and U-18666A significantly reduced the response to agitation from nine motions for the control group to three for these treatment groups (p=0.012), whereas AY9944 and AY9944/U-18666A treatments further reduced the responses to two motions per group for the first minute post-stimulus (p=0.0098). All cholesterol inhibitors treatments failed to significantly reduce the touch-mediated startle response, except for the combined AY9944/U-18666A group where six burst swims were recorded as opposed to nine for the 0.1% (v/v) control group (p=0.042).

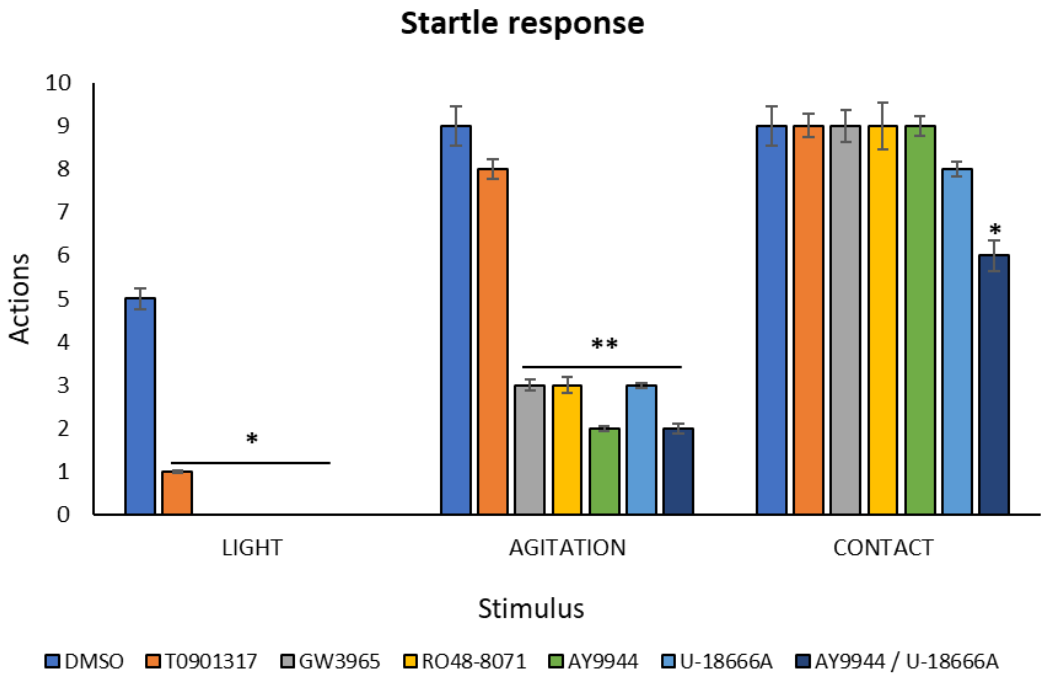


Figure 4.3. Following equilibration to the LED illumination in Figure x, zebrafish larvae were exposed to three different stimuli to assess their startle response. C-starts and burst swims were counted as single actions for one-minute post-stimulus, with each larval group exposed to one stimulus type. A single light flash did not elicit a response from any inhibitor-treated groups apart from the T0901317 zebrafish, which showed a significantly decreased incidence of movement. Light agitation of the growth dishes elicited significantly reduced responses from all inhibitor-treated zebrafish apart from T0901317 larvae. The touch-mediated response was preserved in all groups apart from the AY9944/U-1866A treated fish, which exhibited a

significantly reduced incidence of c-starts and burst swims upon contact. N=10 per treatment group from separate clutches. One-way ANOVA between columns, with * $p<0.05$, and ** $p<0.01$.

### 4.3.3 Pharmacological alteration of cholesterol synthesis in zebrafish larvae results in increased lethality at 5 days post fertilisation

A threshold of 25% lethality was established to determine the maximum viable concentration of each compound and a Kaplan-Meier survival plot (314) was used to analyse the data. Both lxr agonists resulted in low lethality at all tested concentrations, with the minimum survival ratio being 90% at 5 dpf. At 1 µM, T0901317 treatment resulted in 92% survival of larvae and GW3965 in 94% survival with the blank control at 96% and the 0.1% (v/v) DMSO control group at 94% survival at 5 dpf. The medium concentration of 2 µM produced a 92% and 90% survival for GW3965 and T0901317 treated zebrafish at 5 dpf, as compared to 96% and 94% survival of blank control and 0.1% (v/v) DMSO control groups. Finally, at 5 µM both GW3965 and T0901317 treatment resulted in 92% survival, whereas the blank control and 0.1% (v/v) DMSO groups showed 96% survival at 5 dpf. In all cases, the survival ratio of treated zebrafish larvae was not statistically distinct from control groups, as seen in Figure 4.4.

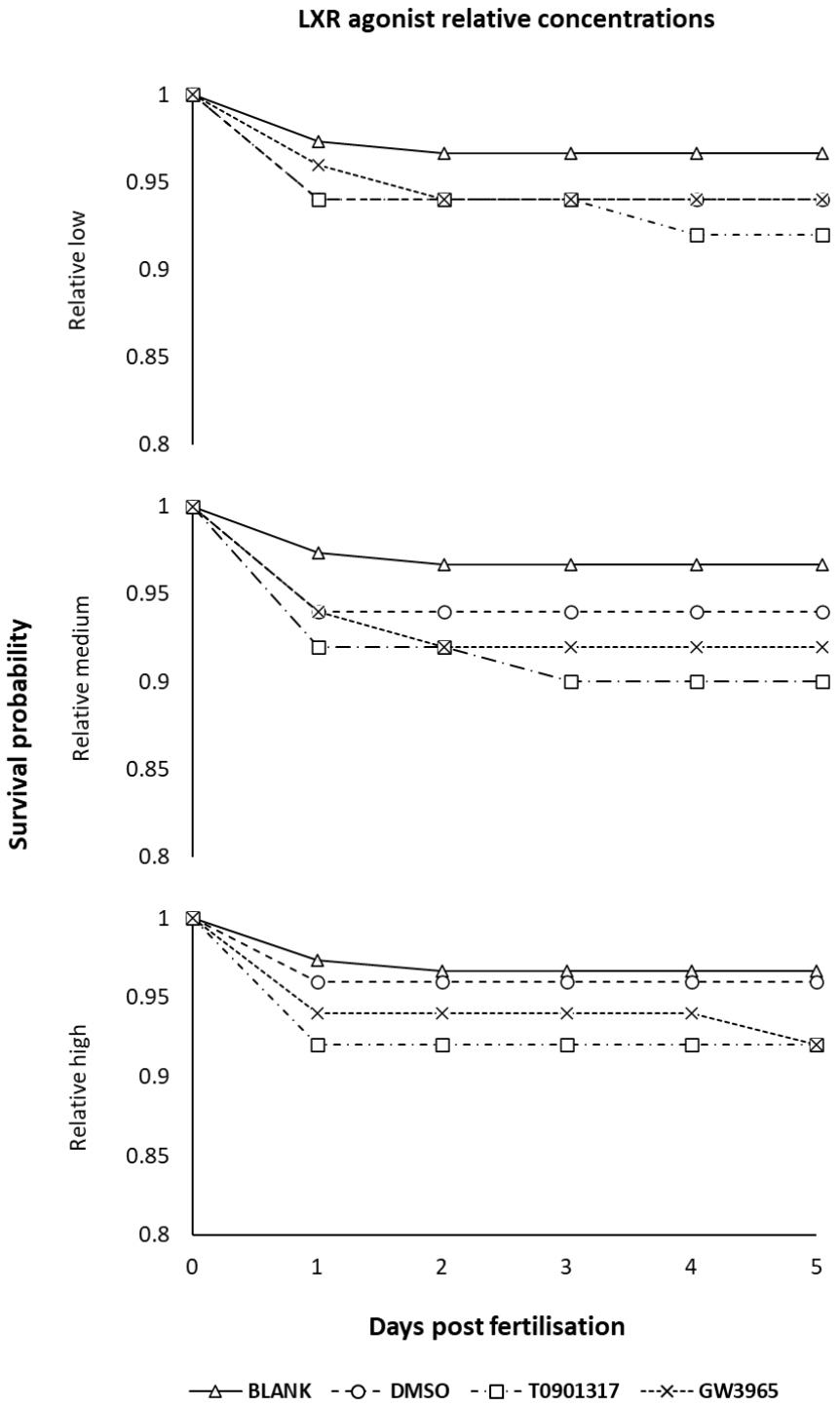


Figure 4.4. LXR agonists were tested against three concentration to assess toxicity. The compounds were administered to dechorionated embryos at 24 hours post fertilisation. All three concentrations showed a low lethality index of under 10% at 5 dpf, which was not significantly increased from the baseline mortality rate at 5 days post fertilisation of the negative and positive controls; n = 50 per treatment group pooled from separate clutches.

Cholesterol inhibitor lethality was significantly increased at relative high concentrations. At the lowest range of tested concentrations, survival of larvae exceeded 90% in all conditions including 94% survival for AY9944 and U-18666A treated groups, 92% survival for AY9944/U-18666A treated zebrafish, and 96% survival for RO48-8071 treated zebrafish as compared to the 97% survival of blank and 0.1% DMSO groups. Similar lethality ranges were recorded for the medium range concentrations of inhibitors with all treatments scoring a 90% survival and both control groups 94%, except for the combined AY9944/U-18666A treatment resulting in 100% lethality at 4 dpf as seen in Figure 4.5. As such, a higher concentration range for AY9944/U-18666A was not pursued. At the highest concentration range tested, AY9944 and U-18666A treatments resulted in 100% lethality at 2 dpf and 3 dpf respectively. At the maximum concentration of 5 µM, RO48-8071 failed to meet the minimum 25% lethality criterium resulting in a survival ratio of 72%, while the control groups exhibited a 96% and 94% survival for the blank and 0.1% (v/v) DMSO as seen in Figure 4.5.

From the data summarised in Table 4.1, the maximum viable concentration for each cholesterol inhibitor treatment was selected and analysed further. The concentrations used in all following sections are 2 µM RO48-8071, 10 µM U-18666A, 10 µM AY9944, and 10 µM each AY9944 and U-18666A for the combination treatment groups.

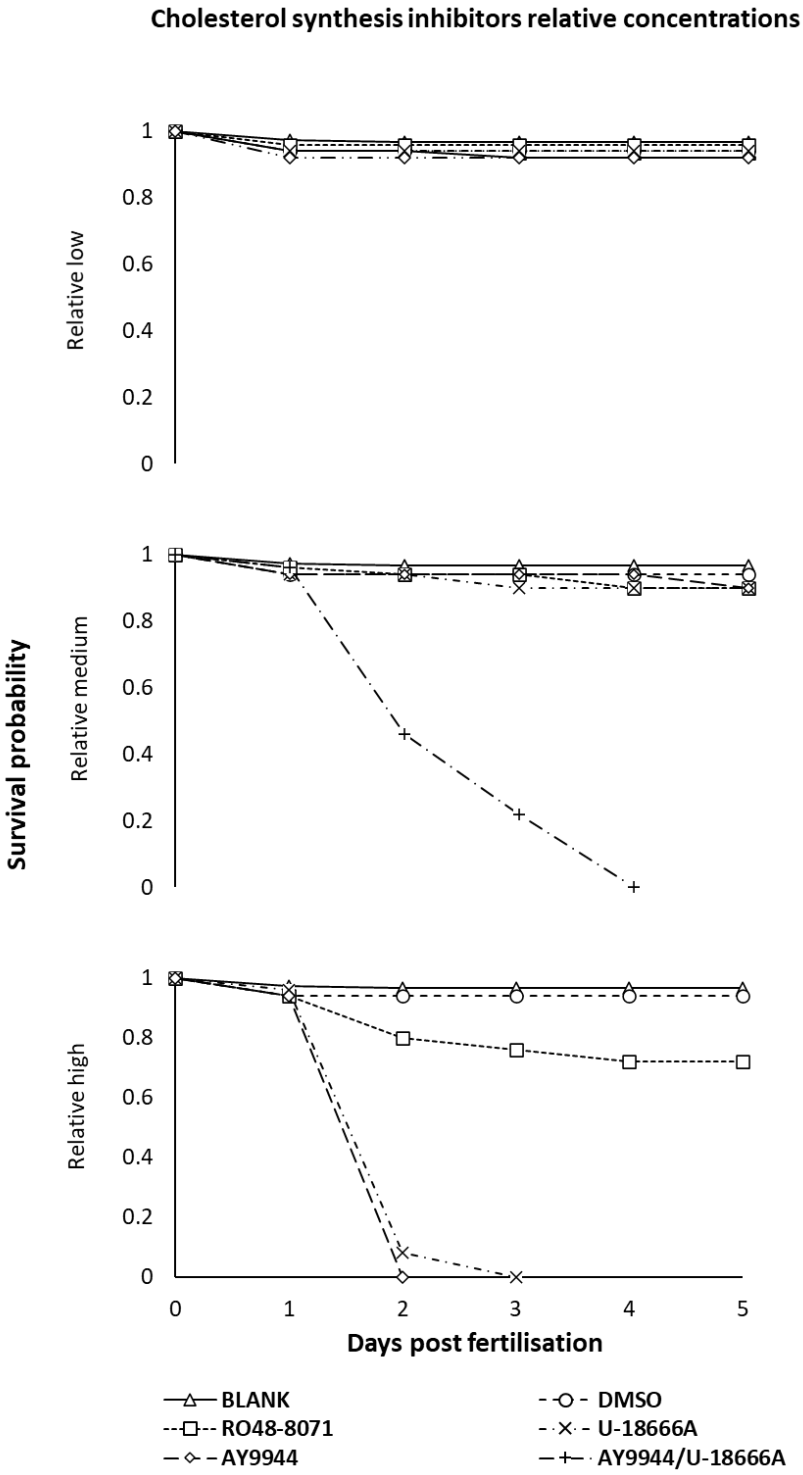


Figure 4.5. Pharmacological cholesterol synthesis inhibitors were tested against increasing concentrations to assess toxicity. The compounds were administered to dechorionated embryos at 24 hours post fertilisation. Combined AY9944/U-1866A treatment at 10 µM resulted at 100% lethality at 4 days post fertilisation, AY9944 and U-18666A treatment at 20 µM resulted in 100% lethality at 2- and 3-days post fertilisation. RO48-8071 treatment at 5 µM resulted in 28% lethality at 5 dpf. N=50 per treatment group pooled from separate clutches.

### 4.3.4 Pharmacological inhibitors of cholesterol synthesis reduce larval body size and yolk size

The physical phenotypes arising from the inhibition of cholesterol synthesis were analysed with respect to the lateral body area, the lateral yolk area, and the lateral eye area of zebrafish to characterise changes in the size of the larvae. Body size was measured using Fiji (309) and expressed as a percentage of the blank control group body area.

All inhibitor treatments significantly reduced the average body size of larvae, with Welch's ANOVA with $\alpha=0.05$ reporting a significant effect of treatment on the reduction of body size ($p < 0.0001$). Games-Howell post hoc analysis revealed no significant effect of 0.1% (v/v) DMSO supplementation on body size ($q=3.39$), whereas RO48-8071 ($q=9.85$), AY9944 ($q=7.56$), U-18666A ($q=12.77$), and AY9944/U-18666A ($q=4.29$) treatment significantly reduced body size as compared to the DMSO control group as seen in Figure 4.6.

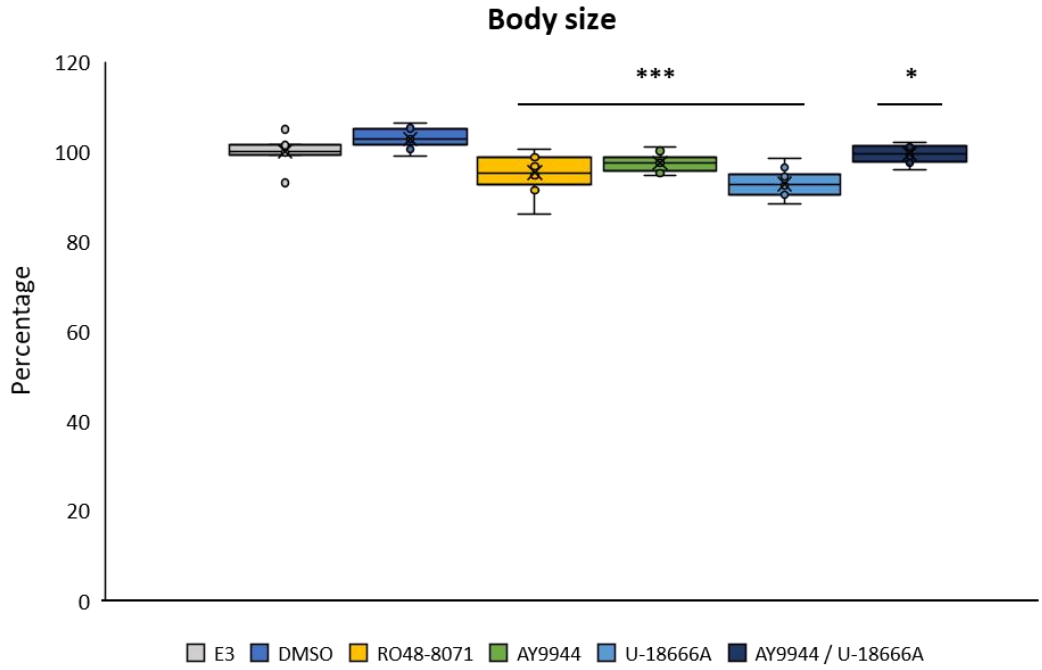


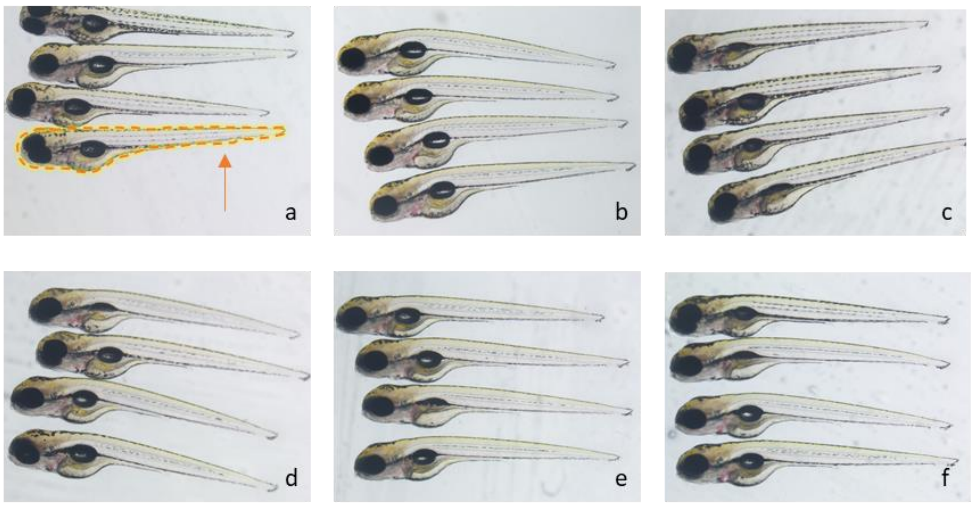

Figure 4.6. Zebrafish treated at 24 hours post fertilisation were assessed for body size at 5 dpf. Recorded decreases in body size, in ascending order, U-18666A showed a mean decrease of 7.3%, RO48-8071 a decrease of 4.7%, AY9944 a decrease of 2.48%, and the combination treatment of AY9944/U-18666A a decrease of 0.43%. All groups showed significant decrease in body size as compared to the 0.1% (v/v) DMSO vehicle control. No statistically significant difference was found between the 0.1% (v/v) DMSO vehicle control when compared to the growth media blank negative control. N=50 per treatment group pooled from separate clutches. Zebrafish at 5 dpf captured at 30X magnification: a) blank E3 only control, b) 0.1% (v/v) DMSO control, c) 5 µM RO48-8071, d) 10 µM AY9944, e) 10 µM U-18666A, f) 10 µM AY9944 plus 10 µM U-18666A. The area measured is highlighted in orange (a). Welch's ANOVA between groups, with Games-Howell post hoc analysis of medians (* $p<0.05$, *** $p<0.001$).

Similarly, all inhibitor treatments resulted in reduced yolk size as compared to both the blank and 0.1% (v/v) DMSO groups ($p<0.0001$). The positive control 0.1% (v/v) DMSO fish did not exhibit significantly different yolk size as compared to the blank E3 only control group ($q=3.24$), while RO48-8071 ($q=7.94$), AY9944 ($q=13.72$), U-18666A ($q=18.79$), and AY9944/U-18666A ($q=15.82$) treatments all produced zebrafish with significantly reduced yolk size at 5 dpf, as seen in Figure 4.7.

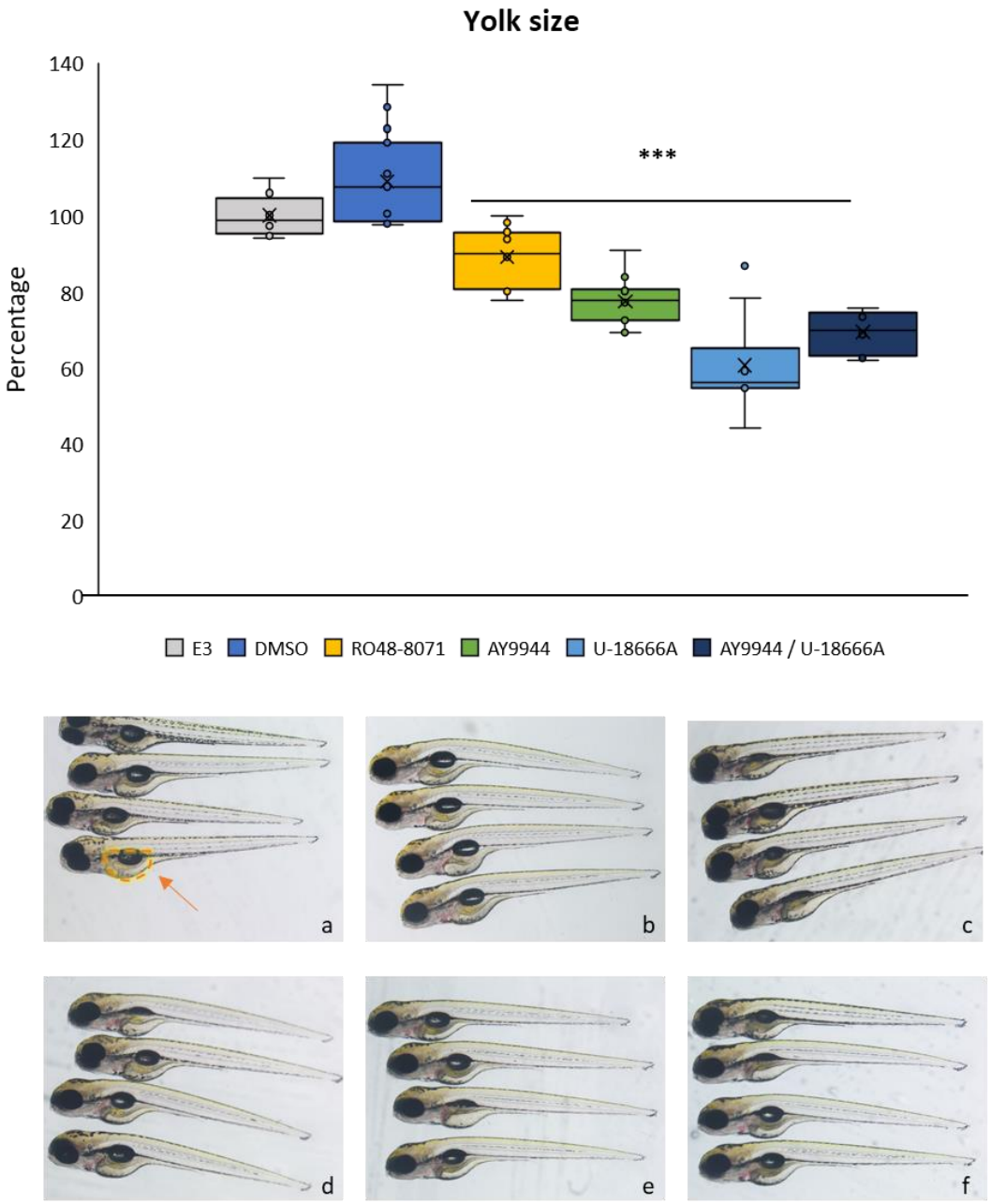


Figure 4.7. Zebrafish treated at 24 hours post fertilisation were assessed for yolk size at 5 dpf. All groups showed significant decreases in yolk size when compared to the 0.1% (v/v) DMSO vehicle control, with U-18666A showing a 47.3% reduction, the combination treatment AYY9944/U-18666A showing a 38.6% reduction, AY9944 showing a 30.6% reduction, and RO48-8071 showing a 18.9% reduction. Yolk size was increased in the 0.1% (v/v) DMSO vehicle control as compared to the growth media blank by 8.9%, though this was not a statistically significant increase. All treatment groups showed a significant decrease as compared to the growth media blank larva, with RO48-8071 treatment decreasing yolk size by 11%, AY9944 treatment by 22.56%, U-18666A by 39.32%, and the combination AY9944/U-1866A treatment decreasing yolk size by 30.59%. N=50 per treatment group pooled from separate clutches. Zebrafish at 5 dpf captured at 30X magnification: a) blank E3 only control, b) 0.1% (v/v) DMSO control, c) 5 µM RO48-8071, d) 10 µM AY9944, e) 10 µM U-18666A, f) 10 µM AY9944 plus 10 µM U-18666A. The area measured is

highlighted in orange (a). Welch's ANOVA between groups, with Games-Howell post hoc analysis of medians (*** p<0.001).

To determine whether the reduction in yolk size was due to a reduction in total body size or due to accelerated consumption of the lipid material by the larvae, yolk size was described as a percentage of body area for each treatment group.

Welch's ANOVA revealed all cholesterol synthesis inhibitor treatments significantly reduced relative yolk size ($p<0.0001$, $\alpha=0.05$). Post hoc analysis showed no significant difference between the blank E3 only and the 0.1% (v/v) DMSO groups ($q=2.05$), while RO48-8071 ($q=4.82$), AY9944 ($q=11.32$), U-18666A ($q=15.49$), and AY9944/U-18666A treatment ($q=14.23$) all resulted in significantly reduced relative yolk size when compared to the positive control as seen in Figure 4.8.

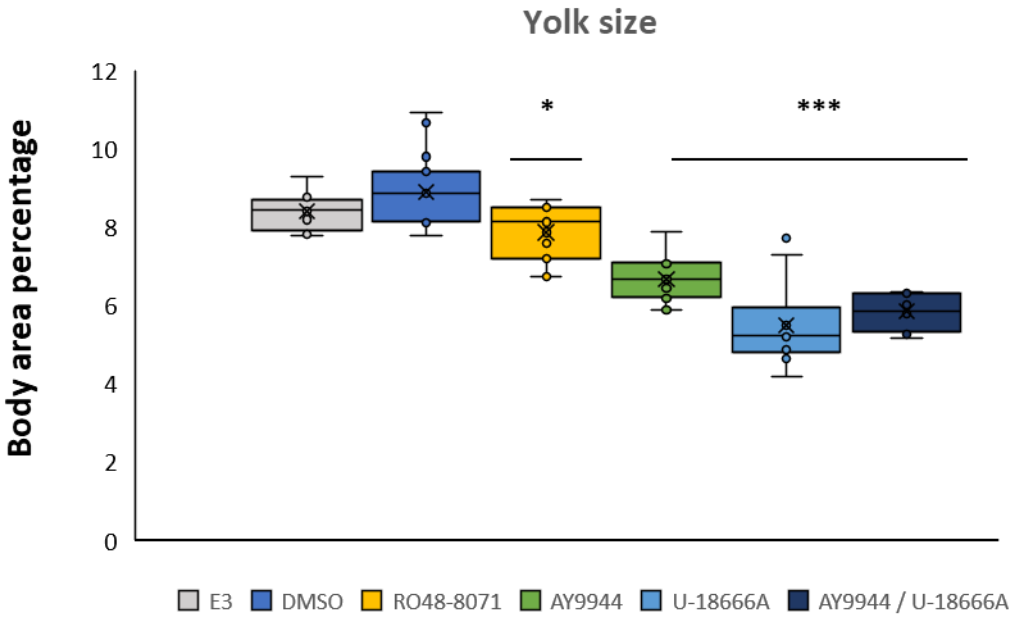


Figure 4.8. Treated zebrafish yolk sac size was expressed as a percentage of body size. All treatment groups showed a significant reduction as compared to the E3 only control group and the DMSO vehicle control. U-18666A treatment produced the most drastic reduction in relative yolk size with a 3.3% reduction as compared to E3 only and a 2.9% reduction as compared to 0.1% (v/v) DMSO. Similarly, the combination treatment of AY994/U-18666A led to a 3.1% and 2.6% reduction respectively, AY9944 treatment to a 2.4% and 1.8% reduction, and RO48-8071 to a 1.1% and a 0.6% relative yolk size reduction. N=50 per treatment group pooled from separate clutches. Welch's ANOVA between groups, with Games-Howell post hoc analysis of medians (* p<0.05, *** p<0.001).

### 4.3.5 Some pharmacological cholesterol synthesis inhibitors reduce eye size in zebrafish larvae, but do not alter eye aspect ratio

The area at maximum diameter and the aspect ratio of each eye was measured in zebrafish at 5 dpf to establish the effect of pharmacological cholesterol synthesis inhibitor treatment on gross eye morphology.

Mean eye lateral area was significantly reduced as compared to the 0.1% (v/v) DMSO control group following treatment with 2 µM RO48-8071 and 10µM U-18666A at 5 dpf ($p<0.0001$, $\alpha=0.05$). No significant difference was noted between the blank E3 and the DMSO control groups ($q=0.23$), as seen in Figure 4.9. Zebrafish treated with 10 µM AY9944 ($q=3.46$) and 10 µM + 10 µM AY9944/U-18666A ($q=2.45$) did not show significantly altered eye area as compared to both control groups.

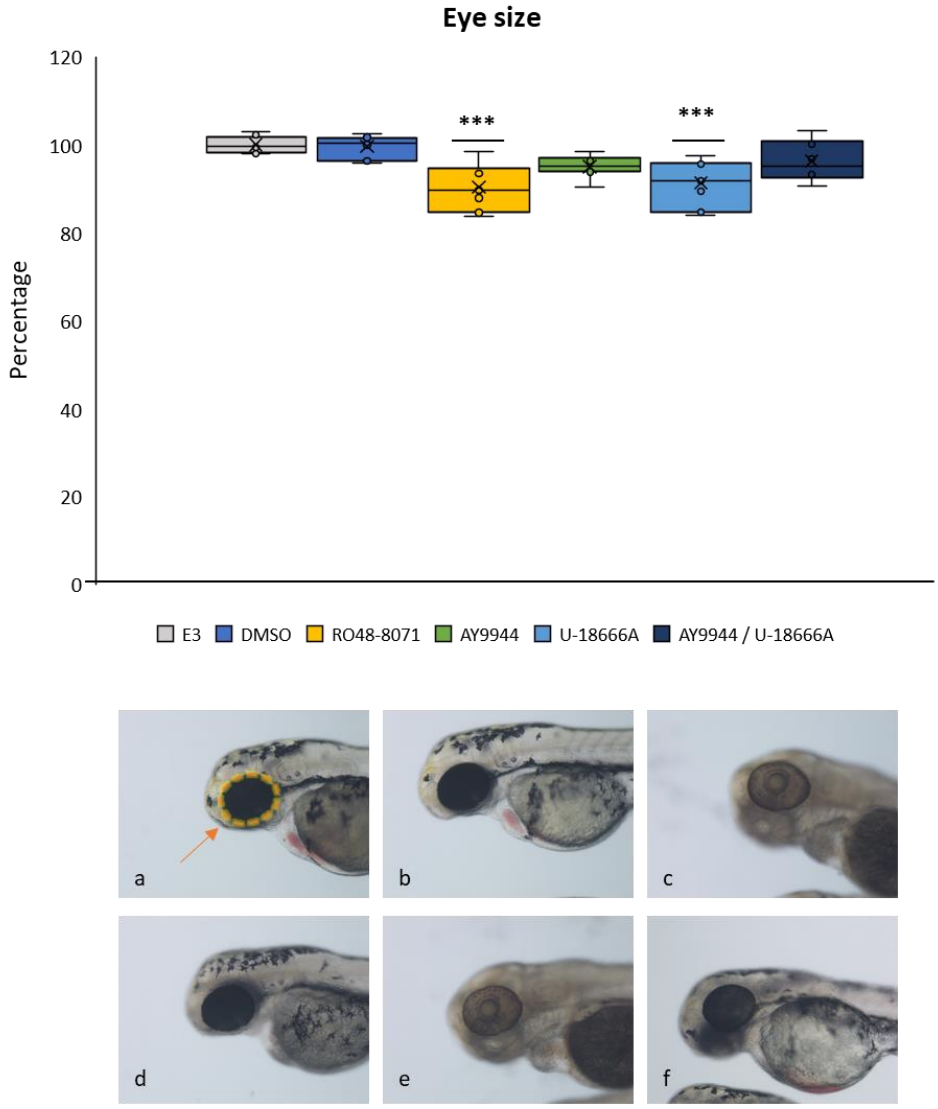


Figure 4.9. Zebrafish treated at 24 hours post fertilisation were assessed for lateral eye size at 5 dpf. Larvae treated with RO48-8071 showed a 9.57% decrease as compared to the E3 only control

and 9.27% as compared to the DMSO, whereas the U-18666A treated group showed an 8.67% and an 8.4% decrease, respectively. All other groups showed no statistically significant differences between them. N=50 per treatment group pooled from separate clutches. Zebrafish at 5 dpf captured at 60X magnification: a) blank E3 only control, b) 0.1% (v/v) DMSO control, c) 5 µM RO48-8071, d) 10 µM AY9944, e) 10 µM U-18666A, f) 10 µM AY9944 plus 10 µM U-18666A. The area measured is highlighted in orange (a). Welch's ANOVA between groups, with Games-Howell post hoc analysis of medians (*** $p<0.001$).

The mean aspect ratio of eyes did not significantly deviate between treatment and control groups ($p=0.084$, $\alpha=0.05$), except for AY9944/U-18666A combination treated zebrafish presenting with moderately more circular eyes as compared to RO48-8071 treated larvae ($q=4.61$) as seen in Figure 4.10.

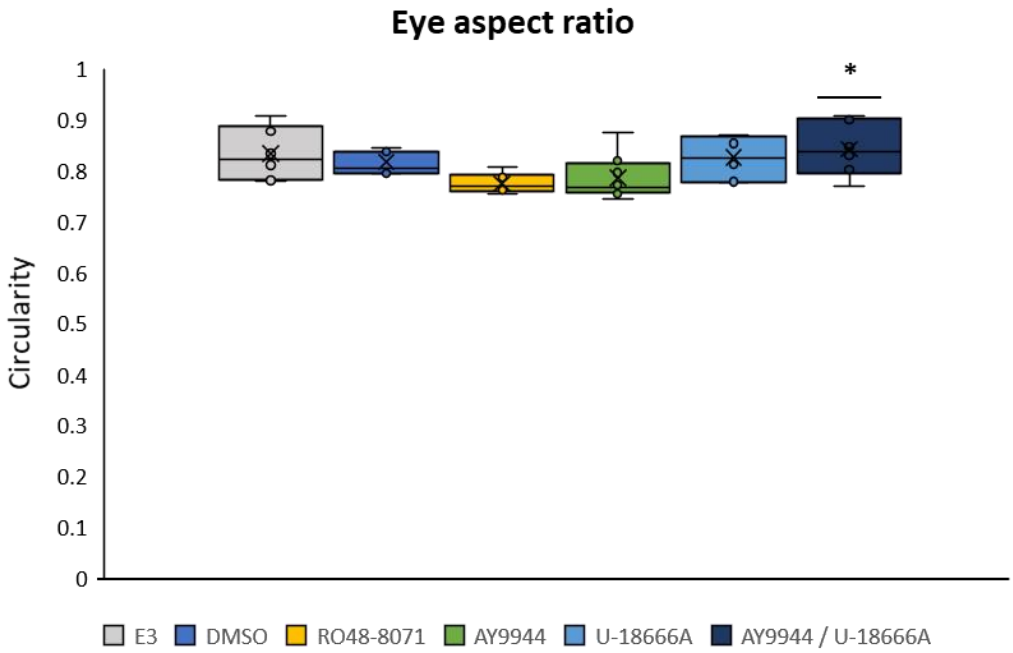


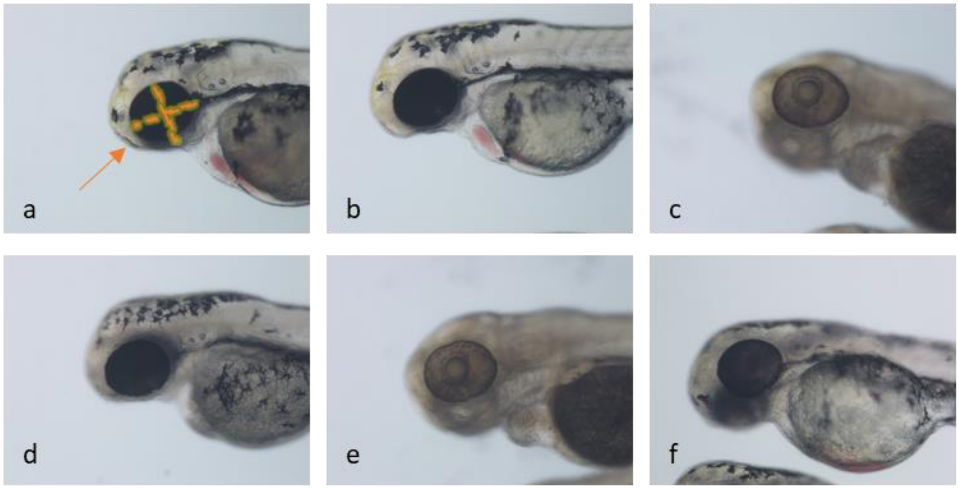


Figure 4.10. Zebrafish treated at 24 hours were assessed for lateral eye aspect ratio at 5 dpf. No treatment groups showed significant deviation from the E3 only and DMSO controls. The combined AY9944/U-18666A treatment group eyes were significantly more circular than the RO48-8071 treatment group by 0.89. N=50 per treatment group pooled from separate clutches. Zebrafish at 5 dpf captured at 60X magnification: a) blank E3 only control, b) 0.1% (v/v) DMSO control, c) 5 µM RO48-8071, d) 10 µM AY9944, e) 10 µM U-18666A, f) 10 µM AY9944 plus 10 µM U-18666A. The dimensions measured are highlighted in orange (a). Welch's ANOVA between groups, with Games-Howell post hoc analysis of medians (* $p<0.05$).

As with the observed reduction in yolk size described in Figures 4.7 and 4.8, the mean eye size was expressed as a percentage of total body size to account for proportionate changes. In

contrast with the significant reductions in eye size observed in Figure 4.9, there was no statistically distinct deviation from the mean between any group comparison ($p=0.33$, $\alpha=0.05$).

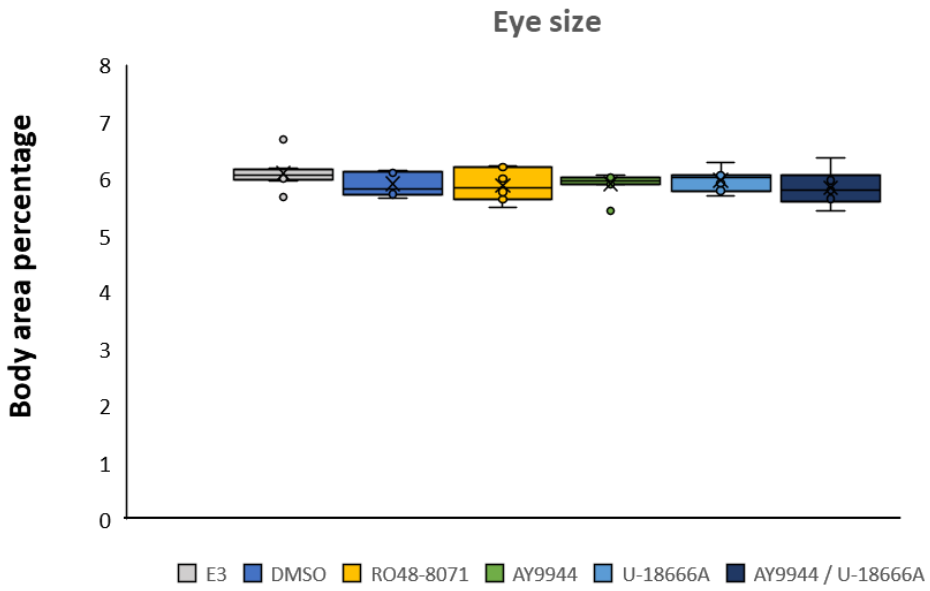


Figure 4.11. Treated zebrafish eye size was expressed as a percentage of body size to account for relative changes. In contrast with absolute eye size as seen in Figure 4.9, no treatment group showed a significant deviation in mean eye size as compared to the E3 only and DMSO controls. N=50 per treatment group pooled from separate clutches. Welch's ANOVA between groups, with Games-Howell post hoc analysis of medians.

## 4.4 Sterol supplementation has a variable effect on phenotype recovery of cholesterol synthesis-inhibited zebrafish larvae

Zebrafish were further supplemented with either lanosterol or cholesterol to assess the rescue effect on physical phenotypes.

The maximum half-life of all pharmacological inhibitors in aqueous solution was determined as the minimum start point for sterol supplementation; as such, sterol introduction was performed either at 30 hpf or 48 hpf and larvae were followed to 5 dpf. The minimum sterol concentration was determined as double the maximum inhibitor concentration to ensure the excess of sterol in solution.

### 4.4.1 Lanosterol and cholesterol supplementation of inhibitor-treated zebrafish is viable in both a concentration-dependent and a treatment-dependent manner

Baseline toxicity assays were performed at 24 hpf, and the survival rate of zebrafish was followed to 5 dpf. Ethanol was used as the positive vehicle control, as supplemental sterols were diluted in 100% EtOH. Neither lanosterol nor cholesterol supplementation at 20 µM showed any significant reduction in survival of treated larvae as compared to the vehicle control 0.1% EtOH, with lanosterol-treated zebrafish exhibiting a 92% survival and cholesterol-treated larvae 96% survival. At 40 µM, lanosterol treatment was 100% lethal by 72 hpf as seen in Figure 4.12, whereas cholesterol treatment showed a 46% lethality which was significantly above the 25% threshold as described in section 4.3.3. Thus, the higher concentrations were rejected for both compounds.

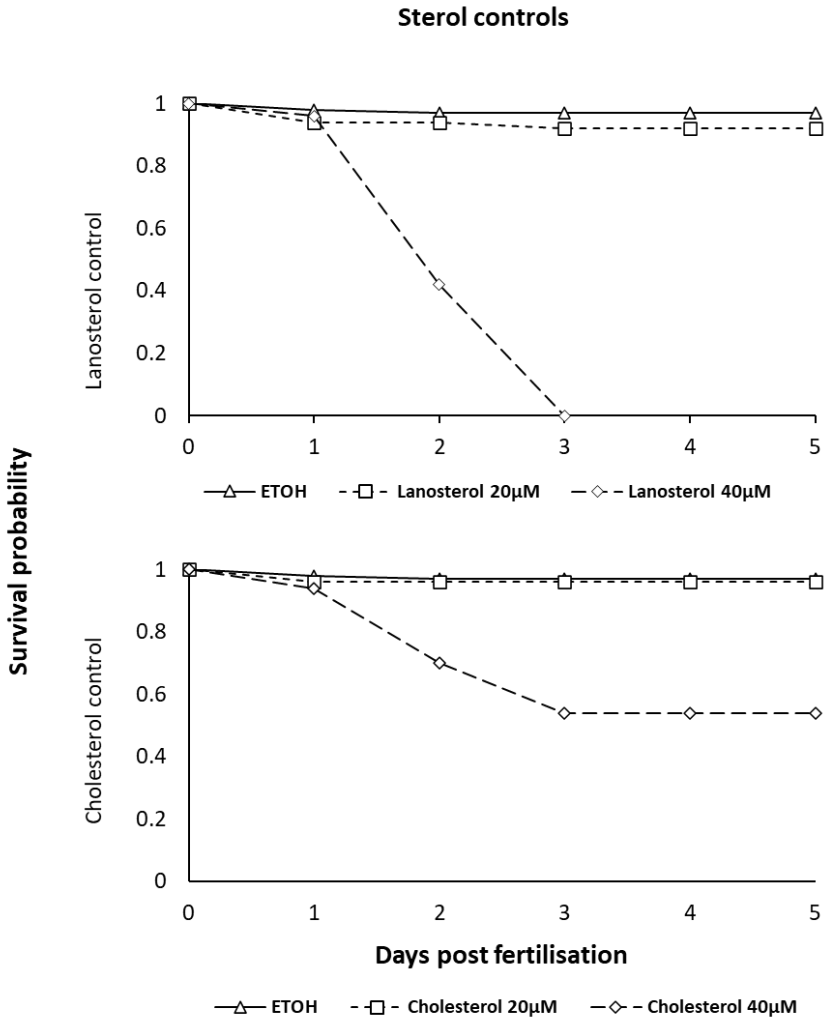


Figure 4.12. The sterol lipids lanosterol and cholesterol were tested against increasing concentrations to assess toxicity. The compounds were administered to dechorionated embryos at 24 hours post fertilisation. Lanosterol did not significantly reduce mortality rates of zebrafish

at 20 µM but resulted in 100% lethality by 3 days post fertilisation at 40 µM. Similarly, cholesterol resulted in 54% survival at 5 dpf at 40 µM but showed no significant reduction at 20 µM as compared to the ethanol vehicle control. N=50 per treatment group pooled from separate clutches.

Rescue supplementation was assessed for larval toxicity as described in section 4.4. Lanosterol introduction at 20 µM did not significantly decrease the survival probability of cholesterol synthesis impaired larvae treated at 30 hpf or 48 hpf, with a total survival of 94% reported in both conditions. Cholesterol supplementation was 100% lethal by 48 and 72 hpf in larvae treated with the inhibitors U-18666A, AY9944/U-18666A, and RO48-8071 respectively, whereas AY9944 only treated larvae did not show a significant reduction in survival as compared to the vehicle control.

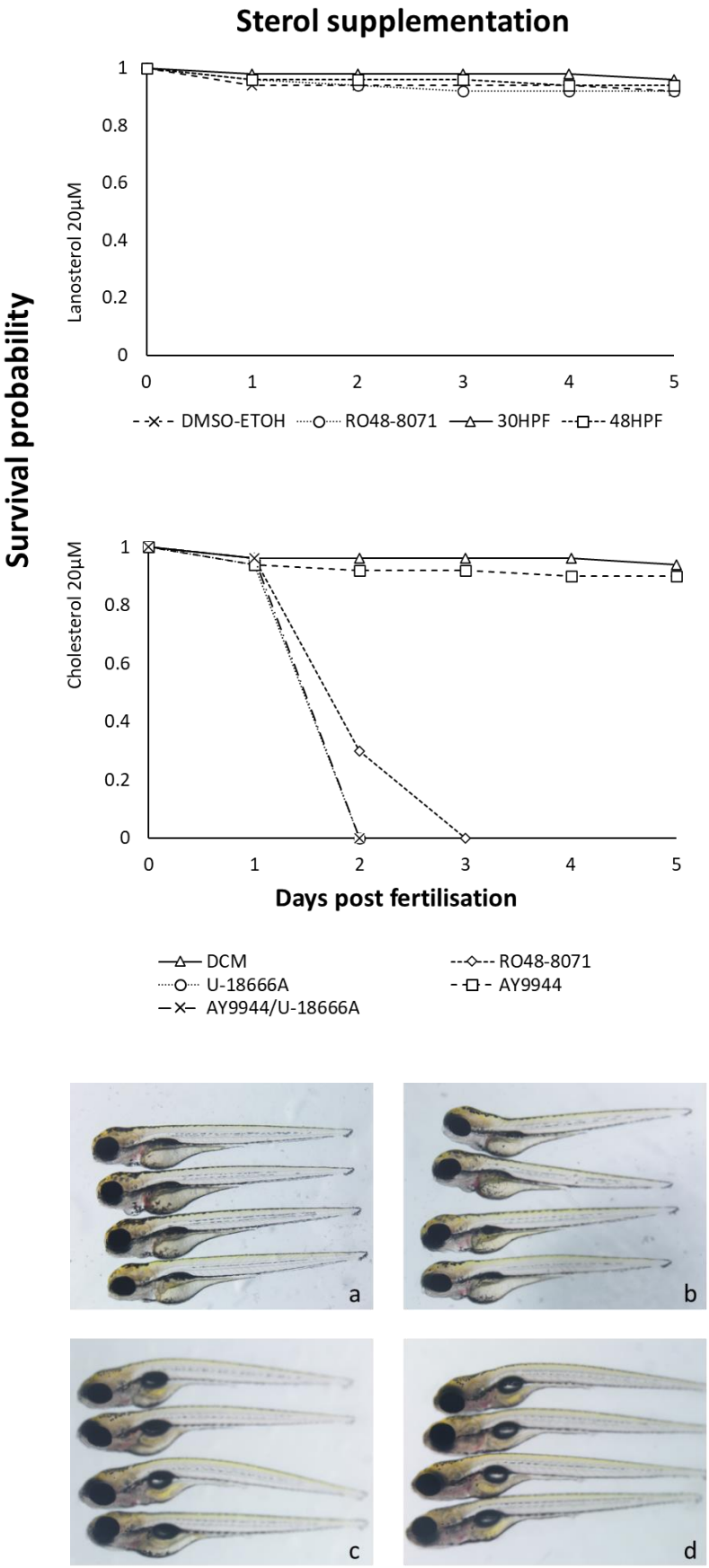


Figure 4.13. Survival rates of cholesterol inhibitor-treated zebrafish which were supplemented with 20µM lanosterol or cholesterol. Zebrafish treated with RO48-8071 to partially inhibit

lanosterol synthesis were supplemented with 20 µM lanosterol at 30 or 48 hours post fertilisation. Neither supplement concentration demonstrated significantly decreased survival at 5 dpf. Cholesterol supplementation at 20 µM resulted in 100% lethality for AY9944 treated and AY9944/U-18666A treated zebrafish at 2 days post fertilisation, and at 3 days post fertilisation for RO48-8071 treated zebrafish. Zebrafish treated with U-18666A only did not show any significant reduction in survival as compared to control groups. Neither lanosterol nor cholesterol supplemented larvae demonstrated any significantly deleterious physical abnormalities, as seen in a (30 hpf 20 µM lanosterol treatment), b (48 hpf 20 µM lanosterol treatment), c (30 hpf 20 µM cholesterol treatment), and d (48 hpf 20 µM cholesterol treatment). N=50 per treatment group pooled from separate clutches.

### 4.4.2 Lanosterol supplementation successfully rescues yolk size, but not body and eye size in RO48-8071 treated zebrafish

Zebrafish larvae treated with RO48-8071 were supplemented with 20 µM lanosterol at 30 or 48 hpf and followed to 5 dpf, when they were assessed for body, yolk, and eye size as described previously. Treatment with the *LSS* inhibitor RO48-8071 significantly reduced the mean body size by 7.68% ($p<0.0001$, $a=0.05$), yolk size by 31.3% ($p<0.0001$, $a=0.05$), and eye size by 8.15% ($p<0.0001$, $a=0.05$) as compared to the 0.1% (v/v) DMSO control group. Lanosterol supplementation at 30 hpf successfully rescued the larval yolk to 93.25% of the control yolk size as compared to 68.7% for RO48-8071 treated zebrafish ($q=11.90$), whereas supplementation at 48 hpf increased the yolk size to 103.85% of the control group ($q=1.68$). Lanosterol-only supplemented zebrafish did not show a significant deviation in mean yolk size, with a 0.42% reduction as compared to the DMSO control larvae ($q=0.188$).

In contrast to the yolk recovery, the body and eye size of lanosterol-supplemented larvae were not restored to control levels. Body size remained decreased at 5 dpf, with larvae supplemented at 30 hpf showing a mean reduction of 14.11% ($q=13.98$) and larvae supplemented at 48 hpf a 6.17% ($q=5.78$) reduction.

Similarly, the eye size of larvae supplemented at 30 hpf were 13.56 % smaller ($q=8.20$) than the control group while larvae supplemented at 48 hpf were 12.97% smaller ($q=7.42$). Both lanosterol supplementation groups presented with smaller eyes as compared to the RO48-8071 treated zebrafish ($q=4.32$ for 30 hpf and $q=3.75$ for 48 hpf), as seen in Figure 4.14.

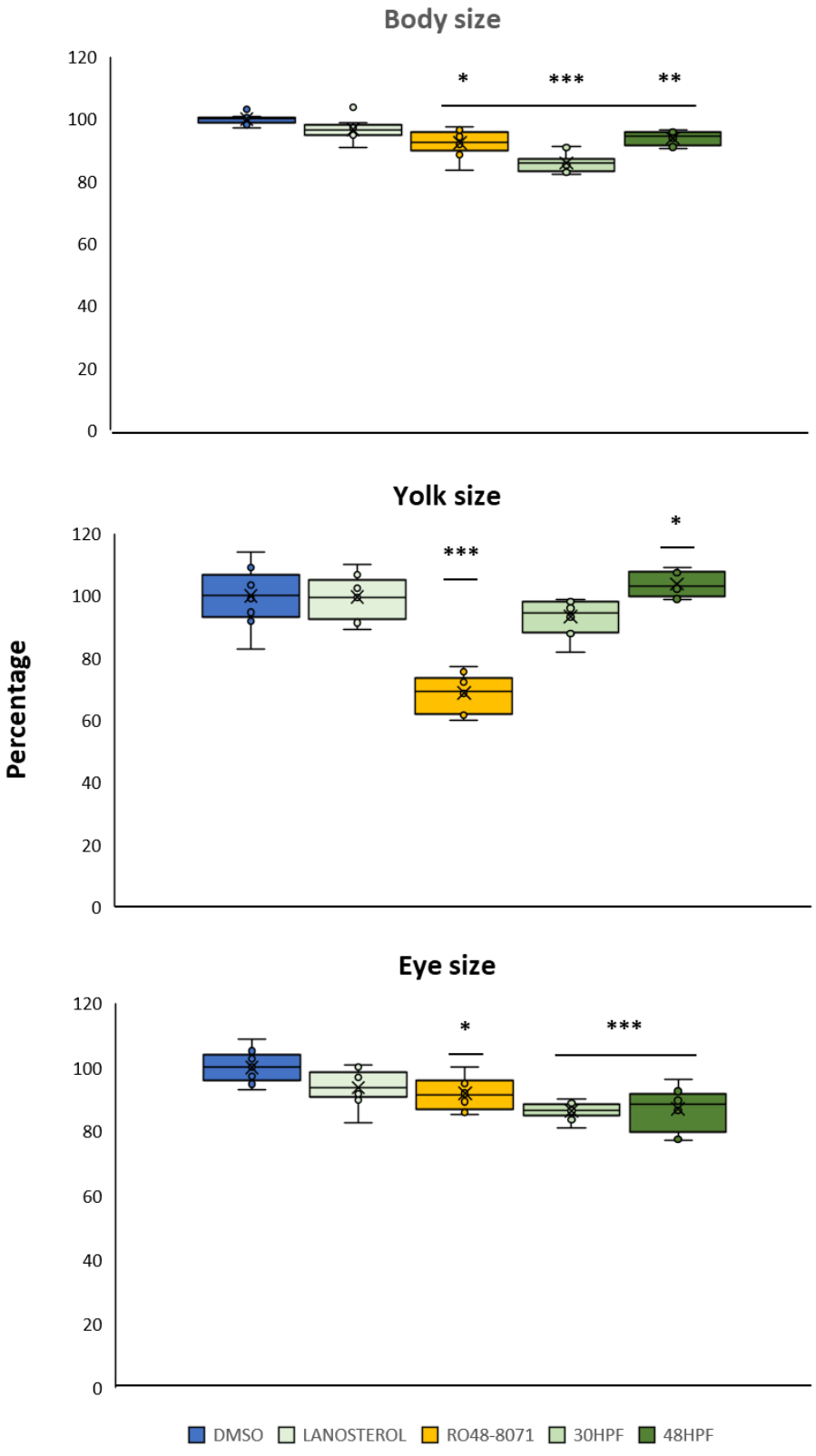


Figure 4.14. Lanosterol supplementation successfully restores yolk size to control levels. Zebrafish treated with RO48-8071 showed a significant decrease in body, yolk, and eye size as compared to the 0.1% (v/v) DMSO control. Supplementation of 20 µM lanosterol only at 30 hpf did not produce any significant deviation in body, yolk, or eye size from the DMSO control group. Supplementation of RO48-8071 treated zebrafish with lanosterol at 30 and 48 hpf restored yolk

size to physiological levels. In contrast, body and eye size remained decreased as compared to the 0.1% (v/v) DMSO and lanosterol only controls for zebrafish treated with RO48-8071 and subsequently supplemented with lanosterol. N=50 per treatment group pooled from separate clutches. Welch's ANOVA between groups, with Games-Howell post hoc analysis of medians (* $p<0.05$, ** $p<0.01$, *** $p<0.001$).

When expressed as a percentage of body size, the mean yolk size of RO48-8071 treated zebrafish was significantly reduced as shown in Figures 4.8 and 4.15. This reduction was rescued in larvae supplemented with lanosterol at 30 hpf, while larvae supplemented at 48 hpf showed a significant increase ($p<0.05$) in yolk size as compared to both the DMSO only control and the lanosterol positive control groups. Similar to the cholesterol synthesis inhibitor treatments, the reduction in zebrafish eye size for lanosterol supplemented groups described in Figure 4.14 was proportional to the overall reduction in body size with relative eye size being consistent across control and treatment/supplementation groups as seen in Figure 4.15.

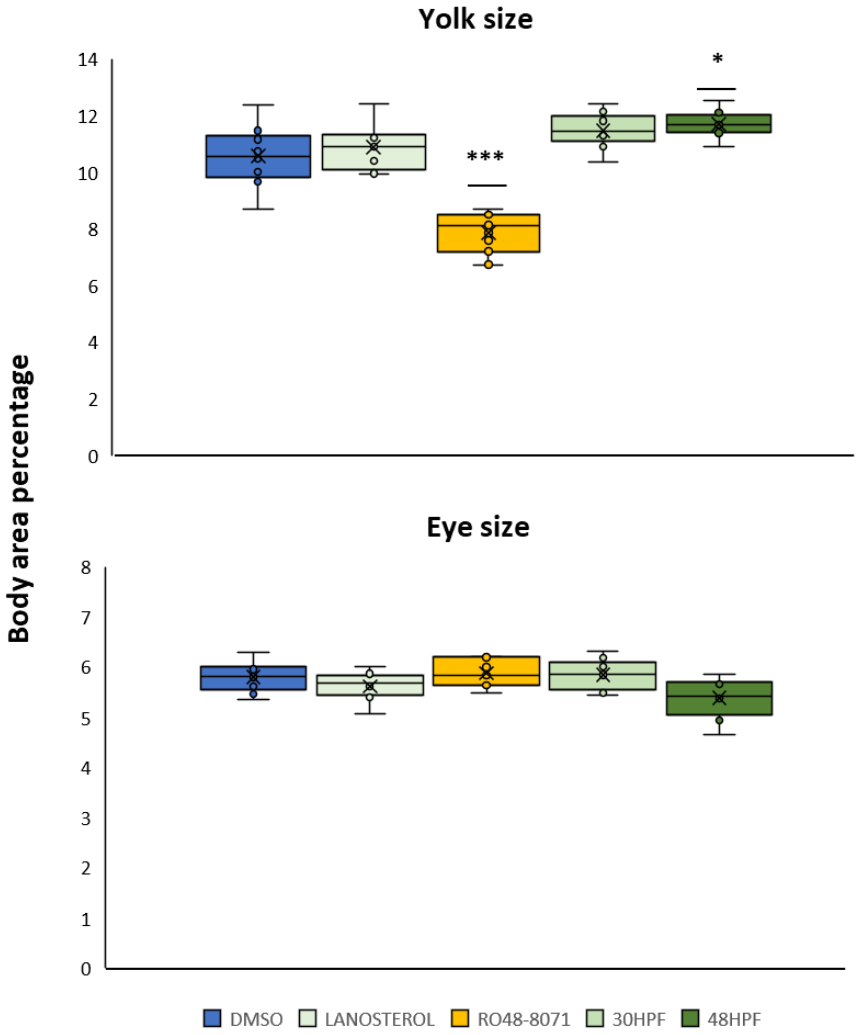


Figure 4.15. Lanosterol supplementation rescues proportionate yolk size and has no effect on relative eye size in zebrafish larvae. RO48-8071 treated zebrafish showed a relative reduction of

yolk size by 3.02%, while lanosterol supplemented larvae showed increased yolk sizes by 0.58% and 0.8% when supplemented at 30 hpf and 48 hpf. Relative eye size remained constant and comparable with control groups for all treatments and supplementations (RO48-8071 = +0.26%, lanosterol 30 hpf = +0.23%, lanosterol 48 hpf = -0.19%). N=50 per treatment group pooled from separate clutches. Welch's ANOVA between groups, with Games-Howell post hoc analysis of medians (* $p<0.05$, *** $p<0.001$).

### 4.4.3 Cholesterol supplementation rescues body and yolk size and increases eye size in AY994 treated zebrafish

Supplementation with 20 µM cholesterol was demonstrated to be lethal in conjunction with all inhibitor treatments apart from 10 µM AY9944, as seen in Figure 4.13. Zebrafish treated with 10 µM AY9944 and supplemented at 30 hpf with 20 µM cholesterol presented with extensive pericardial oedema, microphthalmia, and multiple skeletal deformities at 5 dpf as seen in Figure 4.16, and as such were excluded from further analysis.

Larvae supplemented with 20 µM cholesterol at 48 hpf showed restored body ($q=1.25$) and yolk size ($q=2.05$) to control levels, while AY9944 treated zebrafish bodies ($q=6.14$) and yolks ($q=12.27$) were significantly smaller (body size $p=0.0006$, $\alpha=0.05$; yolk size $p<0.0001$, $\alpha=0.05$). In contrast with other treatment and supplementation combinations, cholesterol supplementation resulted in an increase in eye size as compared to the 0.1% DMSO control group ($p=0.049$, $\alpha=0.05$) at 5dpf.

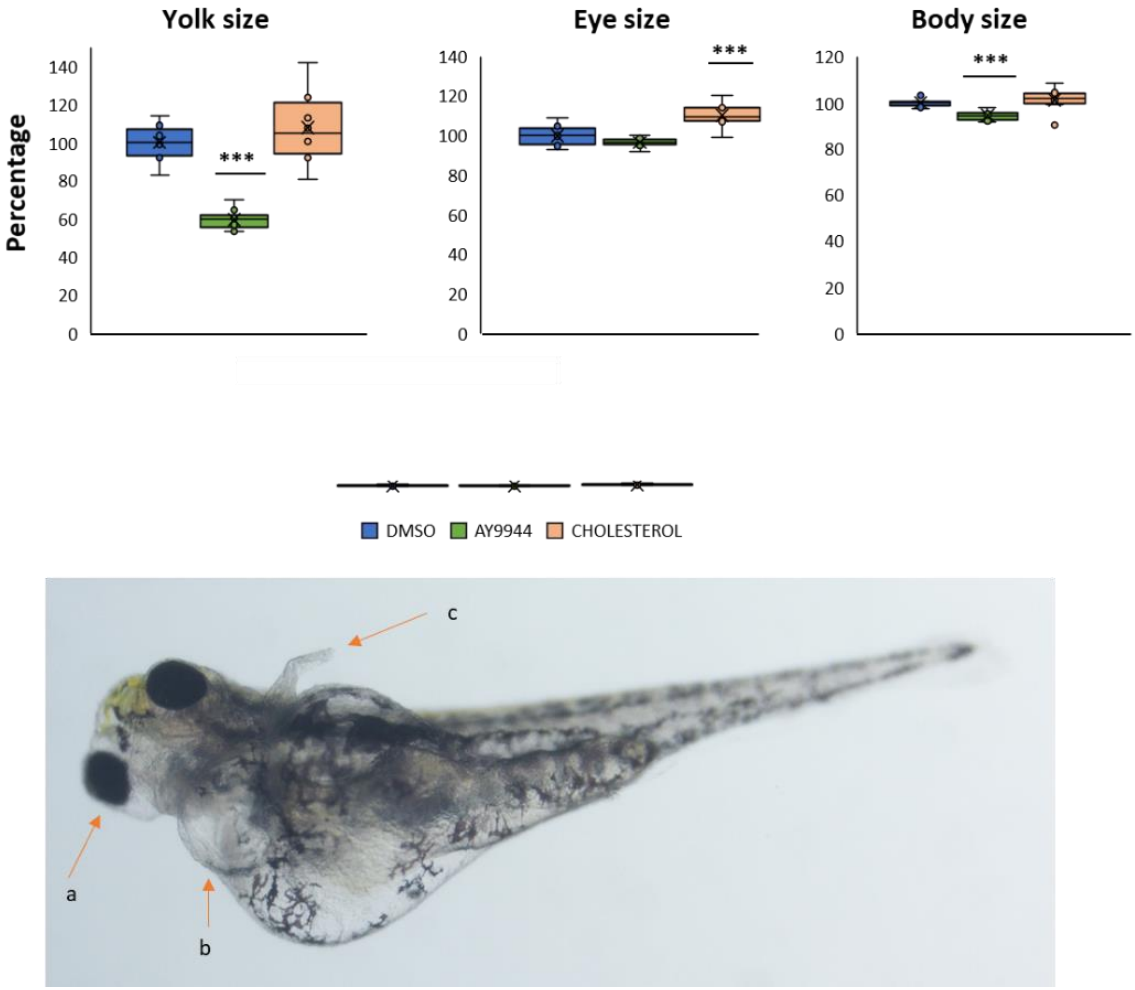


Figure 4.16. Cholesterol supplementation at 48 hpf rescued body and yolk size in AY9944 treated zebrafish and increases eye size. Treatment at 24 hpf with 10 µM AY9944 resulted in significantly decreased body (-5.5%) and yolk size (-40.31%) as compared to 0.1% (v/v) DMSO only control larvae. AY9944-treated zebrafish supplemented with cholesterol at 30 hpf showed extensive pathologies including microphthalmia (a), major pericardial and gastric oedema (b), and severe skeletal deformities of the dorsal fins (c). Though the larvae were active and responsive to external stimuli, they were considered non-viable phenotypes. Supplementation at 48 hpf did not result in any adverse effects, with body (+1.29%) and yolk size (+7.77%) restored to control levels while eye size was significantly increased (+10.35%). N=50 per treatment group pooled from separate clutches. Welch's ANOVA between groups, with Games-Howell post hoc analysis of medians (*** $p<0.001$).

When expressed as a percentage of body size, the mean yolk size of AY9944-treated larvae was significantly decreased ($q=9.31$) as compared to the 0.1% (v/v) DMSO control group, while yolks isolated from cholesterol-supplemented larvae were rescued ($q=1.54$) to a near-physiological size ($p<0.0001$, $\alpha=0.05$), as seen in Figure 4.17. In contrast, the relative eye size of AY9944-treated larvae remained close to control values ($q=0.88$) whereas the cholesterol-

supplemented group presented with significantly increased (q=4.66) mean eye size (p=0.0078, α=0.05).

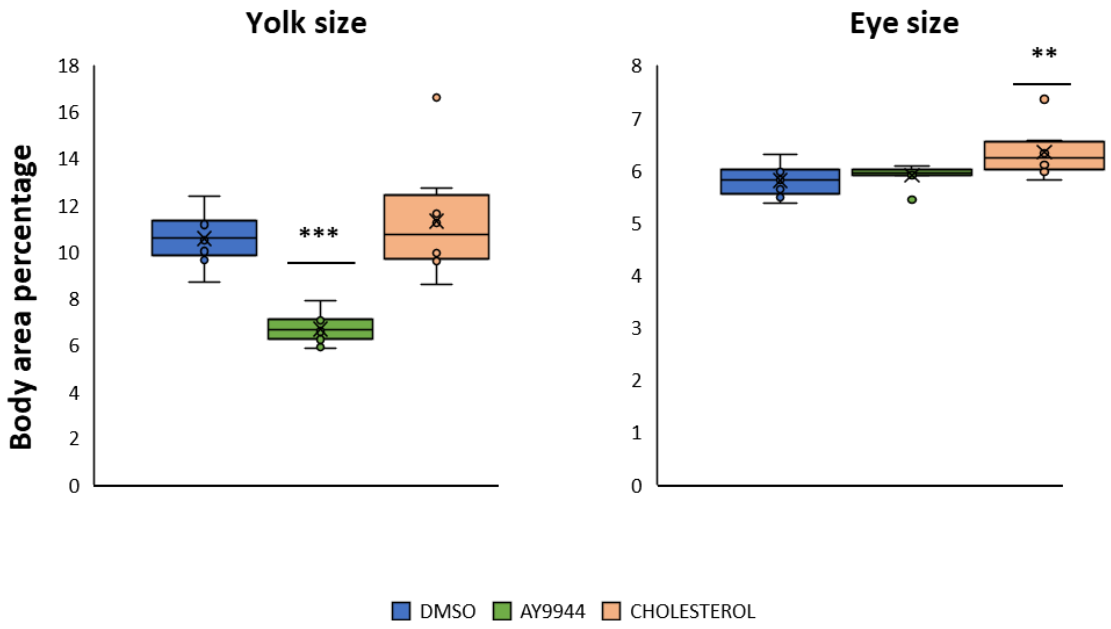


Figure 4.17. Relative eye size is increased in AY9944-treated zebrafish supplemented with cholesterol. The relative yolk size of AY9944-treated zebrafish was decreased by 3.89% as compared to control larvae, while cholesterol supplemented zebrafish showed no significant deviation (-0.74%). In contrast, relative eye size remained stable in AY9944-treated groups (-0.09) while cholesterol supplemented zebrafish showed a significant increase by 0.53% as compared to control larvae. N=50 per treatment group pooled from separate clutches. Welch's ANOVA between groups, with Games-Howell post hoc analysis of medians (** p<0.01, *** p<0.001).

## 4.5 The inhibition cholesterol synthesis impacts lens shape in zebrafish larvae

Live imaging of zebrafish larvae at 5 dpf was performed using SPIM to assess the impact of pharmacological cholesterol synthesis inhibitors on lens morphology.

### 4.5.1 The inhibition of LSS alters larval lens aspect ratio but does not cause microphakia

The mean maximum diameter of lenses was found to remain relatively stable in all treatment groups, with no inhibitor resulting in microphakia (p=0.024, α=0.05), as seen in Figure 4.18. The only significant size difference was noted between RO48-8071 and U-18666A-treated larvae, with the latter showing a reduction in maximum lens diameter of 7.73 µm (q=4.25).

The aspect ratio of lenses was not altered between the control and treatment groups, with the exception of RO48-8071-treated zebrafish which showed a significant elongation of the horizontal diameter of the lens (p=0.0018, α=0.05) and an increased aspect ratio by 0.068 (q=5.14).

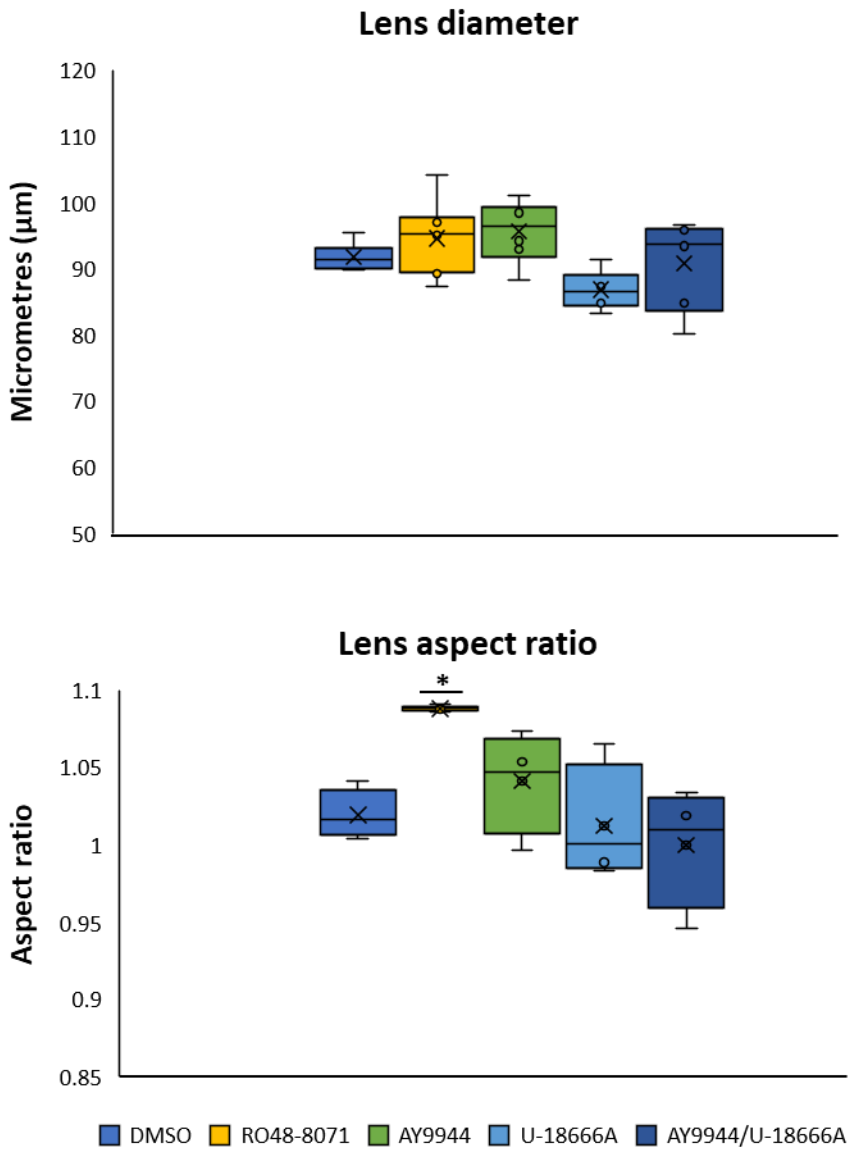


Figure 4.18. Inhibition of LSS alters zebrafish lens aspect ratio. The maximum diameter of treated larvae did not differ significantly between the control group and the inhibitor treatments, with RO48-8071 producing a 2.79 µm increase in diameter, AY9944 a 3.89 µm increase, AY9944 a 4.93 µm reduction, and the combination AY9944/U-18666A a 0.94 µm reduction. The aspect ratio of lenses was not significantly altered for AY9944-treated zebrafish (-0.02), U-18666A (+0.007), and AY9944/U-18666A-treated zebrafish (+0.019). RO48-8071 treatment significantly altered the aspect ratio with pronounced lengthening of the horizontal diameter of lenses (-0.068). N=10 per treatment group pooled from separate clutches. Welch's ANOVA between groups, with Games-Howell post hoc analysis of medians (* p<0.05).

### 4.5.2 The inhibition of cholesterol synthesis results in decreased LEC height

Lens epithelial cells are the precursors of all lens fibre cells. All lenses from inhibitor-treated zebrafish groups were found to have significantly decreased LEC height ($p<0.0001$, $\alpha=0.05$) at the central zone as compared to the 0.1% (v/v) DMSO only control, as seen in Figure 4.19. LEC height in the RO48-8071 group was reduced by 1.3 µm ($q=8.45$), by 1.47 µm ($q=9.22$) in the AY9944 group, 0.98 µm ($q=6.55$) in the U-18666A group, and 1.64 µm in the AY9944/U-18666A group as compared to the mean height of 5.39 µm in control lenses.

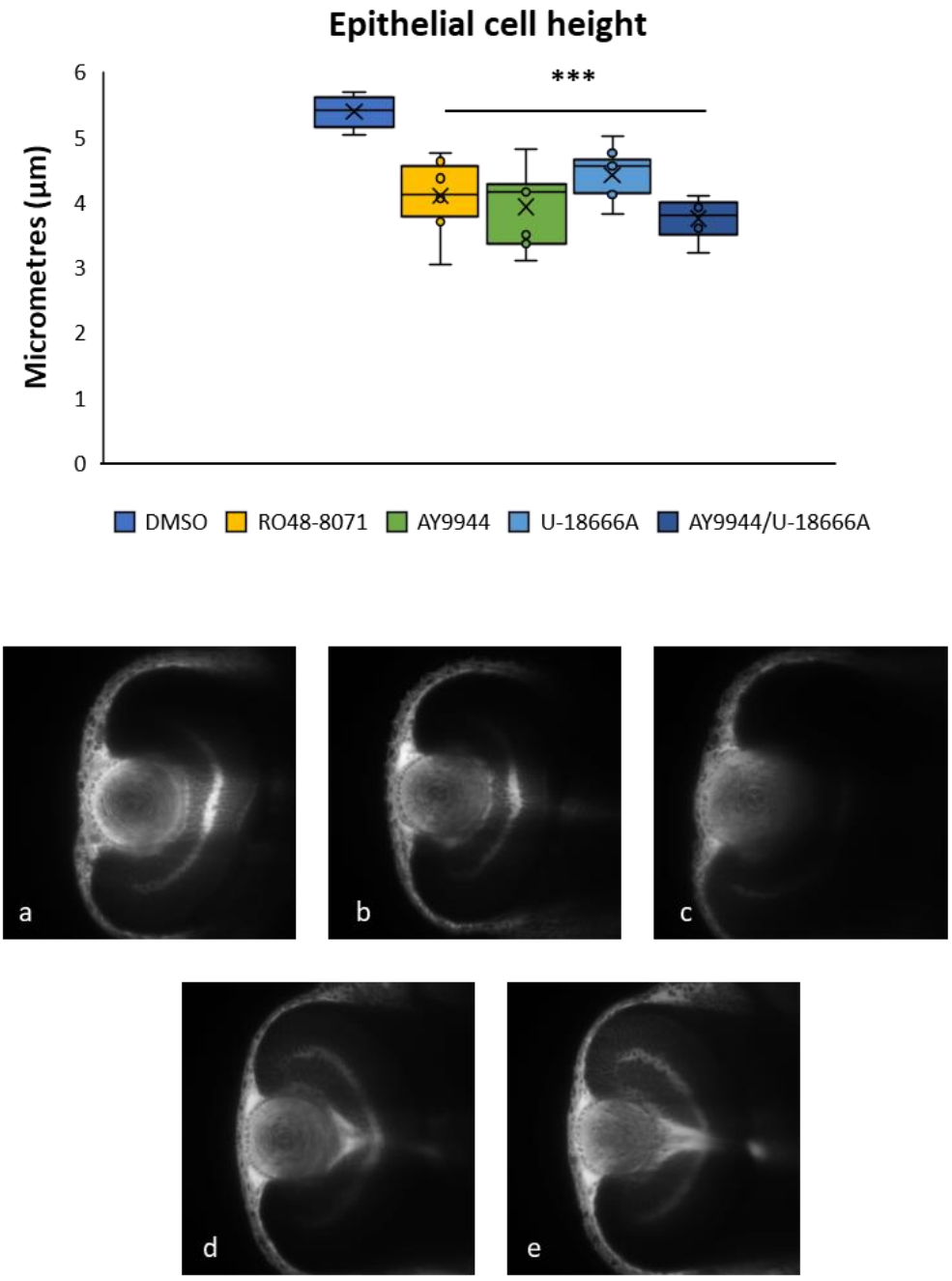


Figure 4.19. The inhibition of cholesterol synthesis decreases zebrafish LEC height. Epithelial lens height was decreased by 1.3 µm in RO48-8071-treated zebrafish, 1.47 µm in AY9944-treated zebrafish, 0.98 µm in U-18666A-treated groups, and 1.64 µm in AY9944/U-18666A-treated

larvae. N=10 per treatment group pooled from separate clutches. Welch's ANOVA between groups, with Games-Howell post hoc analysis of medians (*** p<0.001).

## 4.6 Tracking of sterols in zebrafish larvae

The pharmacological inhibition of cholesterol synthesis was found to produce both behavioural and physical phenotypes in zebrafish larvae, while supplementation with lanosterol or cholesterol mostly rescued the effects of inhibition on lipid rich tissues such as the yolk and eyes.

To assess the direct effect of inhibitors on cholesterol synthesis, treated zebrafish were pooled at 5 dpf and lenses were separated from whole bodies prior to lipid purification. Samples were analysed for total (free and membrane bound) cholesterol content and sterols directly upstream of each inhibition point to examine the accumulation of metabolites in different treatment and supplementation groups.

### 4.6.1 Pharmacological synthesis inhibitors reduce total cholesterol levels in treated zebrafish and lead to the accumulation of upstream metabolites

Lipids purified from pooled, whole larvae showed a decrease in total cholesterol content in all inhibitor-treated groups. Zebrafish treated with RO48-8071 showed the largest decrease in total cholesterol content, followed by the AY9944/U-18666A group, the U-18666A group, and the AY9944-treated group as seen in Figure 4.20. These decreases did not reflect the reductions in physical sizes of larval bodies and yolks seen in Figures 4.7 and 4.8, which are indicative of off-target effects in growth regulation mediated by the tested inhibitors.

Several cholesterol esters were detected at trace amounts which followed the same pattern of reduction in a treatment-dependent manner, suggesting the effect of tested inhibitors is retained downstream in sterol metabolism.

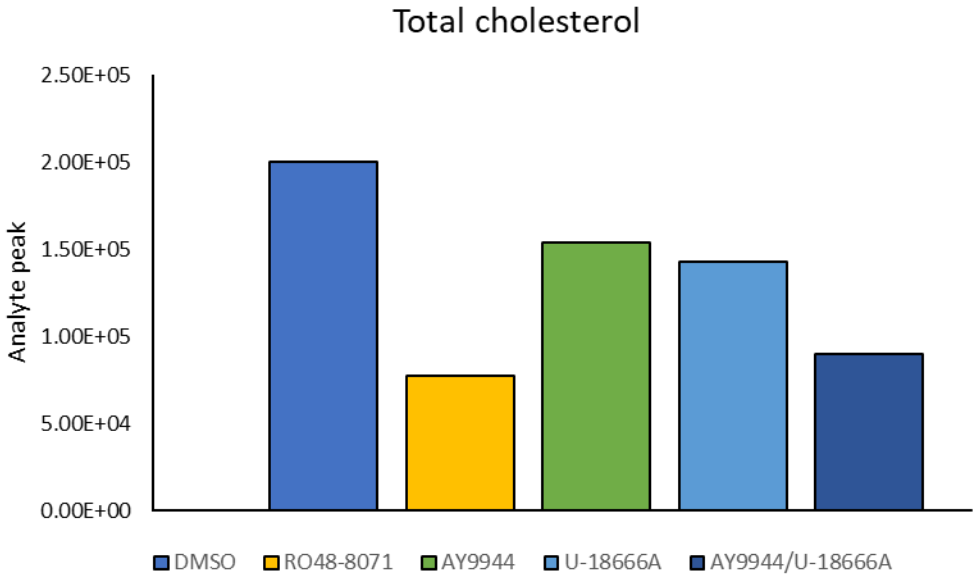


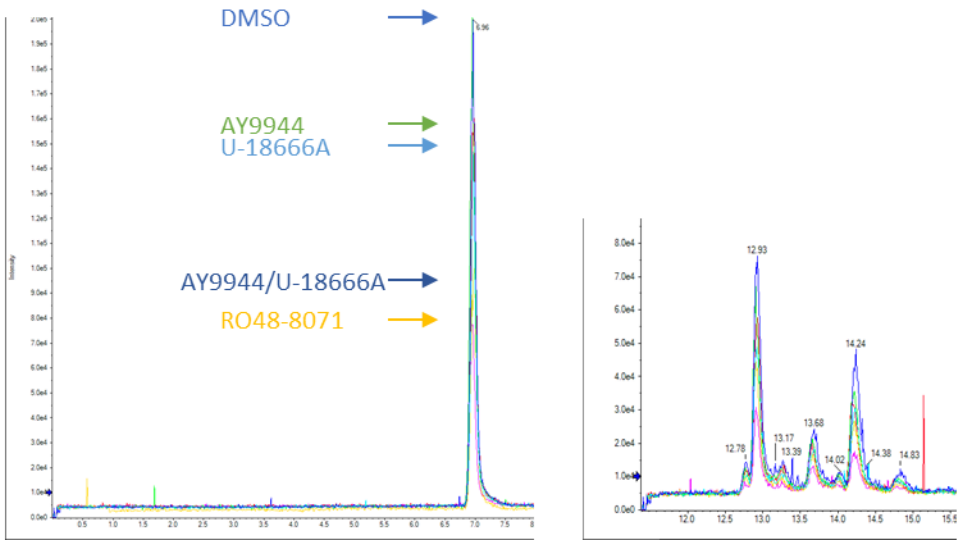


Figure 4.20. Inhibition of cholesterol synthesis with all tested reagents reduces the total cholesterol in zebrafish larvae. Whole body lipids purified from RO48-8071-treated zebrafish showed a 2.57X reduction in total cholesterol content, a 2.21X decrease in AY9944/U-18666A-treated zebrafish, 1.39X decrease in U-18666A-treated groups, and a 1.29X decrease in AY9944-treated larvae. The reduction pattern seen in the cholesterol peak of relevant chromatograms was retained in the elution region of cholesterol esters as seen above, implying the effect of cholesterol depletion is retained throughout downstream metabolism. N=25 per treatment group from separate clutches, technical triplicates pooled.

Lipids purified from isolated whole bodies and isolated whole lenses were analysed for total cholesterol content and oxidosqualene content for RO48-8071-treated zebrafish, 7-dehydrocholesterol for AY9944-treated larvae, and desmosterol for U-18666A-treated fish.

The total cholesterol content was similar in lipids isolated from whole bodies and whole lenses, with the RO48-8071 groups showing the largest decrease, followed by the U-18666A and AY9944 groups. Lens-derived lipids showed proportionately greater decreases in cholesterol content as compared to body-derived lipids, seen in Figure 4.21.

The inhibitory effect of RO48-8071 on LSS was supported by the observed accumulation of oxidosqualene in both bodies and lenses of treated zebrafish, where oxidosqualene content was increased by more than six times as compared to control tissue samples.

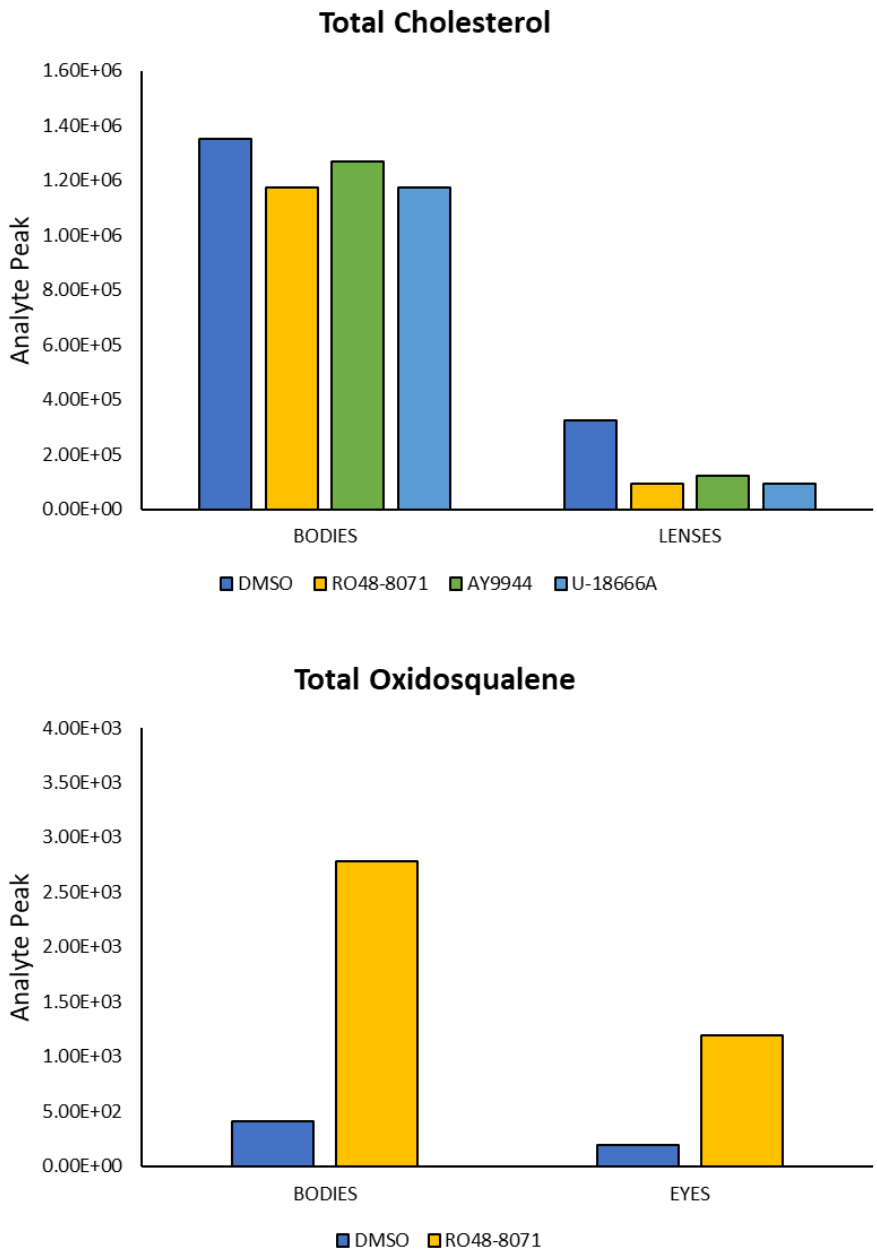


Figure 4.21. Total cholesterol reduction following inhibitor treatment is apparent in whole body and lens tissue samples, while oxidosqualene accumulates in bodies and lenses of RO48-8071-

treated zebrafish. Total cholesterol content was reduced in whole body-derived lipids from RO48-8071-treated zebrafish by 1.14X, 1.06x in AYY9944-treated larvae, and 1.12X in U-18666A. Synthesis inhibition had a more dramatic effect on lens total cholesterol, with the RO48-8071 groups showing a 3.53X decrease, the AY9944 groups a 2.66X decrease, and the U-18666A groups a 3.49X decrease as compared to the 0.1%(v/v) DMSO control. Upstream metabolite accumulation was noted in RO48-8071 zebrafish tissues, with oxidosqualene levels being increased by 6.87X and 6.28X in whole body and whole lens-derived lipids, respectively. N=25 per treatment group from separate clutches, technical triplicates pooled.

Similarly, upstream metabolite accumulation was identified in both AY9944 and U-18666A-treated zebrafish.

A smaller increase in retained 7-dehydrocholesterol was observed in whole-body derived lipids than lens-derived lipids in AY9944-treated zebrafish, while U-18666A-treated larvae showed a comparatively modest retention of desmosterol in whole-body lipids coupled with a decrease of desmosterol in lenses, as seen in Figure 4.22.

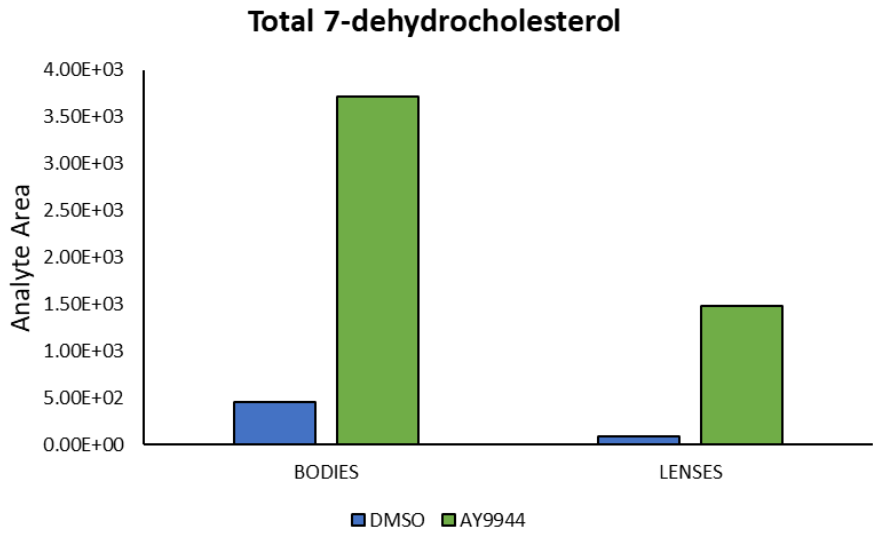


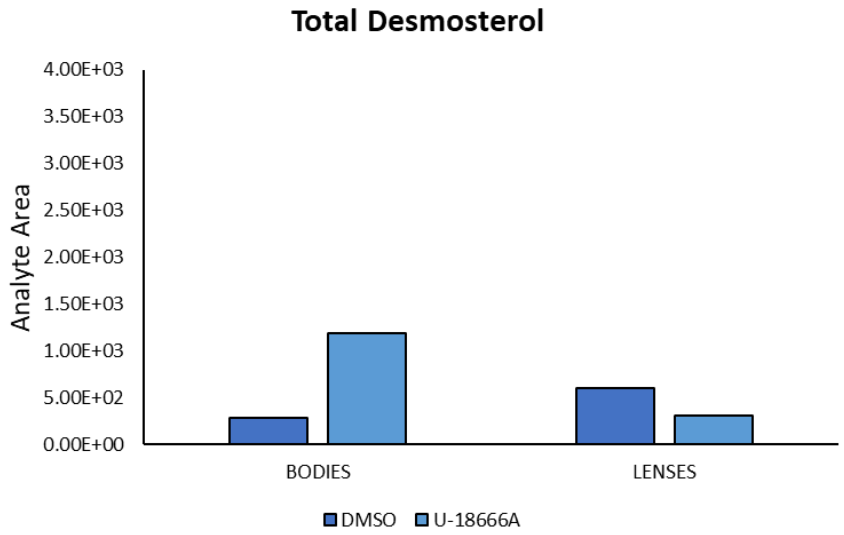


Figure 4.22. 7-dehycrocholesterol accumulates in bodies and lenses of AY9944-treated zebrafish, while U-18666A treatment leads to the accumulation of desmosterol in bodies but not lenses. The total amount of 7-dehucrocholesterol was increased by 8.15X in bodies and 17.55X in lenses of AY9944-treated zebrafish, while desmosterol levels were increased by 4.15X in U-18666A-treated zebrafish. In contrast with all other observations, no accumulation of desmosterol was found in lenses of U-18666A-treated zebrafish, with a 1.9X decrease being noted instead as compared to the 0.1% (v/v) DMSO control groups. N=25 per treatment group from separate clutches, technical triplicates pooled.

### 4.6.2 Lanosterol and cholesterol supplementation partially recover total cholesterol levels in whole bodies and lenses

Inhibitor-treated and sterol supplemented zebrafish were analysed for their whole body and lens cholesterol content to assess the effect of lanosterol and cholesterol supplementation on native lipid levels.

Lanosterol supplementation at 48 hpf partially restored total cholesterol levels in RO48-8071-treated zebrafish in both whole bodies and lenses, with the rescue effect being more prominent in lens-derived lipids. Similarly, cholesterol supplementation at 48 hpf restored total cholesterol levels in AY9944-treated larvae, with lens cholesterol recovery being more efficient as seen in Figure 4.23.

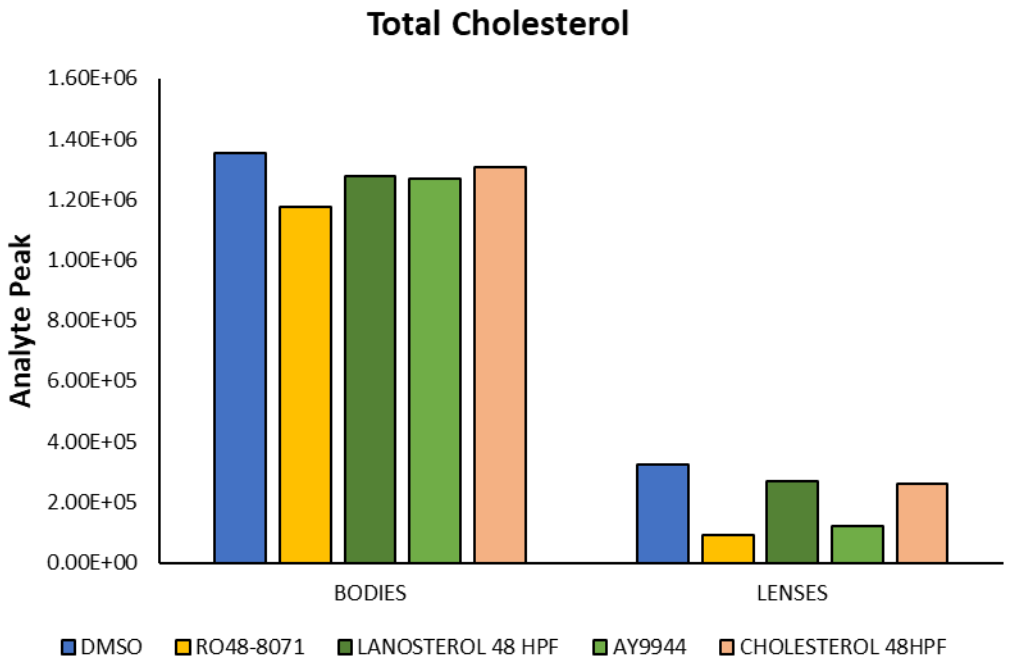


Figure 4.23. Lanosterol and cholesterol supplementation at 48 hpf partially restore total cholesterol levels in bodies and lenses of inhibitor-treated zebrafish. RO48-8071-treated larvae supplemented with lanosterol at 48 hpf showed a 1.08X increase in whole body cholesterol and 2.94X increase in lens cholesterol as compared to the RO48-8071 only zebrafish. Total cholesterol levels were still reduced by 1.05X and 1.2X in whole body and lens-derived lipids respectively as compared to the 0.1% (v/v) DMSO control. Similarly, U-18666A-treated zebrafish supplemented with cholesterol at 48 hpf showed a 1.03X increase and a 2.15X increase in total cholesterol in bodies and lenses as compared to the U-18666A only treated larvae. Total cholesterol was still reduced both in bodies by 1.03X and in lenses by 1.23X as compared to control groups. N=25 per treatment group from separate clutches, technical triplicates pooled.

### 4.6.3 Fluorophore-conjugated cholesterol does not penetrate the lens

Following the identification of increased lens cholesterol levels in sterol-supplemented zebrafish, fluorophore-conjugated and deuterium-tagged sterols were used to monitor supplement uptake and trafficking.

Zebrafish were manually dechorionated at 24 hpf and exposed to 100 µM TopFluor Bodipy cholesterol 488 at the previously established supplementation timepoint of 48 hpf. Live images were captured using a Leica SP5 as described in section 3.4.5.

TopFluor Bodipy cholesterol was detected in the yolk and sclera of supplemented zebrafish larvae from the first recorded timepoint at 5 hours post exposure. The distribution of the compound was not altered at 6 hours post exposure, as seen in Figure 4.24.

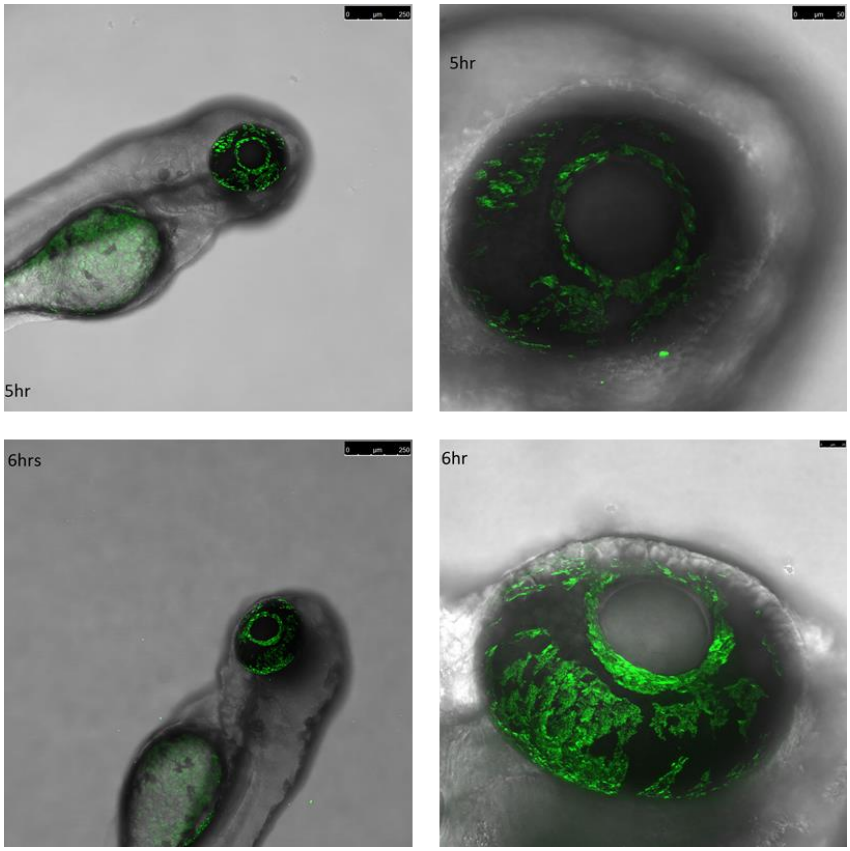


Figure 4.24. TopFluor Bodipy cholesterol 488 penetrates the yolk and sclera of developing zebrafish. At 5 hours post exposure, the compound is visible throughout the yolk of larvae at 10X magnification, and in the sclera of the eye at 40X magnification. The distribution of the compound is identical at 6 hours post exposure. No fluorescence was detected in the lenses of treated zebrafish. Scale bar 250 µm for 10X (left panels, top and bottom) and 50 µm for 40X (right panels, top and bottom). Images are maximum projections of z-stacks overlaying fluorescence and transmission illumination.

This distribution pattern persisted to 18- and 24-hours post cholesterol exposure, with no detected fluorescence in the lens becoming apparent at any point during the time course as seen in Figure 4.25.

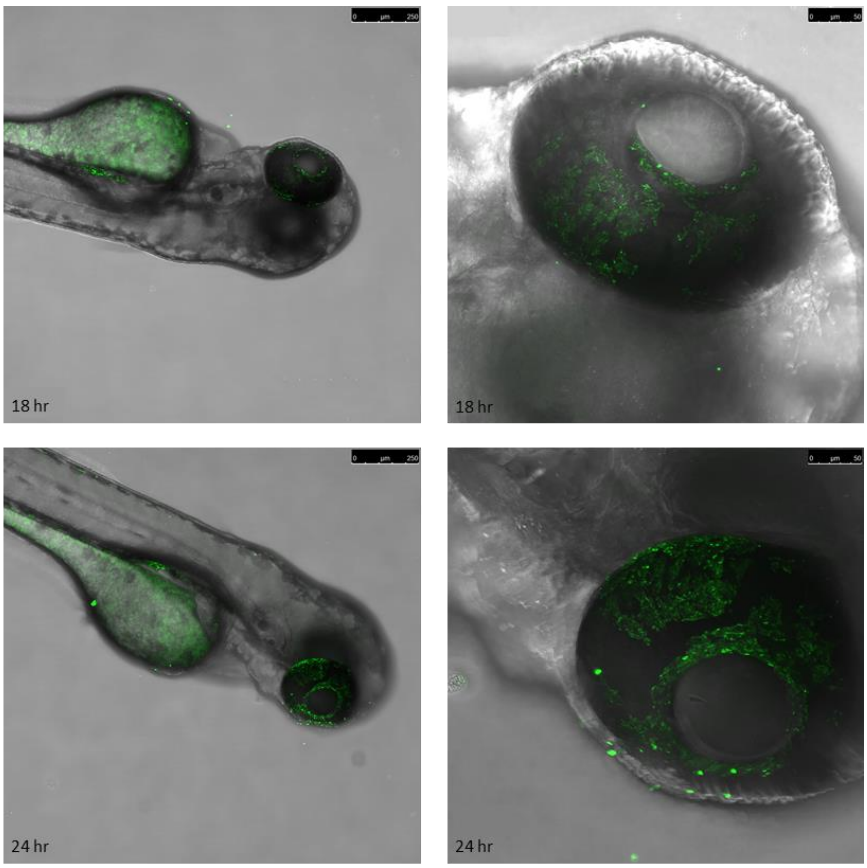


Figure 4.25. TopFluor Bodipy cholesterol 488 penetrates the yolk and sclera of developing zebrafish. At 18 hours post exposure, the compound is visible throughout the yolk of larvae at 10X magnification, and in the sclera of the eye at 40X magnification. The distribution of the compound is identical at 24 hours post exposure, as it is in 5- and 6-hours post exposure. No fluorescence was detected in the lenses of treated zebrafish. Scale bar 250 µm for 10X (left panels, top and bottom) and 50 µm for 40X (right panels, top and bottom). Images are maximum projections of z-stacks overlaying fluorescence and transmission illumination.

The supplementation of Bodipy cholesterol at the earlier developmental timepoint of 6 hpf resulted in the modest uptake of the compound into the yolk at 20 hpf, while no detectable fluorescence was noted for any ocular tissues in contrast with the findings in Figures 4.24 and 4.25. Larvae were followed through to 30 hpf, at which point no fluorescence was detected in the yolk as seen in Figure 4.26.

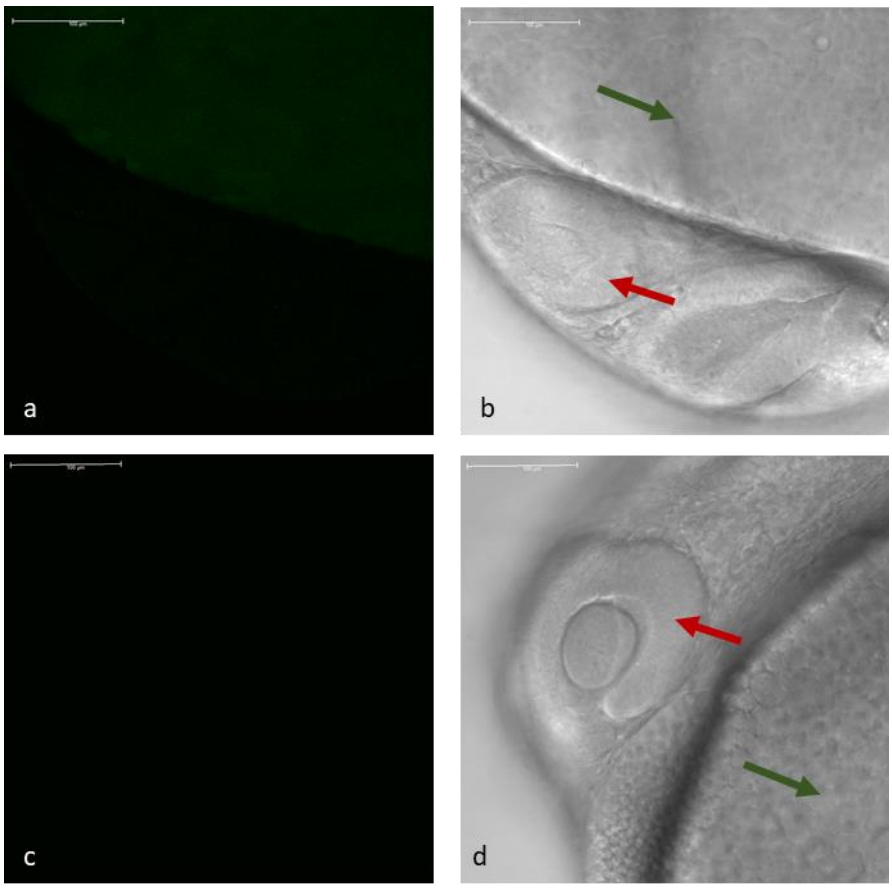


Figure 4.26. TopFluor Bodipy cholesterol is detected at 20 hpf in the yolk of larvae supplemented at 6 hpf but is absent at 30 hpf. At 20 hpf (panels a and b), cholesterol fluorescence is detected uniformly throughout the yolk (green arrow) but is absent in all eye tissues (red arrow). At 30 hpf (panels c and d) there is no detectable fluorescence in the yolk (green arrow) or eye (red arrow). Scale bar 100 µm for 40X (all panels). Images are maximum projections of z-stacks with fluorescence (panels a and c) and transmission illumination (panels b and d).

### 4.6.4 Supplemented sterols are retained and metabolised in zebrafish larvae

To examine whether supplemented sterols are absorbed, trafficked, and metabolised by the zebrafish, larvae were supplemented with d6 cholesterol or d6 lanosterol at two distinct developmental time points. All larvae were manually dechorionated at 70% epiboly 6 hpf, prior to any distinct isolation of the presumptive lens. The first group of zebrafish were supplemented with either deuterated sterol immediately and followed to 20 hpf, when the lens placode is fully formed. The second group were supplemented at 20 hpf and followed to 30 hpf, when the lens has detached from the retina and primary fibre formation is almost complete. Yolks were also collected from each group to analyse its role in sterol absorption and processing.

Lenses from zebrafish collected at 20 hpf showed a modest retention of d6 cholesterol when the larvae were supplemented with d6 cholesterol, while no deuterated sterols were detected

in the equivalent yolks. No deuterated sterols were detected in lenses of zebrafish supplemented with d6 lanosterol, while d6 lanosterol was detected in yolks isolated from the same group as seen in Figure 4.27.

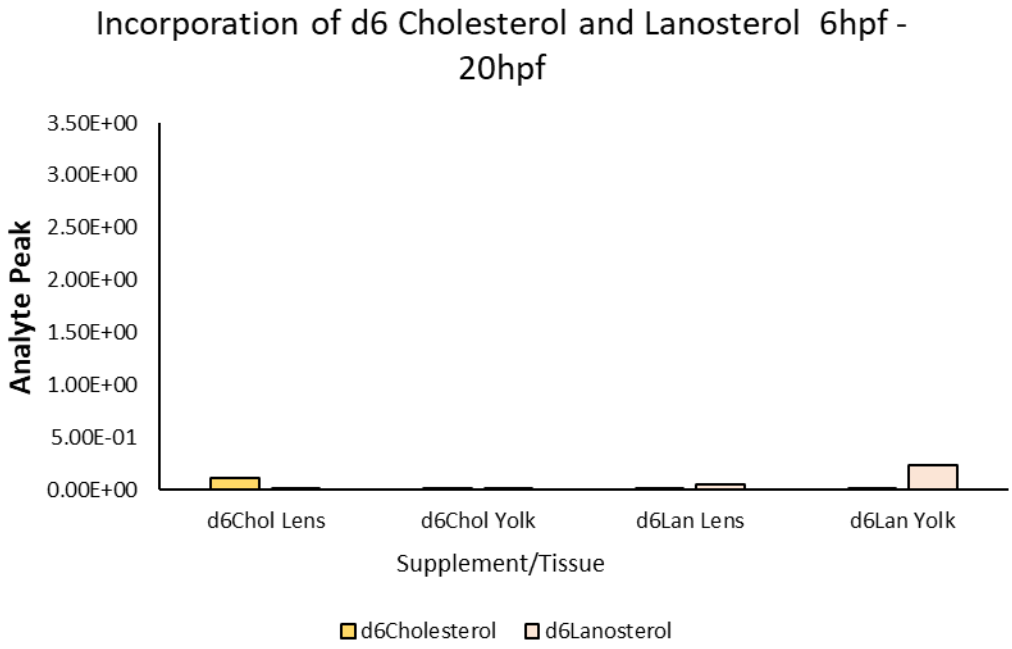


Figure 4.27. D6 cholesterol incorporation was detected in the lens at 20 hpf following d6 cholesterol supplementation, while d6 lanosterol was detected in the yolk at 20 hpf following d6 lanosterol supplementation in zebrafish larvae. N=25 per treatment group from separate clutches, technical triplicates pooled.

Supplementation at 20 hpf resulted in substantially increased detection of d6 cholesterol in lenses of d6 cholesterol supplemented larvae, while minimal amounts of d6 cholesterol were detected in yolks from this group. Lenses isolated from zebrafish supplemented with d6 lanosterol also showed an increased amount of d6 lanosterol and a modest amount of d6 cholesterol, while yolks extracted from these larvae had increased d6 lanosterol levels but no detectable d6 cholesterol, as seen in Figure 4.28.

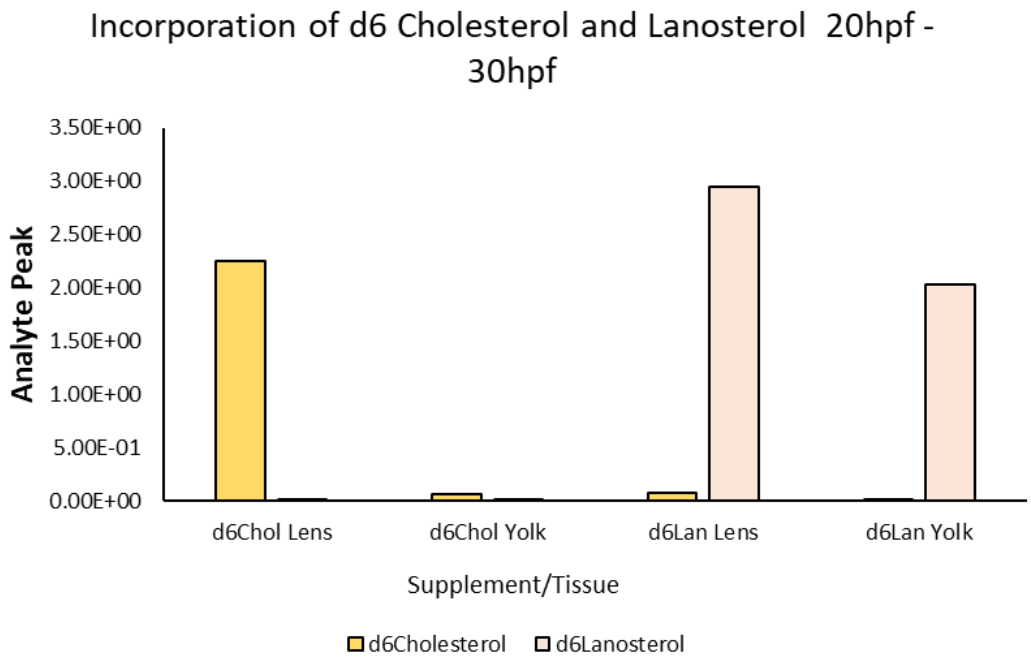


Figure 4.28. Increased d6 cholesterol incorporation was detected in lenses of d6 cholesterol supplemented zebrafish at 30 hpf, while increased d6 lanosterol was detected in both lenses and yolk of d6 lanosterol supplemented larvae. Trace amounts of d6 cholesterol were also detected in lenses of zebrafish supplemented with d6 lanosterol, demonstrating a downstream metabolic processing of supplement lanosterol. N=25 per treatment group from separate clutches, technical triplicates pooled.

The presence of d6 cholesterol in zebrafish supplemented with d6 lanosterol in addition to the relative absence of deuterated sterols in highly active metabolic tissues such as the yolk suggest these sterols are actively processed in the larvae. The d6 deuterium tag is inserted on the 27$^{th}$ carbon of both lanosterol and cholesterol and is not altered during the metabolism of lanosterol to cholesterol. However, the first metabolic step in the degradation of cholesterol involves a hydroxylation of the terminal carbon 27; as such, we analysed lenses and yolks of supplemented zebrafish for the presence of d3, d4, and d6 tagged 27-OHC.

The major identified metabolite in yolks was d3 27-OHC, present in 6 hpf and 20 hpf d6 cholesterol supplemented larvae and in 20 hpf d6 lanosterol supplemented zebrafish. No significant amount of either metabolite was detected in lenses from any supplementation group except for 20 hpf d6 lanosterol supplemented zebrafish, where minor amounts of d3, d4 and d6 27-OHC were identified as seen in Figure 4.29.

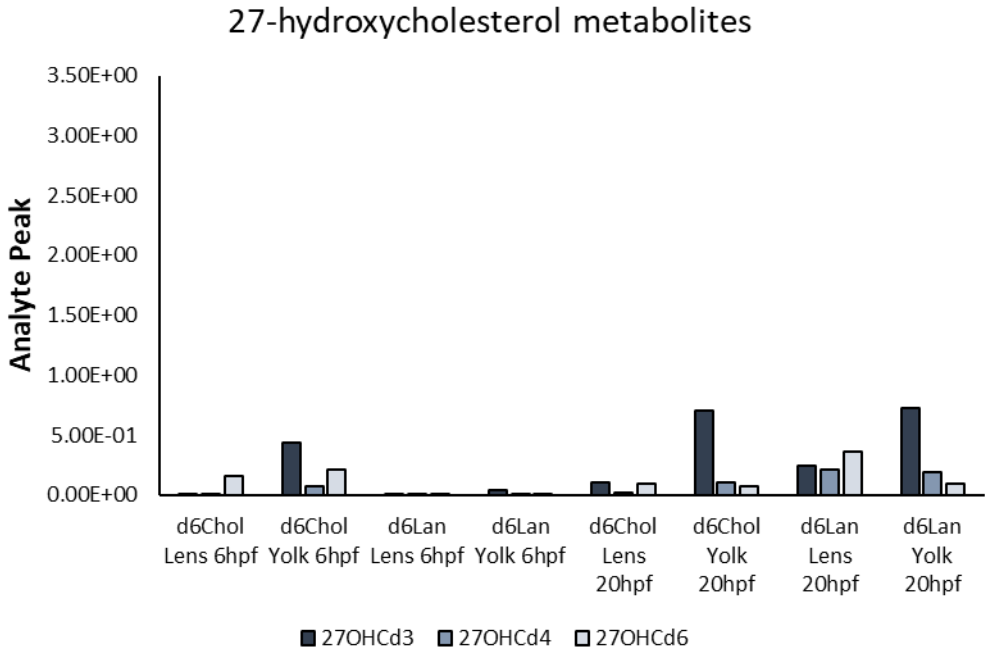


Figure 4.29.D3 27-hydroxycholesterol was detected as the major metabolite in yolks from d6 cholesterol and d6 lanosterol supplemented zebrafish. The conversions of d6 lanosterol and d6 cholesterol to d3 27-hydroxycholesterol demonstrate the active metabolic processing of supplemented sterols in the zebrafish larvae. Trace amounts of d3 and d6 27-hydroxycholesterol were detected in lenses of d6 lanosterol supplemented zebrafish. N=25 per treatment group from separate clutches, technical triplicates pooled.

## 4.7 General summary

The partial inhibition of cholesterol synthesis decreases larval independent movement and negatively affects the optomotor response, while proportionately reducing larval size and accelerating yolk consumption. The pharmacological inhibition of cholesterol synthesis has a limited impact on the gross morphology of zebrafish eyes, including the aspect ratio, and a limited effect on lens development and structure, reducing epithelial cell height.

Although lanosterol supplementation rescues the synthesis inhibition-associated reduction in yolk size, cholesterol supplementation is lethal in larval zebrafish for all inhibitors apart from AY9944. Despite this, larvae treated with AY9944 and supplemented with cholesterol are non-viable, highlighting the importance of further understanding the intricacies of sterol metabolism in the context of an oxysterol-associated pharmacotherapy.

The pharmacological inhibition of cholesterol synthesis reduces total cholesterol in zebrafish and results in the accumulation of relevant upstream metabolites, while lanosterol and cholesterol supplementation recover total cholesterol levels in synthesis-inhibited larvae.

The incorporation of supplemental lanosterol and cholesterol in the developing zebrafish is variable and can be traced through downstream metabolic processing events, as seen in Figure 4.30.

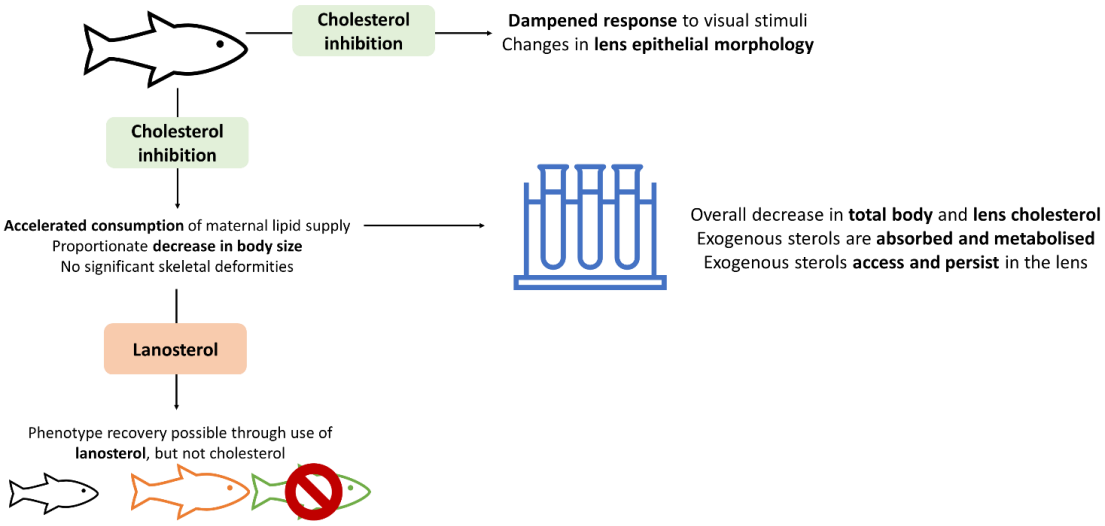


Figure 4.30. The inhibition of cholesterol synthesis in the developing zebrafish larvae impacts whole body and lens development, and may be rescued by the use of exogenous lanosterol.

# 5 Chapter 5: The effect of cholesterol and lanosterol supplementation on lens fibre cell proteins and lipids

## 5.1 Protein-lipid relationships in lens membranes

The unique lipid profile of lens fibre cell membranes, from the age-dependent increase in cholesterol to the species-specific distribution of phospholipids and sphingomyelins provides a canvas to study the preferential interactions of lens proteins with distinct lipid species and bilayer domains.

Previous studies have characterised the protein content of detergent resistant cholesterol rafts and detergent soluble domains (89,221). The localisation of AQP0 to the lateral surface of fibre cells and of CX50 to the apical ends (178) in addition to the sorting of the two proteins in detergent resistant membranes (DRMs) and detergent soluble membranes (DSMs) provides strong evidence for a necessary specificity in protein-lipid interactions to maintain lens health. Further, the loss of cholesterol rafts in cataractous lenses (72) supports the hypothesis that protein function is dependent on the lipid composition of fibre cells membranes.

Independent of transmembrane proteins, the interactions of cytoskeletal proteins with lipid rafts have been shown to be influenced by the lipid composition of these domains, with the loss of raft cholesterol leading to an increase in cellular rigidity and cytoskeleton-membrane attachment (72,326) through actin polymerisation. The cataract-causing Niemann-Pick C1 disease has been associated with hypophosphorylation of vimentin due to reduced protein kinase C (PKC) activity, limiting cholesterol transport and increasing the amount of insoluble vimentin in cells (327). Vimentin has also been associated with the transport of cholesterol from lipid droplets to mitochondria (318), revealing a broad potential for intermediate filament and cytoskeleton interactions in lens epithelial and fibre cells.

The role of soluble α-crystallin in the maintenance of lens transparency and in the pathogenesis of cataract has been characterised (82,190,218) and discussed in section 1.3.2., with high molecular weight crystallin aggregates exhibiting a markedly increased membrane binding capacity (191,194) and providing a platform for the propagation of deleterious oxidative events. Data have indicated that α-crystallin binds to free lens membrane lipids (195), while pharmacological cataract reversal studies have proposed an oxysterol-mediated solubilisation of misfolded α-crystallin (299) indicating a the potential for crystallin-lipid interactions both in the context of membrane bilayers and free lipids.

The use of oxysterols as pharmaceutical interventions to prevent or reverse cataract will have to consider off-target interactions with lipid membrane domains and soluble lens proteins. As

such, we have examined the effect of lanosterol and cholesterol co-incubation on the solubility status of crude lens fibre cell extracts which include the lipid bilayer and its transmembrane proteins, cytoskeletal proteins, and crystallins.

## 5.2 Bovine lens membrane proteins have distinct sedimentation profiles

The serial extraction of bovine lens membranes yields two primary lipid membrane/protein fractions which are enriched for distinct proteins, as seen in Figures 5.1 and 5.2. “High protein content” membranes, as described in section 3.1.2, were derived from cortical and nuclear lens fibre cells serially extracted in NaCl, KCl, and $CH_5NO_3$, with the insoluble fraction retained from each step. These fractions contain both high and low molecular weight proteins as seen in Figure 5.1, including cytoskeletal filaments, transmembrane proteins, and crystallins. Further extraction with urea and NaOH as described in section 3.1.3. yields “low protein content” membranes, which include the fibre cell lipid bilayer and integral membrane proteins.

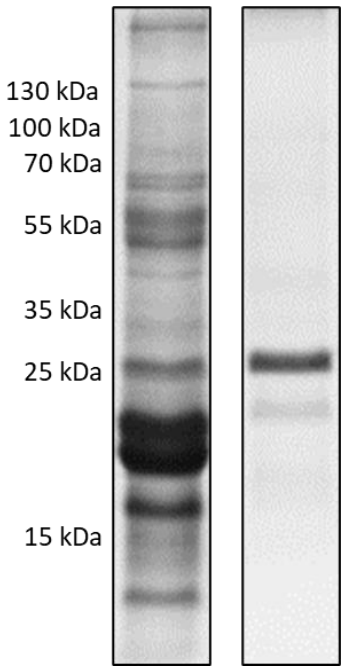


Figure 5.1. Protein profile of bovine lens cortex membranes prior to and following fractionation in an 8M urea buffer. High protein content lysate prior to urea extraction (left) and integral membrane protein lysate following urea extraction (right) Enrichment of the two 18 kDa and 17 kDa bands can be seen in the high protein content lysate, while enrichment of the 26 kDa band can be seen in the integral lens membrane protein preparation. SDS-PAGE stained with Coomassie Brilliant Blue R-250, 5 µg wet weight per lane extracted from a pool of 24 lenses.

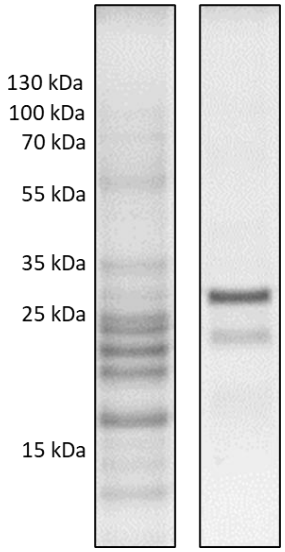


Figure 5.2. Protein profile of bovine lens nucleus membranes prior to and following fractionation in an 8M urea buffer. High protein content lysate prior to urea extraction (left) and integral membrane protein lysate following urea extraction (right). Similar to the cortex-derived material, enrichment of the 26 kDa band can be seen in the integral lens membrane protein preparation. SDS-PAGE stained with Coomassie Brilliant Blue R-250, 5 µg wet weight per lane extracted from a pool of 24 lenses.

The further sedimentation of high protein content membranes produced a mix of insoluble and soluble material with cortex- and nucleus-specific profiles, as illustrated in Figure 5.3. The centrifugation of cortical membranes at 200k x g ($RCF_{AVG}$) produced a protein-enriched insoluble fraction, while further centrifugation of the supernatant at 400k x g ($RCF_{AVG}$) produced soluble and insoluble fractions containing two major bands between 15 kDa-25 kDa. A similar sedimentation profile was observed for nucleus-derived membranes, with the majority of material found in the insoluble fraction of the 200k x g centrifugation.

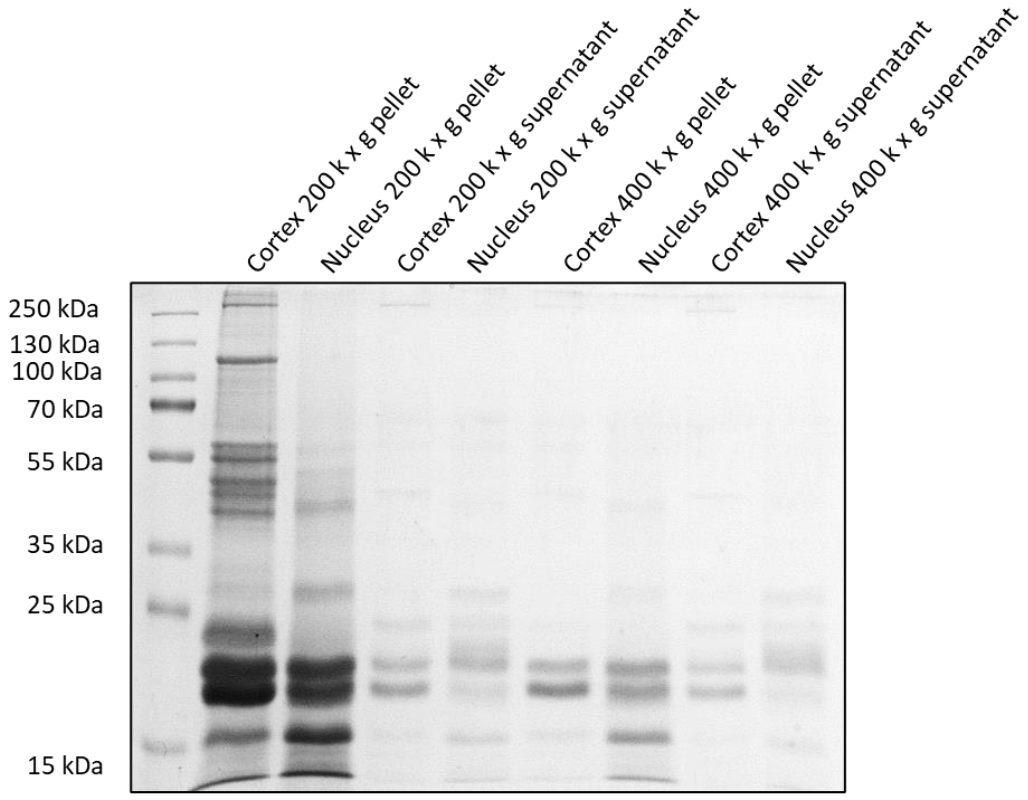


Figure 5.3. Sequential centrifugation of high protein content bovine lens membranes yields different sedimentation profiles for cortex-derived and nucleus-derived protein, SDS-PAGE

analysis. Most of the high and low molecular weight protein content of cortical and nuclear lens membranes was successfully isolated in the insoluble fraction after a 200k x g centrifugation, while small amounts of material remained soluble. These soluble fractions further yielded insoluble and soluble fractions at 400k x g, with the major enriched protein bands being apparent in the 15-35 kDa range. SDS-PAGE stained with Coomassie Brilliant Blue R-250, 5µg wet weight per lane extracted from a pool of 24 lenses.

### 5.2.1 Transmembrane bovine lens proteins sediment in cholesterol-rich fractions

The lipid content of insoluble and soluble high protein content membranes was analysed following a 200k x g centrifugation to identify the ratio of cholesterol and phosphatidylcholine.

Cholesterol enrichment was found in both cortical and nuclear lens fibre cell membranes, as seen in Figure 5.4. The concentration (µM) of total cholesterol was 97X in the insoluble fraction as compared to the soluble fraction; in contrast, the total cholesterol in the insoluble fraction of cortex-derived membranes was 26.14X the concentration identified in the soluble fraction. Similarly, the sedimentation of phosphatidylcholine was enriched in nuclear lens fibre cell membranes with a 20X increase detected in the insoluble fraction as compared to a 10X increase in cortical membranes.

The relative enrichment of cholesterol as compared to phosphatidylcholine was substantially increased in nuclear fibre cell membranes, with a 48.5X cholesterol/phosphatidylcholine concentration ratio in nucleus-derived membranes and 12.2X in cortex-derived membranes, as seen in Figure 5.4.

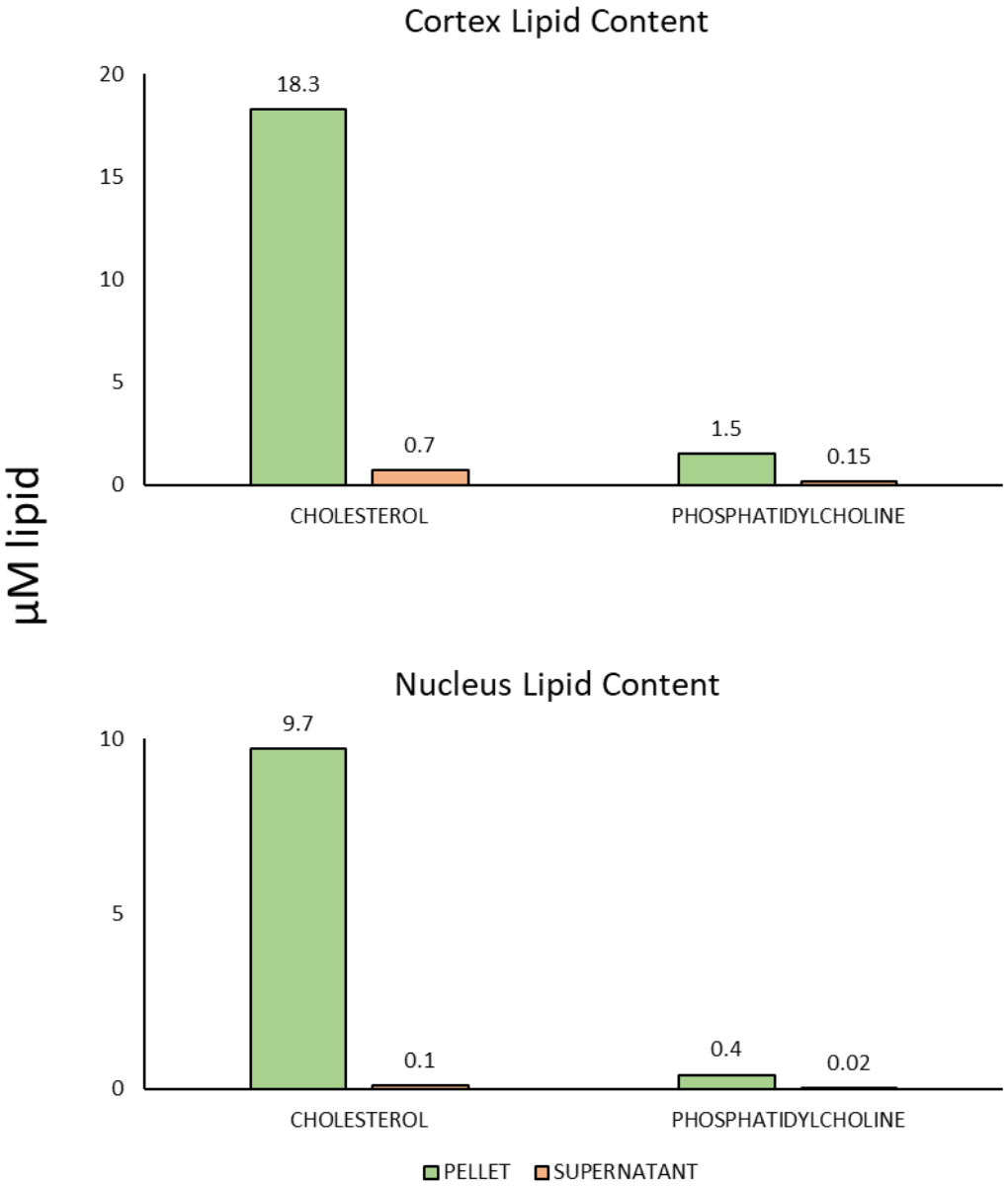


Figure 5.4. The enrichment of cholesterol in pelletable cortex and nucleus membranes is substantially increased as compared to the enrichment of phosphatidylcholine. In insoluble cortex-derived membranes, cholesterol is enriched by 12.2X as compared to phosphatidylcholine, whereas the same ratio is 48.5 in nucleus-derived membranes. These enrichment profiles are not retained in soluble material from either lens fraction, as the cholesterol/phosphatidylcholine ratio is 4.6 in cortex and 5 in nucleus membrane supernatants. Biological samples extracted from a pool of 24 lenses, 10 mg wet weight material per sample.

The transmembrane proteins AQP0, CX50, and CAV-1 were identified in the cholesterol enriched insoluble cortex and nucleus fractions isolated from the 200k x g centrifugation, as seen in Figure 5.5. Cortical AQP0 presented with a major band at 26 kDa and a minor band at 50 kDa, while nuclear AQP0 was found at a minor 26 kDa band. CAV-1 was present in cortex

membranes only at 50 kDa, while CX50 was detected in cortex as a major 55 kDa band and two groups of minor bands ranging from 35-50 kDa and 70-100 kDa.

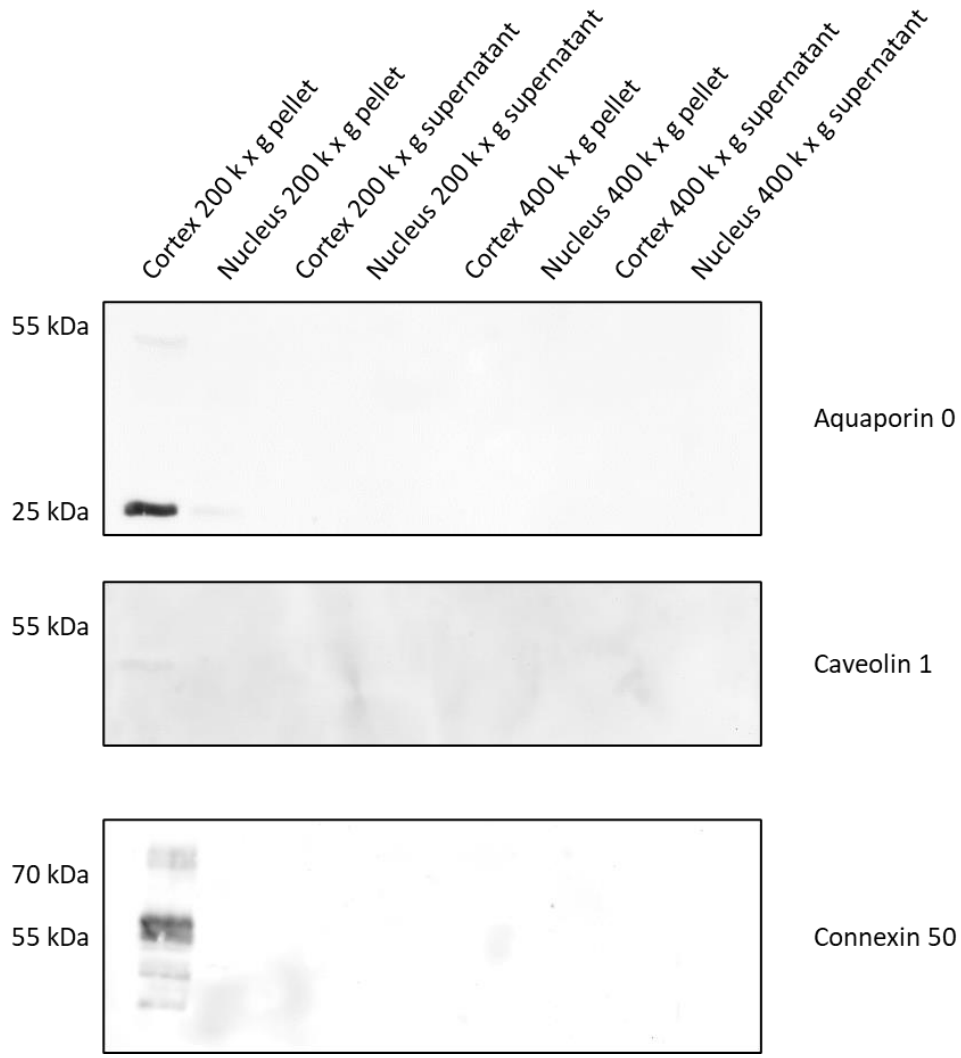


Figure 5.5. The major membrane-associated proteins AQP0, CAV-1, and CX50 are enriched in insoluble cortical lens membranes. AQP0 was detected in the insoluble fraction of 200k x g cortical lens membranes as 26k Da and 50 kDa forms, while it was only detected as a 26k Da band in nuclear membranes. CAV-1 was detected as a 50 kDa band in the insoluble fraction of 200k x g cortical lens membranes, while CX50 was detected in the same fraction with two major bands between 55-60 kDa, two minor bands between 35-45 kDa, and two further minor bands between 70-100 kDa. All lanes 5 µg wet weight per lane extracted from a pool of 24 lenses.

### 5.2.2 Cytoskeletal filaments have variable sedimentation profiles in bovine lens membranes

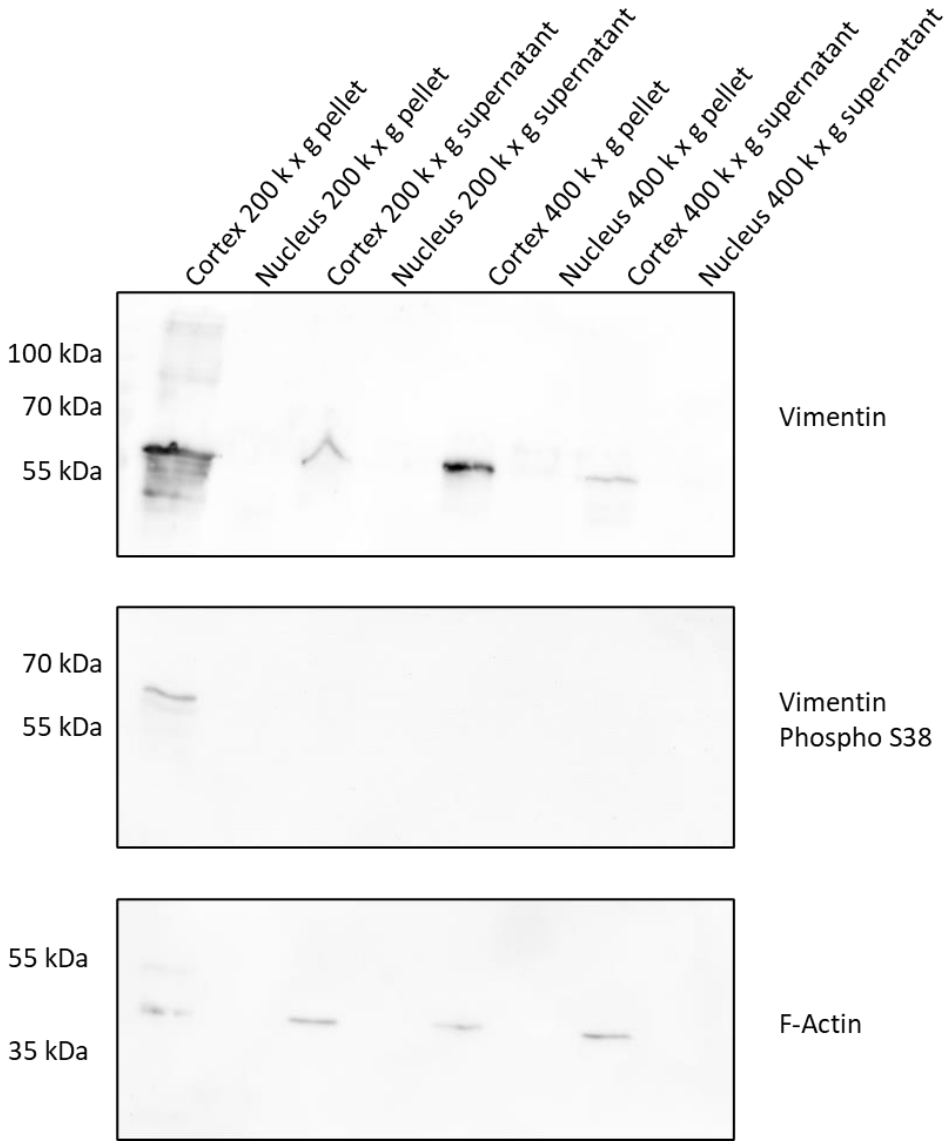


The filament proteins vimentin and actin were identified in all cortex fractions, as seen in Figure 5.6. Vimentin was enriched as a major band at 60 kDa in insoluble fractions following centrifugation at 200k x g and 400k x g, while minor bands were identified in the 200k x g insoluble fraction ranging between 50kDa-130 kDa. The major 60 kDa band was retained in all other cortex fractions. Phosphorylated vimentin was detected as a major-minor 60 kDa band pair in the insoluble cortex fraction produced from the 200k x g centrifugation, while f-actin was identified at equal concentrations in all cortex fractions.

Figure 5.6. The cytoskeleton proteins vimentin and actin were detected in cortical lens membranes. Vimentin was detected as a major 65 kDa band in soluble and insoluble cortical lens membrane fractions from 200k x g and 400k x g centrifugations, while minor band were detected in the 200k x g insoluble cortical fraction ranging from 45 kDa to 130 kDa (top panel). Phospho-vimentin S39 was detected as a major 65 kDa band in cortical insoluble 200k x g fractions, while a minor ~60 kDa band was also detected under the same sample conditions (middle panel). Similarly, actin was detected as the major 42 kDa band in all insoluble cortex fractions, while a minor ~50 kDa was also detected in the 200k x g insoluble cortex fraction (bottom panel). All lanes 5 µg wet weight per lane extracted from a pool of 24 lenses.

The beaded filament proteins BFSP1 and BFSP2 were detected across all cortex and nucleus fractions, with distinct band enrichment patterns for each sample, as seen in Figure 5.7. Major band regions were identified between 40 kDa-60 kDa in cortical and nuclear insoluble membranes centrifuged at 200k x g, with high molecular weight material at 60 kDa, 70 kDa, and 130 kDa was found in all other cortex fractions. Two minor bands at 25 kDa-30 kDa were identified in all cortex and nucleus samples, with two further low molecular weight (17 kDa-19 kDa) bands were observed in cortex-derived membranes.

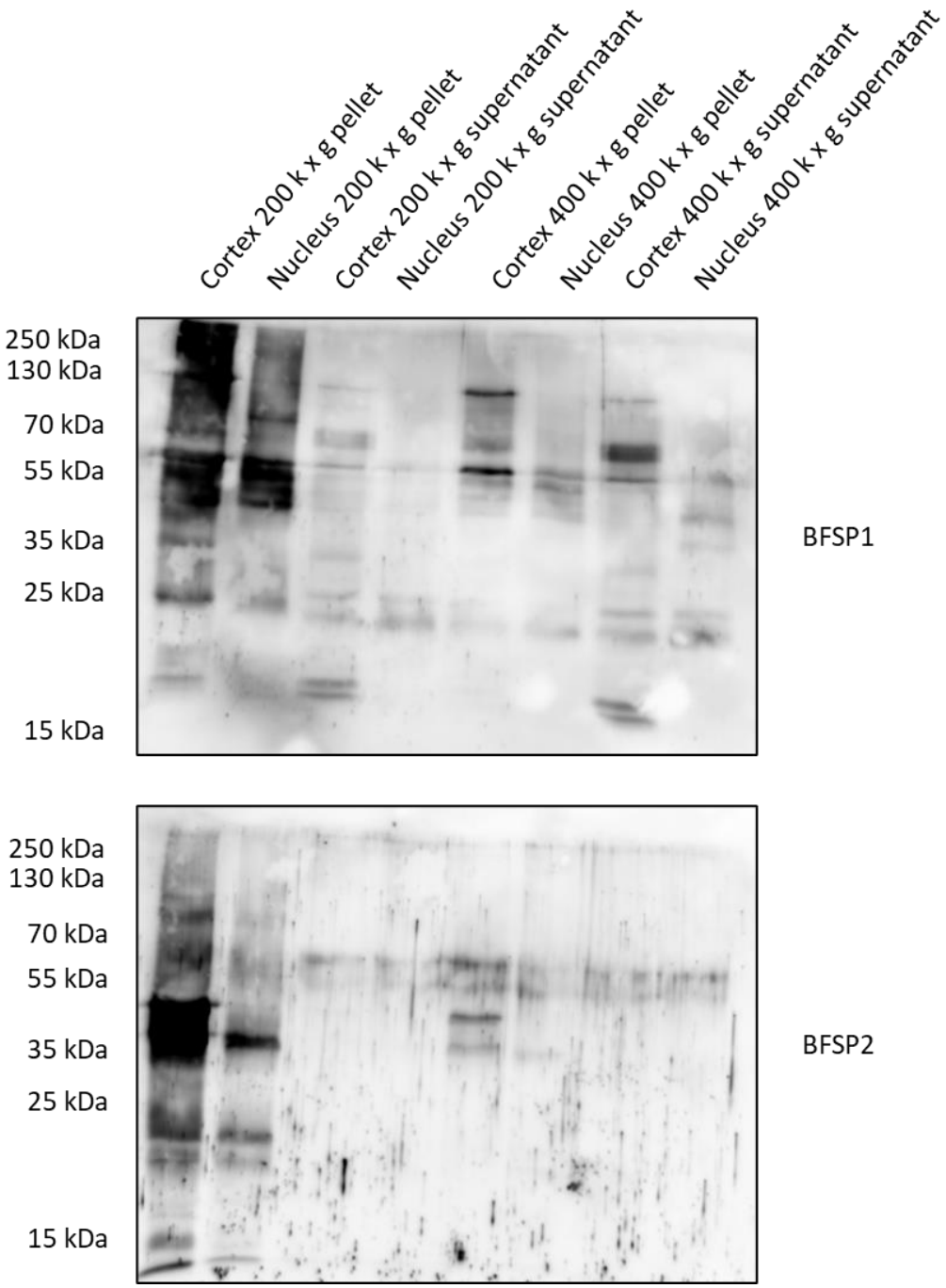


Figure 5.7. The beaded filament proteins BFSP1 and BFSP2 show different sedimentation profiles for their distinct isoforms in cortical and nuclear lens membranes. The 200k x g insoluble fractions show increased BFSP2 enrichment between 35 kDa and 55 kDa in cortex membranes, while a major band is prominent at ~40 kDa in nucleus-derived membranes. Two major enriched BFSP2 bands are present in the soluble 200k x g and both soluble and insoluble 400k x g fractions of cortex and nucleus membranes between 55 kDa and 75 kDa, while two further isoforms were identified in the insoluble 400k x g cortex fraction at 38 kDa and 50 kDa. Multiple isoforms were identified in cortical and nuclear membranes probed for BFSP1, with the majority of material isolated in the insoluble 200k x g fraction. Isoform enrichment differed dependent both on the

origin of the material (cortex or nucleus) and the centrifugal force applied. A minor band at 25 kDa was identified in all samples. All lanes 5 µg wet weight per lane extracted from a pool of 24 lenses.

The filament protein BFSP2 was enriched in the 35 kDa-55 kDa region in both cortex and nucleus insoluble membranes centrifuged at 200k x g, while a double band region was noted between 55 kDa-70 kDa in all other fractions. Further, two minor bands were retained in the 400k x g cortex insoluble membranes at 40 kDa and 50 kDa.

### 5.2.3 αB crystallin is present in all fractions, while γC-crystallin is enriched in nucleus-derived membranes

A major 22 kDa αB-crystallin band was identified in all samples, with equal enrichment across cortical and nuclear fibre cell membranes. In contrast, γC-crystallin was enriched in nucleus-derived fibre cell membranes, with the majority of the material found in the insoluble 200k x g centrifugation fraction, as seen in Figure 5.8.

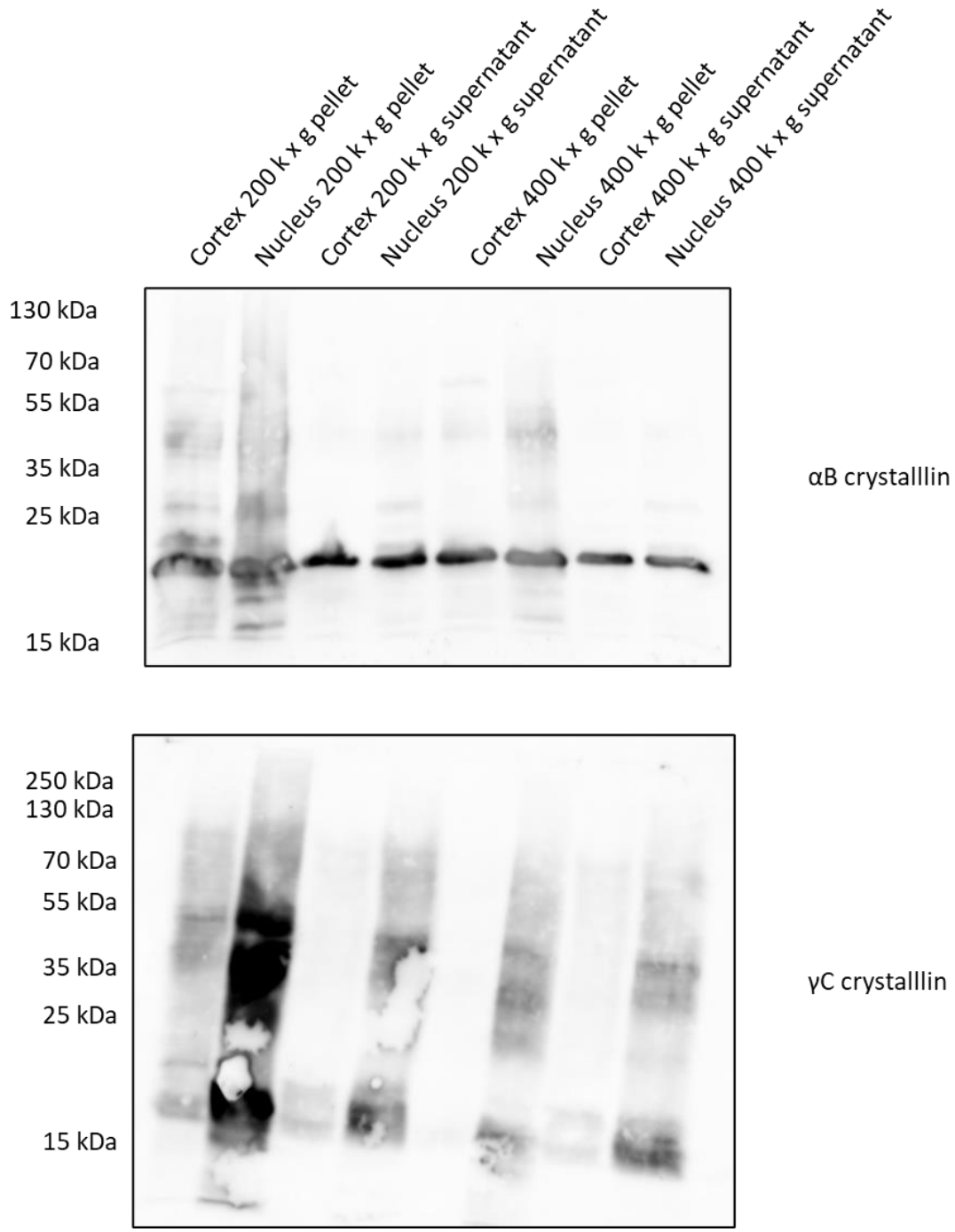


Figure 5.8. Low molecular weight αB-crystallin is enriched ubiquitously in cortex and nucleus-derived lens membranes, while γC-crystallin is enriched in nucleus fractions. The major enriched 22 kDa band for αB-crystallin was present in all fractions, while minor bands were also detected in the 200k x g insoluble cortex and nucleus fractions. Three major staining regions were detected at 17 kDa, 35 kDa, and 45 kDa for γC-crystallin in nucleus-derived membranes and in the insoluble 200k x g cortex fraction. All lanes 5 µg wet weight per lane extracted from a pool of 24 lenses.

## 5.3 High-protein content membranes contain a variably soluble protein fraction

The release of soluble protein from seemingly insoluble lens membrane fractions via centrifugation was further examined to determine whether this is a force-mediated effect or whether it occurs in a temporal manner.

Previous studies have reported variable effects of sterol supplementation on the solubility of α-crystallin (251,269,299) and on the clarity of cataractous lenses (249), and as such we examined the influence of 10 µM lanosterol or 10 µM cholesterol on the sedimentation of high protein content membranes.

Cortical fibre cell high protein content membranes were serially centrifuged at 14k x g to remove native soluble α-crystallin (328,329) and were incubated at 37$^{O}$C in light safe-conditions. Samples were then centrifuged at 14k x g at 30 minutes, 2 hours, 12 hours, 24 hours, and 10 days to examine the solubility status of the total protein content.

Cortex-derived membranes showed a temporal increase in the release of a soluble fraction which consisted of a distinct subset of proteins from the original sample, including six identifiable major bands at 60 kDa, 50 kDa, 20 kDa, 17 kDa, 16 kDa, and 20 kDa. Nucleus-derived membranes showed a significantly reduced temporal release of soluble material between 15 kDa-35 kDa, as seen in Figure 5.9.

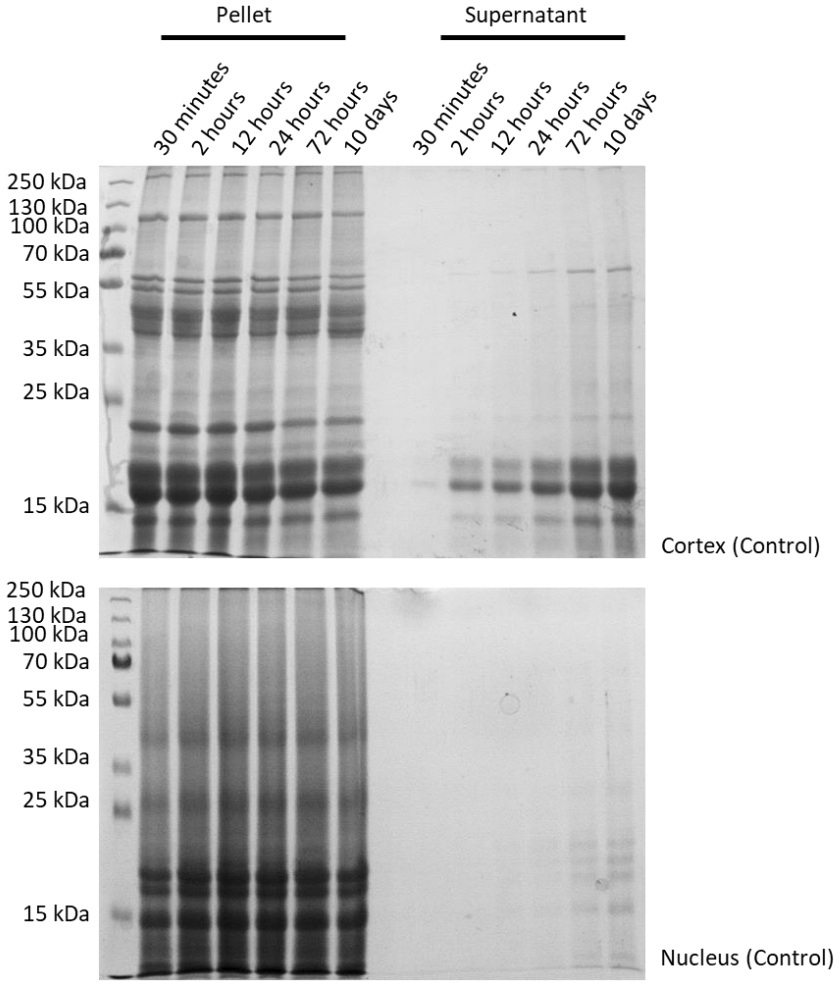


Figure 5.9. High protein content lens membrane fractions release soluble protein material in a temporal manner. Cortex membranes are subject to the increasing solubilisation of two major protein clusters at 50-70 kDa and 15-25 kDa, while nucleus membranes show significantly less time-dependent release of material. All starting samples are 5 µg wet weight extracted from a pool of 24 lenses.

No discernible effect on the speed of release or identity of the bands was noted following the co-incubation of the high protein content membranes with 10 µM lanosterol or 10 µM cholesterol, as seen in Figures 5.10 and 5.11.

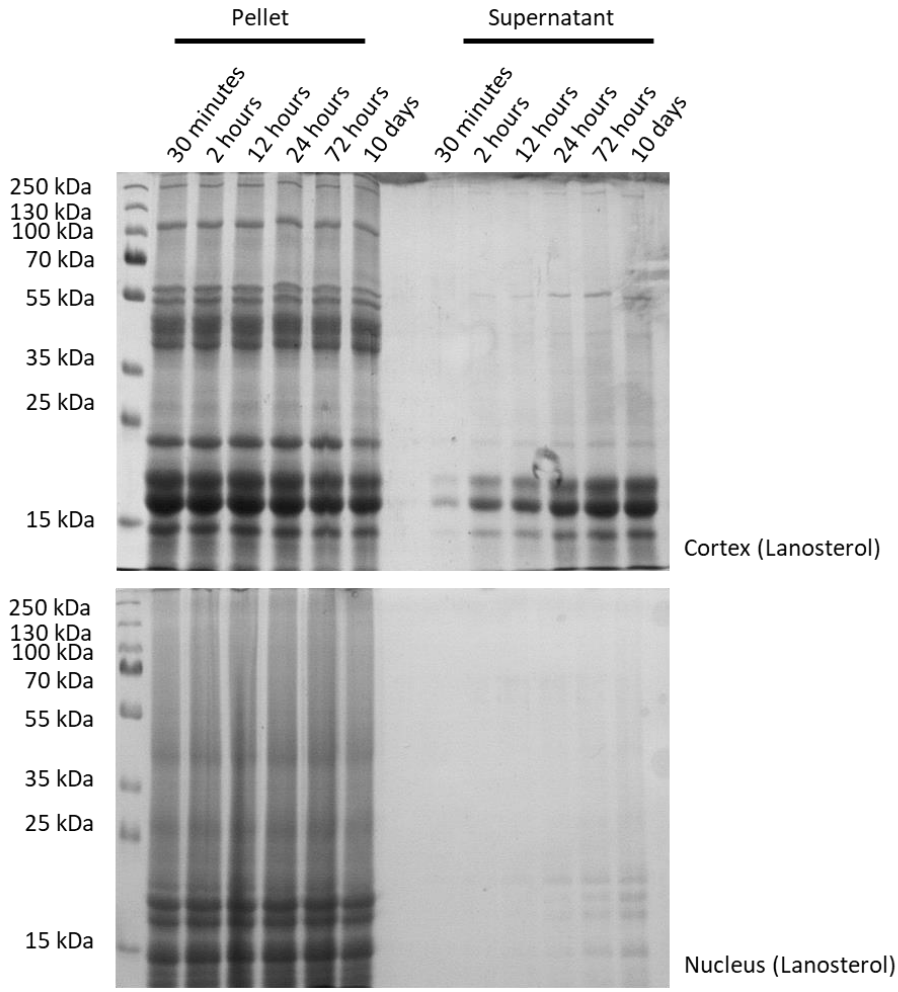


Figure 5.10. High protein content lens membrane fractions release soluble protein material in a temporal manner following co-incubation with 10 µM lanosterol at 37$^{O}$C in light-safe conditions. Cortex membranes are subject to the increasing solubilisation of two major protein clusters at 50-70 kDa and 15-25 kDa, while nucleus membranes show significantly less time-dependent release of material. All starting samples are 5 µg wet weight extracted from a pool of 24 lenses.

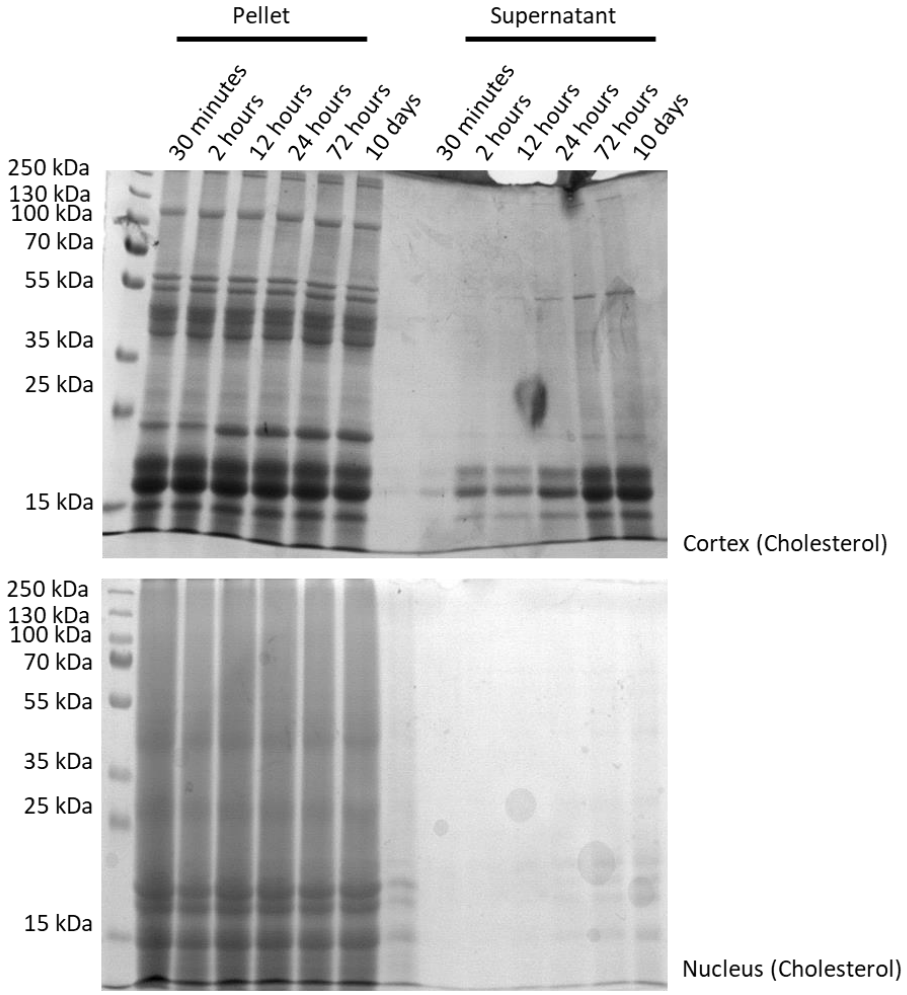


Figure 5.11. High protein content lens membrane fractions release soluble protein material in a temporal manner following co-incubation with 10 µM cholesterol at 37$^{O}$C in light-safe conditions. Cortex membranes are subject to the increasing solubilisation of two major protein clusters at 50-70 kDa and 15-25 kDa, while nucleus membranes show significantly less time-dependent release of material. All starting samples are 5 µg wet weight extracted from a pool of 24 lenses.

The solubilisation effect observed in control, lanosterol-incubated, and cholesterol-incubated membranes was studied in respect to the major lens proteins AQP0, CX50, vimentin, BFSP1, and αB-crystallin.

### 5.3.1 Aquaporin 0 is present in soluble and insoluble membrane fractions, in contrast with insoluble connexin 50

AQP0 was detected as a major 26 kDa band in all insoluble membrane fractions, with no fluctuation between timepoints. A minor 50 kDa band was detected in all insoluble fractions, and in increasing concentration in the 24 hour, 72 hour, and 10 day timepoints in the soluble membrane fractions of the control and cholesterol co-incubated samples and is most likely an AQP0 dimer. No AQP0 was detected in the soluble fractions of high protein content membranes co-incubated with lanosterol, as seen in Figure 5.12.

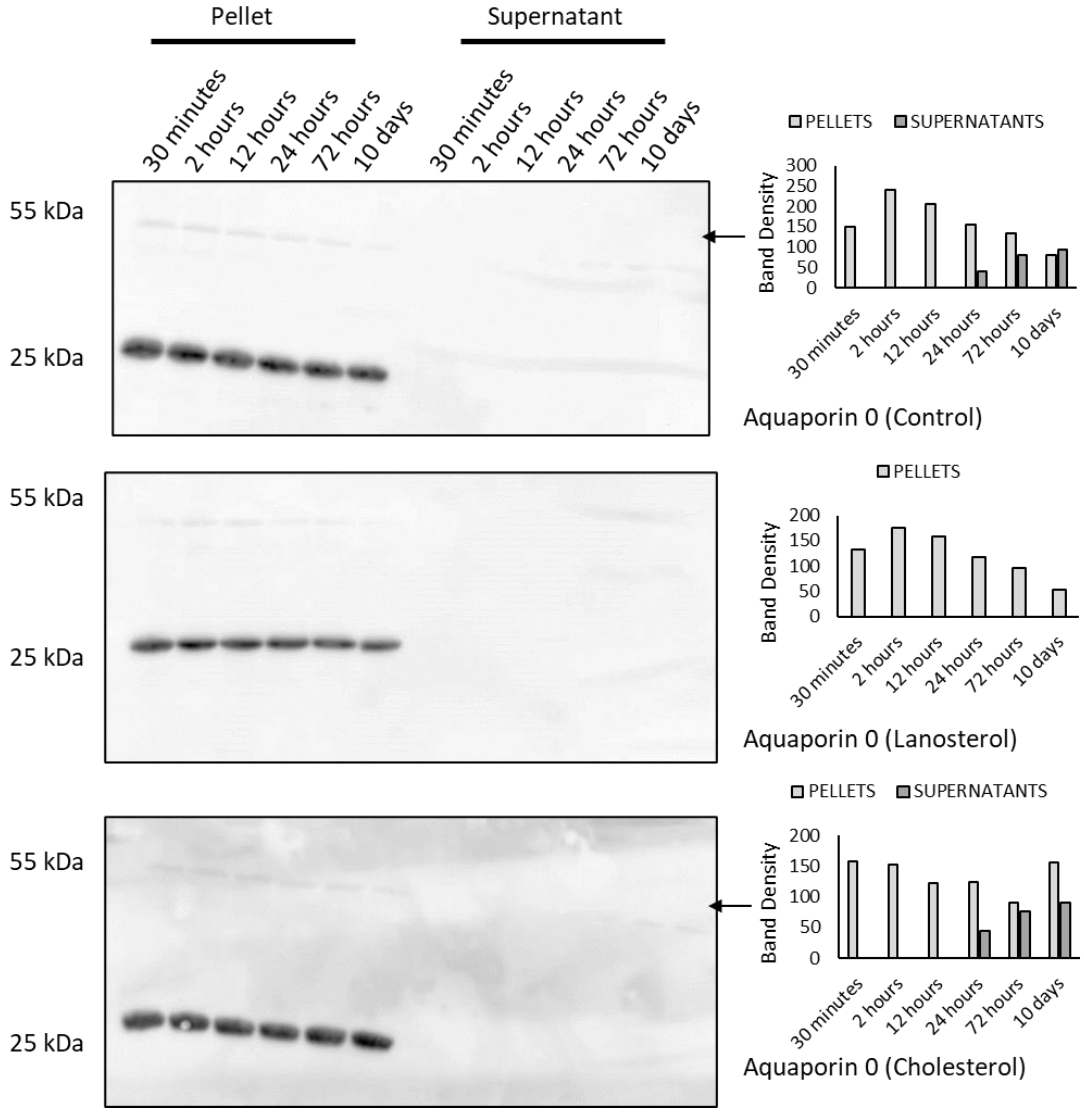


Figure 5.12. The time-dependent solubilisation of high molecular weight AQP0 is inhibited by lanosterol co-incubation in lens cortex membranes. The 26 kDa major AQP0 band shows no substantial fluctuation in the insoluble fraction, while the 50 kDa minor band shows a time-dependent increase in soluble material in control samples and in samples co-incubated with 10 µM cholesterol at 37$^{O}$C in light-safe conditions, as shown in the first and third graphs. No 50kDa material was detected in samples co-incubated with 10 µM lanosterol, as indicated in the second graph. All starting samples are 5 µg wet weight extracted from a pool of 24 lenses.

One major band doublet was identified in the insoluble membrane fractions for CX50 at 55kDa, with three minor bands at 70 kDa, 45 kDa, and 25 kDa; no material was detected in the soluble membrane fractions, in addition to no temporal fluctuations in band density.

The co-incubation of membranes with 10 µM cholesterol produced no effect on the solubility and enrichment profile of CX50. In contrast, co-incubation with 10 µM lanosterol resulted in the relative enrichment of the 25 kDa band, as seen in Figure 5.13.

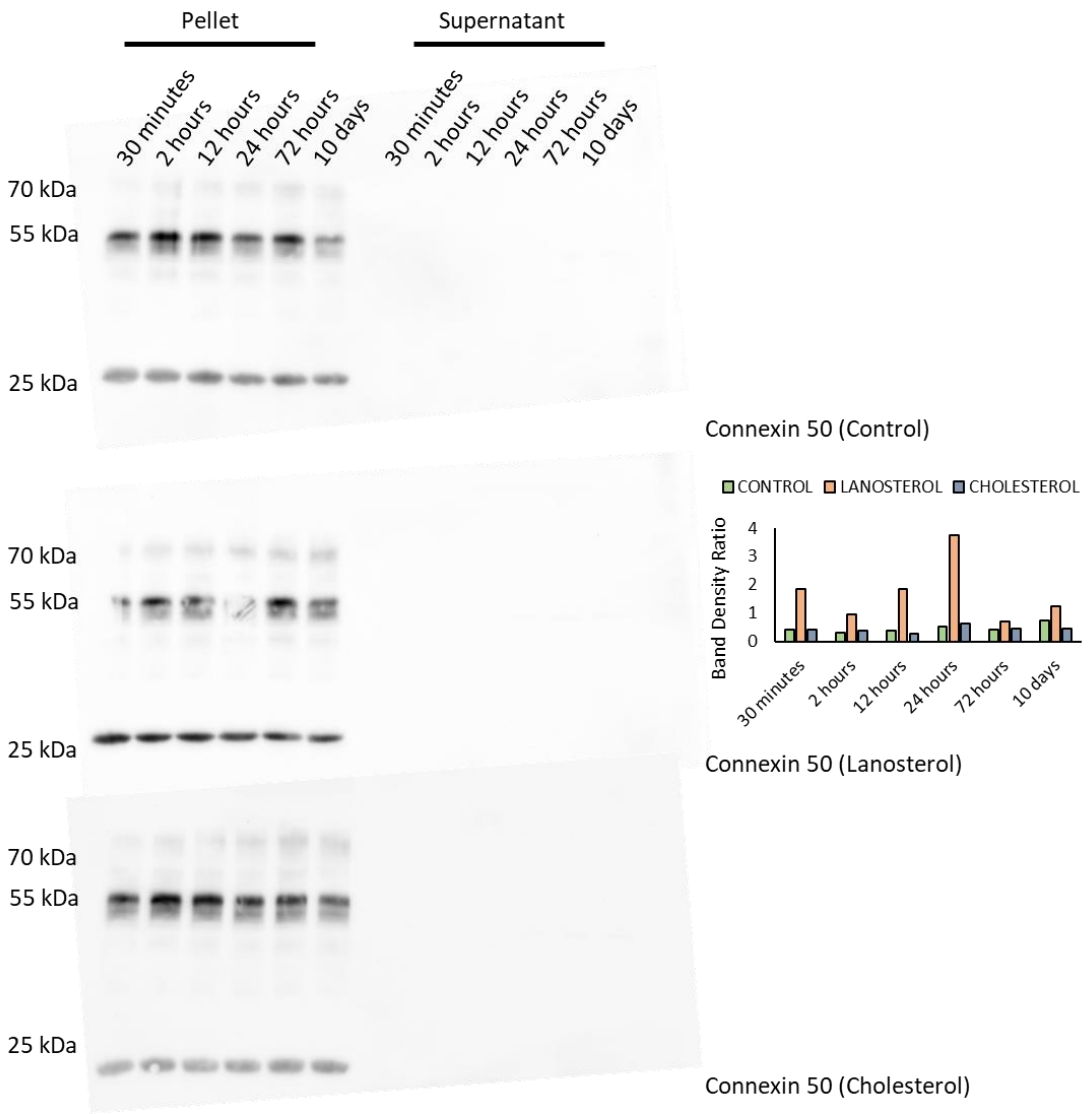


Figure 5.13. Neither lanosterol nor cholesterol co-incubation influence the sedimentation of Cx50 in lens cortex membranes. The two major bands at 55 kDa and 20 kDa, in addition to the two minor bands at ~70 kDa and 50 kDa, remained in the insoluble fraction at all recorded timepoints. All starting samples are 5 µg wet weight extracted from a pool of 24 lenses.

### 5.3.2 The filaments vimentin and BFSP1 are found in insoluble and soluble lens fractions

Both filament proteins vimentin and BFSP1 were found in insoluble and soluble cortex membrane fractions, with a time-dependent solubilisation being apparent as seen in Figures 5.14 and 5.16. the major vimentin band at 60 kDa showed a transition of material from the insoluble to the soluble membrane fraction from 2 hours post centrifugation, while a major ~45 kDa BFSP1 band showed a moderate transition to the soluble fraction from 72 hours post centrifugation.

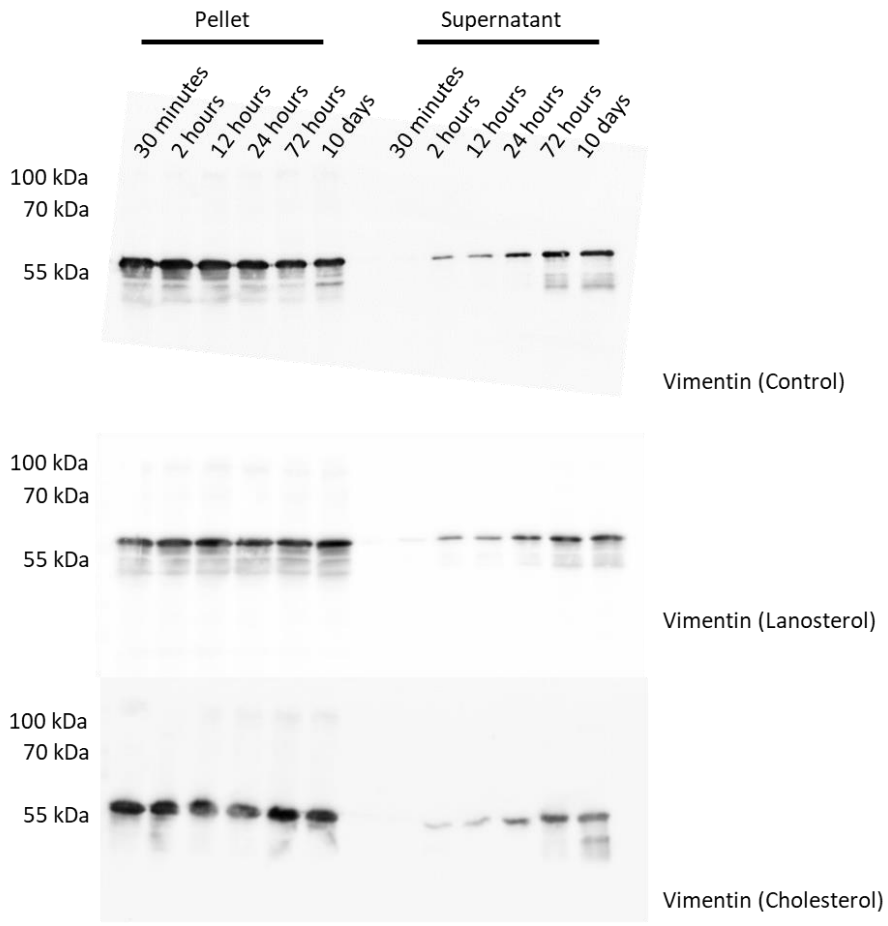


Figure 5.14. Vimentin is subject to a time-dependent, increasing solubilisation in cortex-derived lens membranes. All starting samples are 5 µg wet weight extracted from a pool of 24 lenses.

The co-incubation of cortical membranes with 10 µM cholesterol did not influence the solubility status of vimentin, while the co-incubation with 10 µM lanosterol resulted in a significant reduction of soluble protein at 72 hours and 10 days post centrifugation as seen in Figure 5.15.

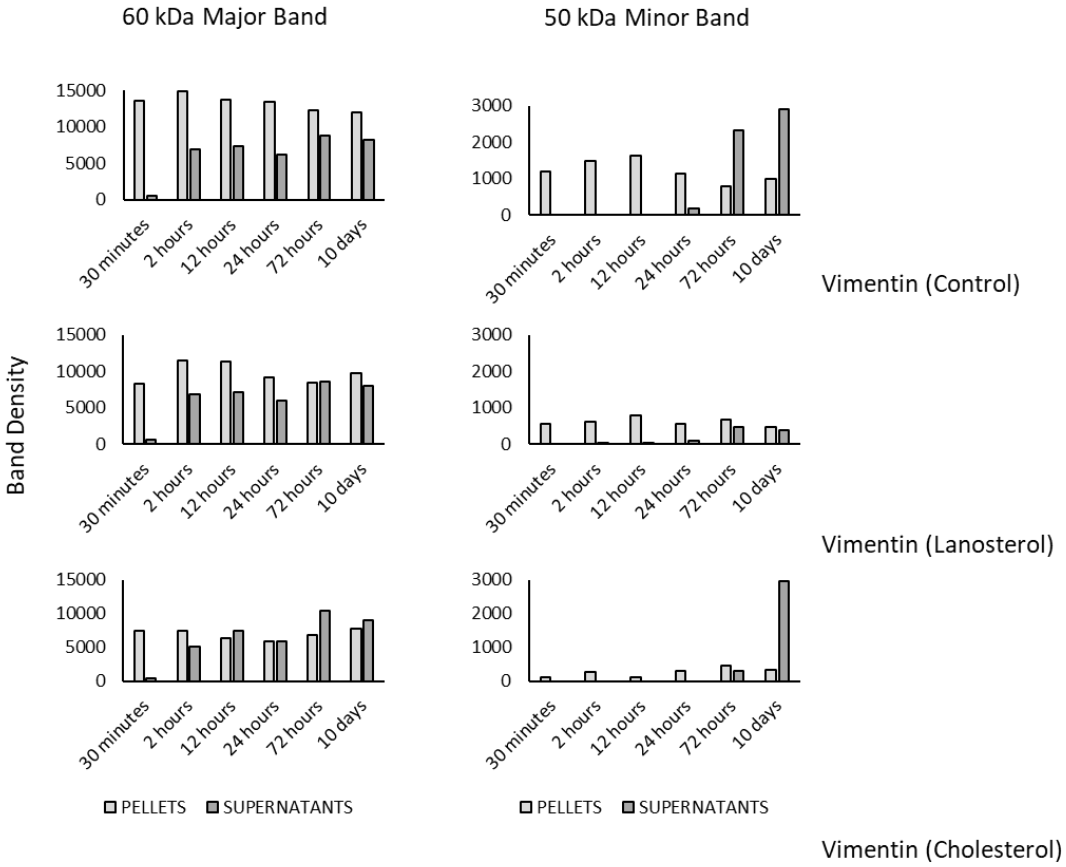


Figure 5.15. Lanosterol co-incubation suppresses the solubilisation of the ~50 kDa minor band, while neither lanosterol nor cholesterol co-incubation have any effect on the major 60 kDa band. All starting samples are 5 µg wet weight extracted from a pool of 24 lenses.

The co-incubation of cortical high protein content lens membranes with 10 µM lanosterol or 10 µM cholesterol resulted in the accelerated release of a 45 kDa BFSP1 band, as seen in Figure 5.16. Control fractions showed the first instance of detectable soluble protein at 24 hours post centrifugation, followed by a modest increase through to 10 days as seen in the first panel and graph. Membranes co-incubated with lanosterol or cholesterol showed detectable soluble BFSP1 from 30 minutes post centrifugation, followed by a steady increase in soluble material and a proportionate decrease of the equivalent insoluble protein through to 10 days post centrifugation as seen in the second and third panels and graphs in Figure 5.16.

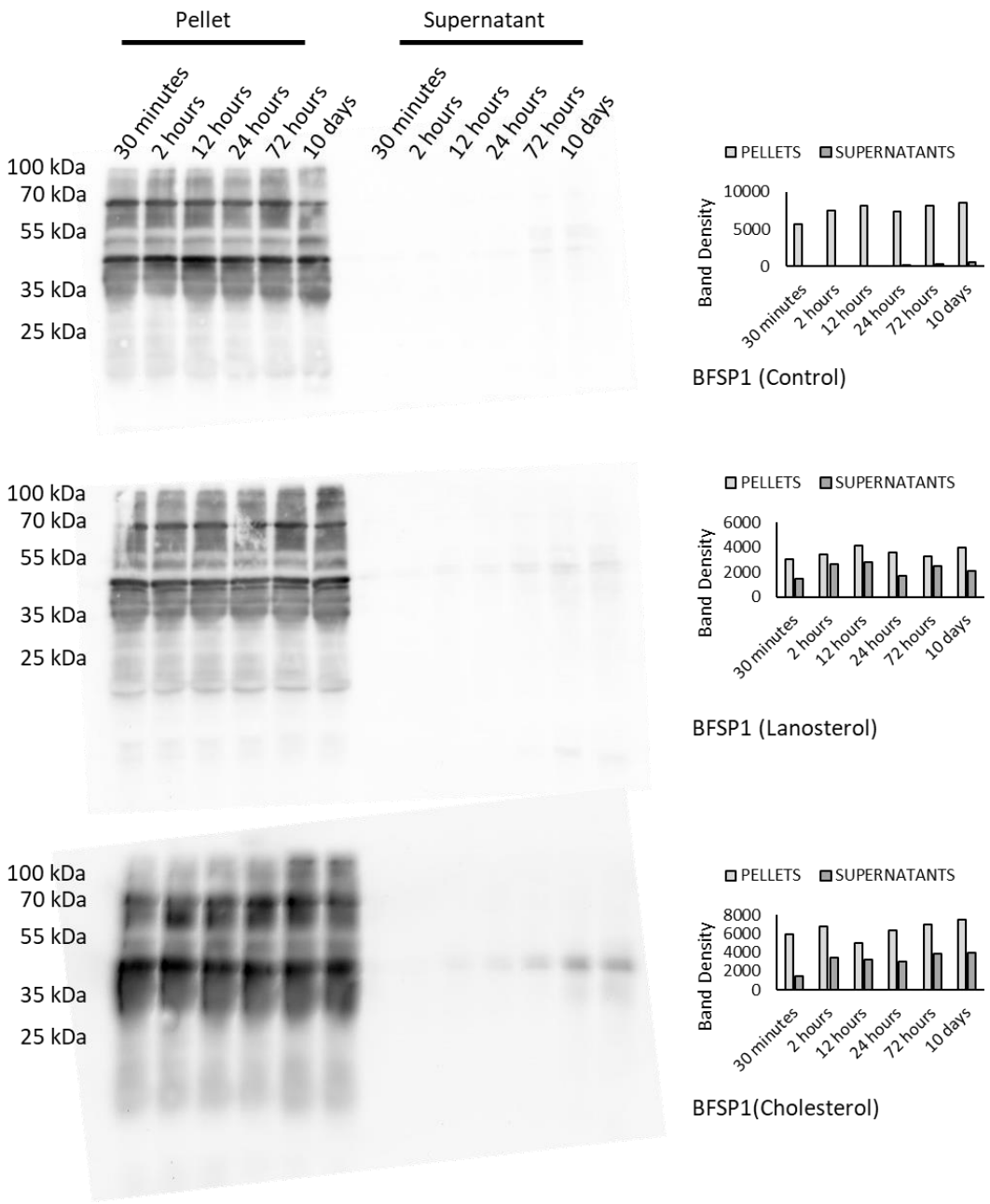


Figure 5.16. BFSP1 is subject to a time-dependent, increasing solubilisation in cortex-derived lens membranes. Co-incubation with 10 µM lanosterol or 10 µM cholesterol increase the release of a 45kDa band. All starting samples are 5 µg wet weight extracted from a pool of 24 lenses.

### 5.3.3 αB-crystallin is enriched in soluble membrane fractions in a temporal, sterol supplementation-independent manner

Similar to the cytoskeletal filament proteins, αB-crystallin in cortical high protein content membranes exhibited a temporal transition of material from the insoluble to the soluble fraction. The major band at 22 kDa presented with a soluble fraction from 30 minutes post centrifugation, followed by an increase through to 10 days, as seen in Figure 5.17. The minor band at 15 kDa also exhibited the release of a temporally soluble fraction from 12 hours post centrifugation.

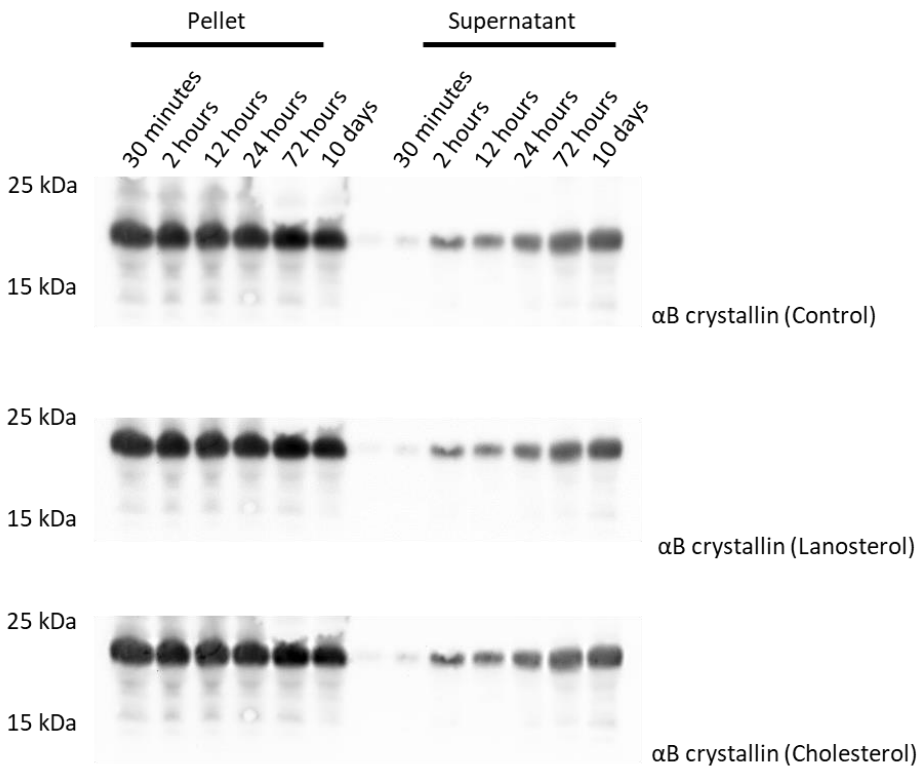


Figure 5.17. The time-dependent solubilisation of αB-crystallin in cortex-derived lens membranes. All starting samples are 5 µg wet weight extracted from a pool of 24 lenses.

The co-incubation of membranes with 10 µM lanosterol or 10 µM cholesterol had no effect on the temporal solubilisation of either the major or minor αB-crystallin band, nor on the ratio of protein distribution between bands of different molecular weight as seen in Figure 5.18.

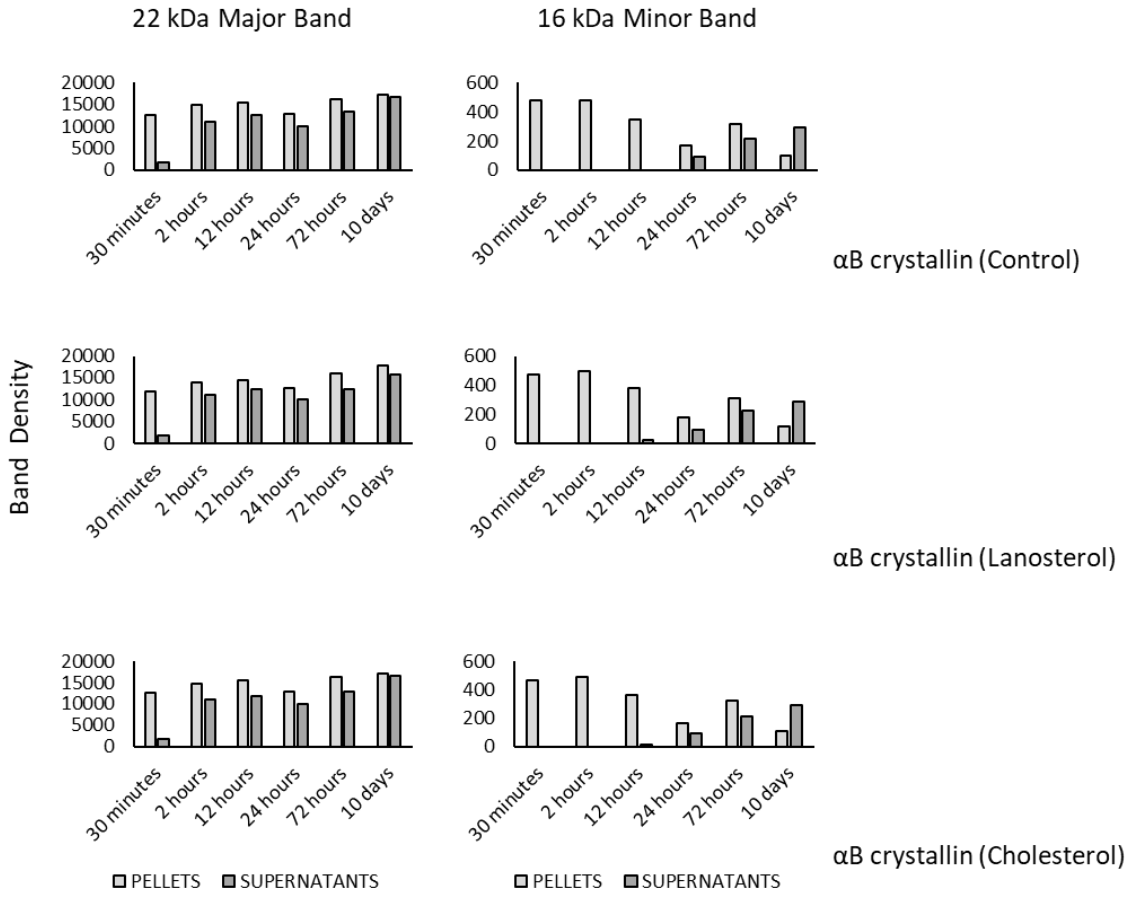


Figure 5.18. Co-incubation of cortex lens membranes with 10 µM lanosterol or 10 µM cholesterol has no effect on the time-dependent solubilisation of αB-crystallin. All starting samples are 5 µg wet weight extracted from a pool of 24 lenses.

## 5.4 Co-incubation with lanosterol or cholesterol does not alter the solubility of endogenous cholesterol in bovine lens membranes

The co-incubation of high protein content membranes with cholesterol was not noted to have any significant effect on the solubility of the major lens protein AQP0, CX50, vimentin, and αB-crystallin, while it promoted the temporal solubilisation of BFSP1. In contrast, co-incubation of cortical fibre cell membranes with lanosterol resulted in the elimination of soluble high molecular weight AQP0, the increase in insoluble 25 kDa CX50, the suppression of the solubilisation of 40 kDa vimentin, and the increased temporal solubilisation of BFSP1. Considering the variable effects of both sterols on the solubility profiles of these proteins, we examined their effect on the distribution of endogenous cholesterol and lanosterol and identified their sedimentation patterns in high protein content lens membranes.

The amount of total cholesterol isolated from cortical and nuclear fibre cell membranes showed no temporal fluctuations between the pellet and supernatant, with the ratio of pelleted to supernatant endogenous cholesterol being 2.46±0.52 in cortex membranes and

2.24±0.08 in nucleus membranes. Following co-incubation with lanosterol these ratios were 2.27±0.11 and 2.25±0.04, and co-incubation with cholesterol 2.26±0.03 and 2.23±0.07 respectively, as seen in Figure 5.19.

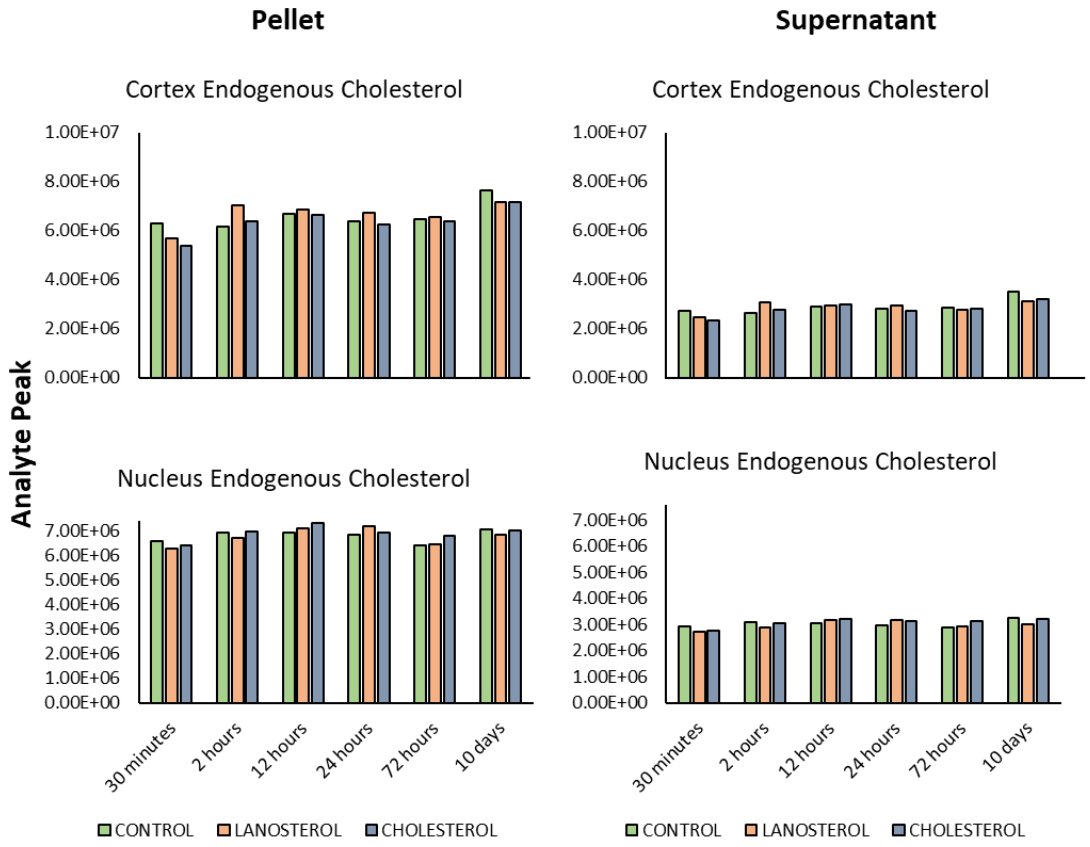


Figure 5.19. The co-incubation of high-protein content lens membranes with lanosterol or cholesterol has no effect on the endogenous total cholesterol content of insoluble and soluble membrane fractions. Nucleus-derived insoluble membrane fractions showed greater but not significant variability in total cholesterol content as compared to soluble membranes and all cortex-derived fractions. Soluble membrane fractions contained reduced levels of cholesterol as compared to the equivalent insoluble membrane fractions. All samples were 10 mg wet weight pooled from 24 lenses. Lipid extractions were conducted in triplicate prior to pooling. All analyte peak values are corrected against spike-in deuterated 25-OHC and normalised against the blank sample values of each relevant metabolite.

Deuterated cholesterol was identified in all cortex and nucleus insoluble fractions of membranes supplemented with d6 cholesterol, with cortex levels remaining stable within error apart from a two-fold increase at 24 hours, as seen in Figure 5.20. Minimal fluctuations were detected in nucleus-derived insoluble membrane fractions.

Analyte peak values in the soluble fractions of cortex and nucleus samples were significantly reduced as compared to the insoluble fractions, with all nucleus d6 cholesterol values registering within error of the equivalent blank sample value.

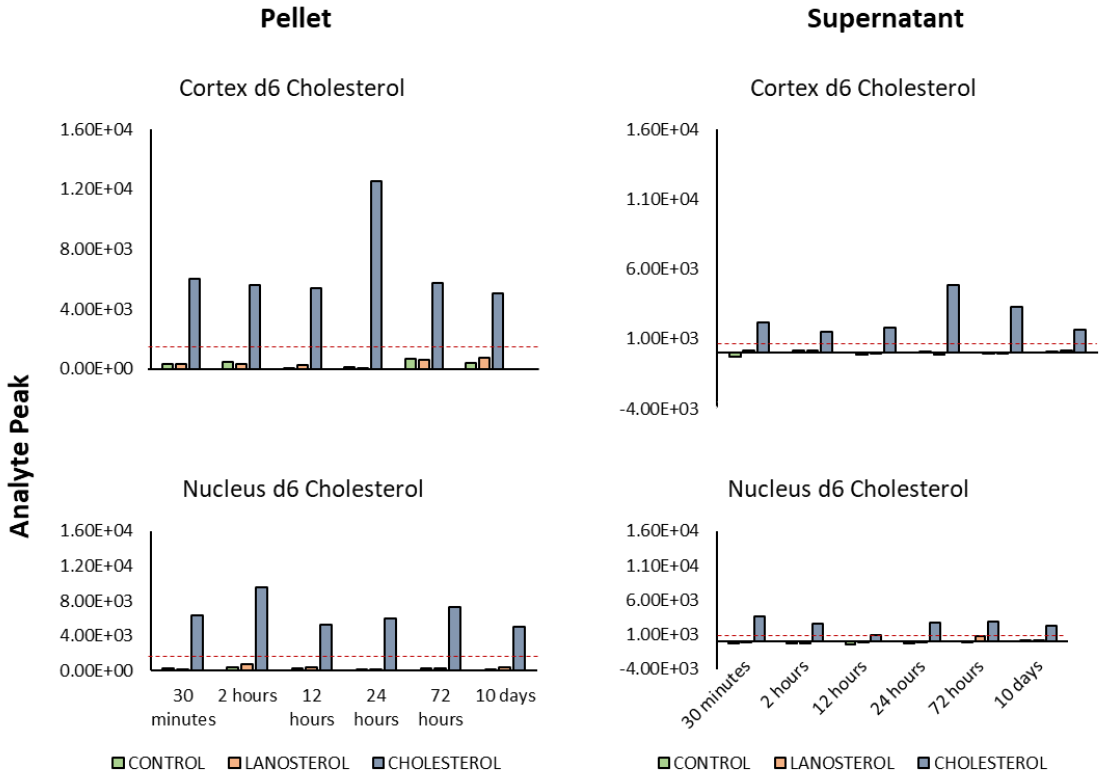


Figure 5.20. Deuterated cholesterol was detected in all cortex and nucleus-derived insoluble fractions co-incubated with d6 cholesterol. D6 cholesterol levels showed no significant fluctuation in insoluble cortical lens membranes, with the exception of a significant increase at 24 hours post-supplementation. Insoluble nucleus fractions showed a temporary increase in d6 cholesterol at 2 hours post-supplementation. Minimal levels of d6 cholesterol were detected in soluble cortex and nucleus fractions, with a transient increase observed at 24 hours post-supplementation in cortical membranes. All samples were 10 mg wet weight pooled from 24 lenses. Lipid extractions were conducted in triplicate prior to pooling. All analyte peak values are corrected against spike-in deuterated 25-OHC and normalised against the blank sample values of each relevant metabolite. The blank analyte peak value of d6 cholesterol is noted by the red dotted line in all graphs.

## 5.5 Co-incubation with lanosterol or cholesterol does not alter the solubility of endogenous lanosterol in bovine lens membranes

In contrast with the observations made for cholesterol, endogenous lanosterol was identified as the dominant analyte in both cortex and nucleus soluble membrane fractions, as seen in Figure 5.21. The ratio of insoluble to soluble endogenous lanosterol was 0.342±0.031 in control cortex membranes and 0.34±0.02 in the equivalent nucleus samples. Co-incubation with

lanosterol or cholesterol had no impact on the solubility of endogenous lanosterol, with the insoluble : soluble ratio being 0.346±0.035/0.0344±0.03 in cortical membranes and 0.343±0.021/0.0345±0.024 in nuclear fibre cell membranes.

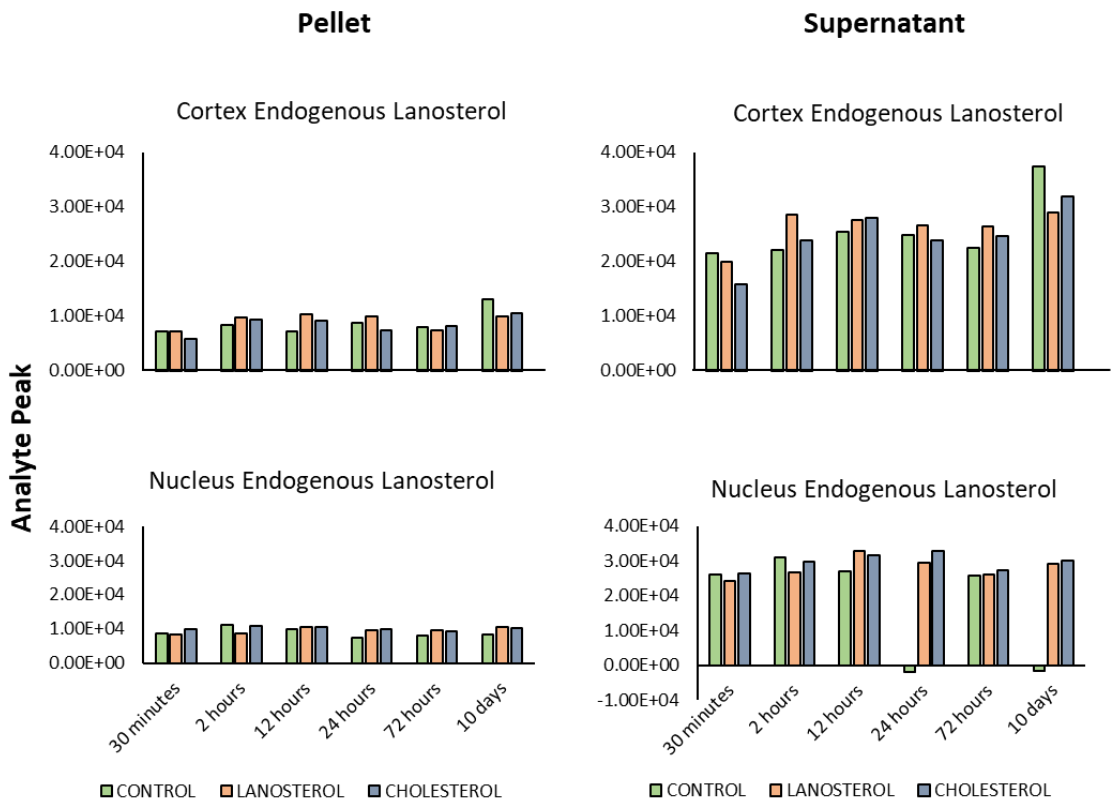


Figure 5.21. No significant fluctuation in endogenous lanosterol levels was recorded for cortex and nucleus membranes co-incubated with cholesterol or lanosterol. A two-fold increase in endogenous lanosterol levels was detected in the soluble fractions of cortex and nucleus-derived membranes for all conditions. All samples were 10 mg wet weight pooled from 24 lenses. Lipid extractions were conducted in triplicate prior to pooling. All analyte peak values are corrected against spike-in deuterated 25-OHC and normalised against the blank sample values of each relevant metabolite.

Deuterated lanosterol was not detected in any examined fraction, as seen in Figure 5.22, despite an effect seen on the distribution of vimentin in Figure 5.14. This finding has been analysed and discussed in section 7.2.3.

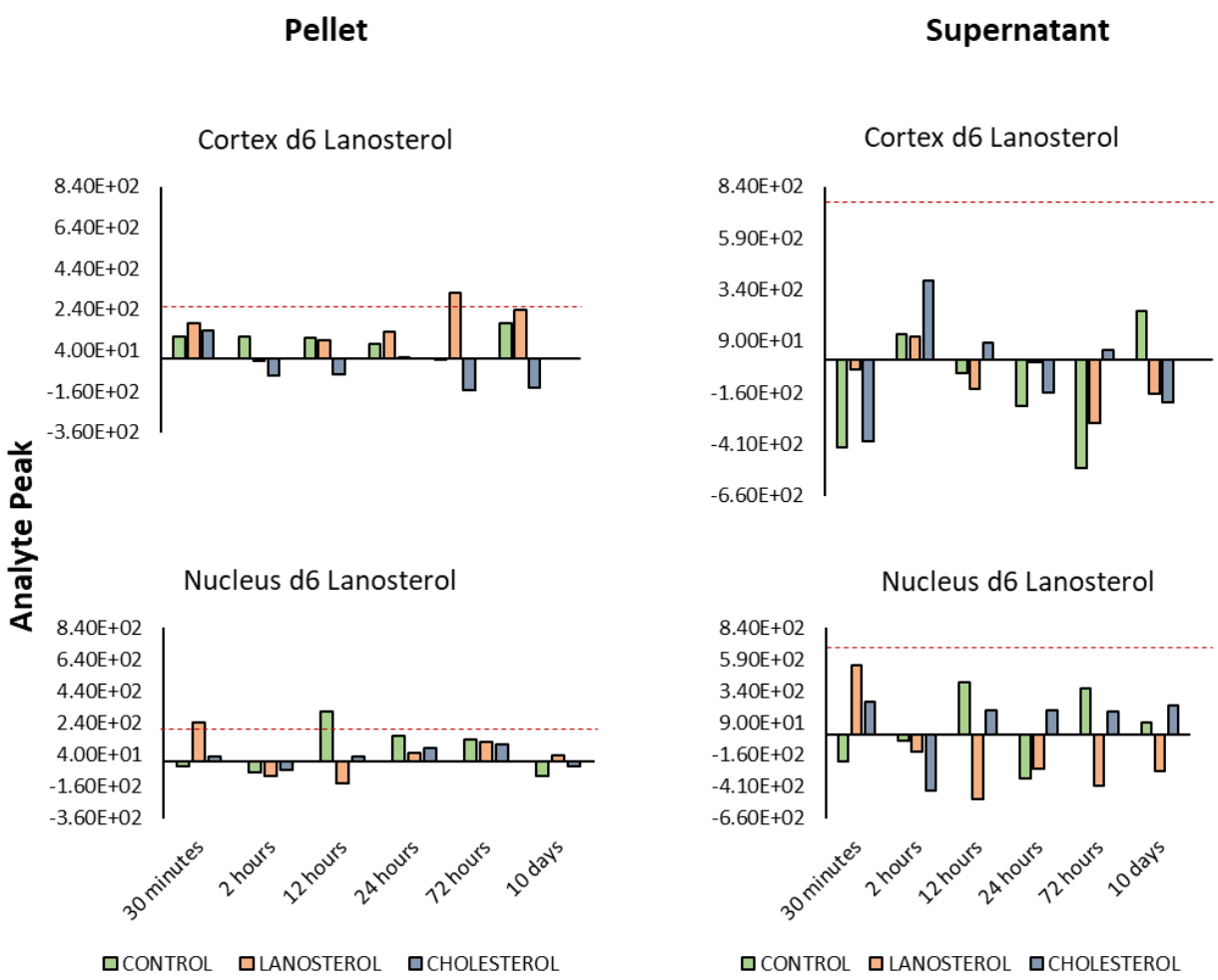


Figure 5.22. Deuterated lanosterol was not detected in any soluble membrane fraction. Minor levels of deuterated lanosterol were detected in the 72 hour insoluble cortex fraction co-incubated with d6 lanosterol, the 30 minute insoluble nucleus fraction co-incubated with d6 lanosterol, and the control insoluble 12 hour nucleus fraction. All detected values were within error of the blank d6 lanosterol analyte peak as indicated by the red dotted line in all four graphs. All samples were 10mg wet weight pooled from 24 lenses. Lipid extractions were conducted in triplicate prior to pooling. All analyte peak values are corrected against spike-in deuterated 25-OHC and normalised against the blank sample values of each relevant metabolite.

## 5.6 General summary

The protein content of isolated lens membranes influences its sedimentation pattern, with structural transmembrane proteins which participate in cell-to-cell adhesion sedimenting in a cholesterol-enriched fraction, demonstrating the maintenance of the bilayer structure in high protein content lens membranes in solution. In contrast, phospholipid enriched supernatants included an array of membrane associated proteins and crystallins.

A cortex-enriched specific lens protein fraction transiently sediments and is partially influenced by lanosterol or cholesterol co-incubation, while neither lanosterol nor cholesterol

supplementation do not alter the sedimentation profile of endogenous lens sterols.

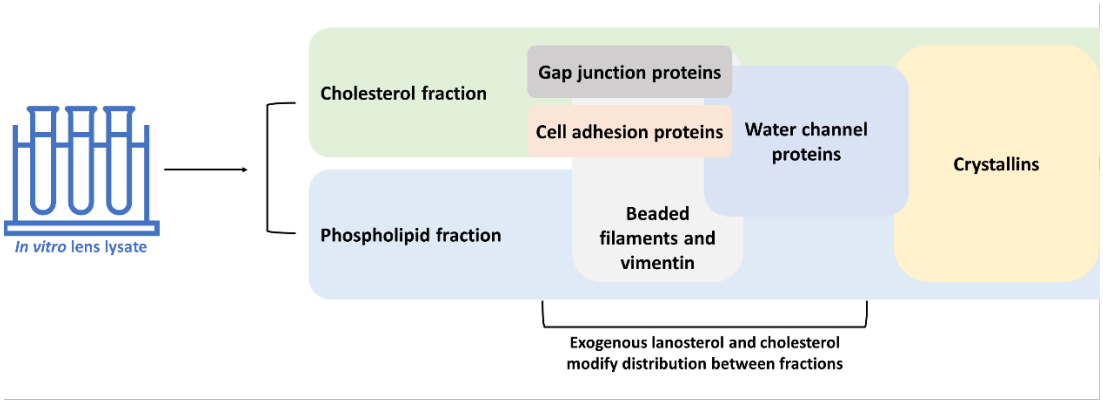


Figure 5.23. Lipid-protein associations remain strong in *in vitro* bovine lens lysates, demonstrating the utility of the structure-function relationship between these macromolecules. Altering the sterol content of lens lysates affects the sedimentation pattern of structural lens proteins.

# 6 Chapter 6: The sedimentation of lens proteins is influenced by α-crystallin

## 6.1 The solubility status of α-crystallin

Crystallins are the most abundant lens protein, making up to 90% of the dry weight of the tissue (9). The physiologically relevant concentration of α-crystallin at approximately 300 $mgmL^{-1}$ creates an environment where controlled protein-protein interactions are essential in the maintenance of long-term health. Whether by molecular crowding or direct macromolecular interactions, α-crystallin is involved in an extensive array of processes from stabilising misfolded and damaged proteins (105,110,234,287,330), to forming decorated beaded filaments with the proteins BFSP1 and BFSP2 (117).

### 6.1.1 Age-dependent changes in α-crystallin of mammalian lenses

The lifelong retention and absence of macromolecule turnover in the lens produces a major hurdle towards maintaining tissue clarity, as damaged proteins are not replaced by younger, functional peptides. The two major roles of α-crystallin in the lens are its chaperone function, whereby α-crystallin stabilises damaged macromolecules and prevents the aberrant formation of light-scattering aggregates (328), and the facilitation of short-range interactions which form the gradient refractive index of the lens via the non-periodic ordering of crystallins (9,93,331). Almost half of all lens proteins are insoluble by the $5^{th}$ decade of life in human lenses (289), including the majority of nuclear α-crystallin. Insoluble α-crystallin has been found to be comprised of a larger proportion of modified and crosslinked oligomers (292) and is commonly associated with the cytoskeleton and is adherent to LFC membranes (191). The age-related accumulation of post translational modifications has been associated with a loss of chaperone activity (208,218), leaving the lens vulnerable to the effects of increased oxidative load and macromolecule damage, which are the hallmarks of cataractogenesis (211).

### 6.1.2 The aggregation of α-crystallin in cataract

The gradual loss of chaperone function and solubility of α-crystallin has been associated with structural and conformational changes, including the accumulation of deleterious post-translational modifications such as deamidations and truncations (213,294). The age-related transition of α-crystallin to a largely insoluble protein fraction, in conjunction with the loss of chaperone activity due to alterations in the protein structure, generates high molecular weight aggregates which cannot be resolved and act as a platform for the propagation of deleterious oxidised products, including lens proteins and lens lipid membrane domains. This increase in cataractogenic load (48) eventually reaches a threshold where aggregates become light-

scattering occlusions and the insoluble load of damaged proteins cannot be amended by the activity of α-crystallin.

## 6.2 The solubility of high protein content membranes fractions can be altered

The release of a soluble fraction from high protein content membranes described in chapter 5 was analysed further in the context of the chaperone role of α-crystallin. Membranes were incubated at different temperatures and in the presence of serine and cysteine inhibitors to examine their effect on the efficiency of soluble fraction release.

### 6.2.1 High protein content membranes from cataractous lenses do not contain a temporally soluble fraction

The total protein concentration was analysed from the insoluble and soluble high protein content membranes described in chapter 5. High protein content membranes derived from clear bovine lenses showed a temporal release of a soluble fraction, with cortical soluble protein exceeding the amount of insoluble protein at 72 hours post incubation. Similarly, the soluble fraction of nucleus-derived membranes increased in a time-dependent manner, but did not exceed the total insoluble protein, as seen in Figure 6.1.

Membranes obtained from age-matched animals with nuclear cataract showed complete loss of this effect both in nuclear and cortical membranes.

The relative increase in protein content of wet weight-matched cortex and nucleus samples was retained both in clear and cataractous lenses, with nuclear membranes containing almost triple the total protein as compared to cortical membranes from clear lenses. This ratio was decreased in cataractous lenses, with nuclear membranes containing almost twice the amount of total protein as compared to cortex membranes.

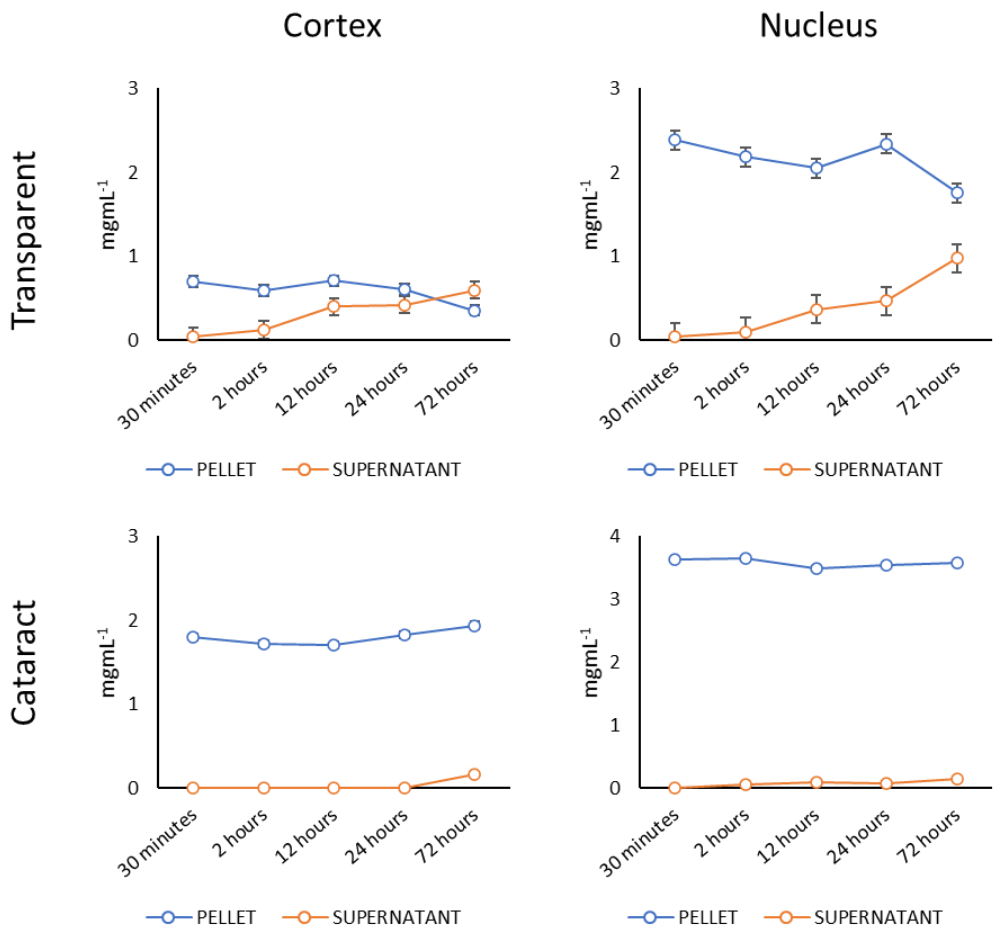


Figure 6.1. High protein content membranes from lenses with nuclear cataract do not show the time-dependent release of soluble material seen in age-matched clear lenses. The rate of release in cortical membranes gradually decreases from 0.05 $mgmL^{-1}$/hour to 0.008 $mgmL^{-1}$/hour by the third day, while the equivalent release in nuclear membranes increases from 0.04 $mgmL^{-1}$/hour to 0.013 $mgmL^{-1}$/hour. The ratio of total protein between wet weight-matched cortex and nucleus membranes was 2.86X in clear lenses and 1.84 in cataractous lenses. All samples are 5 mg wet weight high protein content membranes extracted from a pool of 24 individual bovine lenses, incubated at 37$^{O}$C in light-safe conditions. Assays were repeated in triplicate using material derived from a pool of 24 bovine lenses; error bars are standard error.

### 6.2.2 The release of soluble material from high protein content lens membranes is time and temperature dependent

High protein content membranes were incubated at 4$^{O}$C, 25$^{O}$C, 42$^{O}$C, and 50$^{O}$C to examine the effect of non-physiological temperatures on protein solubility. The temporal release of a soluble protein fraction was greatly diminished in cortical and nuclear membranes incubated at 4$^{O}$C, with a total 0.24 $mgmL^{-1}$ and 0.37 $mgmL^{-1}$ released in the first 30 minutes before reaching equilibrium. Membranes incubated at 25$^{O}$C showed the same solubilisation pattern as membranes incubated at 37$^{O}$C in Figure 5.1, with the total soluble protein overtaking the amount of insoluble protein at 72 hours in cortical but not nuclear membranes. At 42$^{O}$C this

temporal release is retained in cortical membranes only, while the release of soluble material from nuclear membranes is increased but reaches equilibrium after the first 30 minutes. Finally, at 50$^{O}$C this release is completely lost in nucleus-derived membranes, while the release of cortical material peaks at 30 minutes at 0.3 mgmL$^{-1}$, as seen in Figure 6.2.

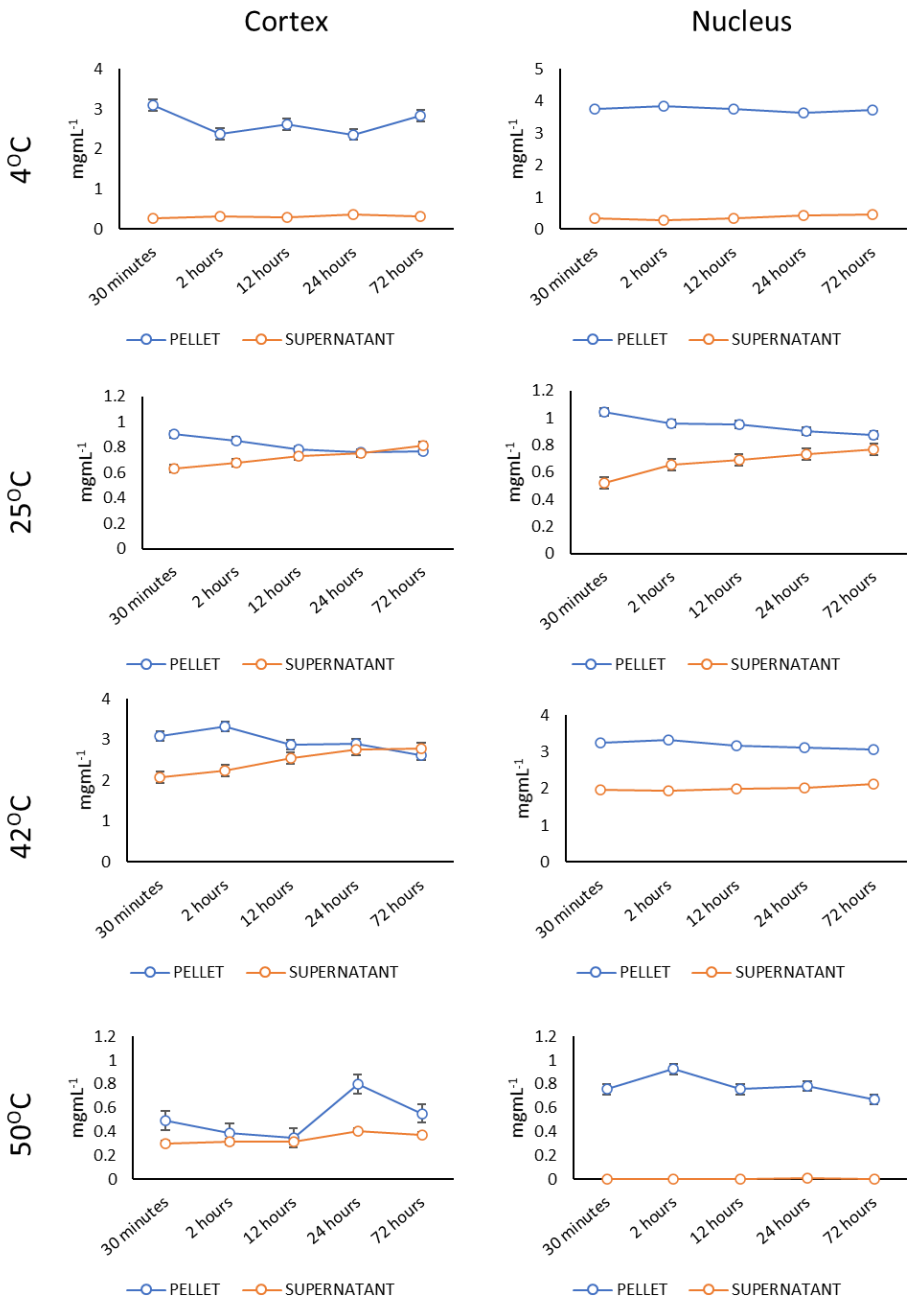


Figure 6.2. The temporal release of soluble material in cortical and nuclear membrane samples is temperature dependent. Cortex-derived membranes release a soluble fraction in a time-dependent manner at 25$^{O}$C and 42$^{O}$C, while nucleus-derived membranes follow this pattern at 25$^{O}$C only. Both cortical and nuclear membranes show limited release of soluble material at 4$^{O}$C which peaks at 30 minutes post-incubation. This limited release by 30 minutes is also exhibited in cortex membranes at 50$^{O}$C and nucleus membranes at 42$^{O}$C, whereas nuclear membranes are rendered insoluble in their entirety at 50$^{O}$C. All samples are 5 mg wet weight high protein

content membranes extracted from a pool of 24 individual bovine lenses. Assays were repeated in triplicate using material derived from a pool of 24 bovine lenses; error bars are standard error.

### 6.2.3 Cysteine and serine protease inhibitors prevent the release of soluble protein from high content membranes

The absence of temporally soluble material in both cortical and nuclear membranes of lenses with nuclear cataract, in conjunction with the relatively stable lipidome of soluble and insoluble membrane fractions described in chapter 5, supports the hypothesis that changes in the lens fibre cell proteome may have a direct effect on the solubility of the membrane fractions.

High protein content membranes were incubated at 37$^{O}$C in light-safe conditions in a NaCl/EDTA buffer or in a NaCl/Protease inhibitor complex buffer to examine the effect of serine and cysteine protein inhibitors on the temporal release of soluble protein. Cortex and nucleus-derived membranes showed the previously characterised time-dependent release of a distinct soluble protein fraction, while membranes suspended in the protease inhibitor complex buffer showed a significant decrease both in the required time and in the total amount of released protein, as seen in Figure 6.3.

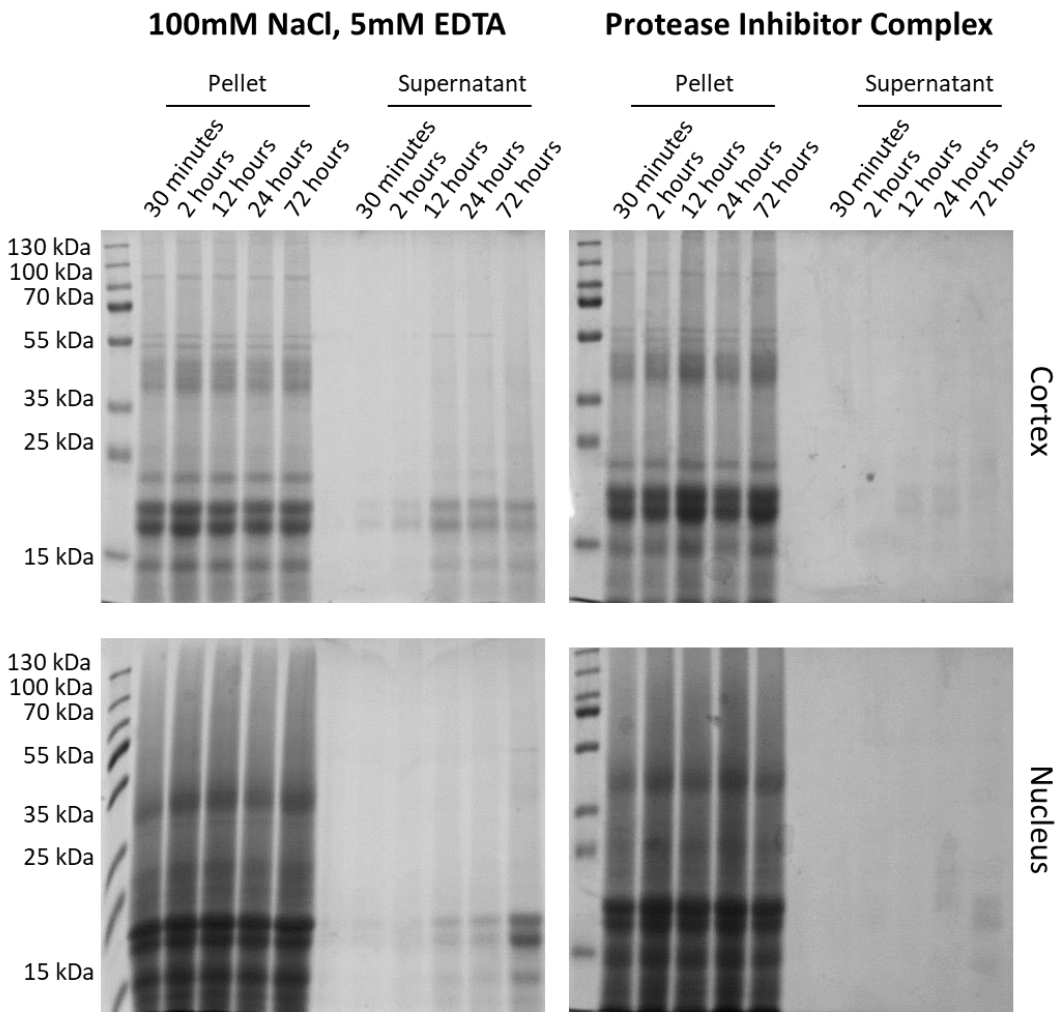


Figure 6.3. The incubation of high protein content membranes in a commercial serine/cysteine protease inhibitor complex greatly reduces the amount of temporally soluble protein in cortex and nucleus-derived membranes. All samples are 5 mg wet weight high protein content membranes extracted from a pool of 24 individual bovine lenses, incubated at 37$^{O}$C in light-safe conditions.

In the absence of a comprehensive list of protease inhibitors included in the commercial complex used in Figure 6.4, a series of cysteine and serine/cysteine/threonine protease inhibitors were used to examine the effect of amino acid-specific interactions on protein solubility.

While iodoacetamide, an irreversible alkylating inhibitor of cysteine peptidases, had no effect on the temporal solubility of cortical membranes, it decreased the total amount of soluble protein released from nuclear membranes by 0.54 mgmL$^{-1}$ at 72 hours post-incubation, as seen in Figure 6.4. In contrast, the commercial inhibitor complex reduced the total soluble protein in cortex membranes to 0.02 mgmL$^{-1}$ and 0.04 mgmL$^{-1}$ in nucleus membranes.

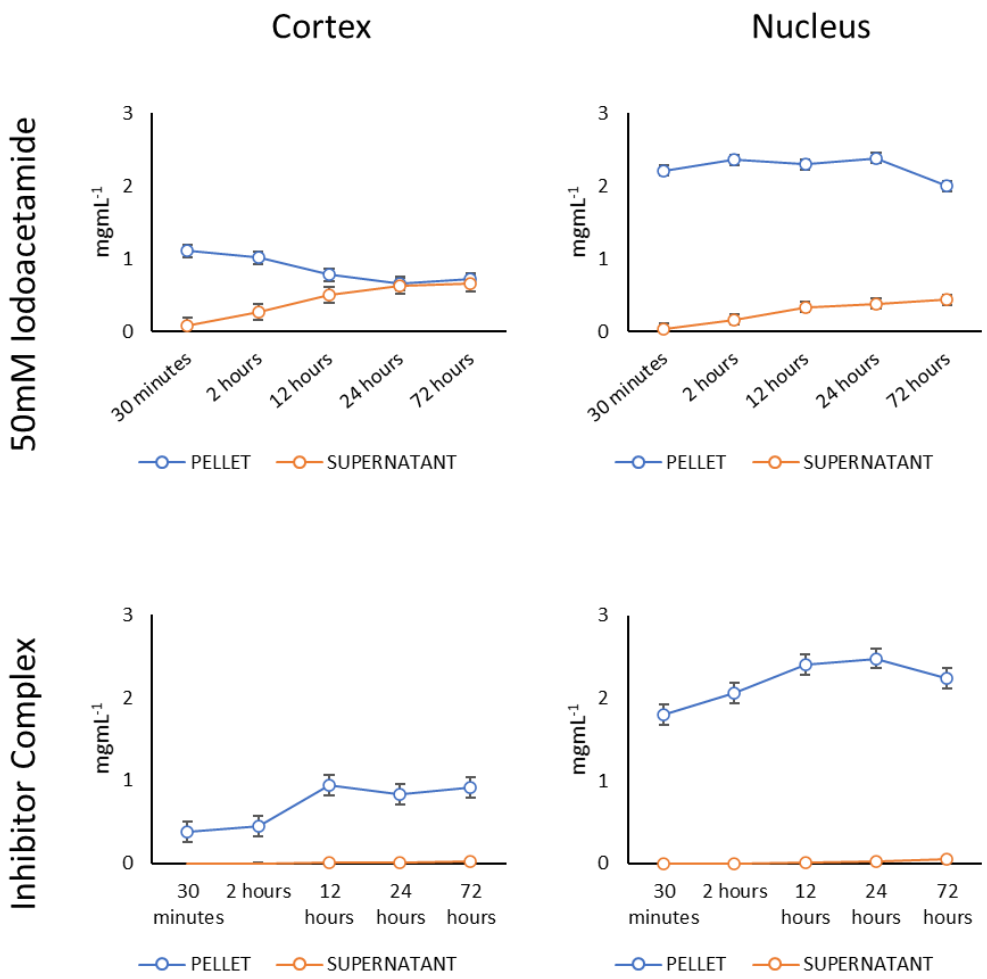


Figure 6.4. Iodoacetamide reduces the total amount of temporally soluble protein in nuclear membranes, but not in cortical membranes. The ratio of soluble to insoluble protein in nucleus-derived membranes was increased in 50mM iodoacetamide-incubated samples by 2.82X as compared to clear control lenses in NaCl/EDTA at 37$^{O}$C. In contrast, incubation with a commercial cysteine/serine/threonine inhibitor complex resulted in the significant elimination of release of soluble protein from both cortex and nucleus high protein content membranes. All samples are 5 mg wet weight high protein content membranes extracted from a pool of 24 individual bovine lenses, incubated at 37$^{O}$C in light-safe conditions. Assays were repeated in triplicate using material derived from a pool of 24 bovine lenses; error bars are standard error.

### 6.2.4 The cysteine protease inhibitor E-64 prevents the release of soluble material more efficiently than the serine/cysteine/threonine protease inhibitor leupeptin

The irreversible cysteine protease inhibitor E-64 and the competitive serine/cysteine/threonine inhibitor leupeptin were used at increasing concentrations to examine their effect on the temporally soluble protein fraction released from cortical and nuclear high protein content membranes. Incubation with leupeptin significantly reduced the

total amount of cortex soluble protein in all three concentrations tested, with 1 µM leupeptin producing a final 0.13 $mgmL^{-1}$ soluble protein, 10 µM leupeptin 0.23 $mgmL^{-1}$, and 100 µM leupeptin a total 0.39 $mgmL^{-1}$ soluble protein.

Incubation with E-64 resulted in the complete suppression temporally soluble protein at 1 µM and 10 µM, while a total of 0.18 $mgmL^{-1}$ was released in cortex membranes at 100 µM, as seen in Figure 6.5.

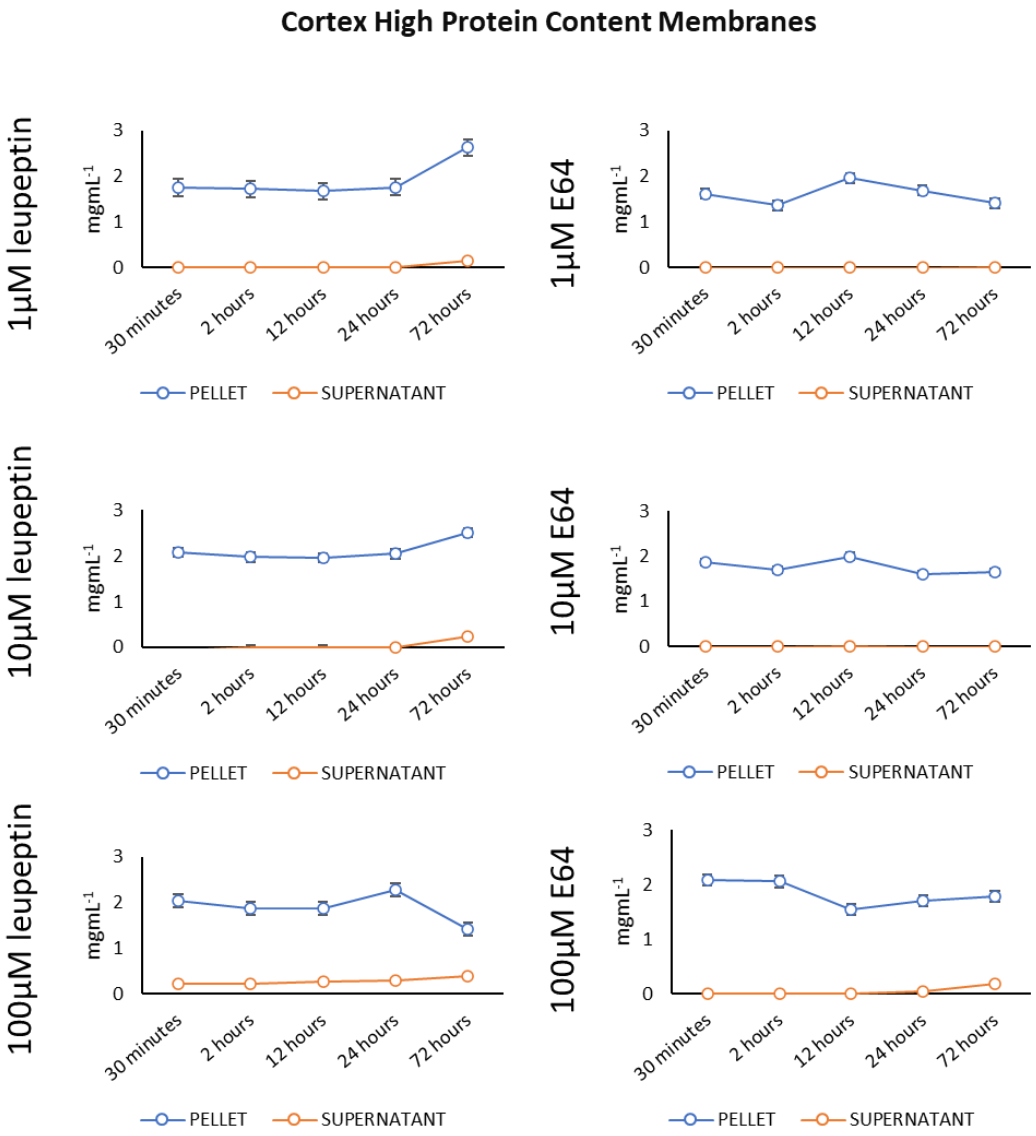


Figure 6.5. E-64 inhibits the temporal release of soluble protein from cortical high protein content membranes more efficiently than leupeptin. Soluble protein was detected at 72 hours post-incubation in membranes incubated with 1 µM and 10 µM leupeptin (0.13 $mgmL^{-1}$ and 0.23 $mgmL^{-1}$), while 100 µM leupeptin resulted in the initial release of 0.21 $mgmL^{-1}$ soluble protein before reaching a maximum final concentration of 0.39 $mgmL^{-1}$. Incubation with E-64 completely prevented the release of soluble protein at 1 µM and 10 µM, while a total of 0.18 $mgmL^{-1}$ was detected at 72 hours in the 100 µM E-64 samples. All samples are 5 mg wet weight high protein

content membranes extracted from a pool of 24 individual bovine lenses, incubated at 37$^{O}$C in light-safe conditions. Assays were repeated in triplicate using material derived from a pool of 24 bovine lenses; error bars are standard error.

Similarly, leupeptin successfully reduced the amount of total soluble protein in nucleus-derived membranes while also increasing the time required for the release of material, as seen in Figure 6.6. At 1 µM and 10 µM, leupeptin incubation resulted in the detection of 0.64$^{-1}$ and 0.5 mgmL$^{-1}$ soluble protein at 72 hours, while 100 µM leupeptin resulted in the detection of 0.26 mgmL$^{-1}$ soluble protein at 12 hours before reaching a maximum of 0.77 mgmL$^{-1}$ at 72 hours. E-64 incubation produced similar results, with 0.17 mgmL$^{-1}$ and 0.23 mgmL$^{-1}$ detected at 72 hours in 1 µM and 10 µM samples, while 0.22 mgmL$^{-1}$ was detected at 12 hours in the 100 µM sample before reaching a maximum of 0.31 mgmL$^{-1}$ at 72 hours.

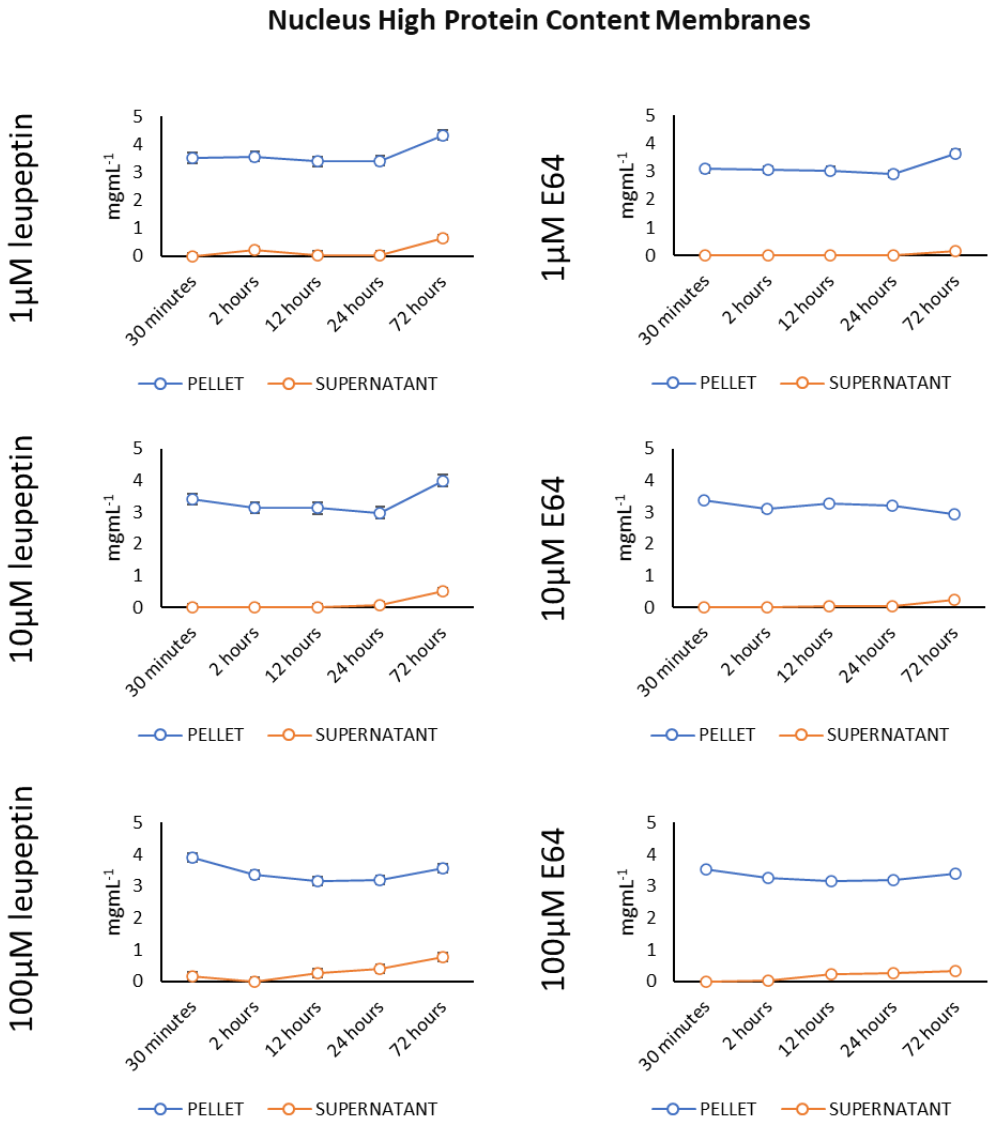


Figure 6.6. Leupeptin and E-64 successfully reduce the amount of temporally soluble protein released from nuclear high protein content membranes isolated from clear lenses. Soluble

protein was detected at 72 hours post-incubation in membranes incubated with 1 µM and 10 µM leupeptin (0.64 $mgmL^{-1}$ and 0.5 $mgmL^{-1}$), while 100 µM leupeptin resulted in the initial release of 0.26 $mgmL^{-1}$ soluble protein at 12 hours before reaching a maximum final concentration of 0.77 $mgmL^{-1}$. Incubation with E-64 prevented the release of soluble protein at 1 µM and 10 µM prior to 72 hours, while a total of 0.22 $mgmL^{-1}$ was detected at 12 hours in the 100 µM samples before reaching a maximum of 0.31 $mgmL^{-1}$ at 72 hours. All samples are 5 mg wet weight high protein content membranes extracted from a pool of 24 individual bovine lenses, incubated at $37^{O}C$ in light-safe conditions. Assays were repeated in triplicate using material derived from a pool of 24 bovine lenses; error bars are standard error.

## 6.3 The co-incubation of lens fibre cell membranes with whole α-crystallin fractions has variable results

As the major protein in the lens, α-crystallin has been proposed as a target for both the treatment and prevention of cataract (302); its *in vivo* chaperone function and broad interactions with other crystallins, cytoskeletal proteins, and membrane lipids fully illustrate the integral role α-crystallin plays in maintaining lens homeostasis and clarity. From this, we have examined the effect of whole bovine α-crystallin fractions on the solubility status of lens fibre cell membrane proteins.

### 6.3.1 The solubility of α-crystallin is fraction and concentration-dependent when co-incubated with integral protein lens membranes

Integral protein membranes, as described in chapter 5, showed no evidence of a temporally soluble protein fraction. Therefore, they provide a canvas for studying the interactions between supplemental α-crystallin and the membrane bilayer itself and to examine whether the solubilisation seen in high protein content membranes can be attributed to membrane-bound material, including membrane-bound crystallins.

No soluble material was detected in integral protein membranes co-incubated with 15 $\mu gmL^{-1}$ commercial bovine α-crystallin, suggesting a binding of the supplemental protein to the insoluble material. Minimal amounts of soluble protein were detected in samples co-incubated with native soluble α-crystallin isolated from high protein content membranes, with 0.03 $mgmL^{-1}$ detected at 2 hours, 0.049 $mgmL^{-1}$ at 12 hours, and 0.033 $mgmL^{-1}$ at 72 hours post-incubation. Size-exclusion chromatography (SEC) isolated α-crystallin showed an immediate inversion with most protein transitioning to the soluble fraction by 30 minutes at an average ratio of 2.5X soluble/insoluble protein. This ratio remained stable within error for the entire time duration examined, as seen in Figure 6.7.

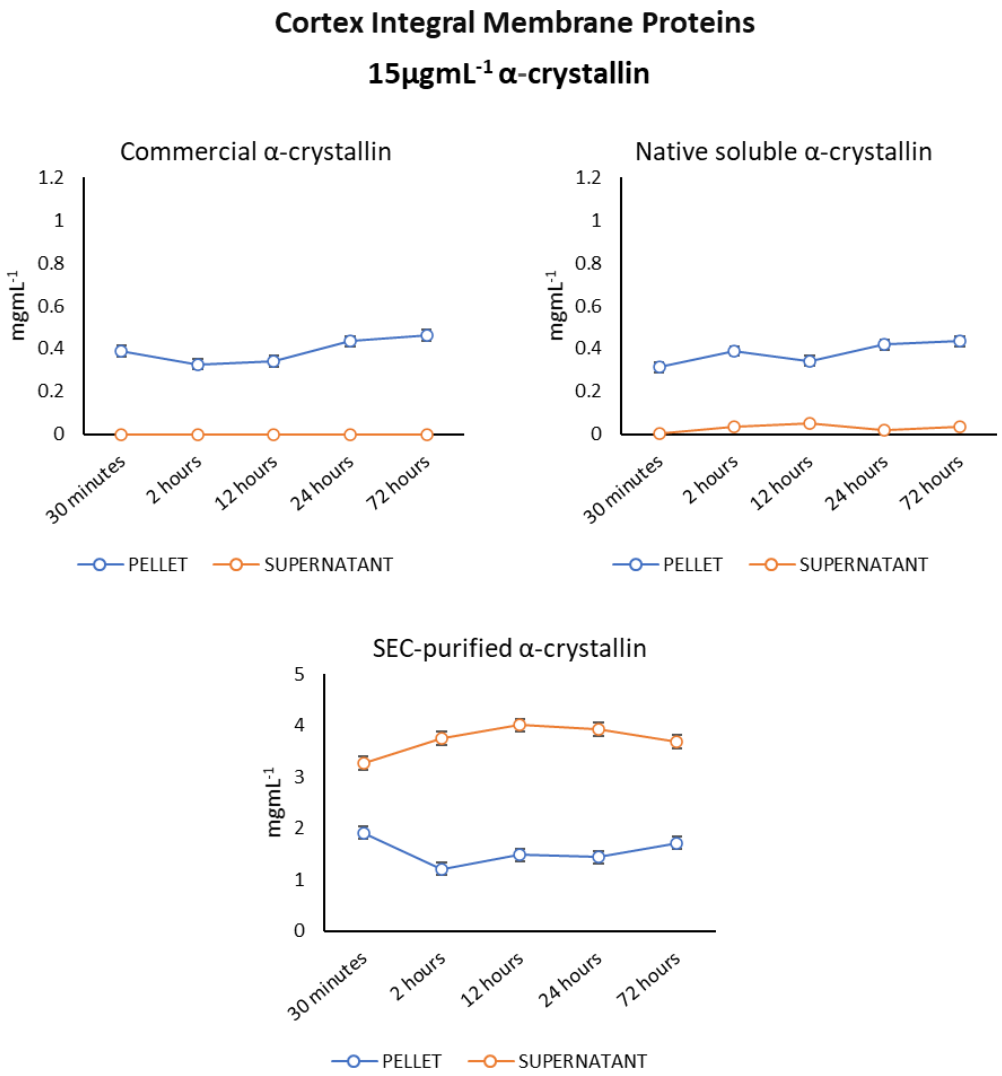


Figure 6.7. Native soluble α-crystallin, but not commercial α-crystallin results in a modest release of soluble protein for integral protein membranes. Size exclusion chromatography-isolated α-crystallin resulted in an inversion of soluble and insoluble material at an average ratio of 2.5. All samples are 5 mg wet weight integral protein membranes extracted from a pool of 24 individual bovine lenses, incubated at 37$^{O}$C in light-safe conditions. Samples incubated with SEC-isolated α-crystallin are 5 mgmL$^{-1}$ starting concentration. Assays were repeated in triplicate using material derived from a pool of 24 bovine lenses; error bars are standard error.

Similar to the 15 µgmL$^{-1}$ supplementation, the addition of commercial bovine α-crystallin at 30 µgmL$^{-1}$ resulted in no release of soluble material. Native soluble α-crystallin produced an increased solubilisation of material from 30 minutes post-incubation at 0.11 mgmL$^{-1}$ before reaching equilibrium at 12 hours with 0.16 mgmL$^{-1}$ soluble protein. The supplementation of SEC-isolated α-crystallin produced the same effect seen previously, with the average ratio of soluble to insoluble protein being 2.4, as seen in Figure 6.8.

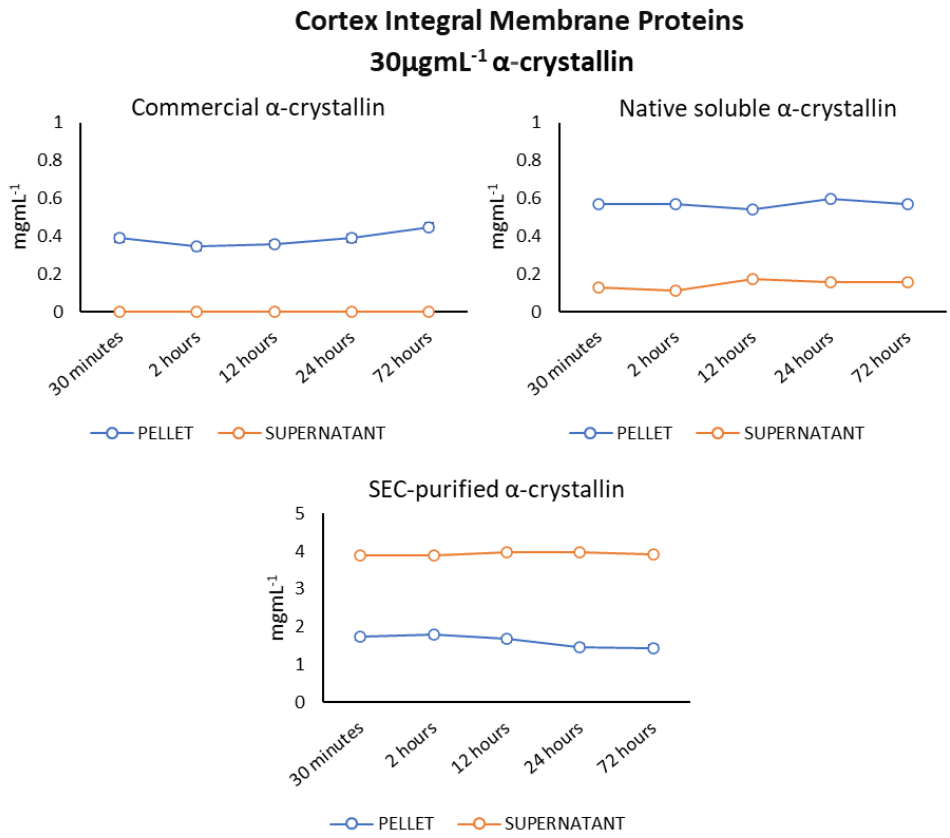


Figure 6.8. Native soluble α-crystallin, but not commercial α-crystallin results in an increased release of soluble protein for integral protein membranes. Size exclusion chromatography-isolated α-crystallin resulted in an inversion of soluble and insoluble material at an average ratio of 2.4. All samples are 5 mg wet weight integral protein membranes extracted from a pool of 24 individual bovine lenses, incubated at 37$^{O}$C in light-safe conditions. Samples incubated with SEC-isolated α-crystallin are 5 mgmL$^{-1}$ starting concentration. Assays were repeated in triplicate using material derived from a pool of 24 bovine lenses; error bars are standard error.

An increase of the supplemental commercial α-crystallin to 60 µgmL$^{-1}$ produced a transient emergence of 0.05 mgmL$^{-1}$ soluble protein at 24 hours, while native soluble α-crystallin at the same concentration resulted in an initial inversion of the insoluble to soluble protein ratio but was followed by a time-dependent decrease in soluble protein. Integral membrane proteins co-incubated with SEC-isolated α-crystallin showed the same pattern as described in Figures 6.7 and 6.8, with the average ratio of insoluble to soluble protein being 2.25 as seen in Figure 6.9.

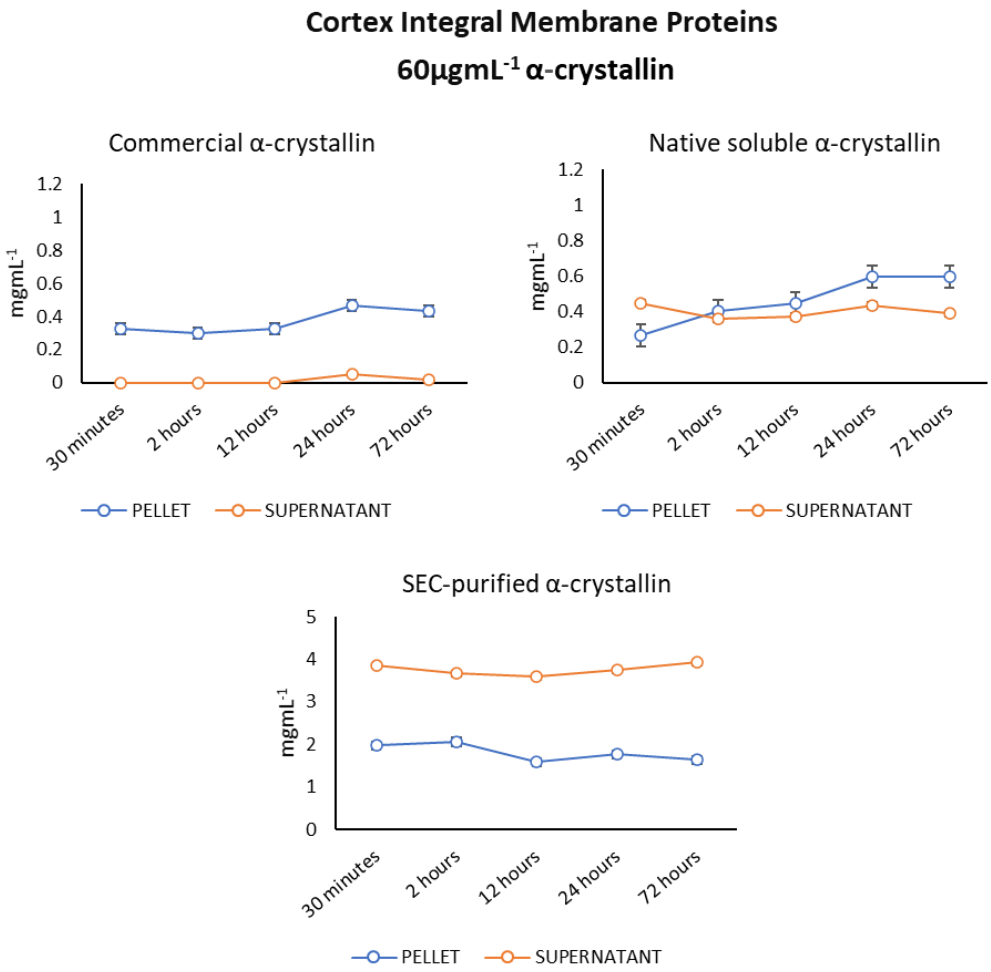


Figure 6.9. Native soluble α-crystallin produces an initial inversion of the insoluble to soluble protein ratio of integral membrane proteins but is followed by a temporal increase in insoluble material. Size exclusion chromatography-isolated α-crystallin resulted in an inversion of soluble and insoluble material at an average ratio of 2.25. All samples are 5mg wet weight integral protein membranes extracted from a pool of 24 individual bovine lenses, incubated at 37 $^{O}$C in light-safe conditions. Samples incubated with SEC-isolated α-crystallin are 5 mgmL$^{-1}$ starting concentration. Assays were repeated in triplicate using material derived from a pool of 24 bovine lenses; error bars are standard error.

A further increase of all fractions of supplemental α-crystallin to 120 µgmL$^{-1}$ resulted in a static ratio of insoluble to soluble protein. Commercial α-crystallin co-incubation produced a 0.64 mgmL$^{-1}$ soluble protein fraction as compared to the 2.72 mgmL$^{-1}$ insoluble protein at 30 minutes, and the average ratio remained at 4 throughout the timepoints examined. Similarly, the co-incubation with native soluble α-crystallin resulted in a release of 1.36 mgmL$^{-1}$ protein at 30 minutes, and the ratio of insoluble to soluble protein remained at an average of 1.5. In contrast with lower concentrations, SEC-isolated α-crystallin also produced a larger proportion of insoluble protein at an average ratio of 1.7, as seen in Figure 6.10.

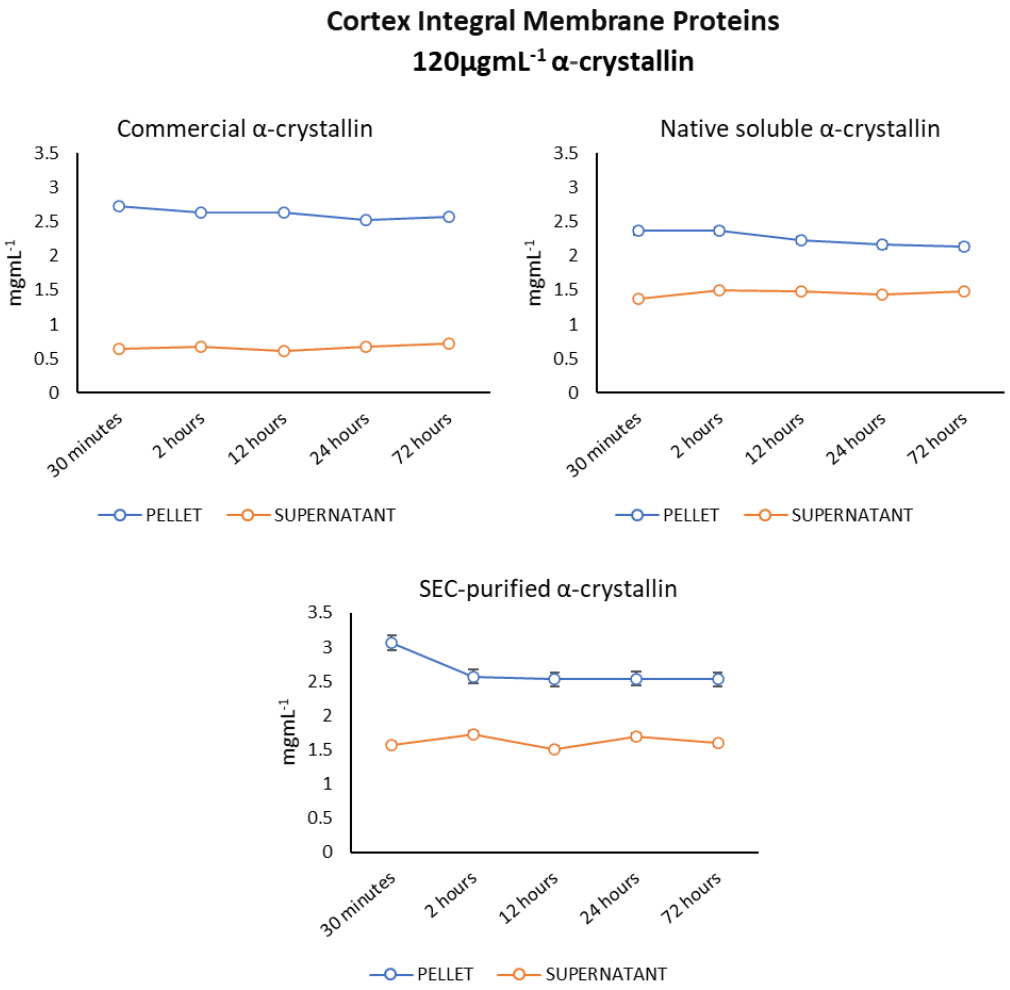


Figure 6.10. All α-crystallin fractions produce a static release of a soluble protein fraction from integral protein lens membranes at 120 µgmL$^{-1}$. The ratio of insoluble to soluble total protein was greatest in the commercial α-crystallin samples at an average of 4, followed by an average of 1.7 in SEC-isolated α-crystallin fractions, and 1.5 in native soluble α-crystallin samples. All samples are 5 mgmL$^{-1}$ integral protein membranes extracted from a pool of 24 individual bovine lenses, incubated at 37$^{O}$C in light-safe conditions. Assays were repeated in triplicate using material derived from a pool of 24 bovine lenses; error bars are standard error.

### 6.3.2 The solubility of α-crystallin is fraction and concentration-dependent when co-incubated with high protein content lens membranes treated with cysteine/serine/threonine protease inhibitors

The commercial protease inhibitor complex, the cysteine/serine/threonine protease inhibitor leupeptin, and the irreversible cysteine peptidase inhibitor E-64 all reduced the amount of temporally soluble protein in high protein content membranes to levels directly comparable with those obtained from cataractous lenses seen in Figure 6.1. Since fractions of whole α-crystallin were shown to be capable of altering the solubility status of integral membrane

proteins, we examined their effect on high protein content membranes rendered insoluble through the use of the inhibitor described in section 6.2.3.

The co-incubation of inhibitor complex treated membranes with 15 $\mu gmL^{-1}$ commercial bovine α-crystallin showed no effect on the solubility of the total protein, while the same concentration of native soluble α-crystallin produced a minimal temporally soluble fraction starting at 12 hours with 0.03 $mgmL^{-1}$ before reaching a maximum of 0.05 $mgmL^{-1}$ at 72 hours. SEC-isolated α-crystallin produced an inversion of the physiological solubilisation pattern, with an initial concentration of 3.84 $mgmL^{-1}$ soluble and 1.97 $mgmL^{-1}$ insoluble protein which gradually exchanged to a final concentration of 1.87 $mgmL^{-1}$ soluble and 2.45 $mgmL^{-1}$ insoluble protein, as seen in Figure 6.11.

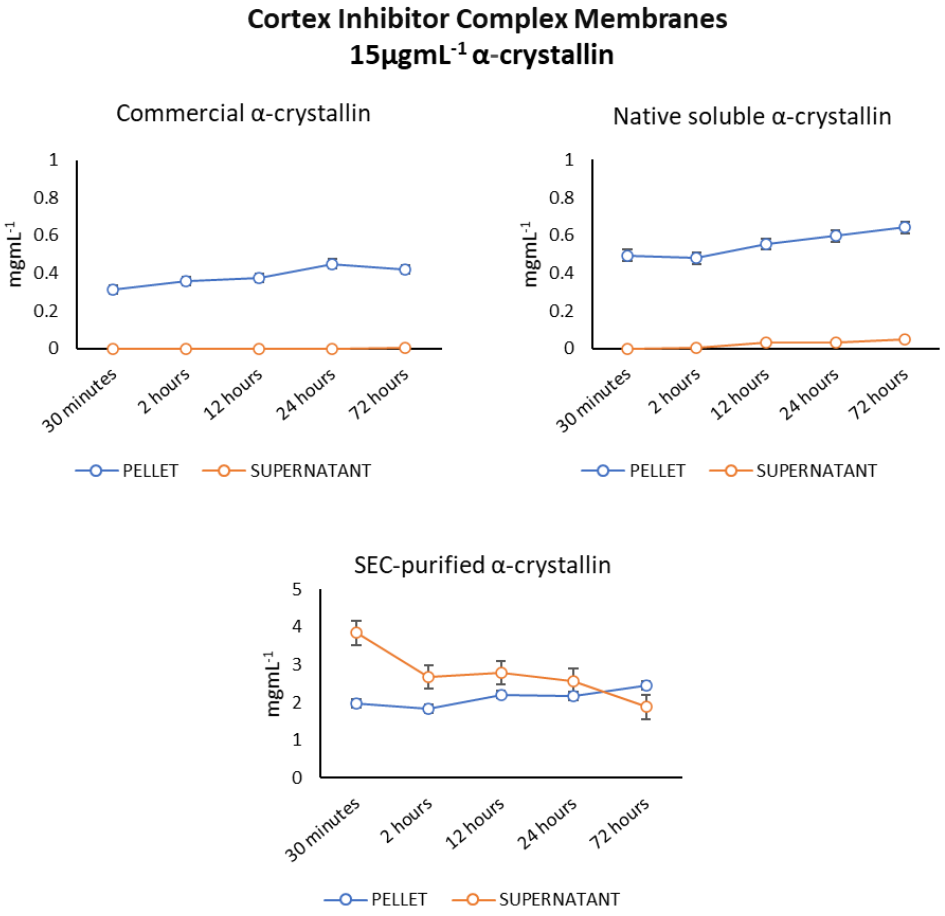


Figure 6.11. Commercial a-crystallin at 15 $\mu gmL^{-1}$ has no effect on the solubility of high protein content membranes treated with an inhibitor protease complex. A minimal release of soluble protein was detected in membranes co-incubated with native soluble a-crystallin, while an inversion in the control solubility profile was observed in membranes co-incubated with SEC-isolated α-crystallin. All samples are 5 mg wet weight high protein content membranes extracted from a pool of 24 individual bovine lenses, incubated at 37$^{O}$C in light-safe conditions. Samples

incubated with SEC-isolated α-crystallin are 5 mgmL$^{-1}$ starting concentration. Assays were repeated in triplicate using material derived from a pool of 24 bovine lenses; error bars are standard error.

An increase of the supplemental α-crystallin to 30 µgmL$^{-1}$ did not alter the solubility status of membranes co-incubated with commercial α-crystallin. As 30 µgmL$^{-1}$ was above the detection threshold for the protein assay, it is evident that the supplemental protein was rendered insoluble during the incubation period. Membranes co-incubated with native soluble α-crystallin showed an increased amount of soluble protein with 0.16 mgmL$^{-1}$ at 30 minutes and a maximum of 0.22 mgmL$^{-1}$ at 72 hours. SEC-isolated α-crystallin resulted in the same pattern seen at 15 µgmL$^{-1}$, with a maximum of 3.44 mgmL$^{-1}$ soluble protein at 30 minutes and a minimum of 2.39 mgmL$^{-1}$ at 72 hours as compared to the equivalent 2.84 mgmL$^{-1}$ and 3.04 mgmL$^{-1}$ insoluble protein respectively, as seen in Figure 5.12.

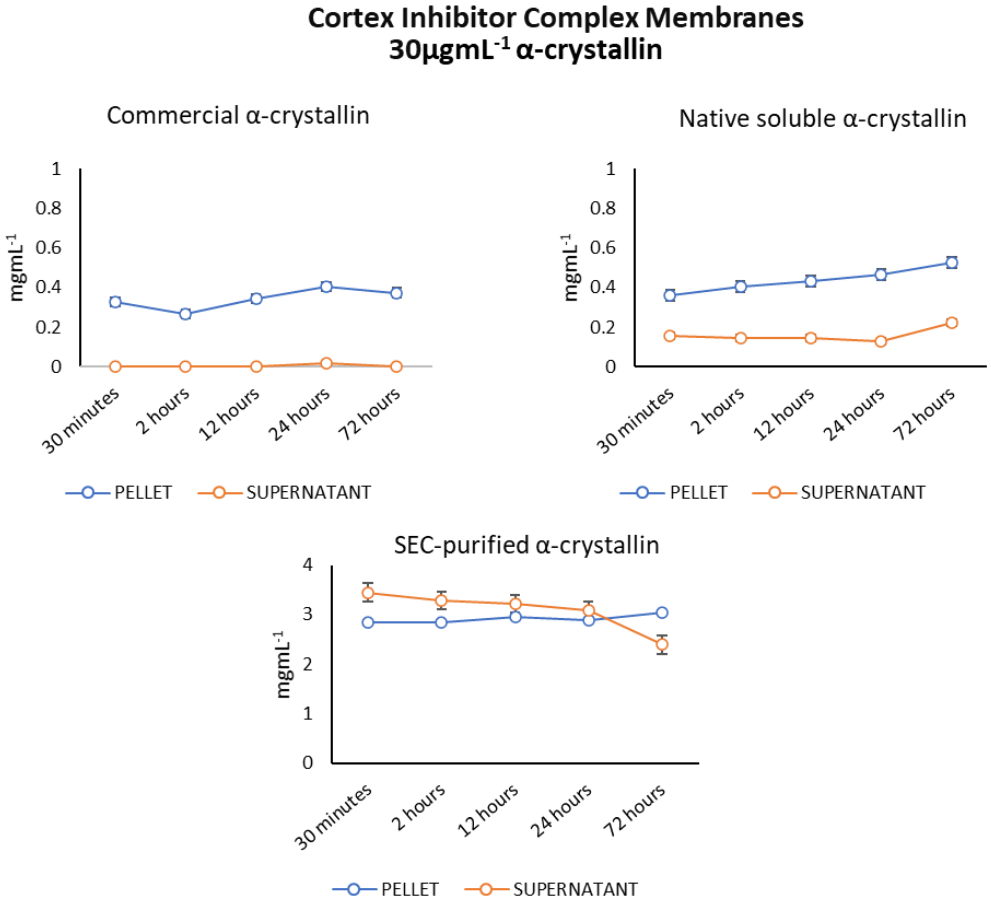


Figure 6.12. Commercial a-crystallin at 30 µgmL$^{-1}$ has no effect on the solubility of high protein content membranes treated with an inhibitor protease complex. An increased release of soluble protein was detected in membranes co-incubated with native soluble a-crystallin, while an inversion in the control solubility profile was observed in membranes co-incubated with SEC-isolated α-crystallin. All samples are 5 mg wet weight high protein content membranes extracted from a pool of 24 individual bovine lenses, incubated at 37$^{O}$C in light-safe conditions. Samples

incubated with SEC-isolated α-crystallin are 5 $mgmL^{-1}$ starting concentration. Assays were repeated in triplicate using material derived from a pool of 24 bovine lenses; error bars are standard error.

A further increase of the supplemental α-crystallin concentration to 60 $\mu gmL^{-1}$ produced a minimal amount of 0.33 $mgmL^{-1}$ soluble total protein at 24 hours in the commercial crystallin samples, while native soluble α-crystallin showed an inversion of the control solubility profile with 0.37 $mgmL^{-1}$ soluble and 0.34 $mgmL^{-1}$ insoluble protein at 30 minutes followed by a final concentration of 0.48 $mgmL^{-1}$ soluble and 0.62 $mgmL^{-1}$ insoluble protein at 72 hours. Membranes incubated with SEC-isolated α-crystallin showed an initial concentration of 3.09 $mgmL^{-1}$ soluble and 3.89 $mgmL^{-1}$ insoluble protein at 30 minutes, which progressed to 3.89 $mgmL^{-1}$ soluble and 3.84 $mgmL^{-1}$ insoluble protein at 72 hours, as seen in Figure 6.13.

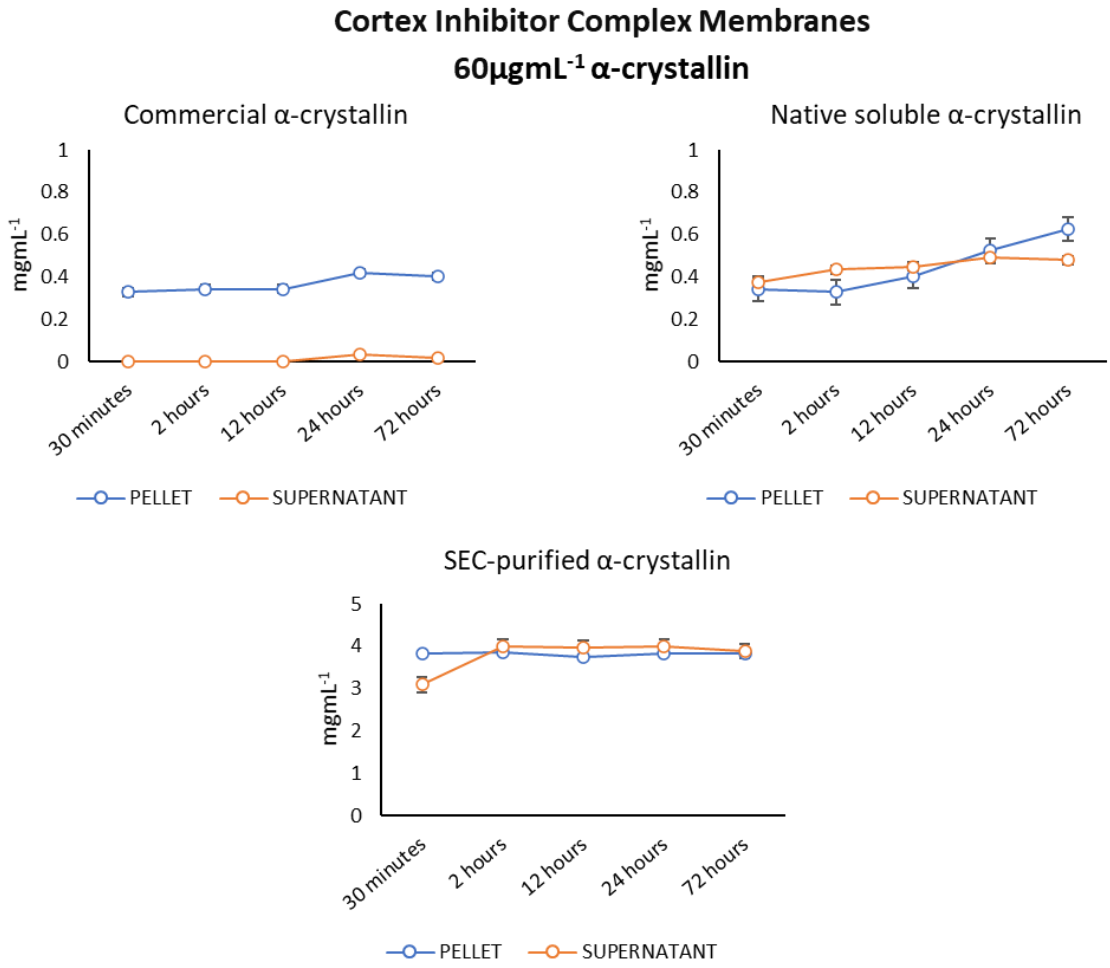


Figure 6.13. Commercial a-crystallin at 60 $\mu gmL^{-1}$ showed a transition of all protein to the insoluble fraction, except for a minimal amount of transiently soluble protein at 24 hours. Membranes co-incubated with native soluble α-crystallin showed a moderate exchange of material with an initial increase of soluble protein and a gradual decrease from 24 to 72 hours. The concentration of soluble and insoluble protein in SEC-isolated α-crystallin membranes was within 0.05 $mgmL^{-1}$from 2 to 72 hours. All samples are 5 mg wet weight high protein content

membranes extracted from a pool of 24 individual bovine lenses, incubated at 37$^{O}$C in light-safe conditions. Samples incubated with SEC-isolated α-crystallin are 5 mgmL$^{-1}$ starting concentration. Assays were repeated in triplicate using material derived from a pool of 24 bovine lenses; error bars are standard error.

At 120 µgmL$^{-1}$, all crystallin fractions produced a relatively stable amount of soluble protein from 30 minutes through to 72 hours of co-incubation, with an excess of insoluble protein at all timepoints. The average ratio of insoluble to soluble protein in commercial α-crystallin membranes was 2.85, followed by 1.46 in native soluble α-crystallin membranes, and 1.09 in SEC-isolated α-crystallin membrane samples as seen in Figure 6.14.

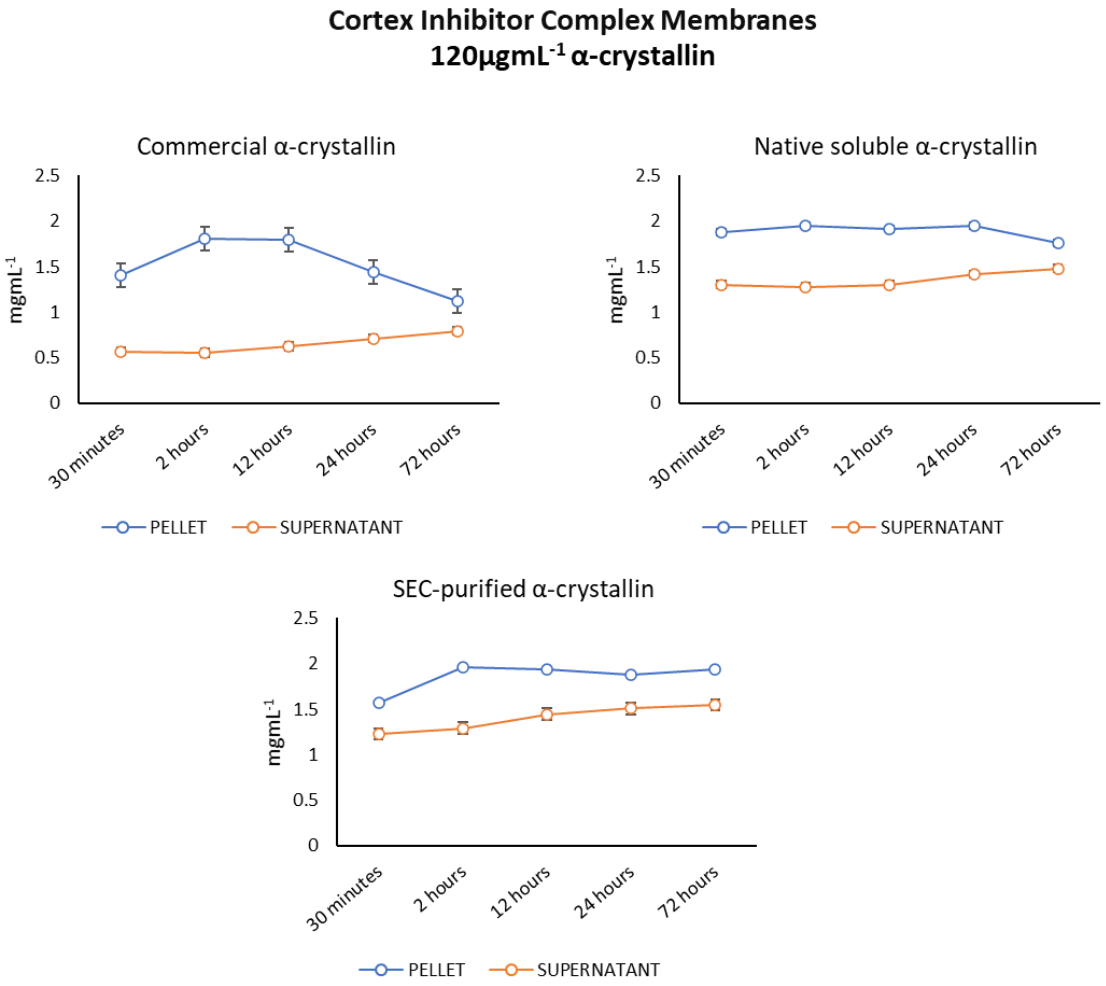


Figure 6.14. All α-crystallin samples produce a relatively static amount of soluble protein, with an excess of insoluble protein at all tested timepoints. All samples are 5mg wet weight high protein content membranes extracted from a pool of 24 individual bovine lenses, incubated at 37$^{O}$C in light-safe conditions. Assays were repeated in triplicate using material derived from a pool of 24 bovine lenses; error bars are standard error.

Considering the above, cortical high protein content membranes were incubated in buffer containing 1 µM leupeptin or 1 µM E-64 for 72 hours and were consequently exposed to 60 $\mu gmL^{-1}$ α-crystallin and co-incubated for a further 72 hours at $37^{O}C$.

In leupeptin-incubated membranes, both commercial and SEC-isolated α-crystallin partially restored the temporal solubilisation seen in control high protein content membranes, with soluble protein in commercial α-crystallin fractions increasing in a temporal manner to reach a maximum of 0.65 $mgmL^{-1}$ and 1.28 $mgmL^{-1}$ in SEC-isolated samples. The ratio of insoluble to soluble protein remained relatively stable in native soluble α-crystallin samples at 1.67, as seen in Figure 6.15.

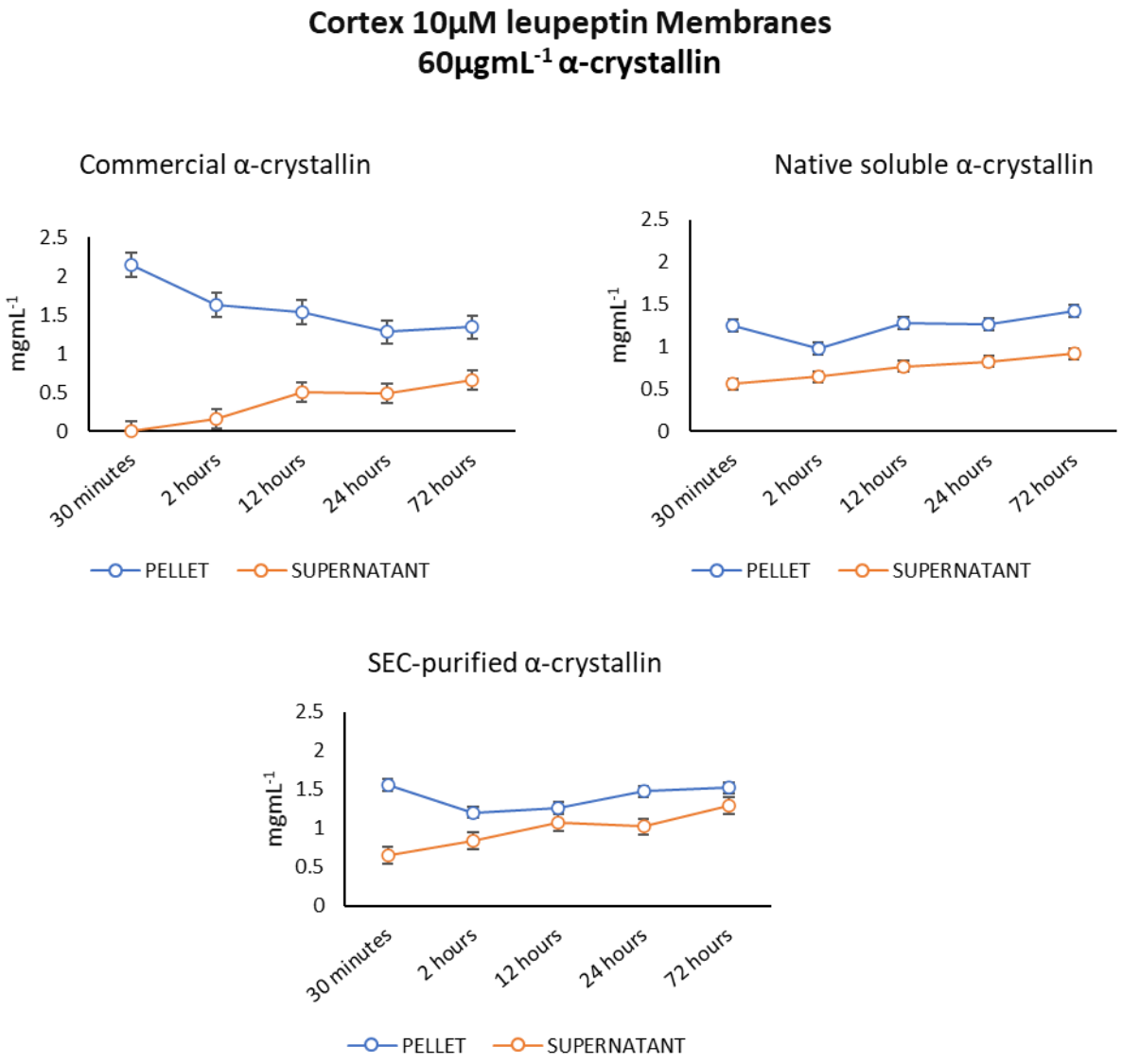


Figure 6.15. Commercial and SEC-isolated α-crystallin partially restore the temporal solubilisation seen in high protein content membranes extracted from clear lenses. The initial ratio of insoluble to soluble protein was 10.86X in commercial α-crystallin membranes at 2 hours which progressed to 2.04 at 72 hours, and 2.4 at 30 minutes in SEC-isolated α-crystallin samples which progressed

to 1.18 at 72 hours. The average ratio of insoluble to soluble protein remained relatively stable in membranes co-incubated with native soluble α-crystallin at 1.67X. All samples are 5 mg wet weight high protein content membranes extracted from a pool of 24 individual bovine lenses, incubated at 37$^{O}$C in light-safe conditions. Assays were repeated in triplicate using material derived from a pool of 24 bovine lenses; error bars are standard error.

Membranes exposed to E-64 showed a restoration of the temporal solubilisation trend seen in control samples with all α-crystallin fractions examined. The soluble protein in membranes co-incubated with commercial α-crystallin presented with an increase from 0mgmL$^{-1}$ at 30 minutes to a maximum of 0.69 mgmL$^{-1}$ at 72 hours, while membranes co-incubated with native soluble α-crystallin showed an increase in soluble protein from 0.43 mgmL$^{-1}$ at 30 minutes to 1.11 mgmL$^{-1}$ at 72 hours. Co-incubation with SEC-isolated α-crystallin resulted in an increase from 0.75 mgmL$^{-1}$ at 30 minutes to 1.21 mgmL$^{-1}$ at 72 hours, as seen in Figure 6.16.

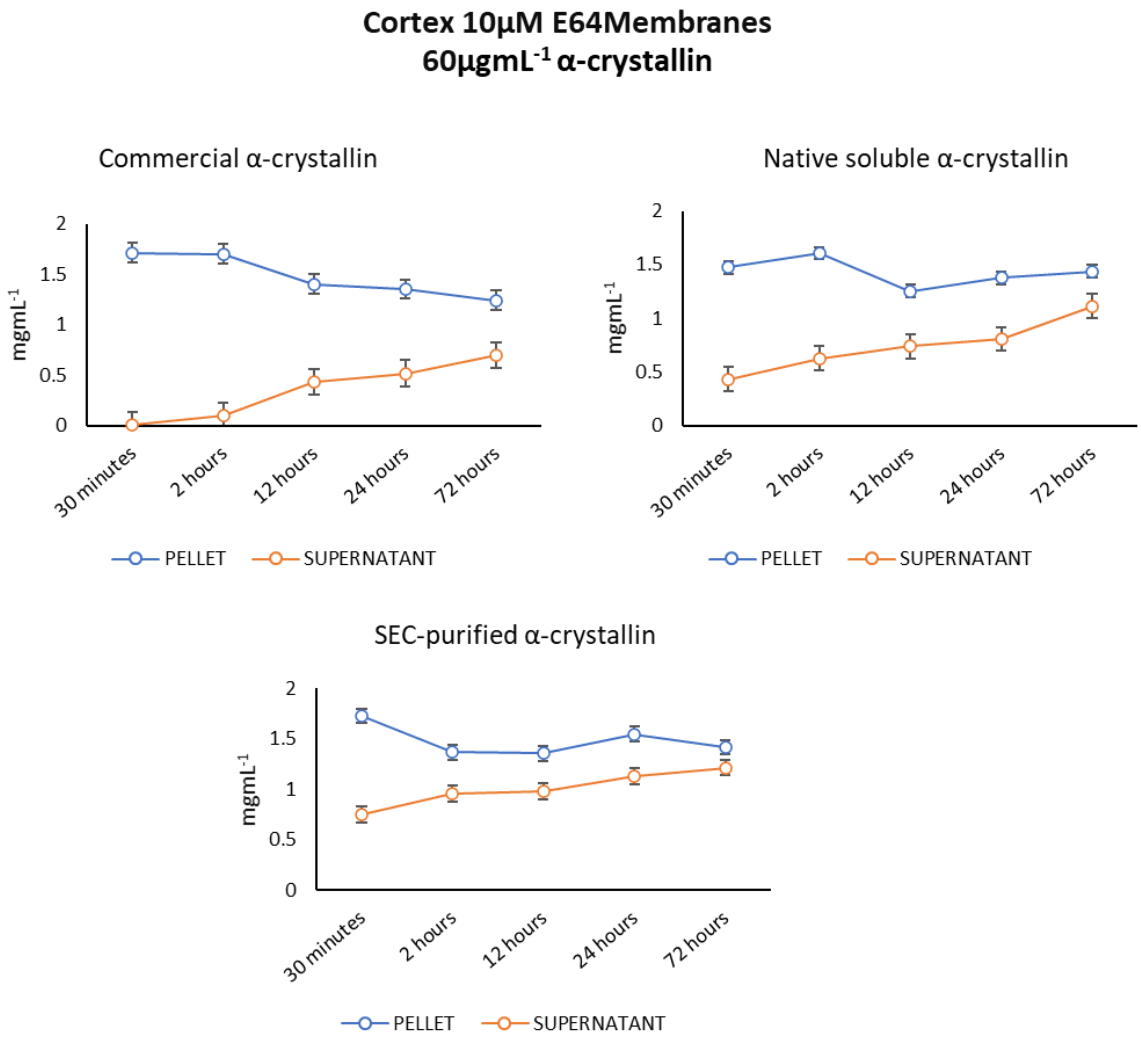


Figure 6.16. All α-crystallin fractions partially restore the temporal increase in released soluble material in membranes pre-treated with E-64. The ratio of insoluble to soluble protein in membranes exposed to commercial a-crystallin decreased from 18.8 at 2 hours to 1.79 at 72

hours, 3.41 at 30 minutes to 1.28 at 72 hours in native soluble α-crystallin membranes, and 2.29X at 30 minutes to 1.16X in membranes co-incubated with SEC-isolated α-crystallin. All samples are 5 mg wet weight high protein content membranes extracted from a pool of 24 individual bovine lenses, incubated at 37$^{O}$C in light-safe conditions. Assays were repeated in triplicate using material derived from a pool of 24 bovine lenses; error bars are standard error.

## 6.4 The sensitisation of α-crystallin fractions with sterols influence the interactions with high protein content lens membranes

Previous reports have highlighted the potential of oxysterols as a pharmacological reagent which restores the native conformation of αB-crystallin in a model of cataract reversal (299). Equally, cholesterol was found to increase the aggregation of α-crystallin and exacerbate the light-scattering aggregates in cataractous lenses. This, in addition to the observations made in section 6.3.2., led us to examine the effect of sterol sensitisation on the efficacy of α-crystallin fractions in the restoration of the temporal solubilisation seen in control cortex membranes.

### 6.4.1 Cholesterol sensitisation increases the efficacy of native soluble α-crystallin in aiding the solubilisation of high protein content membranes

Native soluble α-crystallin was co-incubated in light-safe conditions at 37$^{O}$C for 24 hours with 100 µM, 10 µM, or 1 µM cholesterol prior to use in solubilisation assays.

All cholesterol concentrations produced significantly increased amounts of soluble protein as compared to the α-crystallin only samples described in section 6.3.2. Membranes co-incubated with α-crystallin sensitised against 100 µM cholesterol showed an initial concentration of 1.46 mgmL$^{-1}$ total soluble protein at 30 minutes which increased to 1.51 mgmL$^{-1}$ at 72 hours; α-crystallin sensitised against 10 µM cholesterol produced 1.39 mgmL$^{-1}$ total soluble protein at 30 minutes, increasing to 1.48 mgmL$^{-1}$ at 72 hours, and 1 µM cholesterol produced 1.36 mgmL$^{-1}$ at 30 minutes and 1.43 mgmL$^{-1}$ at 72 hours, as seen in in Figure 6.17.

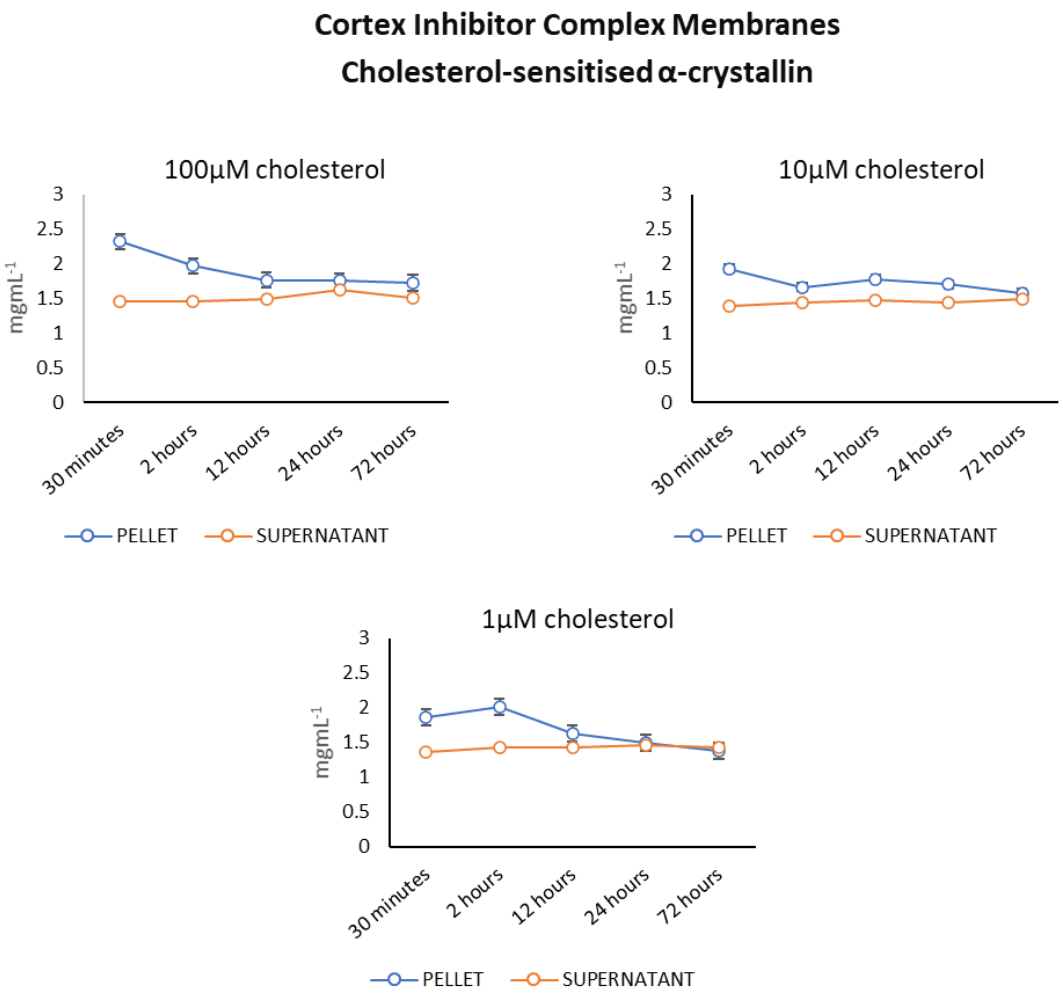


Figure 6.17. Sensitisation of α-crystallin with cholesterol increases the concentration of soluble protein in cortical high protein content membranes incubated with a commercial protease inhibitor complex. The ratio of insoluble to soluble protein in membranes co-incubated with the 100 µM sensitised α-crystallin decreased from 1.58 at 30 minutes to 1.13 at 72 hours, 1.38 at 30 minutes to 1.06 at 72 hours in 10 µM cholesterol sensitised a-crystallin, and 1.36 at 30 minutes to 0.95 at 72 hours in 1 µM cholesterol sensitised α-crystallin. All samples are 5 mg wet weight high protein content membranes extracted from a pool of 24 individual bovine lenses, incubated at 37$^{O}$C in light-safe conditions. Assays were repeated in triplicate using material derived from a pool of 24 bovine lenses; error bars are standard error.

Increased total soluble protein was observed in membranes incubated in E-64 and subsequently co-incubated with cholesterol-sensitised α-crystallin, as seen in Figure 6.18. The temporal increase seen in control membranes was replicated in membranes co-incubated with the 10 µM and 1 µM cholesterol-sensitised α-crystallin, while the soluble protein fraction in the 100 µM cholesterol group remained relatively constant throughout the examined timeframe. The ratio of insoluble to soluble protein in the 100 µM group started at 1.75 at 30 minutes and concluded at 1.4 at 72 hours, while the initial 30 minute ratios of the 10 µM and 1

µM cholesterol groups were 3.15 and 4.63 before progressing to 1.46 and 1.11 at 72 hours respectively.

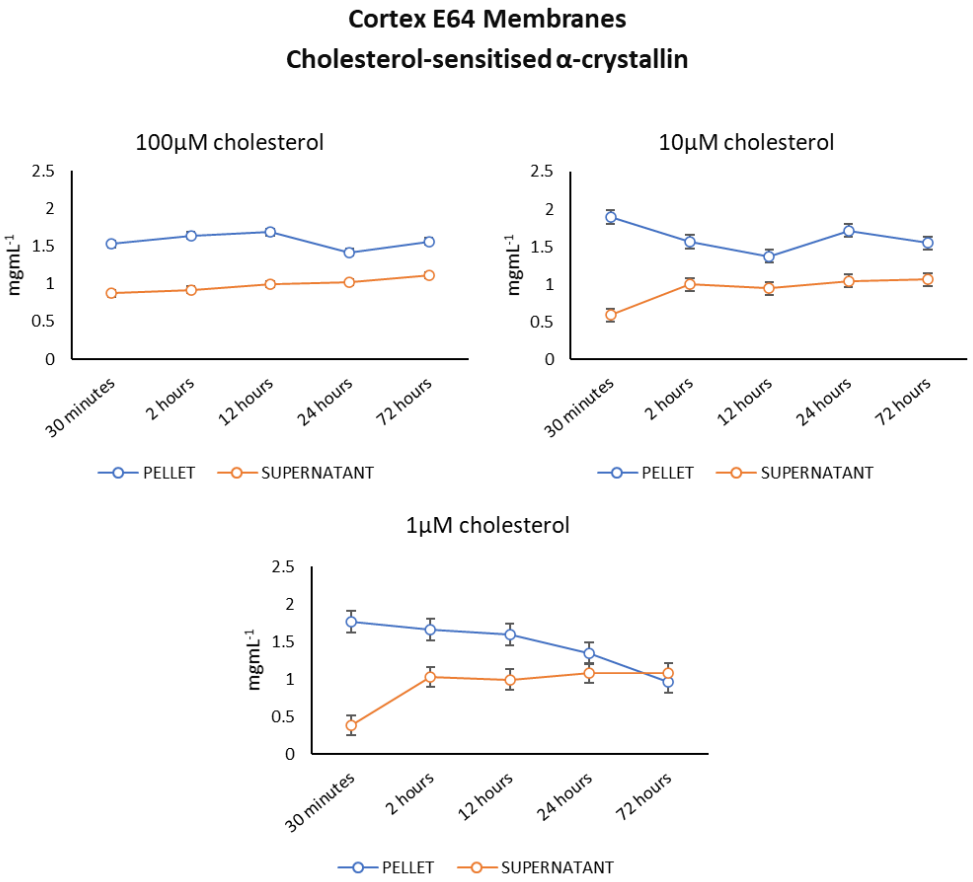


Figure 6.18. Sensitisation of α-crystallin with cholesterol increases the concentration of soluble protein in cortical high protein content membranes incubated with the cysteine peptidase inhibitor E-64. The initial concentrations of soluble protein were 0.87 $mgmL^{-1}$ for the 100 µM cholesterol group, 0.57 $mgmL^{-1}$ for the 10 µM, and 0.38 $mgmL^{-1}$ for the 1 µM cholesterol group. The final concentrations recorded were 1.11 $mgmL^{-1}$, 1.06 $mgmL^{-1}$, and 1.07 $mgmL^{-1}$. All samples are 5 mg wet weight high protein content membranes extracted from a pool of 24 individual bovine lenses, incubated at 37$^{O}$C in light-safe conditions. Assays were repeated in triplicate using material derived from a pool of 24 bovine lenses; error bars are standard error.

### 6.4.2 25-hydroxycholesterol sensitisation increases the amount of total soluble protein but does not restore the temporal solubilisation seen in control membrane samples

Increased total soluble protein was observed in both membranes incubated in the commercial protease inhibitor complex and the cysteine peptidase inhibitor E-64, and subsequently co-incubated with 25-hydroxycholesterol (25-OHC)-sensitised α-crystallin, as seen in Figures 6.19 and 6.20. The temporal increase seen in control membranes was replicated in E-64-exposed membranes, but not the inhibitor complex-exposed membranes.

Membranes co-incubated with α-crystallin sensitised against 100 µM 25-OHC showed an initial concentration of 1.4 $mgmL^{-1}$ total soluble protein at 30 minutes which increased to 1.51 $mgmL^{-1}$ at 72 hours; α-crystallin sensitised against 10 µM 25-OHC produced 1.46 $mgmL^{-1}$ total soluble protein at 30 minutes, increasing to 1.48 $mgmL^{-1}$ at 72 hours, and 1 µM 25-OHC produced 1.44 $mgmL^{-1}$ at 30 minutes and 1.44 $mgmL^{-1}$ at 72 hours, as seen in in Figure 6.19. The final concentrations of soluble protein were all comparable to the equivalent samples of cholesterol-sensitised α-crystallin, as seen in Figure 6.17.

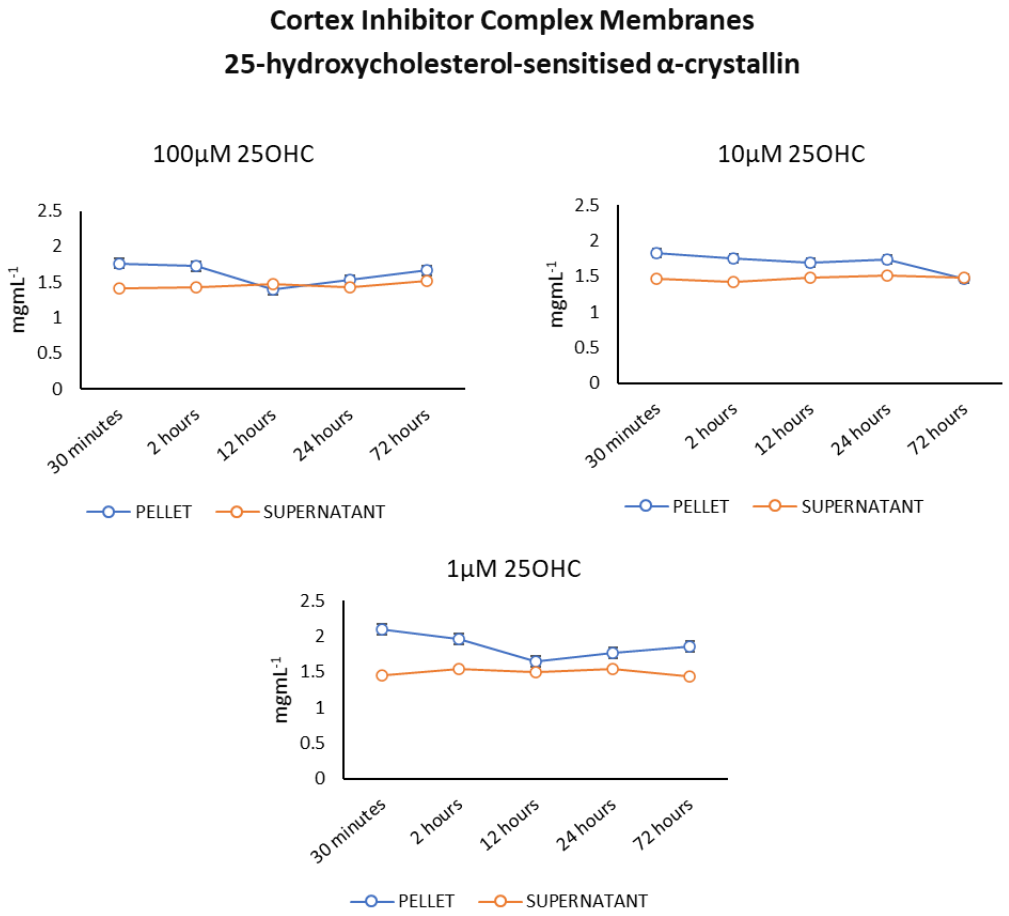


Figure 6.19. Sensitisation of α-crystallin with 25-hydroxycholesterol increases the concentration of soluble protein in cortical high protein content membranes incubated with a commercial protease inhibitor complex. The ratio of insoluble to soluble protein in membranes co-incubated with the 100 µM sensitised α-crystallin decreased from 1.25 at 30 minutes to 1.09 at 72 hours, 1.25 at 30 minutes to 0.98 at 72 hours in 10 µM 25-OHC sensitised a-crystallin, and 1.45 at 30 minutes to 1.29 at 72 hours in 1 µM 25-OHC sensitised α-crystallin. All samples are 5 mg wet weight high protein content membranes extracted from a pool of 24 individual bovine lenses, incubated at 37$^{O}$C in light-safe conditions. Assays were repeated in triplicate using material derived from a pool of 24 bovine lenses; error bars are standard error.

The temporal manner of solubilisation was better retained in membranes exposed to E-64 prior to co-incubation with 25-OHC-sensitised α-crystallin. The ratio of insoluble to soluble

protein in the 100 µM group started at 2.56 at 30 minutes and concluded at 1.17 at 72 hours, while the initial 30 minute ratios of the 10 µM and 1 µM 25-OHC groups were 3.85 and 4.5 before progressing to 1.19 and 1.21 at 72 hours respectively, as seen in Figure 6.20.

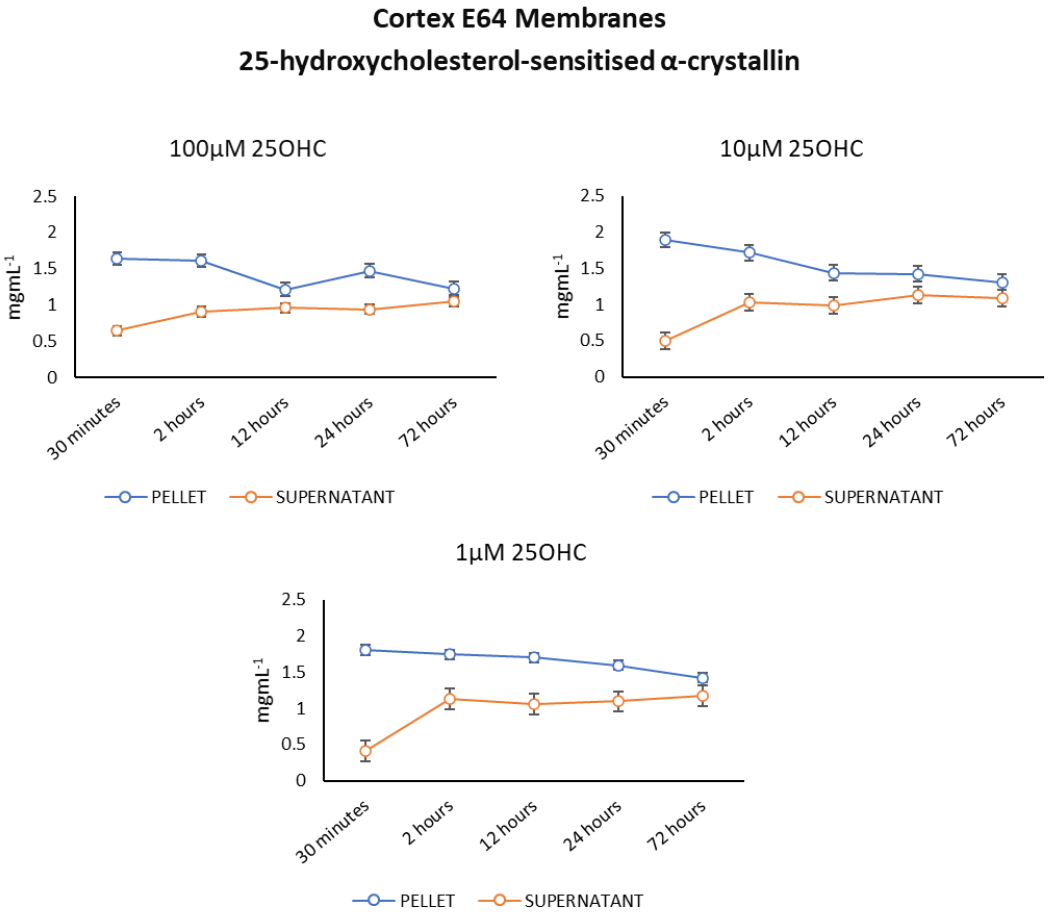


Figure 6.20. Sensitisation of α-crystallin with 25-hydroxycholesterol increases the concentration of soluble protein in cortical high protein content membranes incubated with the cysteine peptidase inhibitor E-64. The initial concentrations of soluble protein were 0.64 $mgmL^{-1}$ for the 100 µM 25-OHC group, 0.49 $mgmL^{-1}$ for the 10 µM, and 0.4 $mgmL^{-1}$ for the 1 µM 25-OHC group. The final concentrations recorded were 1.04 $mgmL^{-1}$, 1.09 $mgmL^{-1}$, and 1.17 $mgmL^{-1}$. All samples are 5 mg wet weight high protein content membranes extracted from a pool of 24 individual bovine lenses, incubated at 37$^{O}$C in light-safe conditions. Assays were repeated in triplicate using material derived from a pool of 24 bovine lenses; error bars are standard error.

### 6.4.3 Lanosterol sensitisation increases the amount of total soluble protein and partially restores the temporal solubilisation in E-64-incubated membranes

The final sensitisation sterol, lanosterol, produced similar results to the cholesterol and 25-OHC sensitised α-crystallin groups seen in Figures 6.17 through to 6.20. Increased total soluble protein was observed in both membranes incubated in the commercial protease inhibitor

complex and the cysteine peptidase inhibitor E-64, and subsequently co-incubated with lanosterol-sensitised α-crystallin, as seen in Figures 6.21 and 6.22. As with the 25-OHC-sensitised groups in Figure 6.20, the temporal increase seen in control membranes was replicated in E-64-exposed membranes, but not the inhibitor complex-exposed membranes.

Membranes co-incubated with α-crystallin sensitised against 100 µM lanosterol showed an initial concentration of 0.72 $mgmL^{-1}$ total soluble protein at 30 minutes which increased to 0.96 $mgmL^{-1}$ at 72 hours; α-crystallin sensitised against 10 µM lanosterol produced 0.87 $mgmL^{-1}$ total soluble protein at 30 minutes, stable through to 72 hours, and 1 µM lanosterol produced 0.81 $mgmL^{-1}$ at 30 minutes and 0.77 $mgmL^{-1}$ at 72 hours, as seen in in Figure 6.21.

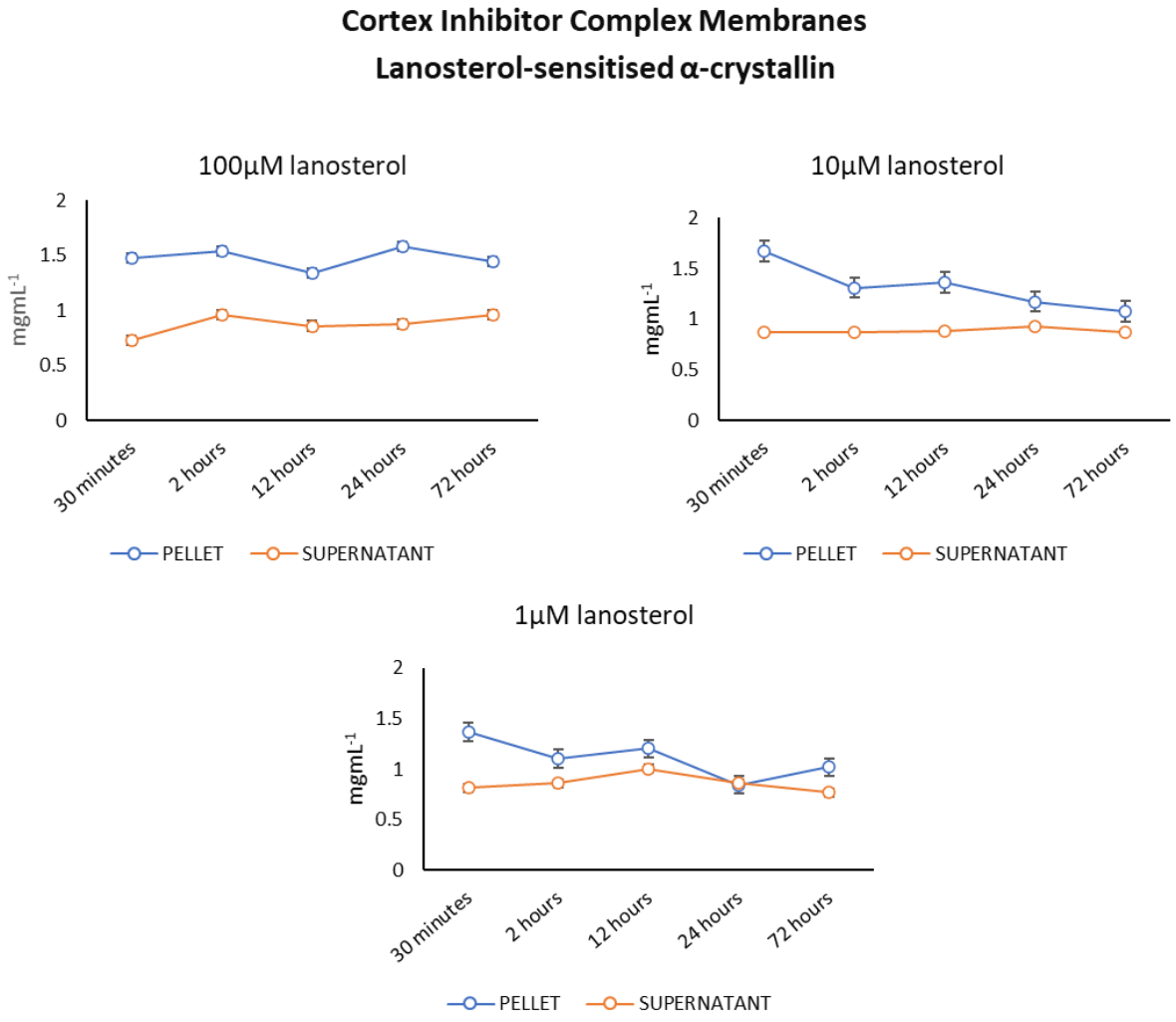


Figure 6.21. Sensitisation of α-crystallin with lanosterol increases the concentration of soluble protein in cortical high protein content membranes incubated with a commercial protease inhibitor complex. The ratio of insoluble to soluble protein in membranes co-incubated with the 100 µM sensitised α-crystallin decreased from 2.04 at 30 minutes to 1.5 at 72 hours, 1.91 at 30 minutes to 1.22 at 72 hours in 10 µM lanosterol sensitised a-crystallin, and 1.67 at 30 minutes to

1.31 at 72 hours in 1 µM lanosterol sensitised α-crystallin. All samples are 5 mg wet weight high protein content membranes extracted from a pool of 24 individual bovine lenses, incubated at 37$^{O}$C in light-safe conditions. Assays were repeated in triplicate using material derived from a pool of 24 bovine lenses; error bars are standard error.

The temporal manner of solubilisation was better retained in membranes exposed to E-64 prior to co-incubation with lanosterol-sensitised α-crystallin. The ratio of insoluble to soluble protein in the 100 µM group started at 2.61 at 30 minutes and concluded at 1.51 at 72 hours, while the initial 30 minute ratios of the 10 µM and 1 µM lanosterol groups were 3.14 and 6.08 before progressing to 1.7 and 1.44 at 72 hours respectively, as seen in Figure 6.20.

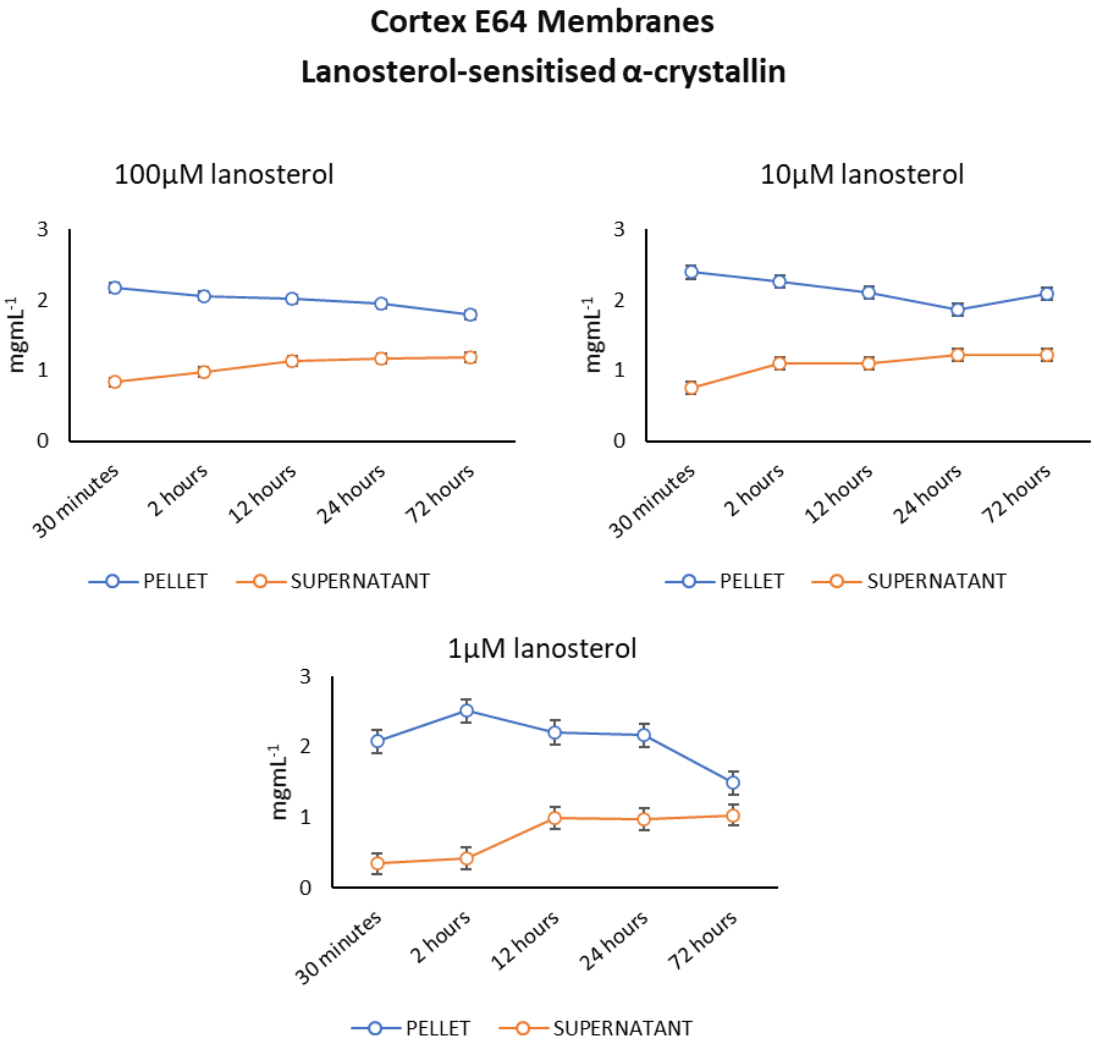


Figure 6.22. Sensitisation of α-crystallin with lanosterol increases the concentration of soluble protein in cortical high protein content membranes incubated with the cysteine peptidase inhibitor E-64. The initial concentrations of soluble protein were 0.83 mgmL$^{-1}$ for the 100 µM lanosterol group, 0.76 mgmL$^{-1}$ for the 10 µM, and 0.344 mgmL$^{-1}$ for the 1 µM lanosterol group. The final concentrations recorded were 1.18 mgmL$^{-1}$, 1.22 mgmL$^{-1}$, and 1.03 mgmL$^{-1}$. All samples

are 5 mg wet weight high protein content membranes extracted from a pool of 24 individual bovine lenses, incubated at 37$^{O}$C in light-safe conditions. Assays were repeated in triplicate using material derived from a pool of 24 bovine lenses; error bars are standard error.

## 6.5 General summary

The temporal release of a soluble protein fraction from high protein content lens membranes is temperature-dependent within the physiological window for chaperone-active α-crystallin and is absent in cataractous lenses. This temporal release for high protein content lens membranes can be inhibited via the use of protease inhibitors including E-46 and leupeptin, as seen in figure 6.23.

Lenticular α-crystallin solutions influence the sedimentation of high protein content membranes treated with protease inhibitors and partially restore the temporal release of material from leupeptin and E-64-treated high protein content membranes at physiological temperatures.

Sterol and oxysterol sensitisation of lenticular α-crystallin solutions has a variable effect on the sedimentation profile of high protein content membranes treated with leupeptin and E-64, highlighting a potential target for crystallin-associated pharmacotherapeutic interventions.

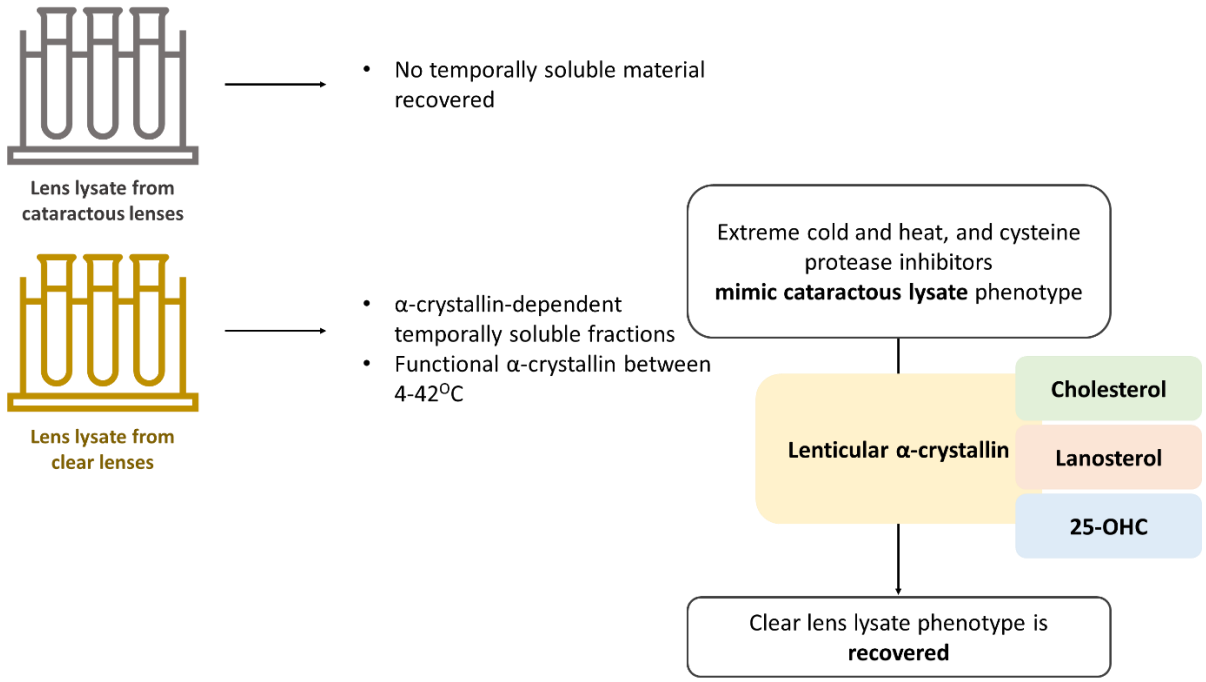


Figure 6.23. Functional α-crystallin, sensitised by oxysterols, recovers the temporal solubility of clear lens lysates in cysteine protease inhibitor-aged lysates which mimic material derived from cataractous lenses.

# 7 Chapter 7: Discussion and general findings

## 7.1 The effect of cholesterol metabolism alteration in the developing zebrafish

### 7.1.1 The partial inhibition of cholesterol synthesis decreases larval independent movement and affects the optomotor response

The pharmacological inhibition of cholesterol synthesis results in a direct but variable reduction of the amount of total cholesterol in the zebrafish larvae, as seen in Figure 4.20. The reduction in cholesterol content of both whole body tissue samples and of lens only samples reveals that the impact of synthesis inhibition is systemic, and as such it is expected that cholesterol-rich tissues such as lens and brain will be significantly impacted. Indeed, this effect is reflected in human cholesterol synthesis syndromes where visual impairment and neurological symptoms including ataxias and intellectual disability are at the core of the condition (249,262,264,270,271).

The analysis of the optomotor response and independent movement of zebrafish larvae provides an initial framework to differentiate between visual impairment and neurological damage (312,313,324). As seen in Figures 4.2 and 4.3, synthesis inhibitors and lxr agonists have a variable effect on these behavioural parameters, with the independent movement of zebrafish at ambient light conditions greatly reduced or entirely eliminated. Zebrafish larvae are light-responsive and highly active by 5 dpf (312) as they consume the last of their maternal yolk sack reserves (319) and begin to independently feed, so any reduction in independent movement is contrary to the behaviour expected for survival. The assessment of independent movement does not provide insight on the mechanism of impairment since it does not indicate whether the defect is due to reduced visual acuity and response to light, or due to motor defects whereby the zebrafish are less mobile as a consequence of neurological damage.

The startle response to specific stimuli was used to directly differentiate between visual and neurological damage, with exposure to light used to assess zebrafish visual acuity, agitation used to assess zebrafish proprioception, and contact used to assess visual acuity and the motor response (312,324).

The response to a single light pulse was eliminated in all groups apart from the T0901317 exposure, where the response was attenuated. Similarly, the response to agitation was significantly reduced in all groups apart from the T0901317 group, and the response to contact was modestly reduced in the U-18666A group and significantly reduced in the U-18666A/AY9944 combination treatment group as seen in Figure 4.3. Since the purely visual

stimulus did not produce a startle response while non-visual stimulus of physical contact did, we can conclude that the damage incurred by the inhibition of cholesterol synthesis is mostly limited to the visual apparatus of the zebrafish. The dampened response to agitation in ambient light conditions implicates neurological damage as part of the observed phenotype since proprioception is not dependent on a functional visual system. From the above, we can conclude that the inhibition of cholesterol synthesis impacts the physiological development of vision in zebrafish and results in neurological impairment which does not affect the motor functions of the larvae.

### 7.1.2 The pharmacological inhibition of cholesterol synthesis proportionately reduces larval size but accelerates yolk consumption

When expressed as an absolute value, the area of synthesis-inhibited zebrafish bodies and yolks was significantly reduced as compared to control groups as seen in Figures 4.6, 4.7, and 4.9.

The total reduction of body size was relatively uniform across the inhibitors used, while the mean eye area was only reduced in the groups treated with RO48-8071 and U-18666A as seen in Figure 4.9. The reduction in yolk size was considerably more pronounced, with U-18666A-treated larvae showing the largest reduction as seen in Figure 4.7.

When expressed as a percentage of body area, the significant reduction in yolk size was retained for all inhibitor-treated groups while the eye area was indistinguishable from control groups, as seen in Figures 4.8 and 4.11. From these findings, we can conclude that the reduced eye area seen in Figure 4.9 is proportionate to the reduction of body size seen in Figure 4.6. In contrast, the significant relative reduction seen in yolk size in Figure 4.8 can be attributed to an accelerated consumption of the maternal yolk lipid reservoir due to decreased *de novo* cholesterol synthesis, an effect which has previously been seen as a result of lxr agonist treatment (319). The U-81666A groups showed the largest reduction in body and yolk size, with a marginally larger decrease in eye are seen in the RO48-8071 treated larvae. As U-18666A is both a DHCR24 inhibitor and a weak inhibitor of hedgehog (hh) signalling and thus intracellular cholesterol transport, it is probable that these phenotypes are a result of improper segmentation in the developing embryos producing a reduced lateral length.

As the cholesterol synthesis inhibitors were not introduced to the zebrafish growth medium until 24 hpf and partially reduced the total cholesterol levels as seen in Figure 4.20, it is increasingly likely that the reduced levels of cholesterol did not fundamentally impact major developmental signalling pathways; indeed, the behavioural effects appear to be limited to

cholesterol-rich tissues which are responsible for the vision-perception portion of the optomotor response.

### 7.1.3 The pharmacological inhibition of cholesterol synthesis has a limited impact on the gross morphology of zebrafish eyes

The overall decrease in eye lateral area in zebrafish groups treated with RO48-8071 and U-18666A was found to be proportionate to the overall decrease in body size, as seen in Figure 4.11. Similarly, marginal changes in the lateral aspect ratio of larval eyes were detected for all synthesis inhibitor treatments as seen in Figure 4.10, with the exception of the combination AY9944/U-18666A group which saw a significant increase in the circularity of the eye due to a decrease in the horizontal diameter. The appropriate development of the ocular apparatus was largely expected as by 24 hpf larvae respond to the visual stimulus of light (312), and the experiment was designed to target the initial formation of secondary fibre cells which occurs between 26 and 30 hpf (332). Furthermore, as neither microphthalmia nor microcornea have commonly been associated with syndromic cholesterol metabolism disorders in the presence of congenital cataract (249,262,265,270) it is not entirely unexpected that the overall lateral morphology of the eye was not found to vary from control groups.

### 7.1.4 Lanosterol supplementation rescues the synthesis inhibition-associated reduction in yolk size, but cholesterol supplementation is lethal for all inhibitors apart from AY9944

The restoration of the yolk area of lanosterol-supplemented zebrafish treated with RO48-8071 larvae, in addition to the minor but significant enlargement of the yolk when lanosterol was added at 48 hpf as seen in Figures 4.14 and 4.15, is an initial indicator that supplemental sterols can be absorbed by the larvae. This finding is further supported by the morphology of the yolk sack as seen in Figure 4.13, as only sporadic evidence of abdominal oedema was found at 5 dpf following the control supplementation with lanosterol or cholesterol. The significant relative increase in yolk area between larvae supplemented with lanosterol at 30 and 48 hpf could be interpreted as evidence to support both the yolk-mediated uptake of sterol and the subsequent metabolism or transport through the YSL, which is discussed further in section 7.1.8.

The decrease in body size seen in lanosterol-supplemented and RO48-8071 treated larvae in Figure 4.14 as compared to control groups highlights the importance of maintaining appropriate cholesterol metabolism during development, and demonstrates that the developmental defects conferred by cholesterol synthesis inhibitors may not be rescuable once damage has occurred. Interestingly, lanosterol supplementation at 30 hpf resulting in a

significant decrease in mean body area as compared to the 0.1% (v/v) DMSO (q=13.98), the lanosterol only control (q=10.65), the RO48-8071 (q=6.73), and the 48 hpf lanosterol groups (q=7.62) as seen in Figure 4.14. Further phenotypic data beyond 5 dpf would clarify the longevity of these phenotypes and whether they are a transient effect due to the dysregulation of the cholesterol synthesis pathway or whether they are persistent and irreversible. Treatment of larvae with RO48-8071 results in the accumulation of oxidosqualene which is retained through to 5 dpf as discussed in section 7.1.6 and although not much is known about the biological implications, data suggest that the inhibition of cholesterol synthesis at LSS results in the growth arrest of multiple cell types including human endothelial cells and supress tumour growth and metastasis by limiting angiogenesis (333–337). Regardless, the increase in oxidosqualene levels will undoubtedly influence the rate of cholesterol biosynthesis due to its limited conversion to cholesterol.

Similar to the overall mean body size, the lateral area of eyes was significantly reduced in zebrafish supplemented with lanosterol at 30 and 48 hpf which had been treated with RO48-8071 at 24 hpf, as seen in Figure 4.14. This reduction is not preserved when expressed as a percentage of body size as seen in Figure 4.15, meaning the lateral eye area is proportionately reduced and indicative of a systemic effect.

Unlike lanosterol, cholesterol supplementation was shown to be 100% lethal in combination with RO48-8071 and U-18666A treatment as seen in Figure 4.13. This complete lethality was also observed in larvae treated with AY9944/U-18666A, seen in Figure 4.13. While no data were recovered which could offer insight into a relevant mechanism, the physical phenotype of AY9994-treated surviving larvae may provide some clues.

Zebrafish treated with AY9944 and supplemented with cholesterol at 30 hpf presented with severe developmental abnormalities at 5 dpf, in contrast with control larvae treated with AY9944 only as seen in Figures 4.16 and 4.6, respectively. A combination of extensive pericardial and abdominal oedema, skeletal deformities of the dorsal fins, and increased circularity of the lateral eye face in addition to severe ocular oedema were immediately apparent, with a relative increase in eye are also being apparent as seen in Figure 4.17. After exclusion of the oedema, the yolk area was also restored to physiological levels in AY9944-treated and cholesterol-supplemented zebrafish.

Recent studies have shown that the inhibition of cholesterol synthesis at the rate-limiting step of HMG-CoA produce structural defects in cilia by disrupting the formation of cholesterol-rich domains at the transition zone in the base of the cilium (316). This results in an inhibition of Hedgehog signalling in the cilium (338), impairing ciliary function and producing phenotypes

such as pericardial oedema, left-right asymmetry, and microcephaly (316); all these are also found in patients diagnosed with SLOS which commonly presents with postnatal cataract (271). Cholesterol supplementation has been shown to be effective in rescuing the cilium-dependent phenotypes associated with HMG-CoA inhibition (316) and as an effective early intervention in SLOS (273). Although the phenotype seen in AY9944-treated and cholesterol-supplemented zebrafish is typical of severe ciliopathy, further characterisation of each tissue is required to understand why this phenotype arises after the supplementation with cholesterol and not in the synthesis-inhibited larvae. It is possible that the sudden influx of supplementary cholesterol promotes a dramatic downregulation of cholesterol synthesis, but extensive biochemical work is required to elucidate the mechanism behind this phenotype.

### 7.1.5 The inhibition of cholesterol synthesis has a limited effect on lens development and structure

Although no statistically significant deviation was found in lens diameter on the optical axis of cholesterol synthesis inhibited zebrafish, the range of values was increased in all groups as compared to the 0.1% (v/v) DMSO control as seen in Figure 4.18. A similar effect was seen in the lens aspect ratio, except for lenses from larvae treated with RO48-8071 which were significantly more ellipsoidal due to an increase in the equatorial diameter. The mechanism behind the development of lenses into to spherical or lenticular shapes is poorly understood, but transition events have been identified in the mouse which are related to changes in the epithelial density pattern (339).

A significant reduction in LEC height was found in all zebrafish groups treated with cholesterol synthesis inhibitors, with the most dramatic reduction seen in AY9944/U-18666A treated larvae. This decrease could be indicative of a loss of cell architecture, with biochemical characterisation of cytoskeletal and cell-to-cell adhesion proteins required to fully understand this effect.

The simplest mechanism behind the transition of a lens from a spherical to lentoid shape is an increase in the ratio of differentiation to proliferation, where a greater number of new LFCs are deposited along the equator leading to a regional thickening of the tissue. This can arise from a change in the concentration of FGF and BMP which regulate LEC proliferation and cell cycle exit (8,11,24) or a change in the sensitivity of LECs to these factors. Changes in cell architecture and membrane composition, such as those seen in Figures 4.19 and 4.21 could have an impact on cell fate, and as such further analysis of the pathways involved in cell cycle control needs to be undertaken in order to understand these phenotypes.

### 7.1.6 The pharmacological inhibition of cholesterol synthesis reduces total cholesterol in zebrafish and results in the accumulation of relevant upstream metabolites

A decrease in total cholesterol was seen across all cholesterol synthesis inhibitor-treated zebrafish groups, with the RO48-8071 group showing the largest reduction. This trend was retained in detected cholesterol esters, as seen in Figure 4.20. Tissue-specific analysis of the total cholesterol content and intermediate metabolites revealed the overall reduction in cholesterol was more dramatic in the lenses of all inhibitor-treated groups as compared to the equivalent whole body samples, as seen in Figure 4.21.

The accumulation of immediate upstream metabolites was seen in all whole body tissue samples, with RO48-8071 and AY9944 resulting in a larger increase of oxidosqualene and 7-dehydrocholesterol respectively, while U-18666A treatment produced only a modest increase of desmosterol, as seen in Figures 4.21 and 4.22. The lenticular accumulation of upstream metabolites was varied, with AY9944 treatment resulting in a two-fold increase in the ratio of 7-dehydrocholsterol as compared to whole body samples. The ratio of accumulated oxidosqualene in lenses of larvae treated with RO48-8071 was similar to that of whole-body tissue samples. Interestingly, the amount of detected desmosterol was reduced in U-18666A-treated zebrafish lenses in contrast with the modest accumulation seen in the equivalent whole-body samples.

From the above, it is possible to consider that the main pathway of cholesterol production in the lens is the Kandutsch-Russell pathway via the production of 7-dehydrocholesterol (317), since the use of AY9944 resulted in the most dramatic increase of this upstream metabolite while the use of U-18666A did not result in the accumulation of desmosterol which is the major precursor in the Bloch pathway. This relatively modest decrease in total cholesterol and modest accumulation of desmosterol in zebrafish treated with U-18666A can be attributed to the accelerated consumption of the maternal yolk lipid reserve seen in Figure 4.8.

A more appropriate comparison of the effect of cholesterol synthesis inhibition at these different levels would be achieved by modifying the concentrations of RO48-8071, AY9944, and U-18666A to equally reduce the amount of total larval cholesterol. A standard cholesterol content across zebrafish groups would allow a better analysis of the effects of each inhibitor, including phenotypes attributed to the accumulation of upstream metabolites and off-target effects due to changes in cholesterol-dependent signalling pathways.

### 7.1.7 Lanosterol and cholesterol supplementation recover total cholesterol levels in synthesis-inhibited larvae

The supplementation of RO48-8071 and AY9944-treated zebrafish with lanosterol and cholesterol respectively resulted in a modest increase in the amount of total cholesterol isolated from whole body samples, as seen in Figure 4.23. The equivalent amount of total lens cholesterol was drastically increased, though values were not restored to physiological levels.

These findings further evidence that supplemental sterols are absorbed and metabolised by the synthesis-inhibited zebrafish, with further discussion on this found in section 7.1.8.

### 7.1.8 The incorporation of supplemental lanosterol and cholesterol in the developing zebrafish is variable and subject to downstream metabolism

Fluorescent and deuterated sterols were used to examine the absorption and incorporation of supplemental lanosterol and cholesterol in the developing zebrafish. The use of fluorescent sterols, including Bodipy-cholesterol, has been well documented in the analysis of cholesterol tracking in the developing zebrafish. Previous studies have shown that Bodipy-cholesterol, with its 24-hydrocarbon-linked fluorophore, is targeted to lipid-rich regions of the brain, neural retina, and the yolk when injected directly into the yolk sac (340,341).

The zebrafish lens is a fully encapsulated tissue by 24 hpf, as separation from the cornea occurs at 23 hpf (332). As such, any compound introduced at this time can only enter the lens through an appropriate transport pathway. Bodipy-cholesterol was introduced to the growth medium of dechorionated zebrafish at 24 hpf and was found to be targeted to the yolk and sclera of the eye at all subsequent timepoints analysed as seen in Figures 4.24 and 4.25. Added at 6 hpf, when the presumptive lens cells are still part of the surface ectoderm (332), Bodipy-cholesterol was detected only in the yolk at 20 hpf and was absent at 30 hpf as seen in Figure 4.26. The inability of the fluorophore to penetrate the lens after separation from the cornea or to be incorporated in the developing lens could be interpreted either as metabolic processing of the cholesterol resulting in cleavage of the fluorophore, or as an incompatibility of the fluorophore-conjugated cholesterol form and the sterol transport mechanisms used by presumptive and mature lens cells. The degradation of the fluorophore through other means is unlikely, as Bodipy-cholesterol is a bright and stable compound (340) and data from Figures 4.24 and 4.25 demonstrate a clear persistence of at least 24 hours after embedding into the larval tissue.

To assess whether the conjugated fluorophore is a barrier to lens incorporation, deuterated d6 lanosterol and d6 cholesterol were used to track sterol absorption to the yolk and any subsequent trafficking and metabolic processing in the yolk or the lens. At 20 hpf, minimal

incorporation of supplemental d6 cholesterol was detected in the lens and d6 lanosterol in the yolk as seen in Figure 4.27, while at 30 hpf an accumulation of supplemental d6 cholesterol was detected in the lens and d6 lanosterol was detected in the lens and the yolk as seen in Figure 4.28. The drastically increased detection of d6 lanosterol in the lens at 30 hpf following d6 lanosterol supplementation at 6 hpf is an important finding in the context of pharmacological treatment of cataract (249,302) as it demonstrates that compound trafficking is possible after the lens has budded into an encapsulated, avascular tissue at 23 hpf. Similarly, the increased detection of d6 cholesterol at 30 hpf following d6 cholesterol supplementation shows that the encapsulated lens has a functional sterol transport apparatus, at least in the zebrafish. In addition to these findings, the detection of minor amounts of d6 cholesterol in the lenses of larvae supplemented with d6 lanosterol evidences downstream metabolic processing of the sterol but does not provide any insight on whether this is an extralenticular or intralenticular event. Further analysis of the long term retention of these metabolites is essential to understanding their transport, partitioning, and function in the lens either through standard LC-MS or MALDI-based imaging techniques (213).

Deuterated sterols such as d6 lanosterol and d6 cholesterol carry three deuterium isotopes on the 26$^{th}$ carbon and three on terminal 27$^{th}$ carbon of their acyl chain, which is not processed in the Kandutsch-Russell or Bloch pathways of cholesterol synthesis (317) between the cyclisation of oxidosqualene to lanosterol and the reduction of desmosterol or 7-dehydrocholesterol to cholesterol. This renders these compounds as ideal candidates to study the metabolism of supplemental lanosterol in the zebrafish, but also offers the opportunity to track the downstream metabolism of supplemental cholesterol through either the retention or loss of the deuterium isotopes. The hydroxylation of cholesterol to 27-hydroxycholesterol by the action of CYP27A1 is of particular interest due to its deficiency in CTX patients (264) which present with juvenile or congenital cataracts. The major downstream metabolite detected in yolks of zebrafish supplemented with d6 lanosterol or d6 cholesterol was d3 27-OHC, demonstrating the three-hydrogen exchange that takes place during the oxidation of carbon 26 which has not been previously shown *in vivo*.

### 7.1.9 General conclusion and future work

As evidenced by the relevant human syndromes (249,261,271), the importance of physiological cholesterol synthesis is significant in the appropriate development of cholesterol-rich tissues and organs such as the brain, the central nervous system, and the lens. Reductions in the amount of synthesised cholesterol can have a broad spectrum of effects ranging from direct cell architecture consequences of lipid-rich organs (319,341,342) through to systemic defects in the development of cilia (316). Through the use of physiologically relevant

cholesterol synthesis inhibitors ranging from the cyclisation of squalene to cholesterol through to the final two steps in cholesterol synthesis of either pathway (317), we have generated a behavioural-physical disease phenotype in the developing zebrafish which includes impairment of the optomotor response due to defects in the vision-perception pathway which are accompanied by physical changes in lens architecture and an increased absorption rate of the maternal yolk supply. The effective decrease of total cholesterol in both whole body samples and isolated lenses, in addition to the accumulation of direct upstream metabolites evidences the efficacy of these pharmacological inhibitors. Though appropriate sterol supplementation only restores the larval yolk supply, we have evidenced that supplemental sterols including cholesterol and lanosterol are targeted to and accumulated in the lens following its encapsulation.

Long-term observations are required to both evaluate the retention or metabolism of supplemental sterols in the lens but also to characterise whether the defects conferred by cholesterol synthesis inhibition are reversible. Data from human studies has indicated that extralenticular phenotypes can be improved by early intervention (268,273), but the unique structure of the lens and distinct lack of lipid turnover (48,80) pose a potential barrier to pharmacological interventions aiming to repair LFC membranes. It is essential that the localisation of accumulated supplemental sterols is characterised in the lens, ideally through MALDI-based imaging (213), to understand the structural interactions between native lens lipids and exogenously introduced lipids due to the unique and specific lipidome of lens membranes (76).

Beyond the lens-specific structure function studies of lipid incorporation, a whole-body approach also needs to be undertaken to evaluate the effect of cholesterol synthesis inhibition and sterol supplementation on the regulation of relevant signalling pathways. As free cholesterol is an important factor in Sonic Hedgehog (SHH) signalling by mediating the paracrine trafficking of N-terminal SHH (343), an RNA-seq analysis of the major sterol transporters in organs which participate in the optomotor response such as the lens, the retina, and the brain in addition to the YSL and the inner ear would provide targets for further protein-based studies. Though cholesterol-reducing drugs such as statins have limited deleterious effects (257,258) in light of the positive outcomes they provide, long-term use has been associated with increased incidence of cataract (253–255) and therefore it is imperative that we have a better understanding of the metabolic aspects of cholesterol synthesis inhibition before we move to using sterols and oxysterols as a pharmacological intervention.

## 7.2 The sedimentation of lens material is dependent on the protein and lipid content of lens fractions

Lipid-protein interactions have been shown to be crucial to lens health, through relationships such as the targeting of membrane proteins AQP0 and Cx50 to cholesterol-rich and phospholipid-rich domains respectively (91,171,226), but are also instrumental in the ageing of the lens and the development of cataract through the increased binding of high molecular weight α-crystallin aggregates to membrane lipids (191,232). Therefore, the framework for lipid-protein interactions both in terms of endogenous membrane lipids and exogenously introduced free lipids already exists in the lens and can potentially be a key to approaching the pharmacological treatment of cataract. Studies using oxysterols to resolve opacities in cataractous lenses have relied on the stabilisation of α-crystallin aggregates via sterol supplementation (249,251,269,299), though these interventions are in vain should off-target interactions with other structural proteins or lipid elements occur in a manner which fundamentally alters lens homeostasis. As discussed in section 7.1.8, supplemental sterols including lanosterol and cholesterol are transported and accumulate *in vivo* in the lens; subsequently, it is essential to characterise the effect of sterol supplementation on the lipid bilayer and its proteins.

### 7.2.1 The protein content of isolated lens membranes influences its sedimentation pattern

The serial fractionation by centrifugation of bovine lens lipid membranes aims to yield a terminal fraction which contains the lipid bilayer, transmembrane proteins, and any residual proteins that are covalently bound to the bilayer. Initial studies of this fraction showed that the membrane material forms clear vesicles of various sizes (344), with the major enriched protein being AQP0. The protein profile of this integral membrane protein fraction is relatively bare as compared to the protein-enriched fraction retrieved prior to incubation with 8M urea for both cortex and nucleus-derived membranes, as seen in Figures 5.1 and 5.2.

As each serial fraction is collected from sedimented material at 17640 x g, material was stored long term under the assumption that the high protein content pellet contained water-insoluble protein (344). In contrast, and as seen in Figure 5.9, we identified a temporally soluble protein fraction derived from the original pellet which did not sediment under further centrifugation at the same force. To further study this phenomenon, high protein content membranes were serially centrifuged at 200k x g and the soluble fraction was further centrifuged at 400k x g as seen in Figure 5.3. A persistently non-sedimenting protein fraction was identified and analysed for lipid and protein content.

As per previous reports (42,72,74,76), the sedimented fraction at 200k x g showed a significant enrichment of cholesterol as compared to the supernatant, with the ratio of enrichment increased for the nuclear fraction as seen in Figure 5.4. Though significantly lower in concentration, phosphatidylcholine was also enriched in the sedimented fractions. Minimal amounts of lipid material were also identified in the supernatants of these high-protein content fractions, presenting the possibility that not all bilayer material is irreversibly water-insoluble despite it being selected for as an insoluble fraction.

### 7.2.2 Lens proteins are associated with distinct lipid fractions

The distribution of major lens proteins, including transmembrane, cytoskeletal, and crystallin proteins were analysed as seen in Figures 5.5 to 5.8. Transmembrane proteins AQP0, Cx50, and CAV-1 were identified in the cholesterol-rich pellet which contained the majority of lipid bilayer, while trace amounts of AQP0 were detected in the 200k x g supernatant, as seen in Figure 5.5. A different sedimentation profile was identified for cytoskeletal proteins, with vimentin found in all pellets and supernatants of cortex fractions, while phosphorylated vimentin was only identified in the initial 200k x g pellet sample, as seen in Figure 5.6. Similar to vimentin, F-actin was equally distributed in all cortex fractions. The beaded filament proteins BFSP1 and BFSP2 were detected in all fractions as seen in Figure 5.7, though the molecular weight of the detected protein in each sample varied significantly. Lasty, αB-crystallin was enriched in all fractions while γC-crystallin was present in all fractions but greatly enriched in nucleus-derived membranes as seen in Figure 5.8.

This sedimentation pattern is not surprising considering the known localisation and interactions of the examined proteins. Transmembrane proteins AQP0, Cx50, and CAV-1 are expected to sediment with the majority of the lipid bilayer material, as no detergent treatment or enzymatic digestion was performed to release them from their lipid matrix. As per the manufacturer's data validation sheet, the antibody used against AQP0 (B-11, sc-376445, Santa Cruz Biotechnology) detects a 43 amino acid sequence in the C-terminus of the protein which is cleaved in the lens nucleus (157,216) and as such no protein was detected in these fractions. As a transmembrane protein, it would be expected that AQP0 would sediment with the membrane bilayer; the trace amount of monomer detected in the soluble supernatant of the 200k x g centrifugation seen in Figure 5.5 could be a part of smaller, non-sedimenting vesicles which are further discussed in section 7.2.3. Since no distinction was made to isolate DRM fractions from the initial pellet, it is unsurprising that Cx50 and CAV-1 also sedimented with the lipid bilayer (72,189,221,225,226).

The distribution of F-actin does not provide much insight on why seemingly insoluble protein does not sediment without additional structural characterisation of the vesicles through electron microscopy and immunolabelling. The majority of the cytoskeleton is removed during the first step of the fractionation in a soluble complex called the plasma membrane cytoskeleton complex (PMCC) (345–347), and as such the actin detected in Figure 5.6 may be a full length (~40kDa) fraction of the protein which has sedimented due to its strong association with the lens membrane. The detection of vimentin in the cortex-derived membrane samples was also expected, as vimentin transitions from a membrane-associated to a beaded filament-associated protein in the remodelling zone of the lens cortex as part of LFC maturation (118,128). Equally, the presence of phosphovimentin in the 200k x g pellet needs to be further analysed with respect to the assembly state of the protein.

The sedimentation profile of the beaded filament proteins BFSP1 and BFSP2 seen in Figure 5.7 reveals a rich multitude of different fragments which are differentially enriched between sedimented and non-sedimented fractions. The 200k x g cortex fraction for both proteins was found to contain all detected forms. The wide variety of both fragments and higher molecular weight bands across pellets and supernatants of cortical and nuclear membrane samples demonstrates the multiple proteolytic post-translational modifications that BFSP1 undergoes (129,130) during the differentiation of LFC and during physiological ageing. The cleavage of BFSP1 into an N-terminal beaded filament-associated and a C-terminal membrane-associated fragment (130), in addition to the interactions of BFSP1 with AQP0 (131,132), BFSP2 (115), tropomodulin (133), vimentin (115,348), and α-crystallin (118) offer insight as to the complex sedimentation profile of the beaded filament proteins seen in Figure 5.7.

Finally, the ubiquitous distribution of αB-crystallin and the nuclear enrichment of γC-crystallin seen in Figure 5.8 are a confirmation of their localisation and function in the lens and their association with other lens proteins, including crystallins (287), cytoskeletal proteins (111,118,129,346), integral membrane proteins (234), and the lipid bilayer itself (195).

### 7.2.3 A cortex-enriched specific lens protein fraction transiently sediments and is partially influenced by lanosterol or cholesterol co-incubation

Both cortex and nucleus-derived high protein content membranes showed a time-dependent release of a specific soluble protein fraction which contained a subset of the total proteins in the pellet, seen in Figure 5.9. This effect was considerably enriched in the cortical samples, with the first instance of soluble protein becoming apparent at 30 minutes post-centrifugation. The co-incubation of these membranes with lanosterol or cholesterol had no discernible effect on the solubility pattern as characterised by SDS-PAGE, seen in Figured 5.10 and 5.11.

In accordance with the data described in section 7.2.2, the temporal solubility profile of major lens proteins was characterised in high protein content membranes and compared to the equivalent samples co-incubated with lanosterol or cholesterol.

Lanosterol was found to suppress the release of an AQP0 dimer, which was detected from 24 hours post incubation in the control and cholesterol co-incubates samples, seen in Figure 5.12. In contrast, all Cx50 polypeptides remained in the pellet as seen in Figure 5.13. Co-incubation with lanosterol decreased the amount of soluble vimentin at 72 hours and 10 days, seen in Figures 5.14 and 5.15, while both lanosterol and cholesterol promoted the release of soluble BFSP1 from 30 minutes post-incubation, as seen in Figures 5.16 and 5.17. Finally, neither sterol influenced the solubility of αB-crystallin, as seen in Figures 5.18 and 5.19.

The release of a soluble protein fraction from an otherwise sedimented sample could arise from the proteolytic degradation of the polypeptides, though no evidence was found in these supernatants to support this since EDTA inclusion would eliminate the action of lens calpains. Instead, the release of proteins appears to occur in a specific series with an αB-crystallin fraction becoming soluble first, which is then followed by vimentin, AQP0, and finally BFSP1 under control conditions. As α-crystallin is the most abundant protein in the lens, and the most enriched protein in this fraction, it is not unreasonable to expect a certain retention of its chaperone activity *in vitro*, particularly considering that α-crystallin is an ATP-independent chaperone protein (71,297). In addition, at near-physiological concentrations α-crystallin solutions form non-Newtonian fluids (349) which could alter the viscosity of protein mixtures during centrifugation. Further discussion of these effects in the context of transient protein sedimentation can be found in section 7.3.

### 7.2.4 Lanosterol or cholesterol supplementation do not alter the sedimentation profile of endogenous lens sterols

The variable effect of sterol co-incubation on different lens proteins cannot be interpreted as a simple modulation of the chaperone activity of α-crystallin. The enrichment of membrane fragments with supplemental lanosterol or cholesterol could influence the stability of these lipid bilayers, and as such the endogenous levels of cholesterol and lanosterol were analysed for each timepoint.

Neither the co-incubation with d6 lanosterol nor d6 cholesterol showed any effect on the distribution of endogenous cholesterol between the pellet and supernatant at 30 minutes to 10 days post-centrifugation, as seen in Figure 5.19. Similarly, no effect was observed on the distribution of endogenous lens lanosterol, as seen in Figure 5.21. The supplemental deuterated cholesterol was detected in both the pellets and supernatants of cortex and

nucleus-derived membranes, with the majority targeted to the sedimented fractions. Minor fluctuations in d6 cholesterol levels were detected, as seen in Figure 5.20, while no d6 lanosterol was reliably detected as seen in Figure 5.22.

The 10,000-fold increase in signal intensity between the maximum value of endogenous cholesterol and the minimum threshold for the reliable detection of the supplemental deuterated sterols is a major contributing factor in the dampening of detection sensitivity at near-noise threshold analyte peaks. We have previously demonstrated that we can reliably detect trace amounts of deuterated lanosterol, as seen in section 4.6.3, and as such the absence of d6 lanosterol from the membrane fractions discussed in this section is most likely due to experimental error arising from the use of the same sample to analyse both endogenous cholesterol and supplemental lanosterol.

## 7.3 The solubility of α-crystallin influences the sedimentation of lens material

The loss of chaperone function and the transition of α-crystallin to the water-insoluble fraction of the lens proteome are crucial events in the early stages of cataractogenesis. The unique architecture of the lens, including the age-related development of a diffusion barrier (57,211,290) and the increased incidence of protein cross-linking (218,284) coupled with the depletion of soluble α-crystallin (191) contribute to the acceleration of cataractogenic load (48). A major role for a-crystallin as a chaperone is to mitigate the effects of oxidative damage on other lens proteins, as discussed in section 1.3.1, and therefore it is understandable that the major attempts at a pharmacological treatment or prevention of cataract target its chaperone function (249,251,302).

The temporal release of a soluble protein fraction enriched in αB-crystallin described in chapter 5 provides an excellent platform to examine whether this is an α-crystallin mediated effect, and whether it can be modulated by the addition of crosslinking agents or sterols.

### 7.3.1 The temporal release of a soluble protein fraction from high protein content lens membranes is temperature-dependent, and is absent in cataractous lenses

The marked absence of temporally soluble material in age-matched bovine lenses presenting with nuclear cataract was a catalyst in confirming that the observed effect was not due to proteolytic degradation of proteins.

The analysis of the total protein concentration of the pellet and supernatant at each timepoint from 30 minutes to 72 hours post-centrifugation revealed that the soluble protein in clear

lenses exceeded the amount of sedimented protein by the end of the study period in cortex-derived membranes, while the amount of soluble proteins in nucleus-derived membranes increased but did not exceed the equivalent sedimented protein, as seen in Figure 6.1. The loss of this effect in both cortical and nuclear fractions derived from cataractous lenses led to the hypothesis that this event is an extension of some physiological function which is active in clear lenses. The lack of soluble cortical protein from age-matched lenses with nuclear cataract, seen in Figure 6.1, further supports this notion: even though the cortex of these lenses was optically clear, it is evident that significant alterations have already occurred on the macromolecular level which influence protein behaviour *in vitro*.

To replicate this reduction in soluble material, high protein content membranes from clear lenses were incubated at a range of different temperatures including and exceeding the optimal chaperone range for α-crystallin (193,351–353). The temporal release of soluble material was suppressed in both cortical and nuclear membranes at 4$^{O}$C, with a minimal constant concentration of soluble protein found at all timepoints. At 25$^{O}$C and 42$^{O}$C, the solubilisation effect seen at 37$^{O}$C and discussed in chapter 5 was retained in cortical membranes but is suppressed in nuclear membranes at 42$^{O}$C where a constant amount of soluble protein was found. Finally, at 50$^{O}$C no soluble protein was detected in nuclear membranes, while a constant but minimised concentration was found in cortical membranes as seen in Figure 5.2. The limited macromolecule turnover in the lens (48) and the continuous internalisation of old LFCs results in the retention of proteins that are as old as the cells found in the nucleus, and as such the increased thermal aggregation and reduced chaperone function of α-crystallin found in nucleus-derived membranes is not an entirely unexpected observation. The optimal chaperone temperature of α-crystallin *in vitro* is approximately 40$^{O}$C (351,352), although evidence and the physiological relevance of the protein support a wide range of physiological function as seen in Figures 6.1 and 6.2.

### 7.3.2 The temporal release of a soluble protein fraction for high protein content lens membranes can be inhibited via the use of protease inhibitors

The distinction between a clear lens and a cataractous lens-associated protein sedimentation pattern offers the opportunity to study this solubilisation event through the modulation of protein-protein interactions, as mentioned in section 7.3. As thermal stress was shown to eliminate the temporal aspect of this effect in cortical membranes and to eliminate the soluble protein altogether in nuclear membranes outside the range of optimal α-crystallin chaperone function, we investigated whether the use of cysteine, serine, and threonine (208,218) protease inhibitors would replicate the sedimentation profile seen in cataractous and thermal stress samples.

The use of a commercially available protease inhibitor cocktail (Roche cOmplete Mini Protease Inhibitor Cocktail, Sigma-Aldrich) significantly reduced the amount of soluble protein and delayed its temporal release in cortex and nucleus-derived membranes, as seen in Figures 6.3 and 6.4, when compared to the EDTA-only buffers used in all other experiments.

Since the list of protease inhibitors included in the commercial cocktail preparation, cysteine, serine, and threonine protease inhibitors were selected for further analysis due to the prevalence of oxidative modifications on these residues in proteins from cataractous lenses (208,218). The use of iodoacetamide had no discernible effect on the sedimentation of cortical membranes, though it did reduce the amount of soluble protein in nuclear membranes while maintaining the temporal aspect of the solubilisation, as seen in Figure 6.4.

Both E-64 and leupeptin have previously been used as calpain inhibitors and to prevent the proteolysis of crystallins *in vivo* and *in vitro*, though their *in vitro* efficacy was shown to be considerably better due to difficulties associated with the penetrability of the lens by the compounds (354). E-64 is an irreversible cysteine peptidase inhibitor, and leupeptin is a competitive cysteine, serine, and threonine peptidase inhibitor. The use of both compounds would allow us to identify whether the inhibition of protein solubilisation in treated membranes is a cysteine-only mediated effect.

Though both inhibitors were successful in reducing the amount of temporally released soluble protein in cortical fractions, leupeptin was less efficient at all concentrations tested as compared to E-64, with leupeptin-treated membranes showing a delayed release of material at 72 hours post-incubation. In contrast, E-64 eliminated all soluble protein in samples treated with 1 µM or 10 µM while a minimal release of soluble protein was observed at 72 hours in the 100 µM-treated samples, as seen in Figure 6.5. This trend was replicated in nuclear membranes, as seen in Figure 6.6, though both E-64 and leupeptin were less efficient at preventing the temporal release of soluble protein as compared to the equivalent cortex samples.

High molecular weight aggregates are a feature of both aged and cataractous lenses (59,82,111,218), though a dramatic increase in the levels of thiol oxidation is associated with the onset of cataract (208,218). The application of cysteine modifying reagents such as E-64 to membrane fractions containing a variety of lens proteins should irreversibly bind a variety of thiols across different proteins. Consequently, an analysis of all peptides via mass spectrometry is essential in identifying bound E-64 to generate a map of modified thiols. This would permit the identification of vulnerable peptides and would address the role of α-crystallin in altering the sedimentation profile of high protein content membranes.

### 7.3.3 Lenticular α-crystallin solutions have a variable effect on the sedimentation of integral membrane protein membrane samples

Low protein content membranes are not subjected to the temporal solubilisation effect seen in high protein content membranes, as all material remains in the water insoluble fraction during long term storage. As mentioned previously, these fractions contain the lipid bilayer, integral lens membrane proteins, and limited amounts of α-crystallin which is covalently bound to the membrane. Due to their stable sedimentation profile, integral protein membrane fractions were used to examine the effect of supplemental soluble α-crystallin on the temporal solubility of the associated proteins.

Soluble bovine α-crystallin was sourced from a commercial supplier (11046-99-4, Sigma-Aldrich), from the first soluble fraction released from high protein content membranes as seen in chapter 5, and from in-house size exclusion chromatography-purified samples. A range of concentrations from 15 $\mu gmL^{-1}$ to 120 $\mu gmL^{-1}$ were co-incubated with integral protein membranes at $37^{O}C$, producing a variable effect on the sedimentation profile of the native lens proteins.

No soluble protein was detected in samples co-incubated with commercial α-crystallin between 15 and 60 $\mu gmL^{-1}$, while a constant concentration of soluble protein exceeding that of the supplemented α-crystallin was seen from 30 minutes to 72 hours post-incubation in the 120 $\mu gmL^{-1}$ sample, as seen in Figures 5.7 to 5.10. Native soluble α-crystallin supplementation resulted in the release of a constant soluble fraction in all concentrations with the exception of 60 $\mu gmL^{-1}$ where the amount of soluble protein exceeded the amount of sedimented protein at 30 minutes prior to inverting by 12 hours post-incubation. Size-exclusion chromatography-isolated α-crystallin had a drastically different effect on the sedimentation profile of the membrane proteins, with the amount of soluble protein exceeding the amount of sedimented protein at 15 to 60 $\mu gmL^{-1}$ and remaining constant throughout the timepoints examined. At 120$\mu gmL^{-1}$, this ratio was inverted though the amount of soluble protein still exceeded the amount of supplemental α-crystallin.

Evidently, not all α-crystallin is made equal. A comprehensive analysis of the assembly state, ratio of αA- to αB-crystallin and post-translational modifications of the three protein sources is required to better understand the variable effects seen in Figures 5.7 to 5.10. Additionally, an assessment of the chaperone activity of each crystallin source should also be performed on a model substrate such as insulin (355) to understand whether the variation in response seen in section 6.3.1 is purely due to the chaperone activity of α-crystallin.

Lens α-crystallin solutions have been shown to covalently bind to model and native lipid membranes (191,194,195), a finding which has been replicated via the use of commercial α-crystallin in Figures 5.7 to 5.9. The release of excess protein from the integral protein membrane fractions via the supplementation of soluble α-crystallin further supports the hypothesis that this is a chaperone activity-mediated effect. In combination with the identification of cholesterol and phosphotidylcholine in the supernatants of 200k x g centrifugations presented in section 5.2.1, it is possible that α-crystallin mediates the remodelling of membrane fragments through the chaperone buffering of lens proteins. This hypothesis is further supported by the identification of the cytoskeletal proteins vimentin and BFSP1 in addition to the transmembrane protein AQP0 in temporally soluble fractions from high protein content membranes, as discussed in section 7.2.3. However, further analysis is required to understand whether an exchange of material occurs between the supplemental α-crystallin and the native sedimented proteome which can be achieved by incorporating fluorescent tags on selected proteins.

### 7.3.4 Lenticular α-crystallin solutions influence the sedimentation of high protein content membranes treated with protease inhibitors and partially restore the temporal release of material from leupeptin and E-64-treated high protein content membranes

To further understand the role of α-crystallin in modifying the sedimentation profile of membrane fractions, exogenous α-crystallin from three sources was introduced to insoluble membrane fractions which had been treated with the commercial inhibitor cocktail, E-64, and leupeptin.

The effect of commercial and native soluble α-crystallin supplementation on inhibitor cocktail-treated membranes was identical to that seen with integral protein membranes, as discussed in section 7.3.3. in contrast, the co-incubation with SEC-isolated α-crystallin resulted in an immediate release of excess soluble protein for 15 and 30 $\mu gmL^{-1}$ before an inversion of the ratio of soluble to sedimented protein after 24 hours post-incubation, as seen in Figures 5.11 and 5.12. At 60 $\mu gmL^{-1}$ the amount of soluble and sedimented protein was equal after 2 hours, whereas the addition of 120 $\mu gmL^{-1}$ α-crystallin produced the same effect seen in the integral protein membrane samples seen in Figure 5.9.

High protein content membranes treated with E-64 or leupeptin were co-incubated with 60 $\mu gmL^{-1}$ soluble α-crystallin, which restored the temporal release of soluble protein seen in control samples for all α-crystallin sources tested as seen in Figures 5.15 and 5.16. The commercial α-crystallin solution produced the closest sedimentation profile to the control

membranes, with no soluble protein being detected at 30 minutes post-incubation and an almost linear release of material seen thereafter. Native soluble and SEC-isolated α-crystallin supplementation resulted in a release of excess protein by 30 minutes, but the trend of increasing soluble material was retained in the subsequent timepoints. In all samples, the rate of release was dampened as compared to control cortical membranes as the concentration of soluble protein did not exceed the concentration of sedimented protein at 72 hours post-incubation.

The restoration of the temporal increase in soluble protein, albeit at a decreased rate, from membranes which had been rendered insoluble confirms that α-crystallin influences the sedimentation of high protein content membranes through its native chaperone action. This finding is not ground breaking *per se*, it does however support the hypothesis that should the chaperone potential of α-crystallin be restored in cataractous lenses the opacities could be resolved (249,251,299,302).

### 7.3.5 Sterol and oxysterol sensitisation of α-crystallin solutions has a variable effect on the sedimentation profile of high protein content membranes treated with leupeptin and E-64

The use of oxysterols as a pharmacological treatment for cataract has produced mixed results as far as the translation from *in vitro* and *in vivo* animal models to human *in vitro* samples are concerned (249,251,299,300). Data indicate that oxysterols restore the native conformation of aggregated mutant α-crystallin (299) and resolve native α-crystallin aggregates *in vitro* (249,251). From these reports, we analysed the effect of cholesterol, 25-hydroxycholesterol, and lanosterol sensitisation on the presumptive chaperone activity of supplemental α-crystallin discussed in section 7.3.4.

The sensitisation of native soluble α-crystallin with cholesterol accelerated the release of soluble protein from inhibitor cocktail-treated and E-64 treated high protein content membranes, as seen in Figures 6.17 and 6.18, with 1 μM cholesterol also restoring the inversion in the ratio of soluble to sedimented protein at 72 hours observed in control membranes. The sensitisation of native soluble α-crystallin with 25-OHC or lanosterol also accelerated the release of soluble protein to under 30 minutes, with no inversion of the ratio of soluble to sedimented protein becoming apparent as seen in Figures 5.19 to 5.22.

This dramatic increase in the rate of release of soluble material from sedimented membranes as compared to the non-sensitised equivalent samples is a clear indicator that the addition of sterols does have an impact on the chaperone activity of α-crystallin at minimum. However, as sensitised α-crystallin is introduced to the sedimented membranes with the co-incubated

sterols it is not possible to specify whether this effect could also be attributed to protein-sterol interactions between free sterols and the native lens proteins from the membranes themselves. The data discussed in section 7.2.3 show that the co-incubation with sterols influences the sedimentation profile of specific lens proteins in untreated high protein content membranes, therefore it is not unreasonable to expect a similar set of interactions in these samples. Regardless, further analysis is required to confirm this ranging from the simple co-incubation of insoluble membranes with cholesterol, 25-OHC, and lanosterol through to fully characterising how oxysterols enhance the chaperone activity of α-crystallin.

### 7.3.6 General conclusions and future work

The association of transmembrane proteins with the lipid-enriched, sedimenting cortex and nucleus fractions demonstrates the maintenance of the bilayer structure in high protein content lens membranes in solution. The variable sedimentation profiles of the cytoskeletal and beaded filament proteins require further characterisation via electron microscopy to be better understood, though a simple hypothesis states that the preferential associations between lens lipids and lens proteins would be replicated *in vitro* in native membrane solutions.

As mentioned in section 7.2.3, it is not unreasonable to expect that lenticular α-crystallin retains part of its chaperone function *in vivo*. Furthermore, α-crystallin solutions form non-Newtonian fluids at near-physiological lens concentrations with a marked decrease in viscosity seen as shear rate increases (349). A hypothesis to be tested concerning the sedimentation of soluble proteins and their time-dependent emergence into solution has the behaviour of α-crystallin at its core: at high concentrations, such as the ones encountered in lens lysates, a less viscous solution will allow smaller buoyant membrane vesicles to sediment more efficiently and will produce a pellet with a mixture of water-insoluble and water-soluble material. Each serial centrifugation and discarding of the supernatant results in the reduction of levels of α-crystallin and thus a gradual increase in viscosity of the solution containing the homogenised pellet. The effect of this gradual increase in viscosity, and thus a continuous elimination of supernatant material, can be seen in the serial centrifugation and clearance of high protein content membranes described in section 5.3. As α-crystallin retains its chaperone function *in vitro* (121,299,328,350), it is possible to consider that stabilising interactions take place between α-crystallin and its major target proteins such as the beaded intermediate filaments (118,129). A chaperone-mediated stabilisation of vimentin and BFSP1 could be behind the effect seen in Figures 5.14 to 5.16; similarly, α-crystallin has been shown to stabilise AQP0 from thermal aggregation *in vitro* (234) therefore the minor solubilisation seen in Figure 5.12 could be an α-crystallin-mediated effect. The temporal emergence of these

proteins, with α-crystallin appearing first in the soluble fraction, further supports the hypothesis that a chaperone-dependent effect modulates the sedimentation and solubilisation of lens proteins *in vitro*.

Extensive work is required to characterise the mechanism behind these events, ranging from simple observational analysis of these protein solutions via electron microscopy through to the construction of model lens vesicles which can be used to examine the effect of α-crystallin concentration on the sedimentation and solubilisation of high protein content lens fractions.

The finding that protein derived from the clear cortex and the opaque nucleus of cataractous bovine lenses does not exhibit the temporal release of soluble material demonstrates that the macromolecular events underpinning cataractogenesis have already occurred in seemingly transparent LFCs. The replication of this effect through thermal stress and more efficiently through the crosslinking of free thiols with E-64 further support the hypothesis that thiol oxidation is a significant event in cataractogenesis (208,211,218). Finally, the restoration of temporal solubility in an α-crystallin dependent manner in addition to the oxysterol-mediated enhancement of this chaperone action highlight the significance of physiological α-crystallin in the maintenance of lens transparency and add credence to the use of oxysterols as a pharmacotherapy against cataract, or even as a prophylactic supplement.

The variable effect of α-crystallin from different sources and different isolation techniques needs to be further investigated to understand the factors contributing to this finding. An extensive characterisation of the commercial, native soluble, and SEC-isolated α-crystallin solutions has to include a full mapping of post-translational modifications, the ratio of αA- to αB-crystallin, and the multimer assembly state which these oligomers preferentially adopt as the chaperone activity of α-crystallin is greatly influenced by all three factors (99,207,356–358). Furthermore, a structural characterisation of the released soluble material is also essential, as it will shed light on whether these membrane fragments and protein form organised vesicles. A preservation of vesicle structure mimicking LFC architecture would illustrate that these protein-protein and lipid-protein interactions do not take place in a vacuum, and consequently any alteration of these components whether by the introduction of exogenous proteins or lipids should take these effects into consideration.

# 8 Chapter 8: Conclusion

The pharmacological treatment of cataract is no longer a pipe dream, as a result of recent progress made in understanding the effect of oxysterols on the chaperone activity of α-crystallin (249,251,299,300). The physiological architecture of the lens, from the cholesterol-rich lipid membranes of LFCs to the antioxidant role of α-crystallin, provides the framework for successful cataract prevention and treatment.

The presence of congenital and juvenile cataracts in systemic cholesterol synthesis syndromes highlights the significance of membrane integrity in developing and maintaining the lens circulation (149) and hypoxic environment (307) required for a reduced oxidative load, in addition to housing the key structural proteins which regulate LFC maturation (89,104,226). The age-related enrichment of membrane cholesterol (73,259,307) and the lifespan-dependent selection for saturated lipids such as sphingomyelins over the oxidation-sensitive glycerolipids (21,77) evidence the essential function of membrane lipid composition in the maintenance of lens transparency. Equally, the dramatic increase in thiol oxidation (208,218) and transition of α-crystallin to the water insoluble protein fraction (82) of the lens, coupled with the increased membrane binding of α-crystallin aggregates to the lipid bilayer (191) illustrate the essential nature of the chaperone activity of α-crystallin in the context of cataractogenic load (48) and cataractogenesis. Together, these factors outline the two essential parameters in the discovery of a successful pharmacotherapy for cataract, namely compatibility with the membrane lipid composition and preservation of the chaperone activity of α-crystallin.

We have found that the partial inhibition of cholesterol synthesis in the developing zebrafish negatively affect the optomotor response due to a reduction in the visual acuity of the larvae, while an accelerated consumption of the maternal yolk lipids accompanies a proportionate decrease in body size. The height of LECs is also decreased by the reduction in cholesterol content of the lens, which could have deleterious effect on the differentiation and maturation of secondary LFCs derived from these progenitor cells.

We have also identified a transiently sedimenting protein fraction in bovine cortical and nuclear LFC membranes which contains cholesterol and phosphatidylcholine, and the proteins AQP0, vimentin, BFSP1, and αB-crystallin. This release of soluble material is a characteristic of clear lenses and is absent in clear cortical and opaque nuclear fractions from age-matched cataractous lenses. Thermal shock beyond the optimal chaperone activity temperature of α-crystallin eliminates this solubilisation effect, as does the treatment with the irreversible cysteine peptidase inhibitor E-64 mimicking the sedimentation behaviour seen in membranes

derived from cataractous lenses. The introduction of exogenous α-crystallin restores the temporal solubility of these protein fractions, and this effect is enhanced via the sensitisation of α-crystallin with cholesterol and the oxysterols lanosterol and 25-OHC.

These findings highlight the efficacy of chaperone-active α-crystallin as a pharmacological intervention against cataract and as a prophylactic compound against protein aggregation in clear lens fractions of cataractous lenses. This effect is further enhanced by the addition of oxysterols, illustrating the crucial role of the interactions between sterols and α-crystallin in the context of a pharmacological treatment of cataract.

We have demonstrated that exogenously introduced oxysterols can be traced throughout the lens *in vivo,* and that the sensitisation of functional α-crystallin with oxysterols can enhance its ability to temporally solubilise sedimented lens proteins in a cataract-mimicking *in vitro* model. As such, this work provides the foundation to hypothesise that oxysterols can be a bioavailable pharmacotherapy following topical application, and they can participate in enhancing the activity of functional α-crystallin in the presence of an artificially aged lens proteome as seen in Figure 8.1.

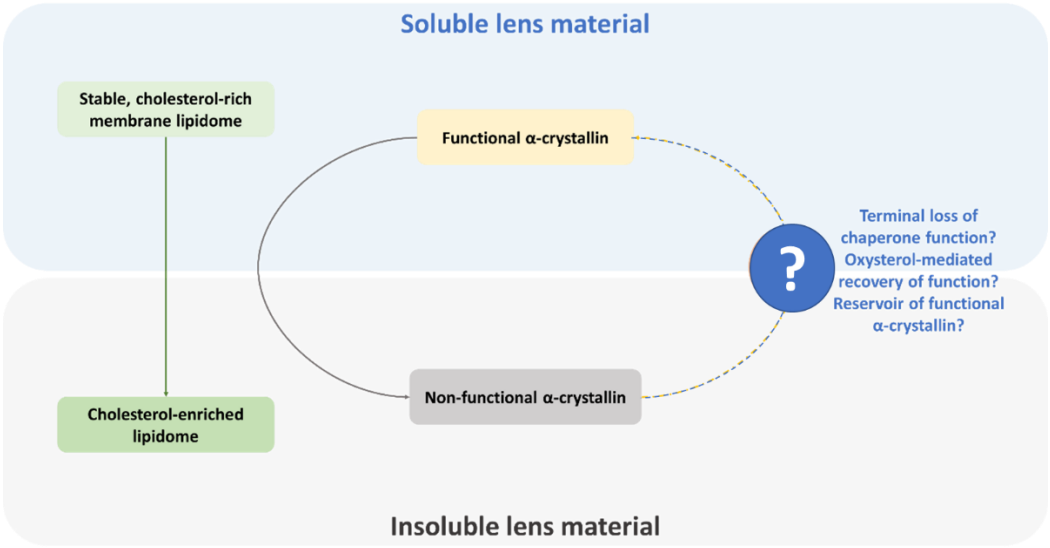


Figure 8.1. The recovery of α-crystallin chaperone function is essential in the reversal of lens lysate sedimentation. A potential role for oxysterols not only in the maintenance of the lens lipidome, but also in the functional activity of α-crystallin is proposed following the observation that oxysterols sensitise exogenous α-crystallin and recover the temporally soluble phenotype of lysates from clear lenses. Although elusive, the role of oxysterols in the pharmacological reversal of cataracts or the extension of the lifespan of functional α-crystallin is plausible, and further work is essential to uncover a potential pharmacological intervention for the global leading cause of blindness.

The development of a safe, effective, and affordable anti-cataractogenic compound is essential in reducing the incidence of blindness worldwide. Currently, the extension and restoration of the chaperone activity of lenticular α-crystallin is the most appealing target for pharmacological intervention; although these data suggest an oxysterol-based treatment could be successful, extensive work is still required to understand the interactions between sterols and the lens proteome before a clinically relevant translation *in vivo* is achieved.

# References


1. Duncan MK, Cvekl A, Kantorow M, Piatigorsky J. Lens Crystallins. In: Lovicu FJ, Robinson ML, editors. Development of the Ocular Lens [Internet]. Cambridge: Cambridge University Press; 2004. p. 119–50. Available from: https://www.cambridge.org/core/books/development-of-the-ocular-lens/lens-crystallins/F93FB3718FBBB68FC576EC88E8F33B36

2. Kalligeraki AA, Isted A, Jarrin M, Uwineza A, Pal R, Saunter CD, et al. Three-dimensional data capture and analysis of intact eye lenses evidences emmetropia-associated changes in epithelial cell organization. Sci Rep [Internet]. 2020;10(1):16898. Available from: https://doi.org/10.1038/s41598-020-73625-9

3. Liu W, Lagutin O V, Mende M, Streit A, Oliver G. Six3 activation of Pax6 expression is essential for mammalian lens induction and specification. EMBO J. 2006;25(22):5383–95.

4. Ashery-Padan R, Marquardt T, Zhou X, Gruss P. Pax6 activity in the lens primordium is required for lens formation and for correct placement of a single retina in the eye. Genes Dev. 2000;14(21):2701–11.

5. Patthey C, Gunhaga L. Signaling pathways regulating ectodermal cell fate choices. Exp Cell Res [Internet]. 2014;321(1):11–6. Available from: http://www.sciencedirect.com/science/article/pii/S0014482713003303

6. Cvekl A, Wang W-L. Retinoic acid signaling in mammalian eye development. Exp Eye Res [Internet]. 2009/05/07. 2009 Sep;89(3):280–91. Available from: https://pubmed.ncbi.nlm.nih.gov/19427305

7. Chauhan BK, Disanza A, Choi S-Y, Faber SC, Lou M, Beggs HE, et al. Cdc42- and IRSp53-dependent contractile filopodia tether presumptive lens and retina to coordinate epithelial invagination. Development [Internet]. 2009 Nov;136(21):3657–67. Available from: https://pubmed.ncbi.nlm.nih.gov/19820184

8. Jarrin M, Pandit T, Gunhaga L. A balance of FGF and BMP signals regulates cell cycle exit and Equarin expression in lens cells. Mol Biol Cell [Internet]. 2012;23(16):3266–74. Available from: http://www.pubmedcentral.nih.gov/articlerender.fcgi?artid=3418319&tool=pmcentrez&rendertype=abstract

9. Bassnett S, Shi Y, Vrensen GFJM. Biological glass: structural determinants of eye lens transparency. Philos Trans R Soc Lond B Biol Sci [Internet]. 2011;366(1568):1250–64. Available from: http://www.pubmedcentral.nih.gov/articlerender.fcgi?artid=3061108&tool=pmcentrez&rendertype=abstract

10. Bassnett S. On the mechanism of organelle degradation in the vertebrate lens. Vol. 88, Experimental Eye Research. 2009. p. 133–9.

11. Bassnett S, Šikić H. The lens growth process. Prog Retin Eye Res. 2017;60:181–200.

12. Augusteyn RC. Growth of the eye lens: I. Weight accumulation in multiple species. Mol Vis [Internet]. 2014 Mar 29;20:410–26. Available from: https://pubmed.ncbi.nlm.nih.gov/24715758

13. Augusteyn RC. Growth of the eye lens: II. Allometric studies. Mol Vis [Internet]. 2014 Mar 30;20:427–40. Available from: https://pubmed.ncbi.nlm.nih.gov/24715759

14. Mohamed A, Augusteyn RC. Human lens weights with increasing age. Mol Vis [Internet]. 2018 Dec 31;24:867–xxx. Available from: https://pubmed.ncbi.nlm.nih.gov/30820139

15. Augusteyn RC. On the contribution of the nucleus and cortex to human lens shape and size. Clin Exp Optom [Internet]. 2017/03/30. 2018 Jan;101(1):64–8. Available from: https://pubmed.ncbi.nlm.nih.gov/28370270

16. Arnold K, Sarkar A, Yram MA, Polo JM, Bronson R, Sengupta S, et al. Sox2(+) adult stem and progenitor cells are important for tissue regeneration and survival of mice. Cell Stem Cell [Internet]. 2011 Oct 4;9(4):317–29. Available from: https://pubmed.ncbi.nlm.nih.gov/21982232

17. Zhou M, Leiberman J, Xu J, Lavker RM. A hierarchy of proliferative cells exists in mouse lens epithelium: implications for lens maintenance. Investig Ophthalmol Vis Sci. 2006;47(7):2997–3003.

18. COLITZ CMH, DAVIDSON MG, McGAHAN MC. Telomerase Activity in Lens Epithelial Cells of Normal and Cataractous Lenses. Exp Eye Res [Internet]. 1999;69(6):641–9. Available from: http://www.sciencedirect.com/science/article/pii/S001448359990739X

19. Andley UP, Rhim JS, Chylack Jr LT, Fleming TP. Propagation and immortalization of human lens epithelial cells in culture. Invest Ophthalmol Vis Sci. 1994 Jun 1;35(7):3094–102.

20. Abe T, Furui S, Sasaki H, Sakamoto Y, Suzuki S, Ishitake T, et al. Quantitative evaluation of light scattering intensities of the crystalline lens for radiation related minimal change in interventional radiologists: A cross-sectional pilot study. J Radiat Res. 2013;54(2):315–21.

21. Huang L, Grami V, Marrero Y, Tang D, Yappert MC, Rasi V, et al. Human lens phospholipid changes with age and cataract. Investig Ophthalmol Vis Sci. 2005;46(5):1682–9.

22. Lovicu FJ, McAvoy JW. Growth factor regulation of lens development. Dev Biol [Internet]. 2005;280(1):1–14. Available from: http://www.sciencedirect.com/science/article/pii/S001216060500045X

23. Petrash JM. Aging and age-related diseases of the ocular lens and vitreous body. Invest Ophthalmol Vis Sci [Internet]. 2013 Dec 13;54(14):ORSF54–9. Available from: https://pubmed.ncbi.nlm.nih.gov/24335070

24. Boswell BA, Overbeek PA, Musil LS. Essential role of BMPs in FGF-induced secondary lens fiber differentiation. Dev Biol [Internet]. 2008/09/18. 2008 Dec 15;324(2):202–12. Available from: https://pubmed.ncbi.nlm.nih.gov/18848538

25. Jia J, Lin M, Zhang L, York JP, Zhang P. The Notch signaling pathway controls the size of the ocular lens by directly suppressing p57Kip2 expression. Mol Cell Biol [Internet]. 2007/08/20. 2007 Oct;27(20):7236–47. Available from: https://pubmed.ncbi.nlm.nih.gov/17709399

26. PIATIGORSKY J. Lens Differentiation in Vertebrates: A Review of Cellular and Molecular Features. Differentiation [Internet]. 1981;19(1):134–53. Available from: http://www.sciencedirect.com/science/article/pii/S0301468111613923

27. Lee A, Morrow JS, Fowler VM. Caspase Remodeling of the Spectrin Membrane Skeleton during Lens Development and Aging. J Biol Chem [Internet]. 2001 Jun 8;276(23):20735–42. Available from: http://www.jbc.org/content/276/23/20735.abstract

28. Cheng C, Nowak RB, Fowler VM. The lens actin filament cytoskeleton: Diverse structures for complex functions. Exp Eye Res. 2017;156:58–71.

29. Fudge DS, McCuaig J V, Van Stralen S, Hess JF, Wang H, Mathias RT, et al. Intermediate filaments regulate tissue size and stiffness in the murine lens. Invest Ophthalmol Vis Sci [Internet]. 2011 Jun 1;52(6):3860–7. Available from: https://pubmed.ncbi.nlm.nih.gov/21345981

30. Bassnett S, Beebe DC. Coincident loss of mitochondria and nuclei during lens fiber cell differentiation. Dev Dyn [Internet]. 1992 Jun 1;194(2):85–93. Available from: https://doi.org/10.1002/aja.1001940202

31. Bassnett S. Mitochondrial dynamics in differentiating fiber cells of the mammalian lens. Curr Eye Res [Internet]. 1992 Jan 1;11(12):1227–32. Available from: https://doi.org/10.3109/02713689208999548

32. Costello MJ, Brennan LA, Basu S, Chauss D, Mohamed A, Gilliland KO, et al. Autophagy and mitophagy participate in ocular lens organelle degradation. Exp Eye Res [Internet]. 2013/09/04. 2013 Nov;116:141–50. Available from: https://pubmed.ncbi.nlm.nih.gov/24012988

33. De Maria A, Shi Y, Kumar NM, Bassnett S. Calpain expression and activity during lens fiber cell differentiation. J Biol Chem [Internet]. 2009/03/06. 2009 May 15;284(20):13542–50. Available from: https://pubmed.ncbi.nlm.nih.gov/19269960

34. Nishimoto S, Kawane K, Watanabe-Fukunaga R, Fukuyama H, Ohsawa Y, Uchiyama Y, et al. Nuclear cataract caused by a lack of DNA degradation in the mouse eye lens. Nature [Internet]. 2003;424(6952):1071–4. Available from: https://doi.org/10.1038/nature01895

35. Nakahara M, Nagasaka A, Koike M, Uchida K, Kawane K, Uchiyama Y, et al. Degradation of nuclear DNA by DNase II-like acid DNase in cortical fiber cells of mouse eye lens. FEBS J [Internet]. 2007 Jun 1;274(12):3055–64. Available from: https://doi.org/10.1111/j.1742-4658.2007.05836.x

36. Ivanov D, Dvoriantchikova G, Pestova A, Nathanson L, Shestopalov VI. Microarray analysis of fiber cell maturation in the lens. FEBS Lett [Internet]. 2005/01/21. 2005 Feb 14;579(5):1213–9. Available from: https://pubmed.ncbi.nlm.nih.gov/15710416

37. Horwitz J. Alpha-crystallin can function as a molecular chaperone. Proc Natl Acad Sci [Internet]. 1992 Nov 1;89(21):10449 LP – 10453. Available from: http://www.pnas.org/content/89/21/10449.abstract

38. Delaye M, Tardieu A. Short-range order of crystallin proteins accounts for eye lens transparency. Nature [Internet]. 1983;302(5907):415–7. Available from: https://doi.org/10.1038/302415a0

39. Tardieu A, Delaye M. Eye Lens Proteins and Transparency: From Light Transmission Theory to Solution X-Ray Structural Analysis. Annu Rev Biophys Biophys Chem [Internet]. 1988 Jun 1;17(1):47–70. Available from: https://doi.org/10.1146/annurev.bb.17.060188.000403

40. Vérétout F, Delaye M, Tardieu A. Molecular basis of eye lens transparency: Osmotic pressure and X-ray analysis of α-crystallin solutions. J Mol Biol [Internet]. 1989;205(4):713–28. Available from: http://www.sciencedirect.com/science/article/pii/0022283689903161

41. Michael R, van Marle J, Vrensen GFJM, van den Berg TJTP. Changes in the refractive index of lens fibre membranes during maturation – impact on lens transparency. Exp Eye Res [Internet]. 2003;77(1):93–9. Available from: http://www.sciencedirect.com/science/article/pii/S0014483503000654

42. Borchman D, Byrdwell WC, Yappert MC. Regional and age-dependent differences in the phospholipid composition of human lens membranes. Invest Ophthalmol Vis Sci. 1994 Oct 1;35(11):3938–42.

43. van den Berg TJ. Light scattering by donor lenses as a function of depth and wavelength. Invest Ophthalmol Vis Sci. 1997 Jun 1;38(7):1321–32.

44. Lynnerup N, Kjeldsen H, Heegaard S, Jacobsen C, Heinemeier J. Radiocarbon Dating of the Human Eye Lens Crystallines Reveal Proteins without Carbon Turnover throughout Life. PLoS One [Internet]. 2008 Jan 30;3(1):e1529. Available from: https://doi.org/10.1371/journal.pone.0001529

45. Augusteyn RC. On the growth and internal structure of the human lens. Exp Eye Res [Internet]. 2010;90(6):643–54. Available from: http://www.sciencedirect.com/science/article/pii/S0014483510000448

46. Hughes JR, Levchenko VA, Blanksby SJ, Mitchell TW, Williams A, Truscott RJW. Correction: No turnover in lens lipids for the entire human lifespan. Elife [Internet]. 2015 Apr 27;4:e08186–e08186. Available from: https://pubmed.ncbi.nlm.nih.gov/25915468

47. Nielsen J, Hedeholm RB, Heinemeier J, Bushnell PG, Christiansen JS, Olsen J, et al. Eye lens radiocarbon reveals centuries of longevity in the Greenland shark (<em>Somniosus microcephalus</em>). Science (80- ) [Internet]. 2016 Aug 12;353(6300):702 LP – 704. Available from: http://science.sciencemag.org/content/353/6300/702.abstract

48. Uwineza A, Kalligeraki AA, Hamada N, Jarrin M, Quinlan RA. Cataractogenic load – A concept to study the contribution of ionizing radiation to accelerated aging in the eye lens. Mutat Res - Rev Mutat Res. 2019;779.

49. Wang Y, Zhang G, Kang L, Guan H. Expression Profiling of DNA Methylation and Transcriptional Repression Associated Genes in Lens Epithelium Cells of Age-Related Cataract. Cell Mol Neurobiol [Internet]. 2017;37(3):537–43. Available from: https://doi.org/10.1007/s10571-016-0393-9

50. Sorte K, Sune P, Bhake A, Shivkumar VB, Gangane N, Basak A. Quantitative assessment of DNA damage directly in lens epithelial cells from senile cataract patients. Mol Vis [Internet]. 2011 Jan 5;17:1–6. Available from: https://pubmed.ncbi.nlm.nih.gov/21224996

51. Huang X-Q, Wang J, Liu J-P, Feng H, Liu W-B, Yan Q, et al. hTERT Extends Proliferative Lifespan and Prevents Oxidative Stress-Induced Apoptosis in Human Lens Epithelial Cells. Invest Ophthalmol Vis Sci [Internet]. 2005 Jul 1;46(7):2503–13. Available from: https://doi.org/10.1167/iovs.05-0154

52. Babizhayev MA, Vishnyakova KS, Yegorov YE. Telomere-dependent senescent phenotype of lens epithelial cells as a biological marker of aging and cataractogenesis: the role of oxidative stress intensity and specific mechanism of phospholipid hydroperoxide toxicity in lens and aqueous. Fundam Clin Pharmacol [Internet]. 2011 Apr 1;25(2):139–62. Available from: https://doi.org/10.1111/j.1472-8206.2010.00829.x

53. Wu JJ, Wu W, Tholozan FM, Saunter CD, Girkin JM, Quinlan RA. A dimensionless ordered pull-through model of the mammalian lens epithelium evidences scaling across species and explains the age-dependent changes in cell density in the human lens. J R Soc Interface. 2015;12(108).

54. Šikić H, Shi Y, Lubura S, Bassnett S. A stochastic model of eye lens growth. J Theor Biol [Internet]. 2015/03/27. 2015 Jul 7;376:15–31. Available from: https://pubmed.ncbi.nlm.nih.gov/25816743

55. Garcí-Porrero JA, Colvée E, Ojeda JL. The mechanisms of cell death and phagocytosis in the early chick lens morphogenesis: A scanning electron microscopy and cytochemical approach. Anat Rec [Internet]. 1984 Jan 1;208(1):123–36. Available from: https://doi.org/10.1002/ar.1092080113

56. Frost LS, Mitchell CH, Boesze-Battaglia K. Autophagy in the eye: implications for ocular cell health. Exp Eye Res. 2014 Jul;124:56–66.

57. SWEENEY MHJ, TRUSCOTT RJW. An Impediment to Glutathione Diffusion in Older Normal Human Lenses: a Possible Precondition for Nuclear Cataract. Exp Eye Res [Internet]. 1998;67(5):587–95. Available from: http://www.sciencedirect.com/science/article/pii/S0014483598905498

58. Minamoto A, Taniguchi H, Yoshitani N, Mukai S, Yokoyama T, Kumagami T, et al. Cataract in atomic bomb survivors. Int J Radiat Biol [Internet]. 2004;80(5):339–45. Available from: http://www.ncbi.nlm.nih.gov/pubmed/15223766

59. Shiels A, Hejtmancik JF. Biology of Inherited Cataracts and Opportunities for Treatment. Annu Rev Vis Sci [Internet]. 2019 Sep 15;5:123–49. Available from: https://pubmed.ncbi.nlm.nih.gov/31525139

60. Chodick G, Sigurdson AJ, Kleinerman RA, Sklar CA, Leisenring W, Mertens AC, et al. The Risk of Cataract among Survivors of Childhood and Adolescent Cancer: A Report from the Childhood Cancer Survivor Study. Radiat Res [Internet]. 2016;185(4):366–74. Available from: http://www.bioone.org/doi/10.1667/RR14276.1%5Cnhttp://www.ncbi.nlm.nih.gov/pubmed/27023263%5Cnhttp://www.pubmedcentral.nih.gov/articlerender.fcgi?artid=PMC4853230

61. Kelley MJ, David LL, Iwasaki N, Wright J, Shearer TR. alpha-Crystallin chaperone activity is reduced by calpain II in vitro and in selenite cataract. J Biol Chem [Internet]. 1993 Sep 5;268(25):18844–9. Available from: http://www.jbc.org/content/268/25/18844.abstract

62. Cumming RG, Mitchell P, Smith W. Diet and cataract: The blue mountains eye study. Ophthalmology [Internet]. 2000 Mar 1;107(3):450–6. Available from: https://doi.org/10.1016/S0161-6420(99)00024-X

63. Litt M, Carrero-Valenzuela R, LaMorticella DM, Schultz DW, Mitchell TN, Kramer P, et al. Autosomal Dominant Cerulean Cataract Is Associated with a Chain Termination Mutation in the Human β-Crystallin Gene CRYBB2. Hum Mol Genet [Internet]. 1997 May 1;6(5):665–8. Available from: https://doi.org/10.1093/hmg/6.5.665

64. Nandrot E, Slingsby C, Basak A, Cherif-Chefchaouni M, Benazzouz B, Hajaji Y, et al. Gamma-D crystallin gene (CRYGD) mutation causes autosomal dominant congenital cerulean cataracts. J Med Genet [Internet]. 2003 Apr;40(4):262–7. Available from: https://pubmed.ncbi.nlm.nih.gov/12676897

65. Gilbert C, Foster A. Childhood blindness in the context of VISION 2020--the right to sight. Bull World Health Organ [Internet]. 2003/07/07. 2001;79(3):227–32. Available from: https://pubmed.ncbi.nlm.nih.gov/11285667

66. Haargaard B, Wohlfahrt J, Rosenberg T, Fledelius HC, Melbye M. Risk Factors for Idiopathic Congenital/Infantile Cataract. Invest Ophthalmol Vis Sci [Internet]. 2005 Sep 1;46(9):3067–73. Available from: https://doi.org/10.1167/iovs.04-0979

67. Haargaard B, Wohlfahrt J, Fledelius HC, Rosenberg T, Melbye M. Incidence and Cumulative Risk of Childhood Cataract in a Cohort of 2.6 Million Danish Children. Invest Ophthalmol Vis Sci [Internet]. 2004 May 1;45(5):1316–20. Available from: https://doi.org/10.1167/iovs.03-0635

68. Hammond CJ, Snieder H, Spector TD, Gilbert CE. Genetic and Environmental Factors in Age-Related Nuclear Cataracts in Monozygotic and Dizygotic Twins. N Engl J Med [Internet]. 2000 Jun 15;342(24):1786–90. Available from: https://doi.org/10.1056/NEJM200006153422404

69. Hammond CJ, Duncan DD, Snieder H, de Lange M, West SK, Spector TD, et al. The Heritability of Age-Related Cortical Cataract: The Twin Eye Study. Invest Ophthalmol Vis Sci. 2001 Mar 1;42(3):601–5.

70. Yonova-Doing E, Forkin ZA, Hysi PG, Williams KM, Spector TD, Gilbert CE, et al. Genetic and Dietary Factors Influencing the Progression of Nuclear Cataract. Ophthalmology [Internet]. 2016/03/23. 2016 Jun;123(6):1237–44. Available from: https://pubmed.ncbi.nlm.nih.gov/27016950

71. Barbazetto IA, Liang J, Chang S, Zheng L, Spector A, Dillon JP. Oxygen tension in the rabbit lens and vitreous before and after vitrectomy. Exp Eye Res. 2004 May;78(5):917–24.

72. Rujoi M, Jin J, Borchman D, Tang D, Yappert MC. Isolation and Lipid Characterization of Cholesterol-Enriched Fractions in Cortical and Nuclear Human Lens Fibers. Invest Ophthalmol Vis Sci [Internet]. 2003 Apr 1;44(4):1634–42. Available from: https://doi.org/10.1167/iovs.02-0786

73. Borchman D, Delamere NA, McCauley LA, Paterson CA. Studies on the distribution of cholesterol, phospholipid, and protein in the human and bovine lens. Lens Eye Toxic Res. 1989;6(4):703–24.

74. Preston Mason R, Tulenko TN, Jacob RF. Direct evidence for cholesterol crystalline domains in biological membranes: role in human pathobiology. Biochim Biophys Acta. 2003 Mar;1610(2):198–207.

75. BORCHMAN D, TANG D. Binding Capacity of α-Crystallin to Bovine Lens Lipids. Exp Eye Res [Internet]. 1996;63(4):407–10. Available from: http://www.sciencedirect.com/science/article/pii/S001448359690130X

76. Borchman D, Lamba OP, Yappert MC. Structural characterization of lipid membranes from clear and cataractous human lenses. Exp Eye Res. 1993 Aug;57(2):199–208.

77. Borchman D, Yappert MC, Afzal M. Lens lipids and maximum lifespan. Exp Eye Res. 2004 Dec;79(6):761–8.

78. Yappert MC, Rujoi M, Borchman D, Vorobyov I, Estrada R. Glycero- versus sphingo-phospholipids: correlations with human and non-human mammalian lens growth. Exp Eye Res. 2003 Jun;76(6):725–34.

79. Paterson CA, Zeng J, Husseini Z, Borchman D, Delamere NA, Garland D, et al. Calcium ATPase activity and membrane structure in clear and cataractous human lenses. Curr Eye Res. 1997 Apr;16(4):333–8.

80. Hughes JR, Deeley JM, Blanksby SJ, Leisch F, Ellis SR, Truscott RJW, et al. Instability of the cellular lipidome with age. Age (Omaha) [Internet]. 2012;34(4):935–47. Available from: https://doi.org/10.1007/s11357-011-9293-6

81. Deeley JM, Mitchell TW, Wei X, Korth J, Nealon JR, Blanksby SJ, et al. Human lens lipids differ markedly from those of commonly used experimental animals. Biochim Biophys Acta. 2008;1781(6–7):288–98.

82. Pescosolido N, Barbato A, Giannotti R, Komaiha C, Lenarduzzi F. Age-related changes in the kinetics of human lenses: prevention of the cataract. Int J Ophthalmol [Internet]. 2016 Oct 18;9(10):1506–17. Available from: https://pubmed.ncbi.nlm.nih.gov/27803872

83. Subczynski WK, Mainali L, Raguz M, O'Brien WJ. Organization of lipids in fiber-cell plasma membranes of the eye lens. Exp Eye Res [Internet]. 2016/03/14. 2017 Mar;156:79–86. Available from: https://pubmed.ncbi.nlm.nih.gov/26988627

84. Mainali L, Raguz M, O'Brien WJ, Subczynski WK. Properties of membranes derived from the total lipids extracted from the human lens cortex and nucleus. Biochim Biophys Acta - Biomembr. 2013;1828(6):1432–40.

85. Pierscionek B, Bahrami M, Hoshino M, Uesugi K, Regini J, Yagi N. The eye lens: age-related trends and individual variations in refractive index and shape parameters. Oncotarget [Internet]. 2015 Oct 13;6(31):30532–44. Available from: https://pubmed.ncbi.nlm.nih.gov/26416418

86. Cheng C, Parreno J, Nowak RB, Biswas SK, Wang K, Hoshino M, et al. Age-related changes in eye lens biomechanics, morphology, refractive index and transparency. Aging (Albany NY) [Internet]. 2019/12/16. 2019 Dec 16;11(24):12497–531. Available from: https://pubmed.ncbi.nlm.nih.gov/31844034

87. Khago D, Bierma JC, Roskamp KW, Kozlyuk N, Martin RW. Protein refractive index increment is determined by conformation as well as composition. J Phys Condens Matter [Internet]. 2018/10/03. 2018 Oct 31;30(43):435101. Available from: https://pubmed.ncbi.nlm.nih.gov/30280702

88. Bassnett S, Wilmarth PA, David LL. The membrane proteome of the mouse lens fiber cell. Mol Vis. 2009 Nov;15:2448–63.

89. Wang Z, Schey KL. Proteomic Analysis of Lipid Raft-Like Detergent-Resistant Membranes of Lens Fiber Cells. Invest Ophthalmol Vis Sci [Internet]. 2015 Dec;56(13):8349–60. Available from: https://pubmed.ncbi.nlm.nih.gov/26747763

90. Greiling TMS, Houck SA, Clark JI. The zebrafish lens proteome during development and aging. Mol Vis. 2009 Nov;15:2313–25.

91. Wenke JL, McDonald WH, Schey KL. Spatially Directed Proteomics of the Human Lens Outer Cortex Reveals an Intermediate Filament Switch Associated With the Remodeling Zone. Invest Ophthalmol Vis Sci. 2016 Aug;57(10):4108–14.

92. Wang Z, Han J, David LL, Schey KL. Proteomics and phosphoproteomics analysis of human lens fiber cell membranes. Invest Ophthalmol Vis Sci. 2013 Feb;54(2):1135–43.

93. Slingsby C, Wistow GJ, Clark AR. Evolution of crystallins for a role in the vertebrate eye lens. Protein Sci [Internet]. 2013 Apr 1;22(4):367–80. Available from: https://doi.org/10.1002/pro.2229

94. Wistow G, Summers L, Blundell T. Myxococcus xanthus spore coat protein S may have a similar structure to vertebrate lens βγ-crystallins. Nature [Internet]. 1985;315(6022):771–3. Available from: https://doi.org/10.1038/315771a0

95. Wistow G, Wyatt K, David L, Gao C, Bateman O, Bernstein S, et al. γN-crystallin and the evolution of the βγ-crystallin superfamily in vertebrates. FEBS J [Internet]. 2005 May 1;272(9):2276–91. Available from: https://doi.org/10.1111/j.1742-4658.2005.04655.x

96. Suman SK, Mishra A, Ravindra D, Yeramala L, Sharma Y. Evolutionary remodeling of βγ-crystallins for domain stability at cost of Ca2+ binding. J Biol Chem [Internet]. 2011/09/26. 2011 Dec 23;286(51):43891–901. Available from: https://pubmed.ncbi.nlm.nih.gov/21949186

97. Lyon YA, Collier MP, Riggs DL, Degiacomi MT, Benesch JLP, Julian RR. Structural and functional consequences of age-related isomerization in α-crystallins. J Biol Chem [Internet]. 2019 May 10;294(19):7546–55. Available from: http://www.jbc.org/content/294/19/7546.abstract

98. Benesch JLP, Ayoub M, Robinson C V, Aquilina JA. Small Heat Shock Protein Activity Is Regulated by Variable Oligomeric Substructure. J Biol Chem [Internet]. 2008 Oct 17;283(42):28513–7. Available from: http://www.jbc.org/content/283/42/28513.abstract

99. Kaiser CJO, Peters C, Schmid PWN, Stavropoulou M, Zou J, Dahiya V, et al. The structure and oxidation of the eye lens chaperone αA-crystallin. Nat Struct Mol Biol [Internet]. 2019;26(12):1141–50. Available from: https://doi.org/10.1038/s41594-019-0332-9

100. Chiesa R, Gawinowicz-Kolks MA, Kleiman NJ, Spector A. Definition and comparison of the phosphorylation sites of the A and B chains of bovine α-crystallin. Exp Eye Res [Internet]. 1988;46(2):199–208. Available from: http://www.sciencedirect.com/science/article/pii/S0014483588800770

101. Robinson ML, Overbeek PA. Differential expression of alpha A- and alpha B-crystallin during murine ocular development. Invest Ophthalmol Vis Sci. 1996 Oct 1;37(11):2276–84.

102. Iwaki T, Kume-Iwaki A, Liem RKH, Goldman JE. αB-crystallin is expressed in non-lenticular tissues and accumulates in Alexander's disease brain. Cell [Internet]. 1989;57(1):71–8. Available from: http://www.sciencedirect.com/science/article/pii/0092867489901736

103. Srinivasan AN, Nagineni CN, Bhat SP. alpha A-crystallin is expressed in non-ocular tissues. J Biol Chem [Internet]. 1992 Nov 15;267(32):23337–41. Available from: http://www.jbc.org/content/267/32/23337.abstract

104. Gangalum RK, Atanasov IC, Zhou ZH, Bhat SP. αB-Crystallin Is Found in Detergent-resistant Membrane Microdomains and Is Secreted via Exosomes from Human Retinal Pigment Epithelial Cells. J Biol Chem [Internet]. 2011 Feb 4;286(5):3261–9. Available from: http://www.jbc.org/content/286/5/3261.abstract

105. Stromer T, Ehrnsperger M, Gaestel M, Buchner J. Analysis of the Interaction of Small Heat Shock Proteins with Unfolding Proteins. J Biol Chem [Internet]. 2003 May

16;278(20):18015–21. Available from: http://www.jbc.org/content/278/20/18015.abstract

106. Dimauro I, Antonioni A, Mercatelli N, Caporossi D. The role of αB-crystallin in skeletal and cardiac muscle tissues. Cell Stress Chaperones [Internet]. 2017/11/30. 2018 Jul;23(4):491–505. Available from: https://pubmed.ncbi.nlm.nih.gov/29190034

107. Abgar S, Vanhoudt J, Aerts T, Clauwaert J. Study of the Chaperoning Mechanism of Bovine Lens α-Crystallin, a Member of the α-Small Heat Shock Superfamily. Biophys J [Internet]. 2001;80(4):1986–95. Available from: http://www.sciencedirect.com/science/article/pii/S0006349501761681

108. Kappé G, Boelens WC, de Jong WW. Why proteins without an α-crystallin domain should not be included in the human small heat shock protein family HSPB. Cell Stress Chaperones [Internet]. 2010;15(4):457–61. Available from: https://doi.org/10.1007/s12192-009-0155-4

109. Kingsley CN, Brubaker WD, Markovic S, Diehl A, Brindley AJ, Oschkinat H, et al. Preferential and specific binding of human αB-crystallin to a cataract-related variant of γS-crystallin. Structure. 2013 Dec;21(12):2221–7.

110. Acosta-Sampson L, King J. Partially folded aggregation intermediates of human gammaD-, gammaC-, and gammaS-crystallin are recognized and bound by human alphaB-crystallin chaperone. J Mol Biol. 2010 Aug;401(1):134–52.

111. Su S, Liu P, Zhang H, Li Z, Song Z, Zhang L, et al. Proteomic Analysis of Human Age-related Nuclear Cataracts and Normal Lens Nuclei. Invest Ophthalmol Vis Sci [Internet]. 2011 Jun 10;52(7):4182–91. Available from: https://doi.org/10.1167/iovs.10-7094

112. Zhao H, Brown PH, Magone MT, Schuck P. The molecular refractive function of lens γ-crystallins. J Mol Biol [Internet]. 2011 [cited 2017 Jun 14];411(3):680–99. Available from: http://www.sciencedirect.com/science/article/pii/S0022283611006322

113. Lapko VN, Smith DL, Smith JB. Expression of βA2-crystallin in human lenses. Exp Eye Res [Internet]. 2003;77(3):383–5. Available from: http://www.sciencedirect.com/science/article/pii/S0014483503001568

114. Wistow G. The human crystallin gene families. Hum Genomics [Internet]. 2012 Dec 1;6(1):26. Available from: https://pubmed.ncbi.nlm.nih.gov/23199295

115. FitzGerald P, Sun N, Shibata B, Hess JF. Expression of the type VI intermediate filament proteins CP49 and filensin in the mouse lens epithelium. Mol Vis [Internet]. 2016 Aug 6;22:970–89. Available from: https://pubmed.ncbi.nlm.nih.gov/27559293

116. Sandilands A, Prescott AR, Carter JM, Hutcheson AM, Quinlan RA, Richards J, et al. Vimentin and CP49/filensin form distinct networks in the lens which are independently modulated during lens fibre cell differentiation. J Cell Sci. 1995 Apr;108 ( Pt 4:1397–406.

117. Perng M-D, Zhang Q, Quinlan RA. Insights into the beaded filament of the eye lens. Exp Cell Res [Internet]. 2007/04/06. 2007 Jun 10;313(10):2180–8. Available from: https://pubmed.ncbi.nlm.nih.gov/17490642

118. Song S, Landsbury A, Dahm R, Liu Y, Zhang Q, Quinlan RA. Functions of the intermediate filament cytoskeleton in the eye lens. J Clin Invest. 2009 Jul;119(7):1837–48.

119. Ireland ME, Wallace P, Sandilands A, Poosch M, Kasper M, Graw J, et al. Up-regulation

of novel intermediate filament proteins in primary fiber cells: an indicator of all vertebrate lens fiber differentiation? Anat Rec. 2000 Jan;258(1):25–33.

120. Goulielmos G, Gounari F, Remington S, Müller S, Häner M, Aebi U, et al. Filensin and phakinin form a novel type of beaded intermediate filaments and coassemble de novo in cultured cells. J Cell Biol. 1996 Feb;132(4):643–55.

121. Perng MD, Cairns L, van den IJssel P, Prescott A, Hutcheson AM, Quinlan RA. Intermediate filament interactions can be altered by HSP27 and alphaB-crystallin. J Cell Sci [Internet]. 1999 Jul 1;112(13):2099 LP – 2112. Available from: http://jcs.biologists.org/content/112/13/2099.abstract

122. Nicholl ID, Quinlan RA. Chaperone activity of alpha-crystallins modulates intermediate filament assembly. EMBO J [Internet]. 1994;13(4):945–53. Available from: http://europepmc.org/abstract/MED/7906647

123. Alizadeh A, Clark JI, Seeberger T, Hess J, Blankenship T, Spicer A, et al. Targeted genomic deletion of the lens-specific intermediate filament protein CP49. Invest Ophthalmol Vis Sci. 2002 Dec;43(12):3722–7.

124. Sandilands A, Prescott AR, Wegener A, Zoltoski RK, Hutcheson AM, Masaki S, et al. Knockout of the intermediate filament protein CP49 destabilises the lens fibre cell cytoskeleton and decreases lens optical quality, but does not induce cataract. Exp Eye Res. 2003 Mar;76(3):385–91.

125. Conley YP, Erturk D, Keverline A, Mah TS, Keravala A, Barnes LR, et al. A juvenile-onset, progressive cataract locus on chromosome 3q21-q22 is associated with a missense mutation in the beaded filament structural protein-2. Am J Hum Genet. 2000 Apr;66(4):1426–31.

126. Jakobs PM, Hess JF, FitzGerald PG, Kramer P, Weleber RG, Litt M. Autosomal-dominant congenital cataract associated with a deletion mutation in the human beaded filament protein gene BFSP2. Am J Hum Genet. 2000 Apr;66(4):1432–6.

127. Ramachandran RD, Perumalsamy V, Hejtmancik JF. Autosomal recessive juvenile onset cataract associated with mutation in BFSP1. Hum Genet. 2007 May;121(3–4):475–82.

128. Costello MJ, Mohamed A, Gilliland KO, Fowler WC, Johnsen S. Ultrastructural analysis of the human lens fiber cell remodeling zone and the initiation of cellular compaction. Exp Eye Res. 2013 Nov;116:411–8.

129. Su S-P, McArthur JD, Truscott RJW, Aquilina JA. Truncation, cross-linking and interaction of crystallins and intermediate filament proteins in the aging human lens. Biochim Biophys Acta. 2011 May;1814(5):647–56.

130. Sandilands A, Prescott AR, Hutcheson AM, Quinlan RA, Casselman JT, FitzGerald PG. Filensin is proteolytically processed during lens fiber cell differentiation by multiple independent pathways. Eur J Cell Biol. 1995 Jul;67(3):238–53.

131. Tapodi A, Clemens DM, Uwineza A, Jarrin M, Goldberg MW, Thinon E, et al. BFSP1 C-terminal domains released by post-translational processing events can alter significantly the calcium regulation of AQP0 water permeability. Exp Eye Res. 2019 Aug;185:107585.

132. Lindsey Rose KM, Gourdie RG, Prescott AR, Quinlan RA, Crouch RK, Schey KL. The C terminus of lens aquaporin 0 interacts with the cytoskeletal proteins filensin and CP49. Invest Ophthalmol Vis Sci. 2006 Apr;47(4):1562–70.

133. Gokhin DS, Nowak RB, Kim NE, Arnett EE, Chen AC, Sah RL, et al. Tmod1 and CP49 synergize to control the fiber cell geometry, transparency, and mechanical stiffness of the mouse lens. PLoS One. 2012;7(11):e48734.

134. Lo W-K, Wen X-J, Zhou C-J. Microtubule configuration and membranous vesicle transport in elongating fiber cells of the rat lens. Exp Eye Res. 2003 Nov;77(5):615–26.

135. Piatigorsky J. Lens cell elongation in vitro and microtubules. Ann N Y Acad Sci. 1975 Jun;253:333–47.

136. Nowak RB, Fischer RS, Zoltoski RK, Kuszak JR, Fowler VM. Tropomodulin1 is required for membrane skeleton organization and hexagonal geometry of fiber cells in the mouse lens. J Cell Biol. 2009 Sep;186(6):915–28.

137. Nowak RB, Fowler VM. Tropomodulin 1 constrains fiber cell geometry during elongation and maturation in the lens cortex. J Histochem Cytochem Off J Histochem Soc. 2012 Jun;60(6):414–27.

138. Weber GF, Menko AS. Actin filament organization regulates the induction of lens cell differentiation and survival. Dev Biol [Internet]. 2006;295(2):714–29. Available from: http://www.sciencedirect.com/science/article/pii/S0012160606002569

139. Liou W, Rafferty NS. Actin filament patterns in mouse lens epithelium: A study of the effects of aging, injury, and genetics. Cell Motil [Internet]. 1988 Jan 1;9(1):17–29. Available from: https://doi.org/10.1002/cm.970090104

140. Rafferty NS, Scholz DL. Polygonal arrays of microfilaments in epithelial cells of the intact lens. Curr Eye Res. 1984 Sep;3(9):1141–9.

141. Rafferty NS, Scholz DL. Actin in polygonal arrays of microfilaments and sequestered actin bundles (SABs) in lens epithelial cells of rabbits and mice. Curr Eye Res. 1985 Jun;4(6):713–8.

142. Ramaekers FC, Boomkens TR, Bloemendal H. Cytoskeletal and contractile structures in bovine lens cell differentiation. Exp Cell Res. 1981 Oct;135(2):454–61.

143. Hayes JM, Hartsock A, Clark BS, Napier HRL, Link BA, Gross JM. Integrin α5/fibronectin1 and focal adhesion kinase are required for lens fiber morphogenesis in zebrafish. Mol Biol Cell. 2012 Dec;23(24):4725–38.

144. Al-Ghoul KJ, Kuszak JR, Lu JY, Owens MJ. Morphology and organization of posterior fiber ends during migration. Mol Vis. 2003 Apr;9:119–28.

145. Cheng C, Nowak RB, Gao J, Sun X, Biswas SK, Lo W-K, et al. Lens ion homeostasis relies on the assembly and/or stability of large connexin 46 gap junction plaques on the broad sides of differentiating fiber cells. Am J Physiol Cell Physiol. 2015 May;308(10):C835-47.

146. Beebe DC, Truscott RJW. Counterpoint: The lens fluid circulation model--a critical appraisal. Invest Ophthalmol Vis Sci. 2010 May;51(5):2302–6.

147. Mathias RT, Kistler J, Donaldson P. The Lens Circulation. J Membr Biol [Internet]. 2007;216(1):1–16. Available from: https://doi.org/10.1007/s00232-007-9019-y

148. Vaghefi E, Walker K, Pontre BP, Jacobs MD, Donaldson PJ. Magnetic resonance and confocal imaging of solute penetration into the lens reveals a zone of restricted extracellular space diffusion. Am J Physiol Regul Integr Comp Physiol. 2012

Jun;302(11):R1250-9.

149. Candia OA, Mathias R, Gerometta R. Fluid circulation determined in the isolated bovine lens. Invest Ophthalmol Vis Sci. 2012 Oct;53(11):7087–96.

150. Gao J, Sun X, Moore LC, White TW, Brink PR, Mathias RT. Lens intracellular hydrostatic pressure is generated by the circulation of sodium and modulated by gap junction coupling. J Gen Physiol. 2011 Jun;137(6):507–20.

151. Chen Y, Gao J, Li L, Sellitto C, Mathias RT, Donaldson PJ, et al. The Ciliary Muscle and Zonules of Zinn Modulate Lens Intracellular Hydrostatic Pressure Through Transient Receptor Potential Vanilloid Channels. Invest Ophthalmol Vis Sci [Internet]. 2019 Oct 22;60(13):4416–24. Available from: https://doi.org/10.1167/iovs.19-27794

152. Gao J, Sun X, Moore LC, Brink PR, White TW, Mathias RT. The effect of size and species on lens intracellular hydrostatic pressure. Invest Ophthalmol Vis Sci. 2013 Jan;54(1):183–92.

153. Gao J, Sun X, White TW, Delamere NA, Mathias RT. Feedback Regulation of Intracellular Hydrostatic Pressure in Surface Cells of the Lens. Biophys J. 2015 Nov;109(9):1830–9.

154. Grey AC, Walker KL, Petrova RS, Han J, Wilmarth PA, David LL, et al. Verification and spatial localization of aquaporin-5 in the ocular lens. Exp Eye Res. 2013 Mar;108:94–102.

155. Patil R V, Saito I, Yang X, Wax MB. Expression of aquaporins in the rat ocular tissue. Exp Eye Res. 1997 Feb;64(2):203–9.

156. Mitchell CA, Risau W, Drexler HC. Regression of vessels in the tunica vasculosa lentis is initiated by coordinated endothelial apoptosis: a role for vascular endothelial growth factor as a survival factor for endothelium. Dev Dyn an Off Publ Am Assoc Anat. 1998 Nov;213(3):322–33.

157. Petrova RS, Schey KL, Donaldson PJ, Grey AC. Spatial distributions of AQP5 and AQP0 in embryonic and postnatal mouse lens development. Exp Eye Res. 2015 Mar;132:124–35.

158. Agre P, King LS, Yasui M, Guggino WB, Ottersen OP, Fujiyoshi Y, et al. Aquaporin water channels--from atomic structure to clinical medicine. J Physiol. 2002 Jul;542(Pt 1):3–16.

159. Barandika O, Ezquerra-Inchausti M, Anasagasti A, Vallejo-Illarramendi A, Llarena I, Bascaran L, et al. Increased aquaporin 1 and 5 membrane expression in the lens epithelium of cataract patients. Biochim Biophys Acta. 2016 Oct;1862(10):2015–21.

160. Ruiz-Ederra J, Verkman AS. Accelerated cataract formation and reduced lens epithelial water permeability in aquaporin-1-deficient mice. Invest Ophthalmol Vis Sci. 2006 Sep;47(9):3960–7.

161. Vorontsova I, Gehring I, Hall JE, Schilling TF. Aqp0a Regulates Suture Stability in the Zebrafish Lens. Invest Ophthalmol Vis Sci. 2018 Jun;59(7):2869–79.

162. Froger A, Clemens D, Kalman K, Németh-Cahalan KL, Schilling TF, Hall JE. Two distinct aquaporin 0s required for development and transparency of the zebrafish lens. Invest Ophthalmol Vis Sci. 2010 Dec;51(12):6582–92.

163. Clemens DM, Németh-Cahalan KL, Trinh L, Zhang T, Schilling TF, Hall JE. In vivo analysis of aquaporin 0 function in zebrafish: permeability regulation is required for lens

transparency. Invest Ophthalmol Vis Sci. 2013 Jul;54(7):5136–43.

164. Wang Z, Schey KL. Identification of a direct Aquaporin-0 binding site in the lens-specific cytoskeletal protein filensin. Exp Eye Res. 2017 Jun;159:23–9.

165. Sindhu Kumari S, Gupta N, Shiels A, FitzGerald PG, Menon AG, Mathias RT, et al. Role of Aquaporin 0 in lens biomechanics. Biochem Biophys Res Commun. 2015 Jul;462(4):339–45.

166. Reichow SL, Clemens DM, Freites JA, Németh-Cahalan KL, Heyden M, Tobias DJ, et al. Allosteric mechanism of water-channel gating by Ca2+-calmodulin. Nat Struct Mol Biol. 2013 Sep;20(9):1085–92.

167. Kumari SS, Varadaraj K, Okamura T, Kasai N, Mathias RT. Cataract Development and Water Transport in the Aquaporin 0 Mutant CatTohm Mouse Lens . Invest Ophthalmol Vis Sci. 2005 May 1;46(13):1844.

168. Fields JB, Németh-Cahalan KL, Freites JA, Vorontsova I, Hall JE, Tobias DJ. Calmodulin Gates Aquaporin 0 Permeability through a Positively Charged Cytoplasmic Loop. J Biol Chem. 2017 Jan;292(1):185–95.

169. Freites JA, Németh-Cahalan KL, Hall JE, Tobias DJ. Cooperativity and allostery in aquaporin 0 regulation by Ca(2). Biochim Biophys acta Biomembr [Internet]. 2019/02/22. 2019 May 1;1861(5):988–96. Available from: https://pubmed.ncbi.nlm.nih.gov/30802427

170. Rose KML, Wang Z, Magrath GN, Hazard ES, Hildebrandt JD, Schey KL. Aquaporin 0-calmodulin interaction and the effect of aquaporin 0 phosphorylation. Biochemistry. 2008 Jan;47(1):339–47.

171. Gutierrez DB, Garland DL, Schwacke JH, Hachey DL, Schey KL. Spatial distributions of phosphorylated membrane proteins aquaporin 0 and MP20 across young and aged human lenses. Exp Eye Res. 2016 Aug;149:59–65.

172. Vaghefi E, Pontre BP, Jacobs MD, Donaldson PJ. Visualizing ocular lens fluid dynamics using MRI: manipulation of steady state water content and water fluxes. Am J Physiol Regul Integr Comp Physiol. 2011 Aug;301(2):R335-42.

173. Ismail VS, Mosely JA, Tapodi A, Quinlan RA, Sanderson JM. The lipidation profile of aquaporin-0 correlates with the acyl composition of phosphoethanolamine lipids in lens membranes. Biochim Biophys Acta - Biomembr [Internet]. 2016;1858(11):2763–8. Available from: http://www.sciencedirect.com/science/article/pii/S0005273616302346

174. Schey KL, Gutierrez DB, Wang Z, Wei J, Grey AC. Novel fatty acid acylation of lens integral membrane protein aquaporin-0. Biochemistry. 2010 Nov;49(45):9858–65.

175. Harris AL. Emerging issues of connexin channels: biophysics fills the gap. Q Rev Biophys. 2001 Aug;34(3):325–472.

176. White TW, Gao Y, Li L, Sellitto C, Srinivas M. Optimal lens epithelial cell proliferation is dependent on the connexin isoform providing gap junctional coupling. Invest Ophthalmol Vis Sci. 2007 Dec;48(12):5630–7.

177. White TW, Bruzzone R, Goodenough DA, Paul DL. Mouse Cx50, a functional member of the connexin family of gap junction proteins, is the lens fiber protein MP70. Mol Biol Cell. 1992 Jul;3(7):711–20.

178. Dahm R, van Marle J, Prescott AR, Quinlan RA. Gap junctions containing alpha8-connexin (MP70) in the adult mammalian lens epithelium suggests a re-evaluation of its role in the lens. Exp Eye Res. 1999 Jul;69(1):45–56.

179. Tjahjono N, Xia C-H, Li R, Chu S, Wang J, Gong X. Connexin 50-R205G Mutation Perturbs Lens Epithelial Cell Proliferation and Differentiation. Invest Ophthalmol Vis Sci [Internet]. 2020 Mar 9;61(3):25. Available from: https://pubmed.ncbi.nlm.nih.gov/32182330

180. Paul DL, Ebihara L, Takemoto LJ, Swenson KI, Goodenough DA. Connexin46, a novel lens gap junction protein, induces voltage-gated currents in nonjunctional plasma membrane of Xenopus oocytes. J Cell Biol. 1991 Nov;115(4):1077–89.

181. Beyer EC, Kistler J, Paul DL, Goodenough DA. Antisera directed against connexin43 peptides react with a 43-kD protein localized to gap junctions in myocardium and other tissues. J Cell Biol. 1989 Feb;108(2):595–605.

182. Rae JL, Bartling C, Rae J, Mathias RT. Dye transfer between cells of the lens. J Membr Biol. 1996 Mar;150(1):89–103.

183. Mathias RT, White TW, Gong X. Lens gap junctions in growth, differentiation, and homeostasis. Physiol Rev. 2010;90(1):179–206.

184. Le AC, Musil LS. Normal differentiation of cultured lens cells after inhibition of gap junction-mediated intercellular communication. Dev Biol. 1998 Dec;204(1):80–96.

185. Boswell BA, Le A-CN, Musil LS. Upregulation and maintenance of gap junctional communication in lens cells. Exp Eye Res. 2009 May;88(5):919–27.

186. Lin JS, Fitzgerald S, Dong Y, Knight C, Donaldson P, Kistler J. Processing of the gap junction protein connexin50 in the ocular lens is accomplished by calpain. Eur J Cell Biol. 1997 Jun;73(2):141–9.

187. Slavi N, Rubinos C, Li L, Sellitto C, White TW, Mathias R, et al. Connexin 46 (cx46) gap junctions provide a pathway for the delivery of glutathione to the lens nucleus. J Biol Chem. 2014 Nov;289(47):32694–702.

188. White TW, Goodenough DA, Paul DL. Targeted ablation of connexin50 in mice results in microphthalmia and zonular pulverulent cataracts. J Cell Biol. 1998 Nov;143(3):815–25.

189. Gu S, Biswas S, Rodriguez L, Li Z, Li Y, Riquelme MA, et al. Connexin 50 and AQP0 are Essential in Maintaining Organization and Integrity of Lens Fibers. Invest Ophthalmol Vis Sci. 2019 Sep;60(12):4021–32.

190. McFall-Ngai MJ, Ding L-L, Takemoto LJ, Horwitz J. Spatial and temporal mapping of the age-related changes in human lens crystallins. Exp Eye Res [Internet]. 1985;41(6):745–58. Available from: http://www.sciencedirect.com/science/article/pii/0014483585901836

191. Cobb BA, Petrash JM. alpha-Crystallin chaperone-like activity and membrane binding in age-related cataracts. Biochemistry [Internet]. 2002 Jan 15;41(2):483–90. Available from: https://pubmed.ncbi.nlm.nih.gov/11781086

192. Roy D, Spector A. Absence of low-molecular-weight alpha crystallin in nuclear region of old human lenses. Proc Natl Acad Sci [Internet]. 1976 Oct 1;73(10):3484 LP – 3487. Available from: http://www.pnas.org/content/73/10/3484.abstract

193. Heys KR, Friedrich MG, Truscott RJW. Presbyopia and heat: changes associated with aging of the human lens suggest a functional role for the small heat shock protein, alpha-crystallin, in maintaining lens flexibility. Aging Cell. 2007 Dec;6(6):807–15.

194. Cobb BA, Petrash JM. Factors influencing alpha-crystallin association with phospholipid vesicles. Mol Vis [Internet]. 2002 Mar 22;8:85–93. Available from: https://pubmed.ncbi.nlm.nih.gov/11951084

195. Cobb BA, Petrash JM. Characterization of alpha-crystallin-plasma membrane binding. J Biol Chem [Internet]. 2000 Mar 3;275(9):6664–72. Available from: https://pubmed.ncbi.nlm.nih.gov/10692476

196. Cheng C, Xia C, Huang Q, Ding L, Horwitz J, Gong X. Altered Chaperone-like Activity of α-Crystallins Promotes Cataractogenesis. J Biol Chem [Internet]. 2010 Dec 24;285(52):41187–93. Available from: http://www.jbc.org/content/285/52/41187.abstract

197. Hooi MYS, Truscott RJW. Racemisation and human cataract. D-Ser, D-Asp/Asn and D-Thr are higher in the lifelong proteins of cataract lenses than in age-matched normal lenses. Age (Dordr). 2011 Jun;33(2):131–41.

198. Gupta R, Srivastava OP. Deamidation Affects Structural and Functional Properties of Human αA-Crystallin and Its Oligomerization with αB-Crystallin. J Biol Chem [Internet]. 2004 Oct 22;279(43):44258–69. Available from: http://www.jbc.org/content/279/43/44258.abstract

199. Hanson SRA, Hasan A, Smith DL, Smith JB. The Major in vivo Modifications of the Human Water-insoluble Lens Crystallins are Disulfide Bonds, Deamidation, Methionine Oxidation and Backbone Cleavage. Exp Eye Res [Internet]. 2000;71(2):195–207. Available from: http://www.sciencedirect.com/science/article/pii/S0014483500908686

200. Srivastava OP. Age-related increase in concentration and aggregation of degraded polypeptides in human lenses. Exp Eye Res [Internet]. 1988;47(4):525–43. Available from: http://www.sciencedirect.com/science/article/pii/0014483588900929

201. Chaves JM, Srivastava K, Gupta R, Srivastava OP. Structural and Functional Roles of Deamidation and/or Truncation of N- or C-Termini in Human αA-Crystallin. Biochemistry [Internet]. 2008 Sep 23;47(38):10069–83. Available from: https://doi.org/10.1021/bi8001902

202. Su S-P, Lyons B, Friedrich M, McArthur JD, Song X, Xavier D, et al. Molecular signatures of long-lived proteins: autolytic cleavage adjacent to serine residues. Aging Cell. 2012 Dec;11(6):1125–7.

203. Yoshida H, Yumoto N, Tsukahara I, Murachi T. The degradation of alpha-crystallin at its carboxyl-terminal portion by calpain in bovine lens. Invest Ophthalmol Vis Sci. 1986 Aug 1;27(8):1269–73.

204. Andley UP, Mathur S, Griest TA, Petrash JM. Cloning, Expression, and Chaperone-like Activity of Human αA-Crystallin. J Biol Chem [Internet]. 1996 Dec 13;271(50):31973–80. Available from: http://www.jbc.org/content/271/50/31973.abstract

205. Hains PG, Truscott RJW. Post-Translational Modifications in the Nuclear Region of Young, Aged, and Cataract Human Lenses. J Proteome Res [Internet]. 2007 Oct 1;6(10):3935–43. Available from: https://doi.org/10.1021/pr070138h

206. Kato K, Inaguma Y, Ito H, Iida K, Iwamoto I, Kamei K, et al. Ser-59 is the major

phosphorylation site in αB-crystallin accumulated in the brains of patients with Alexander's disease. J Neurochem [Internet]. 2001 Feb 1;76(3):730–6. Available from: https://doi.org/10.1046/j.1471-4159.2001.00038.x

207. Peschek J, Braun N, Rohrberg J, Back KC, Kriehuber T, Kastenmüller A, et al. Regulated structural transitions unleash the chaperone activity of αB-crystallin. Proc Natl Acad Sci [Internet]. 2013 Oct 1;110(40):E3780 LP-E3789. Available from: http://www.pnas.org/content/110/40/E3780.abstract

208. Hains PG, Truscott RJW. Proteomic analysis of the oxidation of cysteine residues in human age-related nuclear cataract lenses. Biochim Biophys Acta - Proteins Proteomics [Internet]. 2008;1784(12):1959–64. Available from: http://www.sciencedirect.com/science/article/pii/S1570963908002252

209. Fan X, Zhou S, Wang B, Hom G, Guo M, Li B, et al. Evidence of Highly Conserved β-Crystallin Disulfidome that Can be Mimicked by In Vitro Oxidation in Age-related Human Cataract and Glutathione Depleted Mouse Lens. Mol Cell Proteomics. 2015 Dec;14(12):3211–23.

210. Fan X, Reneker LW, Obrenovich ME, Strauch C, Cheng R, Jarvis SM, et al. Vitamin C mediates chemical aging of lens crystallins by the Maillard reaction in a humanized mouse model. Proc Natl Acad Sci [Internet]. 2006 Nov 7;103(45):16912 LP – 16917. Available from: http://www.pnas.org/content/103/45/16912.abstract

211. Truscott RJW. Age-related nuclear cataract—oxidation is the key. Exp Eye Res [Internet]. 2005;80(5):709–25. Available from: http://www.sciencedirect.com/science/article/pii/S0014483504003549

212. Gao J, Wang H, Sun X, Varadaraj K, Li L, White TW, et al. The effects of age on lens transport. Invest Ophthalmol Vis Sci. 2013 Nov;54(12):7174–87.

213. Wenke JL, Rose KL, Spraggins JM, Schey KL. MALDI Imaging Mass Spectrometry Spatially Maps Age-Related Deamidation and Truncation of Human Lens Aquaporin-0. Invest Ophthalmol Vis Sci. 2015 Nov;56(12):7398–405.

214. Ball LE, Little M, Nowak MW, Garland DL, Crouch RK, Schey KL. Water permeability of C-terminally truncated aquaporin 0 (AQP0 1-243) observed in the aging human lens. Invest Ophthalmol Vis Sci. 2003 Nov;44(11):4820–8.

215. Sindhu Kumari S, Varadaraj K. Intact and N- or C-terminal end truncated AQP0 function as open water channels and cell-to-cell adhesion proteins: end truncation could be a prelude for adjusting the refractive index of the lens to prevent spherical aberration. Biochim Biophys Acta. 2014 Sep;1840(9):2862–77.

216. Gonen T, Sliz P, Kistler J, Cheng Y, Walz T. Aquaporin-0 membrane junctions reveal the structure of a closed water pore. Nature. 2004 May;429(6988):193–7.

217. Wang Z, Friedrich MG, Truscott RJW, Schey KL. Cleavage C-terminal to Asp leads to covalent crosslinking of long-lived human proteins. Biochim Biophys acta Proteins proteomics. 2019 Sep;1867(9):831–9.

218. Wang B, Hom G, Zhou S, Guo M, Li B, Yang J, et al. The oxidized thiol proteome in aging and cataractous mouse and human lens revealed by ICAT labeling. Aging Cell. 2017 Apr;16(2):244–61.

219. Kanthan GL, Wang JJ, Rochtchina E, Tan AG, Chia E-M, Lee A, et al. Ten-Year Incidence of Age-Related Cataract and Cataract Surgery in an Older Australian Population: The

Blue Mountains Eye Study. Invest Ophthalmol Vis Sci. 2007 May 10;48(13):5675.

220. Klein BEK, Klein R, Lee KE, Gangnon RE. Incidence of Age-Related Cataract over a 15-Year Interval: The Beaver Dam Eye Study. Ophthalmology [Internet]. 2008;115(3):477–82. Available from: http://www.sciencedirect.com/science/article/pii/S0161642007012742

221. Tong J, Briggs MM, Mlaver D, Vidal A, McIntosh TJ. Sorting of lens aquaporins and connexins into raft and nonraft bilayers: role of protein homo-oligomerization. Biophys J [Internet]. 2009 Nov 4;97(9):2493–502. Available from: https://pubmed.ncbi.nlm.nih.gov/19883592

222. Brown DA, London E. Structure and function of sphingolipid- and cholesterol-rich membrane rafts. J Biol Chem. 2000 Jun;275(23):17221–4.

223. Pike LJ. Rafts defined: a report on the Keystone Symposium on Lipid Rafts and Cell Function. Vol. 47, Journal of lipid research. United States; 2006. p. 1597–8.

224. Lin D, Lobell S, Jewell A, Takemoto DJ. Differential phosphorylation of connexin46 and connexin50 by H2O2 activation of protein kinase Cgamma. Mol Vis. 2004 Sep;10:688–95.

225. Cenedella RJ, Sexton PS, Brako L, Lo W-K, Jacob RF. Status of caveolin-1 in various membrane domains of the bovine lens. Exp Eye Res. 2007 Oct;85(4):473–81.

226. Schubert A-L, Schubert W, Spray DC, Lisanti MP. Connexin family members target to lipid raft domains and interact with caveolin-1. Biochemistry. 2002 May;41(18):5754–64.

227. Tong J, Canty JT, Briggs MM, McIntosh TJ. The water permeability of lens aquaporin-0 depends on its lipid bilayer environment. Exp Eye Res. 2013;113:32–40.

228. Raguz M, Mainali L, O'Brien WJ, Subczynski WK. Lipid domains in intact fiber-cell plasma membranes isolated from cortical and nuclear regions of human eye lenses of donors from different age groups. Exp Eye Res. 2015;132:78–90.

229. Subczynski WK, Mainali L, Raguz M, O'Brien WJ. Organization of lipids in fiber-cell plasma membranes of the eye lens. Exp Eye Res. 2016;

230. Ifeanyi F, Takemoto L. Differential binding of alpha-crystallins to bovine lens membrane. Exp Eye Res. 1989 Jul;49(1):143–7.

231. Cenedella RJ, Chandrasekher G. High capacity binding of alpha crystallins to various bovine lens membrane preparations. Curr Eye Res. 1993 Nov;12(11):1025–38.

232. Tang D, Borchman D, Yappert MC, Cenedella RJ. Influence of cholesterol on the interaction of alpha-crystallin with phospholipids. Exp Eye Res. 1998 May;66(5):559–67.

233. Borchman D, Tang D. Binding capacity of alpha-crystallin to bovine lens lipids. Exp Eye Res. 1996 Oct;63(4):407–10.

234. Swamy-Mruthinti S, Srinivas V, Hansen JE, Rao CM. Thermal stress induced aggregation of aquaporin 0 (AQP0) and protection by α-crystallin via its chaperone function. PLoS One. 2013;8(11):e80404.

235. Liu B-F, Liang JJ. Confocal fluorescence microscopy study of interaction between lens MIP26/AQP0 and crystallins in living cells. J Cell Biochem. 2008 May;104(1):51–8.

236. Billingsley G, Santhiya ST, Paterson AD, Ogata K, Wodak S, Hosseini SM, et al. CRYBA4, a novel human cataract gene, is also involved in microphthalmia. Am J Hum Genet [Internet]. 2006/08/17. 2006 Oct;79(4):702–9. Available from: https://pubmed.ncbi.nlm.nih.gov/16960806

237. Sun H, Ma Z, Li Y, Liu B, Li Z, Ding X, et al. Gamma-S crystallin gene (CRYGS) mutation causes dominant progressive cortical cataract in humans. J Med Genet [Internet]. 2005 Sep;42(9):706–10. Available from: https://pubmed.ncbi.nlm.nih.gov/16141006

238. Stephan DA, Gillanders E, Vanderveen D, Freas-Lutz D, Wistow G, Baxevanis AD, et al. Progressive juvenile-onset punctate cataracts caused by mutation of the gammaD-crystallin gene. Proc Natl Acad Sci U S A [Internet]. 1999 Feb 2;96(3):1008–12. Available from: https://pubmed.ncbi.nlm.nih.gov/9927684

239. Wang KJ, Wang S, Cao N-Q, Yan Y-B, Zhu SQ. A novel mutation in CRYBB1 associated with congenital cataract-microcornea syndrome: the p.Ser129Arg mutation destabilizes the βB1/βA3-crystallin heteromer but not the βB1-crystallin homomer. Hum Mutat [Internet]. 2011/01/25. 2011 Mar;32(3):E2050–60. Available from: https://pubmed.ncbi.nlm.nih.gov/21972112

240. Wang KJ, Wang B Bin, Zhang F, Zhao Y, Ma X, Zhu SQ. Novel β-Crystallin Gene Mutations in Chinese Families With Nuclear Cataracts. Arch Ophthalmol [Internet]. 2011 Mar 1;129(3):337–43. Available from: https://doi.org/10.1001/archophthalmol.2011.11

241. Riazuddin SA, Yasmeen A, Yao W, Sergeev Y V, Zhang Q, Zulfiqar F, et al. Mutations in βB3-Crystallin Associated with Autosomal Recessive Cataract in Two Pakistani Families. Invest Ophthalmol Vis Sci [Internet]. 2005 Jun 1;46(6):2100–6. Available from: https://doi.org/10.1167/iovs.04-1481

242. Bateman JB, von-Bischhoffshaunsen FRB, Richter L, Flodman P, Burch D, Spence MA. Gene Conversion Mutation in Crystallin, β-B2 (CRYBB2) in a Chilean Family with Autosomal Dominant Cataract. Ophthalmology [Internet]. 2007 Mar 1;114(3):425–32. Available from: https://doi.org/10.1016/j.ophtha.2006.09.013

243. Bateman JB, Geyer DD, Flodman P, Johannes M, Sikela J, Walter N, et al. A New βA1-Crystallin Splice Junction Mutation in Autosomal Dominant Cataract. Invest Ophthalmol Vis Sci. 2000 Oct 1;41(11):3278–85.

244. Qi Y, Jia H, Huang S, Lin H, Gu J, Su H, et al. A deletion mutation in the βA1/A3 crystallin gene (CRYBA1/A3) is associated with autosomal dominant congenital nuclear cataract in a Chinese family. Hum Genet [Internet]. 2004;114(2):192–7. Available from: https://doi.org/10.1007/s00439-003-1049-7

245. Mackay DS, Andley UP, Shiels A. Cell death triggered by a novel mutation in the alphaA-crystallin gene underlies autosomal dominant cataract linked to chromosome 21q. Eur J Hum Genet [Internet]. 2003;11(10):784–93. Available from: https://doi.org/10.1038/sj.ejhg.5201046

246. Pras E, Frydman M, Levy–Nissenbaum E, Bakhan T, Raz J, Assia EI, et al. A Nonsense Mutation (W9X) in CRYAA Causes Autosomal Recessive Cataract in an Inbred Jewish Persian Family. Invest Ophthalmol Vis Sci. 2000 Oct 1;41(11):3511–5.

247. Yang J, Zhu Y, Gu F, He X, Cao Z, Li X, et al. A novel nonsense mutation in CRYBB1 associated with autosomal dominant congenital cataract. Mol Vis [Internet]. 2008 Apr 18;14:727–31. Available from: https://pubmed.ncbi.nlm.nih.gov/18432316

248. Shiels A, Bennett TM, Hejtmancik JF. Cat-Map: putting cataract on the map. Mol Vis [Internet]. 2010 Oct 8;16:2007–15. Available from: https://pubmed.ncbi.nlm.nih.gov/21042563

249. Zhao L, Chen X-J, Zhu J, Xi Y-B, Yang X, Hu L-D, et al. Lanosterol reverses protein aggregation in cataracts. Nature [Internet]. 2015;523(7562):607–11. Available from: https://doi.org/10.1038/nature14650

250. Mori M, Li G, Abe I, Nakayama J, Guo Z, Sawashita J, et al. Lanosterol synthase mutations cause cholesterol deficiency-associated cataracts in the Shumiya cataract rat. J Clin Invest. 2006 Feb;116(2):395–404.

251. Chen X-J, Hu L-D, Yao K, Yan Y-B. Lanosterol and 25-hydroxycholesterol dissociate crystallin aggregates isolated from cataractous human lens via different mechanisms. Biochem Biophys Res Commun. 2018 Dec;506(4):868–73.

252. Chen P, Dai Y, Wu X, Wang Y, Sun S, Xiao J, et al. Mutations in the ABCA3 gene are associated with cataract-microcornea syndrome. Invest Ophthalmol Vis Sci. 2014 Nov;55(12):8031–43.

253. Machan CM, Hrynchak PK, Irving EL. Age-related cataract is associated with type 2 diabetes and statin use. Optom Vis Sci Off Publ Am Acad Optom. 2012 Aug;89(8):1165–71.

254. Lai C-L, Shau W-Y, Chang C-H, Chen M-F, Lai M-S. Statin use and cataract surgery: a nationwide retrospective cohort study in elderly ethnic Chinese patients. Drug Saf. 2013 Oct;36(10):1017–24.

255. Leuschen J, Mortensen EM, Frei CR, Mansi EA, Panday V, Mansi I. Association of statin use with cataracts: a propensity score-matched analysis. JAMA Ophthalmol. 2013 Nov;131(11):1427–34.

256. de Vries AC, Cohen LH. Different effects of the hypolipidemic drugs pravastatin and lovastatin on the cholesterol biosynthesis of the human ocular lens in organ culture and on the cholesterol content of the rat lens in vivo. Biochim Biophys Acta. 1993 Mar;1167(1):63–9.

257. Newman CB, Preiss D, Tobert JA, Jacobson TA, Page RL 2nd, Goldstein LB, et al. Statin Safety and Associated Adverse Events: A Scientific Statement From the American Heart Association. Arterioscler Thromb Vasc Biol. 2019 Feb;39(2):e38–81.

258. Mach F, Ray KK, Wiklund O, Corsini A, Catapano AL, Bruckert E, et al. Adverse effects of statin therapy: perception vs. the evidence - focus on glucose homeostasis, cognitive, renal and hepatic function, haemorrhagic stroke and cataract. Eur Heart J. 2018 Jul;39(27):2526–39.

259. Widomska J, Subczynski WK. Why Is Very High Cholesterol Content Beneficial for the Eye Lens but Negative for Other Organs? Nutrients. 2019 May;11(5).

260. Cenedella RJ, Sexton PS. Probing cataractogenesis associated with mevalonic aciduria. Curr Eye Res. 1998 Feb;17(2):153–8.

261. Berginer VM, Abeliovich D. Genetics of cerebrotendinous xanthomatosis (CTX): an autosomal recessive trait with high gene frequency in Sephardim of Moroccan origin. Am J Med Genet. 1981;10(2):151–7.

262. Berginer VM, Gross B, Morad K, Kfir N, Morkos S, Aaref S, et al. Chronic diarrhea and

juvenile cataracts: think cerebrotendinous xanthomatosis and treat. Pediatrics. 2009 Jan;123(1):143–7.

263. Khan AO, Aldahmesh MA, Mohamed JY, Alkuraya FS. Juvenile cataract morphology in 3 siblings not yet diagnosed with cerebrotendinous xanthomatosis. Ophthalmology. 2013 May;120(5):956–60.

264. Mignarri A, Magni A, Del Puppo M, Gallus GN, Björkhem I, Federico A, et al. Evaluation of cholesterol metabolism in cerebrotendinous xanthomatosis. J Inherit Metab Dis. 2016 Jan;39(1):75–83.

265. Mignarri A, Gallus GN, Dotti MT, Federico A. A suspicion index for early diagnosis and treatment of cerebrotendinous xanthomatosis. J Inherit Metab Dis. 2014 May;37(3):421–9.

266. Berginer VM, Salen G, Shefer S. Long-term treatment of cerebrotendinous xanthomatosis with chenodeoxycholic acid. N Engl J Med. 1984 Dec;311(26):1649–52.

267. Mandia D, Chaussenot A, Besson G, Lamari F, Castelnovo G, Curot J, et al. Cholic acid as a treatment for cerebrotendinous xanthomatosis in adults. J Neurol. 2019 Aug;266(8):2043–50.

268. Mondelli M, Sicurelli F, Scarpini C, Dotti MT, Federico A. Cerebrotendinous xanthomatosis: 11-year treatment with chenodeoxycholic acid in five patients. An electrophysiological study. J Neurol Sci. 2001 Sep;190(1–2):29–33.

269. Song S, Liang JJN, Mulhern ML, Madson CJ, Shinohara T. Cholesterol-derived bile acids enhance the chaperone activity of α-crystallins. Cell Stress Chaperones [Internet]. 2011/03/06. 2011 Sep;16(5):475–80. Available from: https://pubmed.ncbi.nlm.nih.gov/21380614

270. Goodwin H, Brooks BP, Porter FD. Acute postnatal cataract formation in Smith-Lemli-Opitz syndrome. Am J Med Genet A. 2008 Jan;146A(2):208–11.

271. Nowaczyk MJM, Irons MB. Smith-Lemli-Opitz syndrome: phenotype, natural history, and epidemiology. Am J Med Genet C Semin Med Genet. 2012 Nov;160C(4):250–62.

272. Kapphahn RJ, Richards MJ, Ferrington DA, Fliesler SJ. Lipid-derived and other oxidative modifications of retinal proteins in a rat model of Smith-Lemli-Opitz syndrome. Exp Eye Res [Internet]. 2018/08/14. 2019 Jan;178:247–54. Available from: https://pubmed.ncbi.nlm.nih.gov/30114413

273. Elias ER, Irons MB, Hurley AD, Tint GS, Salen G. Clinical effects of cholesterol supplementation in six patients with the Smith-Lemli-Opitz syndrome (SLOS). Am J Med Genet. 1997 Jan;68(3):305–10.

274. Fliesler SJ, Richards MJ, Miller C, Peachey NS, Cenedella RJ. Retinal structure and function in an animal model that replicates the biochemical hallmarks of desmosterolosis. Neurochem Res. 2000 May;25(5):685–94.

275. Cenedella RJ. Cholesterol synthesis inhibitor U18666A and the role of sterol metabolism and trafficking in numerous pathophysiological processes. Lipids. 2009 Jun;44(6):477–87.

276. Klein BE, Klein R, Lee KE. Incidence of age-related cataract: the Beaver Dam Eye Study. Arch Ophthalmol (Chicago, Ill 1960) [Internet]. 1998;116(2):219–25. Available from: http://www.ncbi.nlm.nih.gov/pubmed/9488275

277. Lu Z-Q, Sun W-H, Yan J, Jiang T-X, Zhai S-N, Li Y. Cigarette smoking, body mass index associated with the risks of age-related cataract in male patients in northeast China. Int J Ophthalmol. 2012;5(3):317–22.

278. Ye J, He J, Wang C, Wu H, Shi X, Zhang H, et al. Smoking and risk of age-related cataract: a meta-analysis. Invest Ophthalmol Vis Sci. 2012 Jun;53(7):3885–95.

279. Hennis A, Wu S-Y, Nemesure B, Leske MC. Risk factors for incident cortical and posterior subcapsular lens opacities in the Barbados Eye Studies. Arch Ophthalmol (Chicago, Ill 1960). 2004 Apr;122(4):525–30.

280. Borchman D, Lamba OP, Salmassi S, Lou M, Cecilia Yappert M. The dual effect of oxidation on lipid bilayer structure. Lipids [Internet]. 1992 Apr 1;27(4):261–5. Available from: https://doi.org/10.1007/BF02536472

281. Duran MJ, Pierre S V, Lesnik P, Pieroni G, Bourdeaux M, Dignat-Georges F, et al. 7-ketocholesterol inhibits Na,K-ATPase activity by decreasing expression of its α1-subunit and membrane fluidity in human endothelial cells. Cell Mol Biol (Noisy-le-grand). 2010 Nov;56 Suppl:OL1434-41.

282. Delamere NA, Tamiya S. Lens ion transport: from basic concepts to regulation of Na,K-ATPase activity. Exp Eye Res [Internet]. 2008/05/16. 2009 Feb;88(2):140–3. Available from: https://pubmed.ncbi.nlm.nih.gov/18614168

283. Bhuyan KC, Master RW, Coles RS, Bhuyan DK. Molecular mechanisms of cataractogenesis: IV. Evidence of phospholipid . malondialdehyde adduct in human senile cataract. Mech Ageing Dev. 1986 May;34(3):289–96.

284. Bhuyan KC, Bhuyan DK. Molecular mechanism of cataractogenesis: III. Toxic metabolites of oxygen as initiators of lipid peroxidation and cataract. Curr Eye Res. 1984 Jan;3(1):67–81.

285. Micelli-Ferrari T, Vendemiale G, Grattagliano I, Boscia F, Arnese L, Altomare E, et al. Role of lipid peroxidation in the pathogenesis of myopic and senile cataract. Br J Ophthalmol. 1996 Sep;80(9):840–3.

286. Tang D, Borchman D, Schwarz AK, Yappert MC, Vrensen GFJM, Marle J va., et al. Light scattering of human lens vesicles in vitro. Exp Eye Res [Internet]. 2003;76(5):605–12. Available from: http://www.sciencedirect.com/science/article/pii/S0014483503000265

287. Mchaourab HS, Kumar MS, Koteiche HA. Specificity of αA-crystallin binding to destabilized mutants of βB1-crystallin. FEBS Lett [Internet]. 2007;581(10):1939–43. Available from: http://www.sciencedirect.com/science/article/pii/S0014579307003791

288. MA Z, HANSON SRA, LAMPI KJ, DAVID LL, SMITH DL, SMITH JB. Age-Related Changes in Human Lens Crystallins Identified by HPLC and Mass Spectrometry. Exp Eye Res [Internet]. 1998;67(1):21–30. Available from: http://www.sciencedirect.com/science/article/pii/S0014483598904821

289. Friedrich MG, Truscott RJW. Membrane association of proteins in the aging human lens: profound changes take place in the fifth decade of life. Invest Ophthalmol Vis Sci. 2009 Oct;50(10):4786–93.

290. Friedrich MG, Truscott RJW. Large-scale binding of α-crystallin to cell membranes of aged normal human lenses: a phenomenon that can be induced by mild thermal stress. Invest Ophthalmol Vis Sci. 2010 Oct;51(10):5145–52.

291. Truscott RJ, Augusteyn RC. The state of sulphydryl groups in normal and cataractous human lenses. Exp Eye Res. 1977 Aug;25(2):139–48.

292. Truscott RJ, Augusteyn RC. Oxidative changes in human lens proteins during senile nuclear cataract formation. Biochim Biophys Acta. 1977 May;492(1):43–52.

293. Truscott RJ, Augusteyn RC. Changes in human lens proteins during nuclear cataract formation. Exp Eye Res. 1977 Feb;24(2):159–70.

294. LUND AL, SMITH JB, SMITH DL. Modifications of the Water-insoluble Human Lens α-Crystallins. Exp Eye Res [Internet]. 1996;63(6):661–72. Available from: http://www.sciencedirect.com/science/article/pii/S0014483596901608

295. Spector A. Oxidative stress-induced cataract: mechanism of action. FASEB J [Internet]. 1995 Sep 1;9(12):1173–82. Available from: https://doi.org/10.1096/fasebj.9.12.7672510

296. MacCoss MJ, McDonald WH, Saraf A, Sadygov R, Clark JM, Tasto JJ, et al. Shotgun identification of protein modifications from protein complexes and lens tissue. Proc Natl Acad Sci [Internet]. 2002 Jun 11;99(12):7900 LP – 7905. Available from: http://www.pnas.org/content/99/12/7900.abstract

297. Barnes S, Quinlan RA. Small molecules, both dietary and endogenous, influence the onset of lens cataracts. Exp Eye Res. 2016;

298. McNeil JJ, Robman L, Tikellis G, Sinclair MI, McCarty CA, Taylor HR. Vitamin E supplementation and cataract: Randomized controlled trial. Ophthalmology [Internet]. 2004 Jan 1;111(1):75–84. Available from: https://doi.org/10.1016/j.ophtha.2003.04.009

299. Makley LN, McMenimen KA, DeVree BT, Goldman JW, McGlasson BN, Rajagopal P, et al. Pharmacological chaperone for α-crystallin partially restores transparency in cataract models. Science (80- ) [Internet]. 2015 Nov 6;350(6261):674 LP – 677. Available from: http://science.sciencemag.org/content/350/6261/674.abstract

300. Daszynski DM, Santhoshkumar P, Phadte AS, Sharma KK, Zhong HA, Lou MF, et al. Failure of Oxysterols Such as Lanosterol to Restore Lens Clarity from Cataracts. Sci Rep [Internet]. 2019;9(1):8459. Available from: https://doi.org/10.1038/s41598-019-44676-4

301. Qi H-P, Wei S-Q, Gao X-C, Yu N-N, Hu W-Z, Bi S, et al. Ursodeoxycholic acid prevents selenite-induced oxidative stress and alleviates cataract formation: In vitro and in vivo studies. Mol Vis. 2012;18:151–60.

302. Heruye SH, Maffofou Nkenyi LN, Singh NU, Yalzadeh D, Ngele KK, Njie-Mbye Y-F, et al. Current Trends in the Pharmacotherapy of Cataracts. Pharmaceuticals (Basel). 2020 Jan;13(1).

303. Royer M-C, Lemaire-Ewing S, Desrumaux C, Monier S, Pais de Barros J-P, Athias A, et al. 7-ketocholesterol incorporation into sphingolipid/cholesterol-enriched (lipid raft) domains is impaired by vitamin E: a specific role for alpha-tocopherol with consequences on cell death. J Biol Chem. 2009 Jun;284(23):15826–34.

304. Mintzer E, Charles G, Gordon S. Interaction of two oxysterols, 7-ketocholesterol and 25-hydroxycholesterol, with phosphatidylcholine and sphingomyelin in model membranes. Chem Phys Lipids. 2010 Jun;163(6):586–93.

305. GIRÃO H, MOTA MC, RAMALHO J, PEREIRA P. Cholesterol Oxides Accumulate in Human

Cataracts. Exp Eye Res [Internet]. 1998;66(5):645–52. Available from: http://www.sciencedirect.com/science/article/pii/S0014483598904651

306. Vejux A, Abed-Vieillard D, Hajji K, Zarrouk A, Mackrill JJ, Ghosh S, et al. 7-Ketocholesterol and 7β-hydroxycholesterol: In vitro and animal models used to characterize their activities and to identify molecules preventing their toxicity. Biochem Pharmacol. 2020 Mar;173:113648.

307. Raguz M, Mainali L, O'Brien WJ, Subczynski WK. Amounts of phospholipids and cholesterol in lipid domains formed in intact lens membranes: Methodology development and its application to studies of porcine lens membranes. Exp Eye Res. 2015;140:179–86.

308. Seng JA, Ellis SR, Hughes JR, Maccarone AT, Truscott RJW, Blanksby SJ, et al. Characterisation of sphingolipids in the human lens by thin layer chromatography–desorption electrospray ionisation mass spectrometry. Biochim Biophys Acta - Mol Cell Biol Lipids. 2014;1841(9):1285–91.

309. Schindelin J, Arganda-Carreras I, Frise E, Kaynig V, Longair M, Pietzsch T, et al. Fiji: an open-source platform for biological-image analysis. Nat Methods [Internet]. 2012;9(7):676–82. Available from: https://doi.org/10.1038/nmeth.2019

310. BLIGH EG, DYER WJ. A rapid method of total lipid extraction and purification. Can J Biochem Physiol. 1959 Aug;37(8):911–7.

311. Kyhse-Andersen J. Electroblotting of multiple gels: a simple apparatus without buffer tank for rapid transfer of proteins from polyacrylamide to nitrocellulose. J Biochem Biophys Methods. 1984 Dec;10(3–4):203–9.

312. Burgess HA, Granato M. Modulation of locomotor activity in larval zebrafish during light adaptation. J Exp Biol [Internet]. 2007 Jul 15;210(14):2526 LP – 2539. Available from: http://jeb.biologists.org/content/210/14/2526.abstract

313. Roberts AC, Chornak J, Alzagatiti JB, Ly DT, Bill BR, Trinkeller J, et al. Rapid habituation of a touch-induced escape response in Zebrafish (Danio rerio) Larvae. PLoS One [Internet]. 2019 Apr 4;14(4):e0214374. Available from: https://doi.org/10.1371/journal.pone.0214374

314. Goel MK, Khanna P, Kishore J. Understanding survival analysis: Kaplan-Meier estimate. Int J Ayurveda Res [Internet]. 2010 Oct;1(4):274–8. Available from: https://pubmed.ncbi.nlm.nih.gov/21455458

315. Benchoula K, Khatib A, Jaffar A, Ahmed QU, Sulaiman WMAW, Wahab RA, et al. The promise of zebrafish as a model of metabolic syndrome. Exp Anim [Internet]. 2019/05/21. 2019 Nov 6;68(4):407–16. Available from: https://pubmed.ncbi.nlm.nih.gov/31118344

316. Maerz LD, Burkhalter MD, Schilpp C, Wittekindt OH, Frick M, Philipp M. Pharmacological cholesterol depletion disturbs ciliogenesis and ciliary function in developing zebrafish. Commun Biol [Internet]. 2019 Jan 29;2:31. Available from: https://pubmed.ncbi.nlm.nih.gov/30729178

317. Afonso MS, Machado RM, Lavrador MS, Quintao ECR, Moore KJ, Lottenberg AM. Molecular Pathways Underlying Cholesterol Homeostasis. Nutrients. 2018 Jun;10(6).

318. Shen W-J, Zaidi SK, Patel S, Cortez Y, Ueno M, Azhar R, et al. Ablation of vimentin results in defective steroidogenesis. Endocrinology [Internet]. 2012/04/24. 2012

Jul;153(7):3249–57. Available from: https://pubmed.ncbi.nlm.nih.gov/22535769

319. Pinto CL, Kalasekar SM, McCollum CW, Riu A, Jonsson P, Lopez J, et al. Lxr regulates lipid metabolic and visual perception pathways during zebrafish development. Mol Cell Endocrinol. 2016;419:29–43.

320. Repa JJ, Liang G, Ou J, Bashmakov Y, Lobaccaro JM, Shimomura I, et al. Regulation of mouse sterol regulatory element-binding protein-1c gene (SREBP-1c) by oxysterol receptors, LXRalpha and LXRbeta. Genes Dev. 2000 Nov;14(22):2819–30.

321. Howe K, Clark MD, Torroja CF, Torrance J, Berthelot C, Muffato M, et al. The zebrafish reference genome sequence and its relationship to the human genome. Nature. 2013 Apr;496(7446):498–503.

322. Asnani A, Peterson RT. The zebrafish as a tool to identify novel therapies for human cardiovascular disease. Dis Model Mech. 2014 Jul;7(7):763–7.

323. Thorpe JL, Doitsidou M, Ho S-Y, Raz E, Farber SA. Germ cell migration in zebrafish is dependent on HMGCoA reductase activity and prenylation. Dev Cell. 2004 Feb;6(2):295–302.

324. Brockerhoff SE, Hurley JB, Janssen-Bienhold U, Neuhauss SC, Driever W, Dowling JE. A behavioral screen for isolating zebrafish mutants with visual system defects. Proc Natl Acad Sci [Internet]. 1995 Nov 7;92(23):10545 LP – 10549. Available from: http://www.pnas.org/content/92/23/10545.abstract

325. Lakstygal AM, Demin KA, Kalueff A V. Chapter 8 - Motor patterns and swim path characteristics: the ethogram of zebrafish. In: Gerlai RTBT-B and NG of Z, editor. Academic Press; 2020. p. 125–40. Available from: http://www.sciencedirect.com/science/article/pii/B9780128175286000085

326. Hissa B, Pontes B, Roma PMS, Alves AP, Rocha CD, Valverde TM, et al. Membrane cholesterol removal changes mechanical properties of cells and induces secretion of a specific pool of lysosomes. PLoS One [Internet]. 2013 Dec 20;8(12):e82988–e82988. Available from: https://pubmed.ncbi.nlm.nih.gov/24376622

327. Tamari F, Chen FW, Li C, Chaudhari J, Ioannou YA. PKC activation in Niemann pick C1 cells restores subcellular cholesterol transport. PLoS One [Internet]. 2013 Aug 15;8(8):e74169–e74169. Available from: https://pubmed.ncbi.nlm.nih.gov/23977398

328. Selivanova OM, Galzitskaya O V. Structural and Functional Peculiarities of α-Crystallin. Biology (Basel). 2020 Apr;9(4).

329. Peschek J, Braun N, Franzmann TM, Georgalis Y, Haslbeck M, Weinkauf S, et al. The eye lens chaperone α-crystallin forms defined globular assemblies. Proc Natl Acad Sci [Internet]. 2009 Aug 11;106(32):13272 LP – 13277. Available from: http://www.pnas.org/content/106/32/13272.abstract

330. Xi J, Bai F, Gross J, Townsend RR, Menko AS, Andley UP. Mechanism of Small Heat Shock Protein Function in Vivo: A KNOCK-IN MOUSE MODEL DEMONSTRATES THAT THE R49C MUTATION IN αA-CRYSTALLIN ENHANCES PROTEIN INSOLUBILITY AND CELL DEATH . J Biol Chem [Internet]. 2008 Feb 29;283(9):5801–14. Available from: http://www.jbc.org/content/283/9/5801.abstract

331. Iribarren R. Crystalline lens and refractive development. Prog Retin Eye Res [Internet]. 2015;47:86–106. Available from: http://www.sciencedirect.com/science/article/pii/S1350946215000087

332. Greiling TMS, Clark JI. Early lens development in the zebrafish: A three-dimensional time-lapse analysis. Dev Dyn [Internet]. 2009 Sep 1;238(9):2254–65. Available from: https://doi.org/10.1002/dvdy.21997

333. Aftab BT, Dobromilskaya I, Liu JO, Rudin CM. Itraconazole inhibits angiogenesis and tumor growth in non-small cell lung cancer. Cancer Res. 2011 Nov;71(21):6764–72.

334. Ho P-Y, Liang Y-C, Ho Y-S, Chen C-T, Lee W-S. Inhibition of human vascular endothelial cells proliferation by terbinafine. Int J cancer. 2004 Aug;111(1):51–9.

335. Chong CR, Xu J, Lu J, Bhat S, Sullivan DJJ, Liu JO. Inhibition of angiogenesis by the antifungal drug itraconazole. ACS Chem Biol. 2007 Apr;2(4):263–70.

336. Maione F, Oliaro-Bosso S, Meda C, Di Nicolantonio F, Bussolino F, Balliano G, et al. The cholesterol biosynthesis enzyme oxidosqualene cyclase is a new target to impair tumour angiogenesis and metastasis dissemination. Sci Rep [Internet]. 2015 Mar 12;5:9054. Available from: https://pubmed.ncbi.nlm.nih.gov/25761781

337. Belter A, Skupinska M, Giel-Pietraszuk M, Grabarkiewicz T, Rychlewski L, Barciszewski J. Squalene monooxygenase - a target for hypercholesterolemic therapy. Biol Chem. 2011 Dec;392(12):1053–75.

338. Garcia-Gonzalo FR, Phua SC, Roberson EC, Garcia G 3rd, Abedin M, Schurmans S, et al. Phosphoinositides Regulate Ciliary Protein Trafficking to Modulate Hedgehog Signaling. Dev Cell. 2015 Aug;34(4):400–9.

339. Kalligeraki AA, Isted A, Jarrin M, Uwineza A, Pal R, Saunter CD, et al. Three-dimensional data capture and analysis of intact eye lenses evidences emmetropia-associated changes in epithelial cell organization. Sci Rep. 2020;10(1).

340. Hölttä-Vuori M, Uronen R-L, Repakova J, Salonen E, Vattulainen I, Panula P, et al. BODIPY-cholesterol: a new tool to visualize sterol trafficking in living cells and organisms. Traffic. 2008 Nov;9(11):1839–49.

341. Anderson JL, Carten JD, Farber SA. Zebrafish lipid metabolism: from mediating early patterning to the metabolism of dietary fat and cholesterol. Methods Cell Biol [Internet]. 2011;101:111–41. Available from: https://pubmed.ncbi.nlm.nih.gov/21550441

342. Anderson RA, Schwalbach KT, Mui SR, LeClair EE, Topczewska JM, Topczewski J. Zebrafish models of skeletal dysplasia induced by cholesterol biosynthesis deficiency. Dis Model Mech [Internet]. 2020 Jun 24;13(6):dmm042549. Available from: https://pubmed.ncbi.nlm.nih.gov/32430393

343. Banavali NK. The Mechanism of Cholesterol Modification of Hedgehog Ligand. J Comput Chem [Internet]. 2020 Mar 5;41(6):520–7. Available from: https://doi.org/10.1002/jcc.26097

344. Alcala J, Lieska N, Maisel H. Protein composition of bovine lens cortical fiber cell membranes. Exp Eye Res [Internet]. 1975;21(6):581–95. Available from: http://www.sciencedirect.com/science/article/pii/0014483575900408

345. FitzGerald PG, Graham D. Ultrastructural localization of alpha A-crystallin to the bovine lens fiber cell cytoskeleton. Curr Eye Res. 1991 May;10(5):417–36.

346. Bloemendal H, Berbers GA, De Jong WW, Ramaekers FC, Vermorken AJ, Dunia I, et al. Interaction of crystallins with the cytoskeletal-plasma membrane complex of the

bovine lens. Ciba Found Symp. 1984;106:177–90.

347. Benedetti EL, Dunia I, Dufier JL, Seng YK, Bloemendal H. Plasma membrane-cytoskeleton complex in the normal and cataractous lens. In: Hesketh JE, Pryme IFBT-TCAM-VT, editors. Cytoskeleton in Specialized Tissues and in Pathological States [Internet]. JAI; 1996. p. 451–517. Available from: http://www.sciencedirect.com/science/article/pii/S1874602096800176

348. Merdes A, Brunkener M, Horstmann H, Georgatos SD. Filensin: a new vimentin-binding, polymerization-competent, and membrane-associated protein of the lens fiber cell. J Cell Biol. 1991 Oct;115(2):397–410.

349. Tiffany JM, Koretz JF. Viscosity of alpha-crystallin solutions. Int J Biol Macromol [Internet]. 2002;30(3):179–85. Available from: http://www.sciencedirect.com/science/article/pii/S0141813002000181

350. Abgar S, Yevlampieva N, Aerts T, Vanhoudt J, Clauwaert J. Chaperone-like Activity of Bovine Lens α-Crystallin in the Presence of Dithiothreitol-Destabilized Proteins: Characterization of the Formed Complexes. Biochem Biophys Res Commun [Internet]. 2000;276(2):619–25. Available from: http://www.sciencedirect.com/science/article/pii/S0006291X00935186

351. Raman B, Ramakrishna T, Rao CM. Temperature dependent chaperone-like activity of alpha-crystallin. FEBS Lett. 1995 May;365(2–3):133–6.

352. Raman B, Rao CM. Chaperone-like activity and temperature-induced structural changes of alpha-crystallin. J Biol Chem. 1997 Sep;272(38):23559–64.

353. Maulucci G, Papi M, Arcovito G, De Spirito M. The thermal structural transition of α-crystallin inhibits the heat induced self-aggregation. PLoS One [Internet]. 2011 May 9;6(5):e18906–e18906. Available from: https://pubmed.ncbi.nlm.nih.gov/21573059

354. Fukiage C, Azuma M, Nakamura Y, Tamada Y, Nakamura M, Shearer TR. SJA6017, a newly synthesized peptide aldehyde inhibitor of calpain: amelioration of cataract in cultured rat lenses. Biochim Biophys Acta - Mol Basis Dis [Internet]. 1997;1361(3):304–12. Available from: http://www.sciencedirect.com/science/article/pii/S0925443997000434

355. Rasmussen T, Tantipolphan R, van de Weert M, Jiskoot W. The molecular chaperone alpha-crystallin as an excipient in an insulin formulation. Pharm Res [Internet]. 2010/03/24. 2010 Jul;27(7):1337–47. Available from: https://pubmed.ncbi.nlm.nih.gov/20333453

356. Jehle S, Vollmar BS, Bardiaux B, Dove KK, Rajagopal P, Gonen T, et al. N-terminal domain of αB-crystallin provides a conformational switch for multimerization and structural heterogeneity. Proc Natl Acad Sci [Internet]. 2011 Apr 19;108(16):6409 LP – 6414. Available from: http://www.pnas.org/content/108/16/6409.abstract

357. Delbecq SP, Klevit RE. One size does not fit all: The oligomeric states of αB crystallin. FEBS Lett [Internet]. 2013;587(8):1073–80. Available from: http://www.sciencedirect.com/science/article/pii/S0014579313000525

358. Kumar LVS, Rao CM. Domain Swapping in Human αA and αB Crystallins Affects Oligomerization and Enhances Chaperone-like Activity. J Biol Chem [Internet]. 2000 Jul 21;275(29):22009–13. Available from: http://www.jbc.org/content/275/29/22009.abstract

# Appendix 1: The synthesis of cholesterol

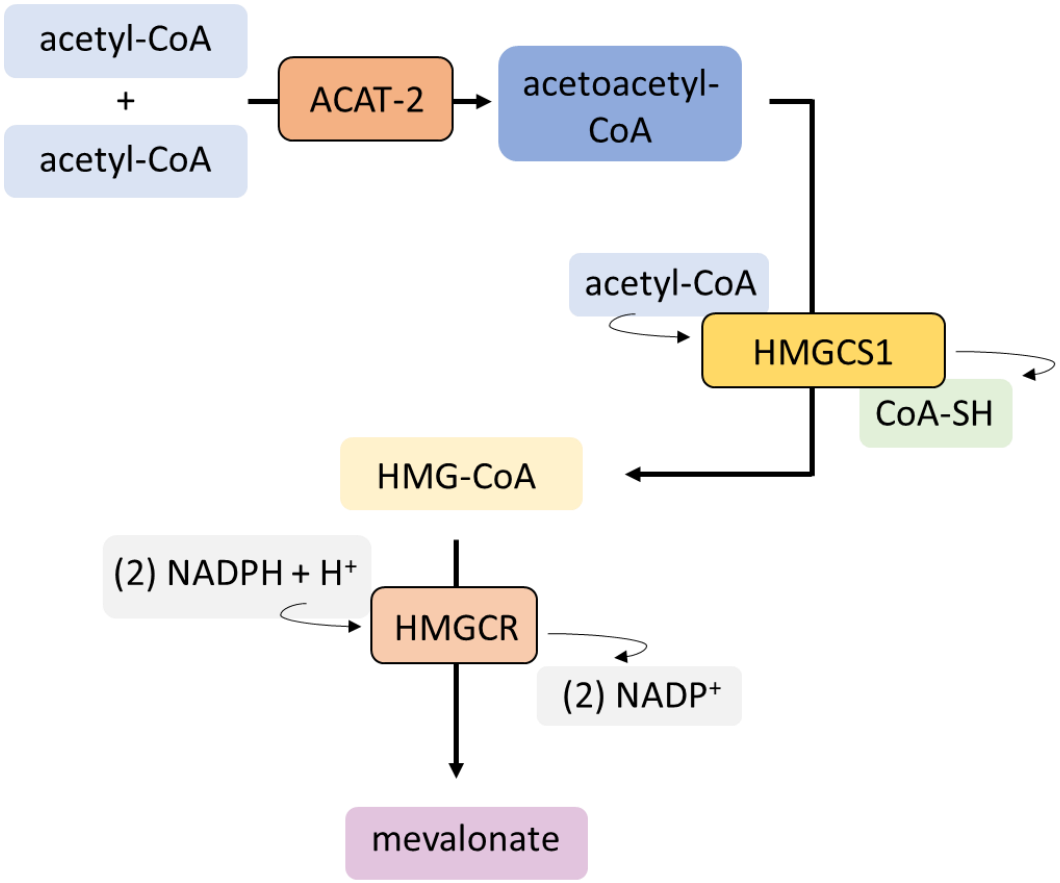


Figure A1. 0-1 Cytosolic synthesis of acetoacetyl-CoA from acetyl-CoA is initiated by the action of acetyl-CoA acetyltransferase 2 (ACAT2) and is followed by a further addition of acetyl-CoA by HGM-CoA synthase (HMGS1) to form HMG-CoA. The endoplasmic reticulum (ER) bound enzyme HMG-CoA reductase (HMGR) then mediates the conversion of HMG-CoA to mevalonate via the consumption of NADPH+, which is the major rate limiting step in cholesterol biosynthesis (316).

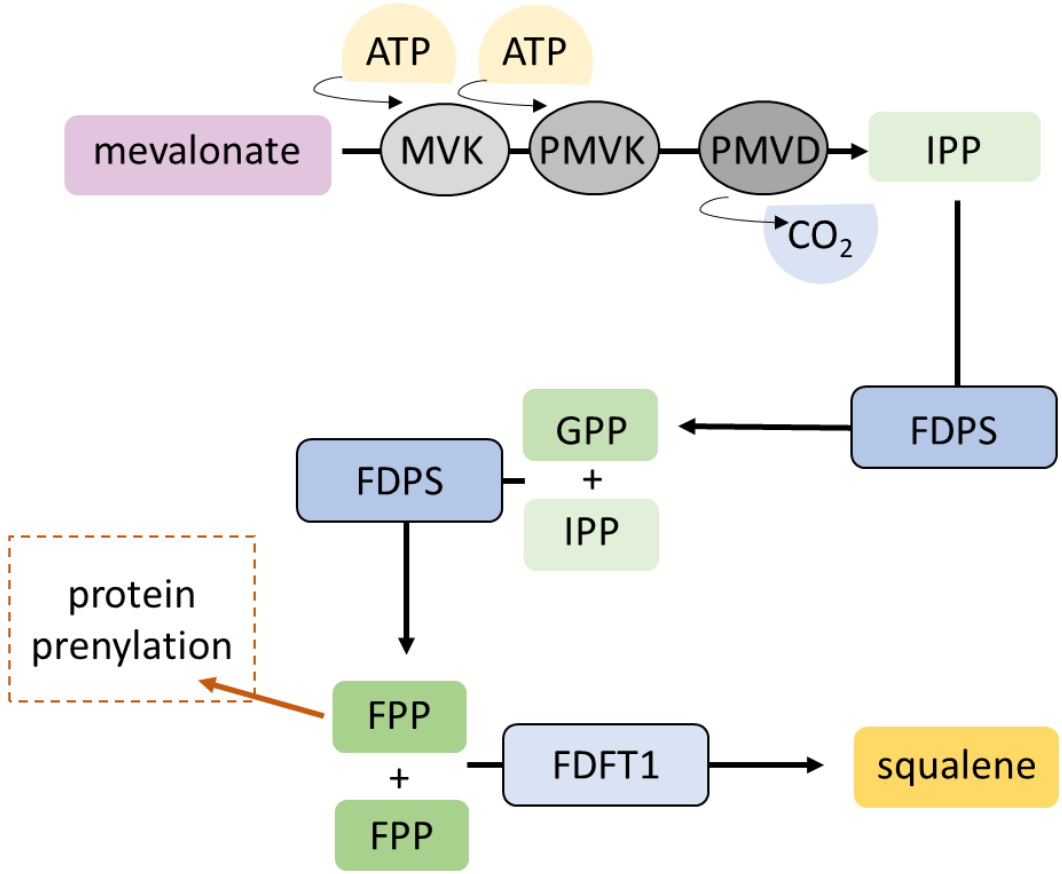


Figure A1. 0-2 Mevalonate is serially phosphorylated in an adenosine triphosphate (ATP) dependent manner by mevalonate kinase (MVK) to produce mevalonate 5-phosphate and then by phosphomevalonate kinase (PMVK) to produce mevalonate 5-diphosphate. Finally, an ATP dependent decarboxylation catalysed by diphosphomevalonate decarboxylase (MVD) converts mevalonate 5-diphosphate to isopentenyl pyrophosphate (IPP). IPP is converted to squalene in three steps. The conversion of IPP to geranyl pyrophosphate (GPP) is followed by its further conversion to farnesyl pyrophosphate (FPP) via the action of farnesyl diphosphate synthase (FDPS). Two molecules of FPP are then used by farnesyl diphosphate farnesyltransferase 1 (FDFT1) to produce squalene.

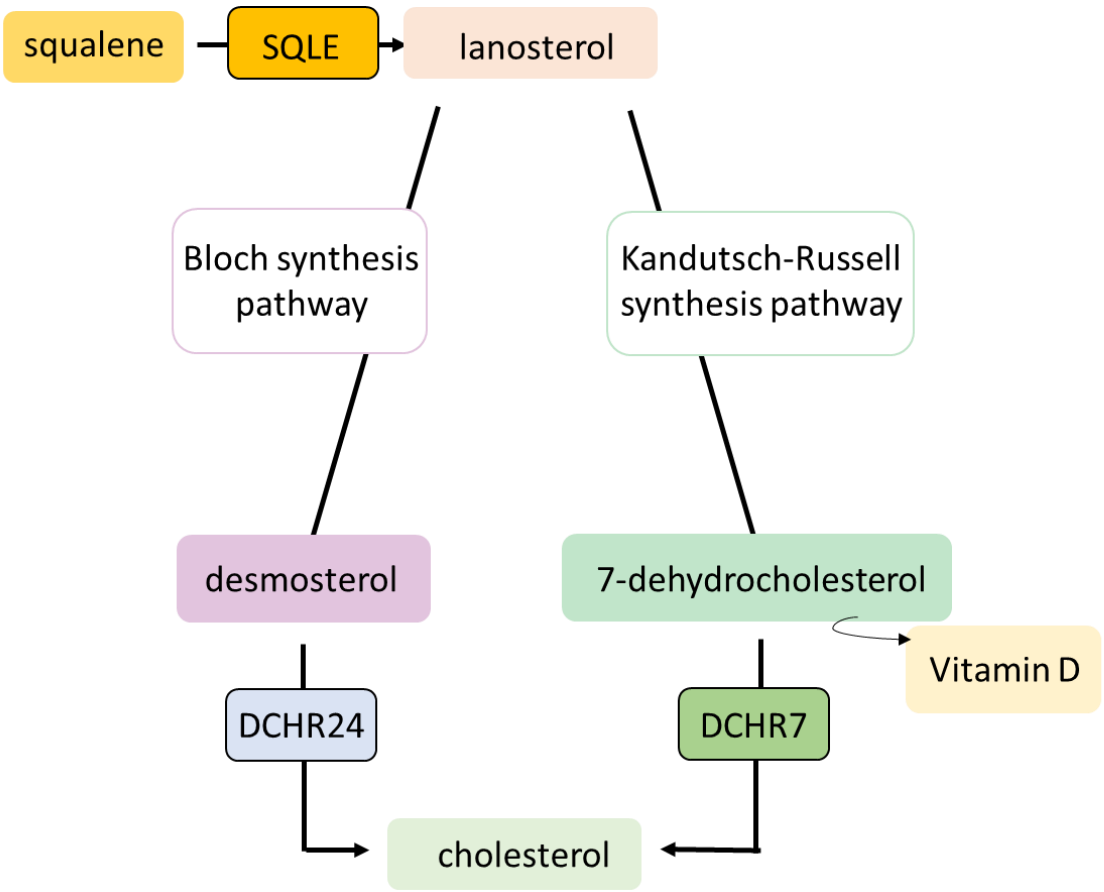


Figure A1. 0-3 Squalene undergoes two serial cyclizations, initially catalysed by squalene epoxidase (SQLE) to produce 2,3-oxidosqualene and followed by lanosterol synthase (LSS) to produce lanosterol. Lanosterol is eventually converted to cholesterol via two distinct pathways which take place in the ER and peroxisomes. In the Bloch pathway (317), four reactions lead to the formation of zymosterol which is the first 27-carbon cholesterol precursor. In the Kandutsch-Russell pathway (317), zymostenol is the equivalent 27-carbon molecule. Zymosterol is converted to desmosterol in three steps in the Bloch pathway, which is then converted to cholesterol in a final step catalysed by dehydrocholesterol reductase 24 (DHCR24), whereas zymostenol is converted to lathosterol and then 7-dehydrocholesterol which is the major cholesterol precursor. Dehydrocholesterol reductase 7 (DHCR7) catalyses the conversion of 7-dehydrocholesterol to cholesterol, with vitamin D being a major alternative product of 7-dehydrocholesterol processing.

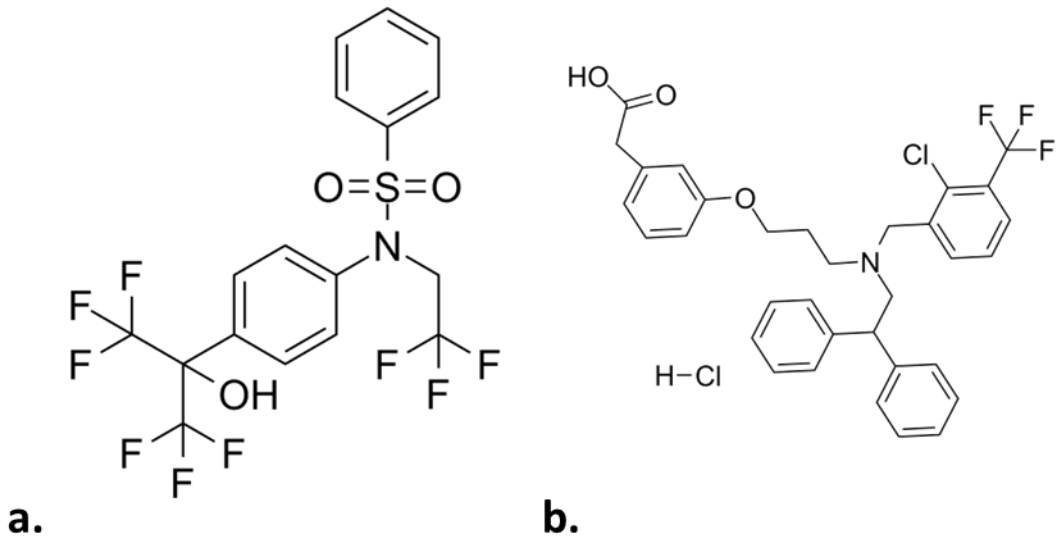


Figure A1. 0.4 The chemical structures of the LXR agonists T0901317 (a) and GW3965 (b). T0901317 is an LXRα-specific agonist, while GW3965 targets both hLXRα and hLXRβ.